OIL FLOW, CAVITATION AND FILM REFORMATION IN JOURNAL BEARINGS INCLUDING AN INTERACTIVE COMPUTER-AIDED DESIGN STUDY

by

A.A.S. Miranda, M.Sc.

A thesis submitted in fulfilment of the requirements for the degree of Doctor of Philosophy

DEPARTMENT OF MECHANICAL ENGINEERING
THE UNIVERSITY OF LEEDS
LEEDS, U.K.

AUGUST 1983

To my family

Lidia,

Vasco and Rafael

ABSTRACT

An interactive computer program for the design of steadily loaded fluid film, hydrodynamic journal bearings based on the procedure of ESDU Item No. 66023 (1966) is presented. The program was developed in two forms, a graphics and a non-graphics version. The computer program procedure enabled a detailed study of the effect of changes in the parameters on the bearing performance, which in turn permitted the design of an optimized bearing.

A theoretical and experimental study of the influence of film reformation on the performance of hydrodynamic journal bearings, and the side flow rate in particular, is also presented. A numerical analysis technique based on a cavitation algorithm proposed by H.G. Elrod was developed. This technique was capable of an automatic determination of the boundaries of the cavitation region and included a consideration of the lubricant inlet conditions (groove geometry and supply pressure). Theoretical data for journal bearings with a single axial groove located at the position of maximum film thickness is presented for a wide range of the values of the bearing design and operating parameters.

An apparatus was designed and commissioned to study the lubricant flow rate in journal bearings. Tests were performed with three glass bushes of width-to-diameter ratio of unity at variable values of eccentricity ratio and lubricant supply pressure. The agreement achieved between theory and experiment for dimensionless side flow rate was excellent. For the location of the film reformation boundary, the correlation between theoretical predictions and experimental measurements was satisfactory, except at low values of eccentricity ratio and dimensionless supply pressure.

A study of the correlation between the predictions of dimensionless load capacity, attitude angle and dimensionless side flow rate obtained from ESDU Item No. 66023 (1966) and those of the new bearing analysis reported in the thesis is presented. Good agreement was observed for the predictions of side flow rate.

ACKNOWLEDGEMENTS

I would like to express deep appreciation to my thesis supervisors, Professor D. Dowson and Dr. C.M. Taylor, for their invaluable guidance and advice. It has been a pleasure to work with people of such calibre.

The suggestions made by Mr. F.A. Martin and Mr. D.R. Garner of The Glacier Metal Co. Ltd., for improvements on the interactive computer program for the design of journal bearings when it was in a crucial stage of development, are gratefully acknowledged. At a later stage, the comments of Mr. C. Clifton and Mr. C. Loughton of ESDU International Ltd., and of Dr. E.H. Smith of Preston Polytechnic, were also appreciated.

I would like to thank Mr. R.T. Harding for his valuable suggestions in relation to the design and the commissioning of the experimental equipment.

Laboratory assistance throughout the duration of the experimental work was provided by Ron Lihoreau and his technical staff, Alan Heald and Luciano Bellon. Photography associated with this thesis was performed by Mr. S. Burridge. This thesis has been typed by Mrs. S. Moor and Mrs. C.M. Goulborn. I am indebted to each and everyone of these people for their contribution.

To carry out this work I was sponsored by the 'Instituto Nacional de Investigacao Cientifica - INIC' on the dependence of the Portuguese Ministry of Education.

CONTENTS

NOMENCLATURE

The following notation is used throughout the thesis. Special notation is defined in the sections to which it applies.

a/b	groove length-to-bearing width ratio
b	bearing width
b/d	bearing width-to-bearing diameter ratio
c	radial clearance
d	bearing diameter
g	Elrod's cavitation index
h	film thickness
p	pressure
p_c	cavitation pressure
p_f	lubricant supply pressure
r	bearing radius
w/d	groove width-to-bearing diameter ratio
x	circumferential coordinate
y	axial coordinate
C_d	diametral clearance
C_d/d	clearance ratio
H	power loss in ESDU Item No. 66023 (1966)
M	number of mesh lines parallel to the bearing axis
N	number of circumferential mesh lines

P resultant film pressure (force)

P_x component of the resultant film pressure (force) perpendicular to the line of centres

P_z component of the resultant film pressure (force) along the line of centres

Q lubricant flow rate

Q_c flow rate into the cavitation region

Q_E theoretical flow rate in ESDU Item No. 66023 (1966)

Q_{gr} net flow rate issuing from the groove

Q_p pressure induced flow rate in ESDU Item No. 66023 (1966)

Q_s flow rate from the bearing sides

Q_v velocity induced flow rate in ESDU Item No. 66023 (1966)

Q_1 flow over the upstream edge of the groove

Q_2 flow over the downstream edge of the groove

Q_3 flow over the groove sides (axial direction)

R_f relaxation factor in Gauss-Seidel iteration

S speed of rotation of the journal

U_1 tangential speed of the shaft surface

U_2 tangential speed of the bush surface

W load on the bearing

α angular coordinate measured from the position of maximum film thickness in the direction of rotation of the journal

α_c angular location of the cavitation boundary

α_r angular location of the reformation boundary at the bearing edge

β bulk modulus of the lubricant

ε eccentricity ratio

η effective viscosity of the lubricant

θ Elrod's variable

ρ lubricant density

ρ_c lubricant density at cavitation pressure

ψ attitude angle

Ω_1 angular velocity of the shaft

Ω_2 angular velocity of the bush

Dimensionless groups

$\bar{h} = \frac{h}{c}$ normalized film thickness

$\bar{p} = \frac{p}{\eta(\Omega_1+\Omega_2)} \left(\frac{c}{r}\right)^2$ normalized pressure

$\bar{x} = \frac{x}{2\pi r}$ normalized x-coordinate

$\bar{y} = \frac{y}{b}$ normalized y-coordinate

$\bar{Q} = \frac{Q}{cb(U_1+U_2)}$ dimensionless flow rate

$\bar{W} = \frac{W}{br\eta(\Omega_1+\Omega_2)} \left(\frac{c}{r}\right)^2$ dimensionless load capacity

$\bar{\beta} = \frac{\beta}{\eta(\Omega_1+\Omega_2)} \left(\frac{c}{r}\right)^2$ bulk modulus parameter

Subscripts

amb	refers to ambient conditions
c	refers to the cavitation region
i	refers to nodes on the circumferential mesh line (i)
j	refers to nodes on the axial mesh line (j)
x	refers to the circumferential direction
y	refers to the axial direction

CHAPTER 1

INTRODUCTION

The role of lubricants in the reduction of friction between surfaces in relative motion has been recognised for hundreds of years. It was, however, the work of Osborne Reynolds in the late nineteenth century that provided the basis of modern scientific studies of fluid film lubrication.

Assuming slow viscous flow and a thin film of lubricant, Reynolds (1886) derived the equation governing the pressure generation in lubricating films by applying the basic equations of motion and continuity to the lubricant. For steady-state operating conditions with an isoviscous, incompressible, lubricant Reynolds' equation can be shown to reduce to the following commonly used form,

$$\frac{\partial}{\partial x}\left[h^3 \frac{\partial p}{\partial x}\right] + \frac{\partial}{\partial y}\left[h^3 \frac{\partial p}{\partial y}\right] = 6\eta \ (U_1+U_2) \ \frac{\partial h}{\partial x} \qquad (1.1)$$

where (p) is the pressure, (h) is the film thickness, (η) is the dynamic viscosity of the lubricant, (U_1,U_2) are the surface speeds in the (x) coordinate direction and the axis are chosen such that there are no surface velocities in the (y) coordinate direction.

In hydrodynamic journal bearings operating under steady-state conditions the journal does not run concentrically within the bush. The position of the centre of the journal with respect to the bush centre

is dependent on the bearing operating conditions. The eccentricity between bush and shaft generates the convergent-divergent shape of the lubricating film observed in journal bearings, making them capable of supporting loads as a result of the generation of hydrodynamic pressures in the convergent part of the film.

The determination of the bearing performance is based on a knowledge of the pressure distribution in the lubricant film in the bearing, which is obtained by integration of equation (1.1). An approximate analytical solution of Reynolds' equation may be obtained by assuming an infinitely wide bearing in which the pressure gradients in the axial direction are taken equal to zero. Reynolds (1886) has determined the pressure generated at specific angular locations in an infinitely wide journal bearing by employing Fourier series to evaluate some of the integrals involved. This approach was, however, restricted to values of eccentricity ratio smaller than or equal to 0.5 due to the requirements for convergence of the series. This difficulty was overcome by Sommerfeld (1904) with the introduction of a new variable (the Sommerfeld variable) which made the evaluation of those integrals straight forward.

The 'short' journal bearing theory of Dubois and Ocvirk (1953) has also provided an approximate analytical solution of the Reynolds' equation which is applicable to bearings of small width-to-diameter ratio. Short bearing theory assumes that the circumferential pressure gradients are negligible in comparison with the axial pressure gradients and is based upon the geometrical condition that the axial length of the journal bearing is small compared with its diameter.

The results obtained using either of these solutions may, however, be very inaccurate when applied to realistic bearings. The width-to-diameter ratio of modern day journal bearings is usually in the range (0.25-1) and hence the solution of the full Reynolds equation is required. This can be achieved by numerical analysis and has been facilitated by the development of digital computers.

The phenomenon known as 'cavitation' usually occurs in the divergent part of the lubricating film in journal bearings. The most common type of cavitation encountered in hydrodynamic lubrication is known as 'gaseous cavitation'. It consists of a disruption of the continuous film of lubricant by the formation of gas cavities caused by ventilation from the surrounding atmosphere or by the emission of dissolved gases from solution when the pressure of the lubricant falls below the saturation pressure. The disrupted film will reform in the vicinity of the position where the film profile begins to converge, depending on the lubricant supply conditions. In the cavitation region, bounded by the rupture and the reformation boundaries, the pressure is usually assumed to be constant and equal to the ambient pressure and Reynolds' equation does not apply. Much attention has been given to the determination of the rupture boundary and various physical models have been proposed for its location. This has not been so with the reformation boundary. Although reformation boundary conditions have been proposed they have rarely been incorporated in theoretical analyses due to the complexities arising from the numerical analysis in their implementation.

A widely used film rupture boundary condition is the Reynolds' boundary condition which assumes that when rupture occurs pressure and pressure gradients both take the value zero. Many of the journal bearing design procedures available have been based on solutions of the

Reynolds' equation which have incorporated the Reynolds' rupture boundary condition and a 'reformation' condition arbitrarily established which assumed that reformation occurred at the position of maximum film thickness where the film pressure was ambient. This is the case, for example, with the data given in the design procedure described in ESDU Item No. 66023 (1966), a commonly used procedure for the design of steadily loaded journal bearings. These boundary conditions and the resulting pressure distribution along the bearing centre line are sketched in Figure 1.1.

In real bearings reformation is not likely to occur at the position of maximum film thickness. Plate 1.1 shows two photographs, from experiments reported in this thesis, of the location of the reformation boundary observed in a journal bearing supplied with lubricant via a hole located at the position of maximum film thickness. Depending on the lubricant supply conditions (grooving arrangement and supply pressure) the beginning of the complete width film may occur upstream or downstream of the position of maximum film thickness. The location of the reformation and of the rupture boundaries determines the extent of the full width film which is an important parameter in relation to the performance of the bearing. For example, the lubricant flow rate may be influenced by the location of the film reformation boundary. The importance of a correct determination of the flow rate in a bearing is crucial; the flow rate affects the lubricant temperature rise and hence its viscosity, which in turn influences the film profile and the load carrying capacity of the bearing. A correct location of the film reformation boundary is, therefore, desirable.

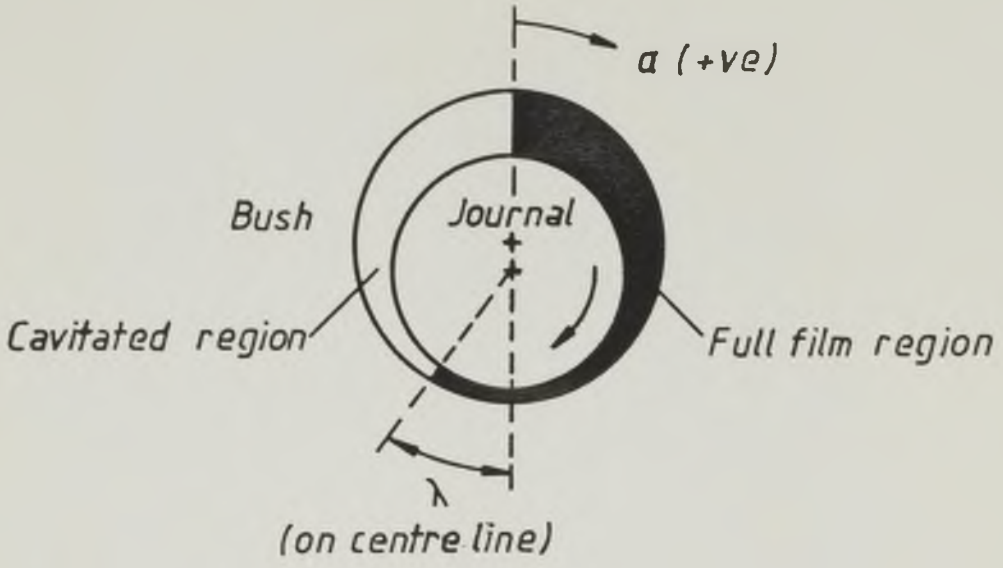

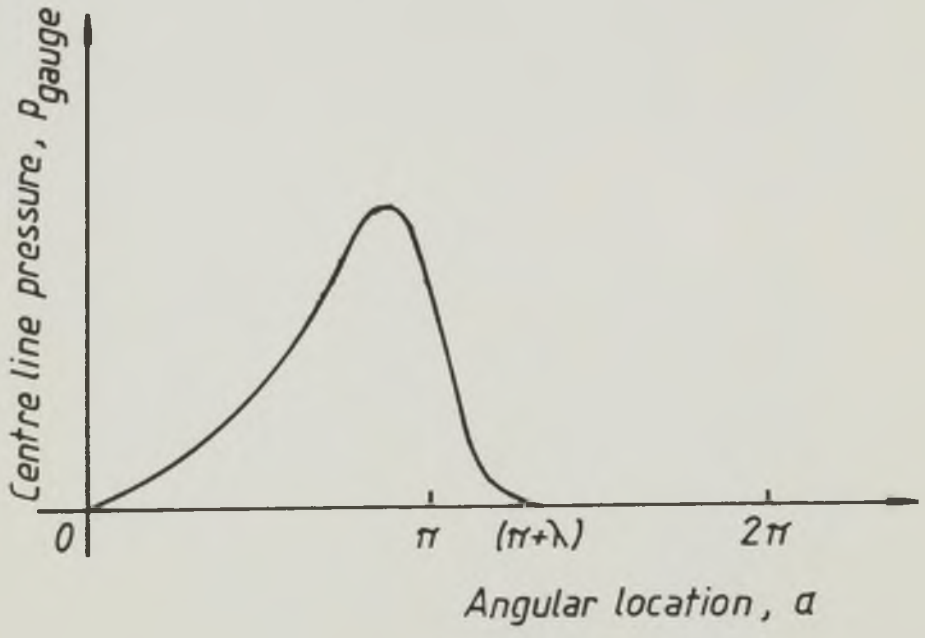

Boundary Conditions:

(1) Film inlet conditions (reformation)

$$p = 0 \text{ at } \alpha = 0$$

(2) Film outlet conditions (rupture)

$$p = \frac{\partial p}{\partial x} = \frac{\partial p}{\partial y} = 0 \quad \text{at rupture}$$

Figure 1.1 A sketch of the boundary conditions commonly adopted in journal bearing analysis and the resulting pressure distribution along the bearing centre line.

(a)

low lubricant

supply pressure

(b)

high lubricant

supply pressure

Plate I.1 Photographs of the location of the film reformation boundary in a journal bearing with oil hole located at the position of maximum film thickness. The direction of shaft rotation was from left to right

Elrod and Adams (1974) and Elrod (1981) proposed a computational algorithm which allowed the automatic determination of the cavitation region without explicit reference to rupture or reformation boundary conditions. Mass flow continuity was achieved at the rupture and reformation boundaries which could be located without encountering the complexities involved in the implementation of the detailed reformation boundary conditions as with more conventional numerical analysis solution schemes.

It was against this background that the present research programme was established. Its objectives were as detailed below.

(1) A commonly used procedure for the design of steadily loaded, fluid film, hydrodynamic journal bearings is described in ESDU Item No. 66023 (1966). It is a 'hand' type design procedure which seemed to have much to gain from modern day computing facilities.

A first objective of the work described in this thesis was the development of techniques which eventually led to the computerization of the ESDU Item No. 66023 (1966) design procedure. These techniques were also expected to be of interest in the computerization of design procedures of a similar type.

The interactive computer program developed, the techniques used and the philosophy adopted will be discussed in Chapter 2 of this thesis.

(2) The second aim of the present research work was to carry out a study of the effect of film reformation considerations on the performance of journal bearings, and on the lubricant flow rate in particular. This investigation was to be initiated for journal bearings having

a single axial groove (or oil hole) located at the position of maximum film thickness. Extension of the investigation to include more practical grooving arrangements will be a future priority. To carry out this study the following procedure was envisaged.

(a) The development of a numerical analysis technique for the analysis of the performance of journal bearings based on Elrod's algorithm. Such an approach will enable a detailed study of the lubricant supply conditions (grooving arrangement and supply pressure). This will be discussed in Chapter 3.

(b) A comparison of the performance predictions of this analysis with those of ESDU Item No. 66023 (1966) which did not incorporate film reformation considerations. This comparative study will be described in Chapter 4.

(c) The determination of the correlation between the predictions of the present analysis and experimental measurements. An experimental apparatus was to be designed and an experimental programme carried out to provide the results required. The description of the apparatus will be presented in Chapter 5 and a discussion of experimental results will be dealt with in Chapter 6.

The overall conclusions of the work undertaken will be presented in Chapter 7.

CHAPTER 2

THE DEVELOPMENT OF AN INTERACTIVE COMPUTER PROGRAM FOR THE DESIGN OF STEADILY LOADED, LIQUID FILM, HYDRODYNAMIC PLAIN JOURNAL BEARINGS

2.1 Introduction

With the advent and development of digital computers numerical analysis techniques acquired new significance and their successful incorporation into theoretical studies became possible with relative ease. In the analysis of fluid film bearings in particular, computers have been used to solve numerically the full Reynolds equation governing the distribution of pressure within the lubicant film. Computer solutions for the bearing performance predictions for a wide range of values of the operating parameters have been made available in the form of charts of dimensionless quantities, and various 'hand' type design procedures based on such solutions have been presented by a number of authors. A good example of this type of design procedure has been developed by the Engineering Sciences Data Unit (ESDU) and is described in ESDU Item No. 66023 (1966) - 'Calculation Methods for Steadily Loaded Pressure Fed Hydrodynamic Journal Bearings'.

'Hand' type bearing design procedures may become tedious and time-consuming in situations where an iterative procedure is used in order to reach a satisfactory solution or when an optimized design is required.

Various computer programs for the design of bearings have been developed in industrial and educational establishments. Taylor (1971) conducted a survey of existing computerized programs which indicated the programs available and the gaps that needed to be filled.

A modern trend in the computer-aided design of bearings appears to be in the application of optimization techniques to the design. In this context, studies on the optimum design of hydrodynamic journal bearings have been presented by Seireg and Ezzat (1969) and Dowson and Ashton (1976).

Computers are not confined to scientific or big business centres. In recent years, mini- and micro-computers of considerable computing power which are small in physical size and sufficiently low in price to make their use acceptable for many applications, have been developed. In many industrial companies the terms 'computer-aided design (CAD)' and 'computer-aided manufacture (CAM)' are already familiar and the tendency to the conversion of 'hand' type design procedures to CAD techniques is expected to continue. Easy communication between the user and the computer has been made possible by means of the visual display unit (VDU) with a keyboard connected directly to the computer. The user's instructions are typed on the keyboard and the answers of the computer are displayed on the VDU. Many engineering design requirements are met by the interactive and the graphics display facilities of modern computer systems. For computerized bearing design in particular, these facilities allow an immediate assessment of the effect of changes in the design parameters on the performance of the bearing making possible the design of optimized bearings.

Siew and Reason (1982) used both the computer/user interaction

and the graphics display facilities in a study of the performance of hydrodynamic journal bearings. They developed computer programs for the study of the influence of the boundary conditions adopted, the lubricant supply pressure and the groove size, on the bearing performance. The development of computer programs for the analyses of misaligned journal bearings and porous journal bearings was also reported.

Most of the existing bearing design computer programs have been developed to respond to specific needs and are often not suitable for the use of other consumers. Few interactive computer programs have been developed and even less (if any) are generally available.

One objective of the work reported in this thesis was the development of an interactive bearing design computer program based on the procedure of ESDU Item No. 66023 (1966). This was the most comprehensive and probably the most commonly used procedure for the design of hydrodynamic journal bearings.

This chapter includes a brief description of the ESDU Item No. 66023 (1966) procedure and a discussion on the interactive computer program developed. A more detailed discussion can be found in Miranda (1983).

2.2 Brief Description of the ESDU Item No. 66023 (1966) Design Procedure

2.2.1 Major Assumptions

The complete assumptions and the limitations of this procedure are listed on pages 9 and 10 of the document. Only the more important are dealt with here:

(i) The viscosity of the lubricant is assumed to be constant around the bearing (termed the effective viscosity).

(ii) The maximum lubricant temperature rise in the load carrying part of the bearing is twice the mean temperature rise. The mean temperature (effective temperature) is obtained by an iterative thermal balance and is used to determine the effective viscosity.

(iii) There is no recirculation of lubricant in the bearing. All the lubricant is assumed to be replaced by fresh lubricant after having travelled 360^{o} around the bearing.

(iv) The lubricant flow rate in the bearing (Q) is the sum of the 'velocity induced flow rate' (Q_v) and the 'feed pressure induced flow rate' (Q_p). For circumferentially grooved bearings (Q_v) equals zero.

2.2.2 Design Criteria

The procedure adopted in ESDU Item No. 66023 (1966) ensures a minimum film thickness at the bearing edge which is safe, and an acceptable maximum temperature of the lubricant in the bearing.

At low speeds, the minimum film thickness should be large enough to prevent asperity contacts between bearing and shaft surfaces. At high speeds, it should be sufficient to prevent the generation of high temperatures in the region of the minimum film thickness, which can cause wiping of the bearing metal. Guidance on the safe value of minimum film thickness is given on Figure 3 of the document.

The limitation on the maximum temperature of the lubricant in the bearing is required to prevent local melting of the bearing surface. The maximum acceptable temperature is dependent on the particular bearing

material employed. For white-metal bearings temperatures up to about 120°C are usually acceptable.

The outlet temperature of the lubricant is used to assess its susceptibility to oxidation. For mineral oils the critical temperature is about 75°C when in contact with the atmosphere.

2.2.3 Design Procedure

The procedure of the ESDU Item No. 66023 (1966) allows the design of both axially and circumferentially grooved bearings and relies extensively on the use of charts of dimensionless quantities.

Load, speed and bearing diameter are assumed to be design specifications.

The procedure involves the following stages.

a) The Initial Approximate Design

An initial design chart gives guidance on the selection of the bearing parameters and the oil type. It may be used to select the clearance ratio (C_d/d), the bearing width-to-bearing diameter ratio (b/d) and the oil characteristics. An estimation of the effective viscosity of the oil can also be obtained and used as a starting value in the thermal iteration to determine the effective viscosity. A load capacity chart (Figure 6 of the document) allows the determination of the operating eccentricity ratio (ε) and a check for operation within the 'Recommended Area'. This is a region bounded by curves of maximum and minimum recommended values of (b/d) (1.25 and 0.2 respectively), and by limiting maximum and minimum loading conditions for a given value of (b/d). Lightly loaded journal bearings are prone to instability but this will not normally occur if the operating point is within the 'Recommended Area'.

b) The Full Design

Having selected the bearing parameters and the oil type, the effective viscosity of the oil is required to calculate the bearing performance characteristics.

The effective temperature is obtained from a thermal balance involving the lubricant flow rate, the power loss and the temperature rise in the bearing. Due to the interconnection between these three quantities an iteration is usually required to calculate the effective operating temperature.

Because of the assumption made regarding lubricant recirculation around the bearing (Section 2.2.1 -(iii)) the primary aim of this procedure is to provide a full width film of lubricant at the groove location whenever possible. A theoretical flow rate (Q_E), required to fill completely the clearance space at the groove, is determined, and the iteration to calculate the effective temperatue is performed involving the flow (Q_E) and the power loss (H). The groove size is then selected, and the lubricant supply pressure required to provide a flow rate in the bearing (Q) such that $Q \geq Q_E$ is then calculated. If the supply pressure required for fully flooded conditions ($Q \geq Q_E$) is too high, the bearing has to be designed for a flow (Q) smaller than the theoretical flow (Q_E) - the bearing is termed 'starved'. In such a case the effective viscosity of the lubricant and the performance characteristics of the bearing have to be recalculated.

c) The Performance Characteristics

If some of the calculated values of the performance characteristics of the bearing are not acceptable, guidance is given on which parameters should be altered, and in what direction, to achieve acceptable operating

conditions. However, a considerable effort and a careful selection of parameters and determination of the corresponding bearing performance, would be required to design an optimized bearing.

Figure 2.1 shows a simplified flow chart of the ESDU Item No. 66023 (1966) design procedure.

2.3 Discussion of an Interactive Computer Program for the Design of Steadily Loaded Hydrodynamic Journal Bearings

Originally, it was intended to develop a program that followed exactly the procedure of the ESDU Item No. 66023 (1966). In its original version, in fact, the program developed followed very closely the philosophy adopted in that document and made extensive use of design charts. An optimization facility was already included in this version.

The program was mounted on the VAX 11/780 Computer in the Department of Mechanical Engineering in the University of Leeds. The language used was Fortran IV and the software involved was the GINO-F Graphics Package.

Not all the diagrams of the ESDU Item No. 66023 (1966) were reproduced on the V.D.U. screen, some were substituted by data stored in tabular form. Graphical interaction was possible by using the cursor mechanism and interpolation routines were used for interpolation in table functions.

A subsidiary program was written which produced the diagrams required in a special code form. The output of this program was stored in a data file, constituting a library of diagrams that could be used by the design program.

A change in philosophy with respect to the approach employed at some particular points of the design procedure was implemented after

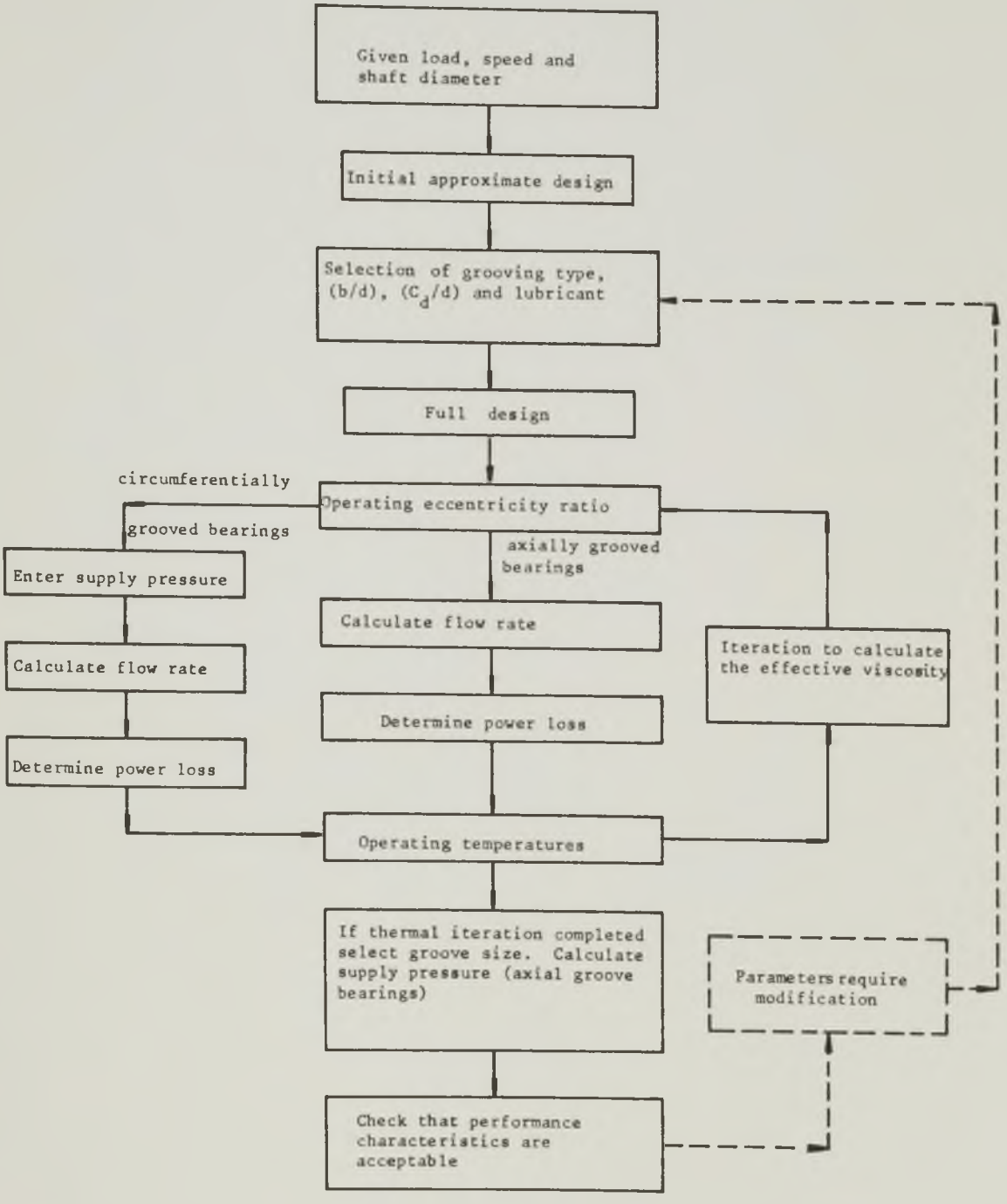

Figure 2.1 Simplified flow chart of the ESDU Item No. 66023 (1966) design procedure

discussions with interested academics and industrialists, and different computer strategies, suggested by the experience of using the original version of the program, were adopted.

It was recognized that the use of diagrams, although being a suitable means of presenting some design features and valuable for less experienced users, nevertheless increased both the time and the storage space required for running the program.

Two new versions resulted from the development of the original form of the computer program:

(1) A graphics version, which employed charts 2B , 6, 12 and 13 of the ESDU Item No. 66023 (1966) and which was able to generate diagrams showing the effect of changes in the parameters on the performance of the bearing. As an alternative to graphical interaction, this version also provided the possibility of using internal calculations from data in tabular form. At the beginning of the program a switch existed which permitted the selection of the graphics or the non-graphics option, according to the type of terminal being used. A Tektronix 4014 terminal was required to run the graphics version of the program under the graphics option.

(2) A non-graphics version, which did not use any diagrams. The procedure followed in this version was similar to that of the graphics version running on the non-graphics option. The reason why this was developed as a separate program was the recognition that such a program would require less memory space and could be a useful version for experienced designers or whenever a suitable graphics terminal was not available.

The two versions of the program were not different in their structure and therefore there is no need to consider them separately.

2.3.1 Selection of the Bearing Parameters

Load and speed were assumed to be design specifications. The bearing diameter, when it was not specified or calculated by strength considerations, was estimated by the program and could be altered at a later stage of the design, if required. The value provided was in the range (25-500 mm) and was obtained according to Figure 5, Section A5 of the Tribology Handbook (1973), assuming b/d = 0.75.

Clearance ratio (C_d/d), bearing width-to-bearing diameter ratio (b/d) and lubricant characteristics, were either inputted directly to the program or selected using the initial design chart. Guidance was given on the chart and the associated instructions for the selection of the parameters.

For each particular design specification , a curve representing the minimum allowable film thickness and lines of maximum (b/d) and limiting maximum temperature, were calculated and drawn on the initial design chart. Curves representing four types of oils were already included in the basic chart. The characteristics of the four types of oil represented (designated Oil 1, Oil 2, Oil 3 and Oil 4) covered a range of lubricating oils and are shown in Table 2.1.

	Dynamic Viscosity at 40°C (Pa.s)	Dynamic Viscosity at 100°C (Pa.s)
Oil 1	0.015	0.0031
Oil 2	0.044	0.0061
Oil 3	0.2	0.0162
Oil 4	0.9	0.04

Table 2.1 Characteristics of the Standard Oils of the ESDU Item No. 66023 (1966)

The computer program allowed the consideration of any other oil along with the standard oils of the ESDU Item No. 66023 (1966). The curve corresponding to this non-standard oil was calculated and drawn on the initial design chart. To perform this calculation the effect of temperature variations on both viscosity and density was considered, and the values of the kinematic viscosity of the oil at $40^{o}C$ and $100^{o}C$, as well as the oil density at a given temperature, were required.

An approximate value of the effective viscosity of the lubricant in the bearing was also obtained from the initial design chart for the design selected. If the alternative of entering the bearing parameters directly was chosen, the oil type and an estimation of the effective temperature of the oil, would be required.

A first check for operation within the 'Recommended Area' was carried out and, if the design was acceptable, the approximate bearing performance characteristics were printed out. Re-selection of the bearing parameters was possible until acceptable operating conditions were reached.

2.3.2 Lubricant Supply Pressure and the Design of the Groove (Axial Groove Bearings)

The primary objective of the ESDU Item No. 66023 (1966) procedure is to achievefully flooded conditions as discussed in Section 2.2.3. The groove size is selected, and the lubricant supply pressure calculated, to provide a full width film of lubricant at the groove location. The maximum acceptable value for supply pressure is considered to be 350 kN/m^2.

A different approach was adopted in the computer program being described. In modern day bearing design lubricant supply pressures of 50 kN/m^2 are common practice and 150 kN/m^2 is considered to be a high supply pressure (Martin (1981)). Thus, perhaps fifty per cent of hydrodynamic bearings operate with 'starved' conditions.

The program provided two alternatives for the design of the groove and the calculation of the supply pressure:

(i) To select the groove size and calculate the lubricant supply pressure for full flow. Changes in the size of the groove were allowed until the value of the supply pressure was considered to be acceptable.

(ii) To select both the groove size and the supply pressure without reference to fully flooded conditions. The degree of starvation (if appropriate) and the performance characteristics of the bearing were then calculated.

2.3.3 Degree of Starvation and the Bearing Performance

The determination of the degree of starvation was based on the concept of a 'starved' bearing adopted by the ESDU Item No. 66023 (1966) and discussed in Section 2.2.3. The following expression was used,

$$\text{Degree of Starvation } (\%) = \left[1 - \frac{Q}{Q_E}\right] \times 100 \qquad (2.1)$$

where (Q) and (Q_E) are the actual and the theoretical flow rates in the bearing, respectively.

The design charts provided by the ESDU Item No. 66023 (1966) and incorporated into the computer program, were based on fully flooded inlet conditions. What would be the error involved when using the information obtained from these charts to calculate the performance of a 'starved' bearing?

Connors (1962) has presented design charts for b/d = 1 where incomplete inlet film conditions were taken into account. Values of the performance characteristics of the bearing calculated using the computer program were compared with those obtained using Connors' design charts. The lubricant flow rates considered were those predicted by the computer program. A bearing with the following characteristics was considered:

Load = 6000 N

Speed = 1200 r.p.m. (20 Hz)

Diameter = 100 mm

Width-to-diameter ratio (b/d) = 1

Clearance ratio (C_d/d) = 0.002

Standard oil No. 2 (ESDU Item No. 66023 (1966))

Oil supplied at atmospheric pressure

Axial groove at the position of maximum film thickness

Groove width-to-bearing diameter ratio (w/d) = 0.15

The groove length-to-bearing width ratio (a/b) was varied in the range (0.3 - 0.9) to provide variable degrees of starvation.

The computed degree of starvation varied from 53.7% (at a/b = 0.9, ε = 0.42) to 82.1% (at a/b = 0.3, ε = 0.51).

The results obtained using Connors' procedure showed smaller values of minimum film thickness, slightly higher maximum temperatures (1-2^{o}C higher) and lower power loss (about 12%), for all degrees of starvation.

The discrepancy observed in minimum film thickness increased from 5.2% at the degree of starvation of 53.7%, to 29.2% with 82.1%

starvation. These results show that there are limitations on the use of the ESDU Item No. 66023 (1966) procedure with high degrees of starvation, but seemed to suggest that this procedure was acceptably accurate with degrees of starvation up to about fifty per cent.

2.3.4 The Bearing Optimization

After the groove size and the supply pressure had been selected, a thermal iteration was performed to calculate the effective viscosity of the lubricant. Final checks for operation within the 'Recommended Area' and for laminar flow conditions, were then carried out.

The bearing parameters selected and the performance characteristics calculated were all printed out on the V.D.U. screen.

In many applications it might be important to minimize power loss, or flow rate, keeping minimum film thickness and maximum temperature at acceptable levels. Any change in a particular bearing parameter will affect the whole performance of the bearing and some compromise has to be adopted by the designer between the desirable and the acceptable.

To give the designer an immediate assessment of the effect of changes in one or more parameters on the performance of the bearing, an optimization procedure was incorporated in the computer program.

a) Effect of Individual Changes in the Parameters

The effect of individual changes in diameter, bearing width, diametral clearance and oil type, on minimum film thickness, oil flow rate, power loss and maximum temperature, was calculated and shown in graphical form. The plots of the variation of minimum film thickness also included the safe minimum film thickness curve in the domain defined for the variation of the parameter. The maximum allowable temperature curve was also represented on the diagrams showing the effect

of changes of a given parameter on maximum bearing temperature.

The domain of variation of the parameter under consideration was defined by the designer and inputted to the program as a fractional change with respect to the value selected in the full design, which was the central point in the field of variation.

b) Effect of Combined Changes in the Parameters on the Bearing Performance

Having studied the effect on the performance of the bearing of individual changes in the parameters, the effect of combined changes could be determined, if required. Only the parameters mentioned in a) and the oil type were allowed to be changed. The groove size and the oil supply pressure were kept unchanged at the values selected in the full design. The performance predictions were shown in tabular form.

There was no limitation in the number of combinations of parameters that could be considered.

Once it had been decided what alterations to adopt, if any, the new values of the parameters and the oil type were inputted and the bearing performance was re-calculated. Checks for operation within the 'Recommended Area' and laminar flow conditions were carried out for the new operating conditions, and the performance characteristics of the optimized bearing were printed out.

2.3.5 The Load-Speed Diagram

Bearing load and shaft speed were assumed to be design specifications. In operation, however, 'off-design' loads or speeds may sometimes occur.

To provide information relating to the effect of 'off-design' conditions on critical performance parameters, such as minimum film

thickness and maximum lubricant temperature, the program was able to calculate and draw a load-speed diagram of the bearing designed. If a graphics facility was not available, the load-speed characteristics of the bearing were shown in the form of pairs of values for load and speed representing points on the load-speed curve.

Figure 2.2 shows a sketch of a typical load-speed diagram. The curve is composed of two portions:

(a) The minimum film thickness portion, is defined by pairs (load, speed) such that the minimum film thickness at the bearing edge is equal to the safe minimum film thickness. At a given speed (S), the maximum allowable load to ensure that the minimum film thickness is safe, is (W_1). For a given load (W), the minimum speed that ensures a safe minimum film thickness is (S_1).

(b) The maximum temperature portion, is the locus of points corresponding to operating conditions such that the maximum temperature of the lubricant equals the maximum allowable temperature. At a given operating speed (S_2), the maximum allowable load to prevent an excessive temperature rise is (W_2), and at a given load (W), the maximum speed permitted is (S_3).

Operating points within the region below the curve will represent safe operating conditions with respect to minimum film thickness and maximum lubricant temperature.

2.3.6 The Program Flow Chart

The structure of the program was somewhat complex due to the numerous calculations involved and the various alternatives offered to the designer anytime a decision was required.

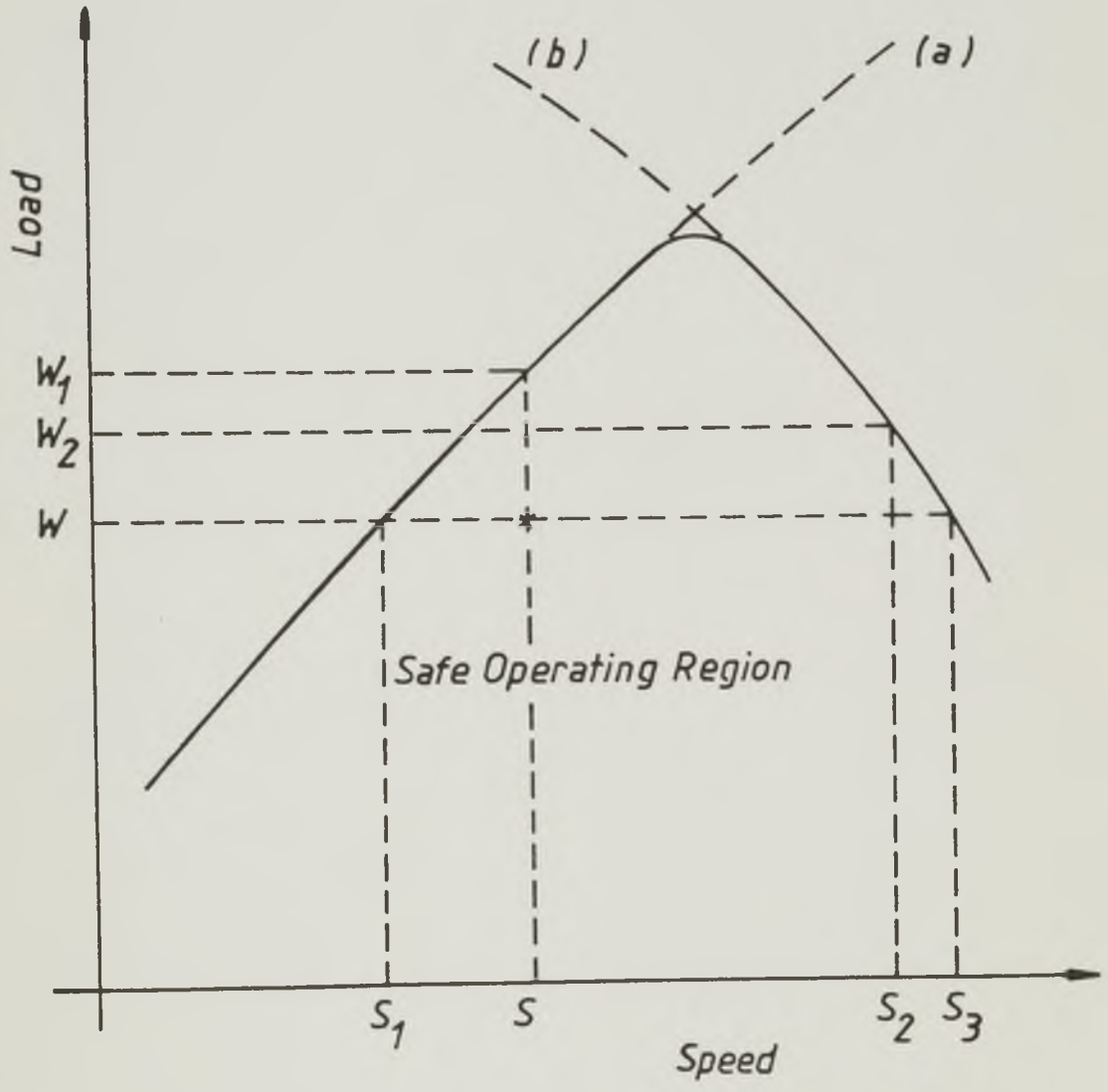

Figure 2.2 Sketch of a load-speed diagram

The graphics version of the program used sixteen routines and had additional complexities connected with the use of charts and graphical interaction. A detailed flow chart is available in Miranda (1983).

A very simplified program flow chart is shown in Figure 2.3. In broad terms, the procedure could be divided into four parts:

(1) The bearing specifications and the selection of parameters
(2) The determination of the effective viscosity of the lubricant
(3) The design of the groove and the calculation of the lubricant supply pressure (Axially grooved bearings)
(4) The optimization process

In part (3), a significant change in philosophy with respect to the ESDU Item No. 66023 (1966) procedure was adopted. The approach employed and its implications have been dealt with in Sections 2.3.2 and 2.3.3.

Bearing design procedures of the 'hand' type are usually not orientated to the design of optimized bearings. This was the case of the procedure described in ESDU Item No. 66023 (1966), although improvements in the design could be made by sensibly changing the bearing parameters. It is the computerization, however, that provides the conditions for an optimization study to be carried out. Such a study was included in the computer program procedure and constituted an important design aid.

2.3.7 Complete Sequence of Pages Produced on the V.D.U. Screen When Running the Graphics Version of the Program

The following example illustrates the use of the program. The design specifications are listed below and the computer output follows.

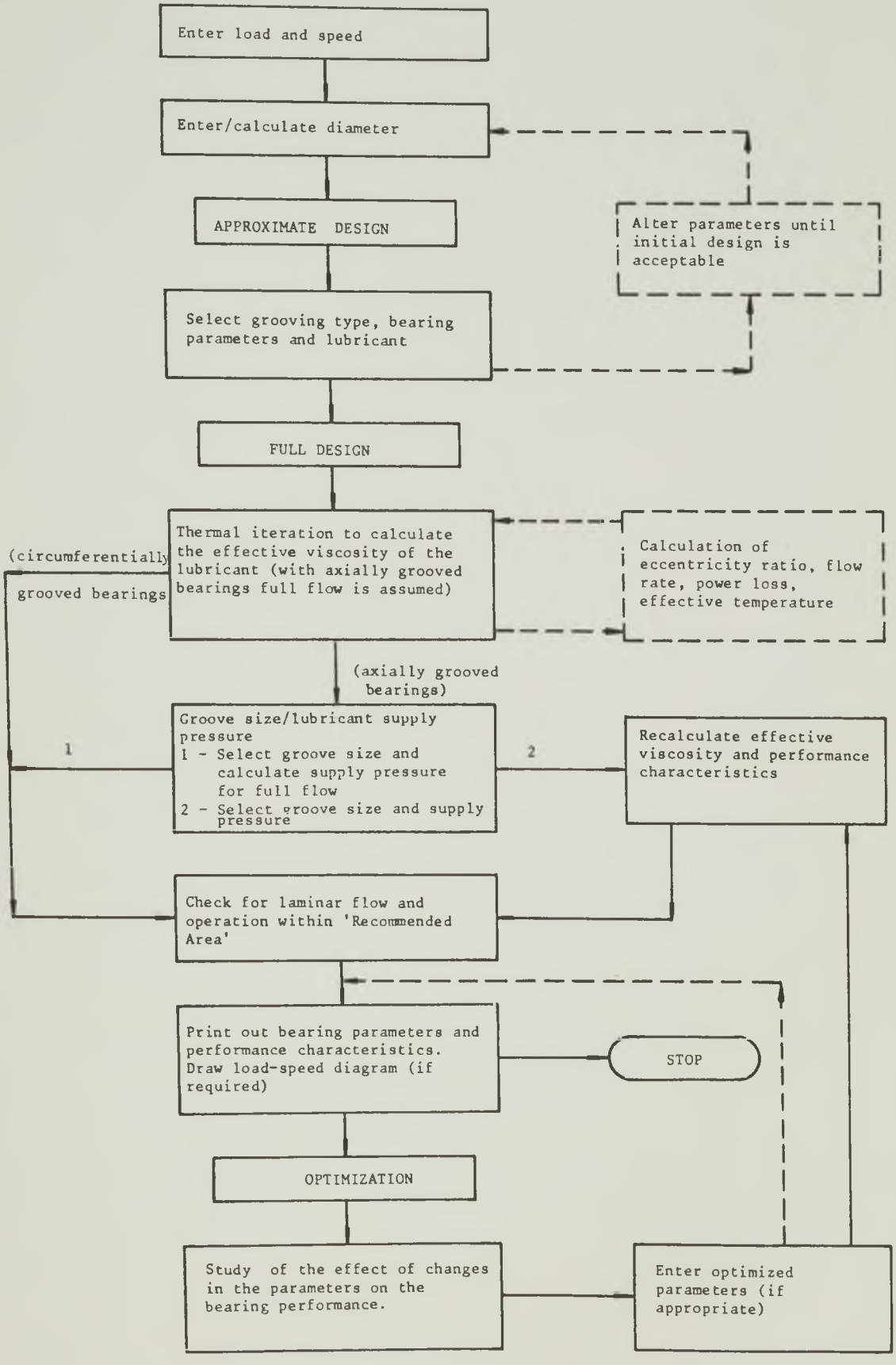

Figure 2.3 Simplified program flow chart

Load = 1000 N

Shaft speed = 1000 r.p.m. (16.66 Hz)

Diameter = 50 mm

Maximum bearing width = 80 mm

Angular misalignment = 0.1×10^{-3} mm/mm

Allowable maximum temperature = $100^{\circ}C$

Inlet oil temperature = $40^{\circ}C$

It is required to consider the possibility of using the SAE 30 engine oil, with the following characteristics:

Kinematic viscosity at $40^{\circ}C$ = 112.7 cSt (112.7×10^{-6} m^2/s)

Kinematic viscosity at $100^{\circ}C$ = 12.52 cSt (12.52×10^{-6} m^2/s)

Density at $40^{\circ}C$ = 875 Kg/m^3

```
     JOURNAL BEARING DESIGN PROGRAM - VERSION 1 -

   THIS IS A PROGRAM TO DESIGN STEADILY LOADED HYDRODYNAMIC
JOURNAL BEARINGS. THIS VERSION IS INTENDED TO BE USED WITH
A GRAPHICS TERMINAL (TEKTRONIX 4014), BUT IT WILL ALSO WORK
WITH A NON-GRAPHICS ONE IF THE USE OF DIAGRAMS IS AVOIDED

TYPE 1 OR 2 ACCORDING TO THE TYPE OF TERMINAL IN USE
1 - A SUITABLE GRAPHICS TERMINAL (TEKTRONIX 4014)
2 - A NON-GRAPHICS TERMINAL
1

                * * *  APPROXIMATE  DESIGN  * * *


ENTER SPEED OF THE SHAFT  (RPM)
1000

IS THE SHAFT/BEARING ARRANGEMENT SIMILAR TO THE FIGURE  (TYPE YES OR NO)
NO
ENTER LOAD (NEWTONS) ON THE BEARING
1000

 CHOICE OF GROOVING TYPE

1-AXIAL GROOVE-IF THE DIRECTION OF THE LOAD DOES NOT VARY WIDELY
2-CIRCUMFERENTIAL GROOVE-IF THAT DIRECTION VARIES BY MORE THAN 180 DEG.
(TYPE 1 OR 2 ACCORDING TO YOUR CHOICE)
1
HAS THE DIAMETER BEEN SPECIFIED  (YES OR NO)
(IF YOU SAY (NO), A STARTING VALUE WILL BE PROVIDED)
YES

ENTER DIAMETER (MM) IN THE RANGE 25-1000 MM
(OUTSIDE THIS RANGE THE VALUE CALCULATED FOR SAFE MINIMUM
FILM THICKNESS CANNOT BE RELIED UPON)
50

ENTER ANGULAR DEFLECTION OF THE SHAFT (MM/M) AT BEARING
LOCATION, DUE TO LOAD
 (IF NO INFORMATION AT ALL, TYPE 0.)
0.1
```

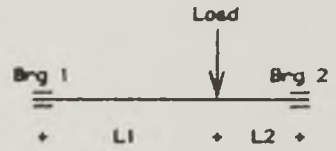

```
DURING THE ASSEMBLY OF THE BEARING SOME ANGULAR MISALIGNMENT
IS EXPECTED TO BE INTRODUCED. IF YOU CAN QUANTIFY IT ENTER
ITS VALUE IN  MM/M, OTHERWISE TYPE 0.
0


SAFE MINIMUM FILM THICKNESS (MM) = 0.0047


ENTER MAXIMUM ALLOWABLE TEMPERATURE IN THE BRG (DEG.C)
 (IF NO INFORMATION TYPE  110)
100
ENTER OIL INLET TEMPERATURE (DEG.C)
(IF NO INFORMATION TYPE  40)
40
WOULD YOU LIKE TO CONSIDER ANOTHER OIL ALONG WITH
THE ESDU 66023 STANDARD OILS 1,2,3 AND 4  (YES OR NO)
YES
ENTER KINEMATIC VISC. (CENTISTOKE) AT 40 DEG.C
112.7
ENTER KINEMATIC VISC. (CENTISTOKE) AT 100 DEG.C
12.52
ENTER OIL DENSITY (KG/M**3) AT A GIVEN TEMPERATURE (DEG.C)
(IF NO INFORMATION ENTER 850 KG/M**3 AT  40 DEG.C)

ENTER DENSITY  (KG/M**3)
875
ENTER TEMPERATURE  (DEG.C)
40
```

```
YOU MUST TAKE ONE OF THE FOLLOWING ALTERNATIVES


1 - EITHER YOU USE THE INITIAL DESIGN CHART, OR

2 - YOU GO DIRECTLY TO THE LOAD CAPACITY CHART. IN THIS
    CASE YOU HAVE TO ENTER VALUES FOR CD/D, B/D,
    OIL TYPE AND EFFECTIVE TEMPERATURE OF THE OIL

    TYPE 1 OR 2 ACCORDING TO YOUR CHOICE
    (YOU MUST TYPE 2 IF USING A NON-GRAPHICS TERMINAL)
1
```

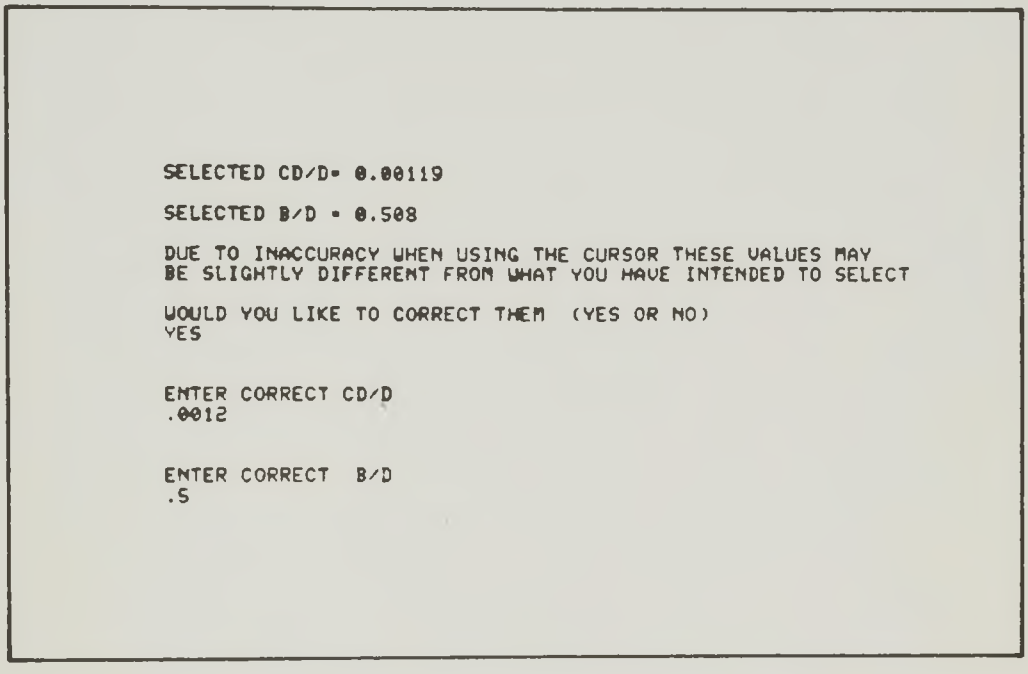
SELECTED CD/D= 0.00119
SELECTED B/D = 0.508
DUE TO INACCURACY WHEN USING THE CURSOR THESE VALUES MAY
BE SLIGHTLY DIFFERENT FROM WHAT YOU HAVE INTENDED TO SELECT
WOULD YOU LIKE TO CORRECT THEM (YES OR NO)
YES
ENTER CORRECT CD/D
.0012
ENTER CORRECT B/D
.5

CHECKING IF THE DESIGN SELECTED WILL OPERATE WITHIN
THE RECOMMENDED REGION

TAKE ONE OF THE FOLLOWING ALTERNATIVES

1 - THE USE OF A LOAD CAPACITY CHART ENABLING A
CHECK OF THE OPERATING POINT WITH RESPECT TO A
RECOMMENDED AREA OF OPERATION
2 - NO DIAGRAM AVAILABLE, THE CHECK BEING MADE BY
INTERNAL CALCULATIONS. GUIDANCE WILL BE GIVEN
FOR CRITICAL OPERATING CONDITIONS

TYPE 1 OR 2 ACCORDING TO YOUR CHOICE
(YOU MUST TYPE 2 IF USING A NON-GRAPHICS TERMINAL)
1

B/D = 0.50

CHECKING IF THE DESIGN FALLS INSIDE THE RECOMMENDED AREA

PROCEDURE TO BE FOLLOWED

1-MOVE HORIZONTAL CURSOR LINE TO SYMBOL +
2-MOVE VERTICAL LINE TO THE INTERSECTION OF THE B/D CURVE
WITH THE HORIZONTAL CURSOR LINE
3-PRESS KEY (E)

DO YOU CONSIDER IT ACCEPTABLE AT THIS STAGE (YES OR NO)
YES

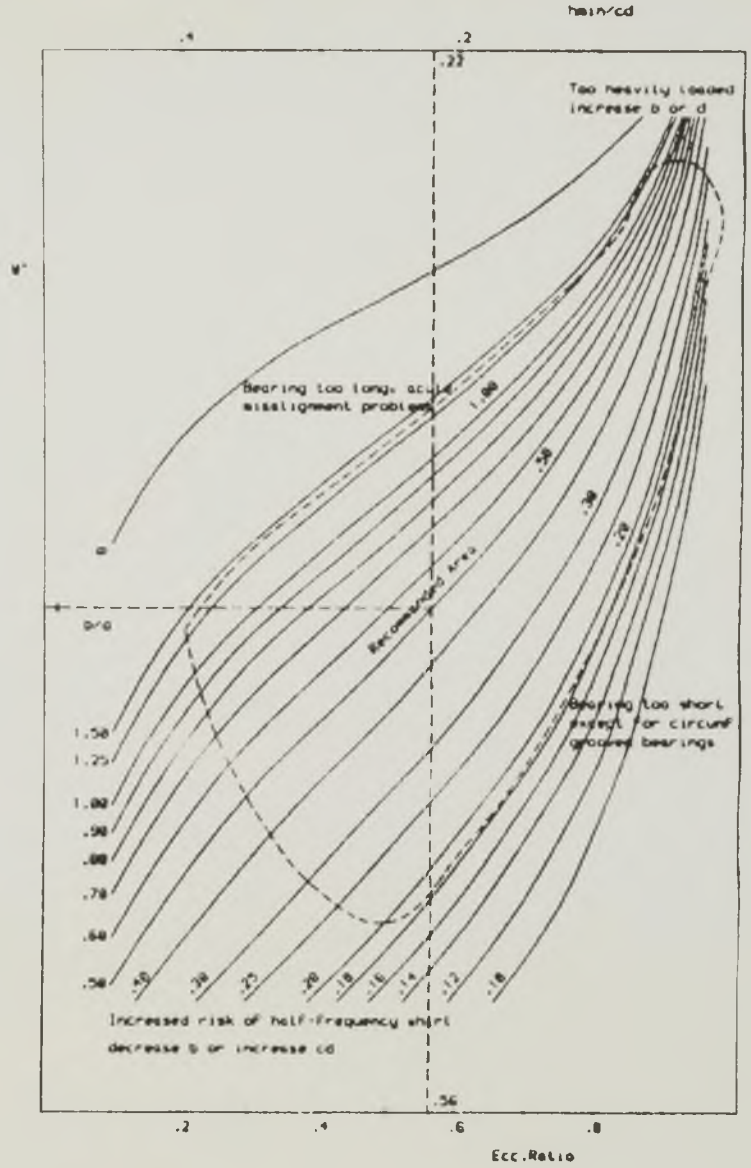

```
INITIAL APPROXIMATE DESIGN

  D      B/D     CD/D      ECC     TMAX     HMIN     HSAFE
(MM)                                (DEG.C)   (MM)     (MM)

  50.   0.50    0.0012    0.56     60.6    0.012    0.005

TO CONTINUE, PRESS <RETURN>
```

```
          *   *   *   FULL  DESIGN   *   *   *


ENTER (HEAT CAPACITY * DENSITY/10**6) FOR THE LUBRICANT (SI UNITS)
(IF NO INFORMATION, TYPE 1.7 FOR OILS, AND 4.2 FOR WATER)
1.7

ENTER THE PROPORTION K  OF HEAT GENERATED IN THE BEARING
TRANSFERRED TO THE LUBRICANT
(IT IS USUALLY SUFFICIENTLY ACCURATE TO TAKE K=0.8)
0.8

CHOICE OF GROOVE POSITION

1-SINGLE AXIAL GROOVE (OR HOLE) AT HMAX.- IT IS THE MOST
  FAVOURABLE LOCATION. BUT THE POSITION OF HMAX. VARIES WITH LOAD AND
  SPEED, SO IT IS ONLY WELL DEFINED FOR CONSTANT OPERATING CONDITIONS
2-SINGLE AXIAL GROOVE (OR HOLE) AT 90 DEG TO THE LOAD LINE -
  SUITABLE FOR SPLIT BEARINGS WITH CONSTANT DIRECTION OF ROTATION
3-TWO DIAMETRALLY OPPOSED AXIAL GROOVES (OR HOLES) AT 90 DEG TO THE
  LOAD LINE - CONVENIENT FOR MANUFACTURE AND ASSEMBLY. ALLOWS
  ROTATION IN EITHER DIRECTION

TYPE  1,2 OR 3 ACCORDING TO YOUR CHOICE
1
```

```
ITERATIVE PROCESS TO CALCULATE THE EFFECTIVE
VISCOSITY OF THE LUBRICANT ASSUMING FULL FLOW

EFF.VISCOSITY WHEN LAST ITERATION WAS STARTED = 0.0293 (N*S/M**2)

EFF.VISCOSITY OBTAINED FROM LAST ITERATION = 0.0294 (N*S/M**2)

NUMBER OF ITERATIONS PERFORMED =    9


DESIGN OF THE GROOVE
DETERMINATION OF THE LUBRICANT SUPPLY PRESSURE

TAKE ONE OF THE FOLLOWING ALTERNATIVES

1 - SELECT GROOVE SIZE AND CALCULATE THE LUBRICANT SUPPLY
    PRESSURE FOR FULL FLOW, OR

2 - SELECT GROOVE SIZE AND ENTER SUPPLY PRESSURE. (FLOW RATE
    POWER LOSS AND TEMPERATURES, WILL BE RECALCULATED)

TYPE 1 OR 2 ACCORDING TO YOUR CHOICE
2


SELECTION OF THE TYPE OF GROOVE


1-SQUARE ENDED AXIAL GROOVE (WIDELY USED)
2-ROUND ENDED AXIAL GROOVE
3-SINGLE HOLE

TYPE  1,2 OR 3 ACCORDING TO YOUR CHOICE
1

THE LENGTH OF THE GROOVE IS THE DIMENSION IN THE AXIAL
DIRECTION OF THE BEARING

ENTER GROOVE LENGTH-TO-BEARING WIDTH RATIO  (A/B)
IN THE RANGE  0.2-0.9
(IF NO EXPERIENCE TO SUGGEST OTHERWISE TYPE  0.8)
0.8

THE WIDTH OF THE GROOVE IS THE DIMENSION IN THE
CIRCUMFERENTIAL DIRECTION OF THE BEARING

ENTER GROOVE WIDTH-TO-BEARING DIAMETER RATIO  (W/D)
IN THE RANGE  0.1-0.3
0.15

ENTER LUBRICANT SUPPLY PRESSURE (KN/M**2)
(USUAL RANGE FOR SUPPLY PRESSURE, 50-350 KN/M**2)
100
```

```
CHECKING IF THE DESIGN SELECTED WILL OPERATE WITHIN
THE RECOMMENDED REGION


TAKE ONE OF THE FOLLOWING ALTERNATIVES

  1 - THE USE OF A LOAD CAPACITY CHART ENABLING A
      CHECK OF THE OPERATING POINT WITH RESPECT TO A
      RECOMMENDED AREA OF OPERATION
  2 - NO DIAGRAM AVAILABLE, THE CHECK BEING MADE BY
      INTERNAL CALCULATIONS. GUIDANCE WILL BE GIVEN
      FOR CRITICAL OPERATING CONDITIONS

TYPE 1 OR 2 ACCORDING TO YOUR CHOICE
(YOU MUST TYPE 2 IF USING A NON-GRAPHICS TERMINAL)
2


B/D = 0.50

ECCENTRICITY RATIO = 0.56

THE DESIGN IS INSIDE THE RECOMMENDED AREA

DO YOU CONSIDER IT ACCEPTABLE AT THIS STAGE (YES OR NO)
Y


CHECK FOR LAMINAR FLOW

REYNOLDS NUMBER =      2.362

THE FLOW IN THE BEARING IS LAMINAR

TO CONTINUE, PRESS <RETURN>
```

DESIGN PARAMETERS OF THE BEARING
****

BEARING DIAMETER (MM) = 50.0

BEARING WIDTH (MM) = 26.0

DIAMETRAL CLEARNCE (MM) = 0.060

LUBRICANT SUPPLY PRESSURE (KN/M**2) = 100.00

LUBRICANT CHARACTERISTICS :

KINEMATIC VISCOSITY (CENTISTOKE) AT 40 DEG.C = 51.76
KINEMATIC VISCOSITY (CENTISTOKE) AT 100 DEG.C = 6.84

SINGLE SQUARE ENDED AXIAL GROOVE AT HMAX.

LENGTH OF THE GROOVE (MM) = 20.0

WIDTH OF THE GROOVE (MM) = 7.5

PERFORMANCE CHARACTERISTICS
****

THE BEARING IS 27.6 % STARVED

ECCENTRICITY RATIO = 0.56

MINIMUM FILM THICKNESS AT THE EDGE (MM) = 0.0120

TOTAL POWER LOSS (WATTS) = 24.86

TOTAL FLOW RATE OF LUBRICANT (M**3/S) = 0.00000107

LUBRICANT OUTLET TEMPERATURE (DEG.C) = 50.9

MAXIMUM TEMPERATURE (DEG.C) = 67.8

ATTITUDE ANGLE (DEG) = 51.2

** SAFE MINIMUM FILM THICKNESS (MM) = 0.0047
(THE SAFETY FACTOR USED WAS 2)
IF ONLY LIMITED ATTENTION HAS BEEN PAID TO MISALIGNMENT
CONSIDERATIONS A LARGER SAFETY FACTOR MAY BE APPROPRIATE
(WITH A SAFETY FACTOR OF 3, HMIN.SAFE BASED ON THE
SURFACE ROUGHNESS CRITERION, IS 0.0070 MM)
** MAXIMUM ALLOWABLE TEMPERATURE (DEG.C) = 100.0
** ASSUMED OIL INLET TEMPERATURE (DEG.C) = 40.0

IS OPTIMIZATION REQUIRED (YES OR NO)
YES

DO YOU WISH TO LOOK AT THE LOAD-SPEED CHARACTERISTICS
OF THE BEARING DESIGNED (YES OR NO) YES

TYPE 1 OR 2 ACCORDING TO YOUR CHOICE

1 - SHOWN IN THE FORM OF A DIAGRAM
2 - IN A TABULAR FORM
(YOU MUST TYPE 2 IF USING A NON-GRAPHICS TERMINAL) 1

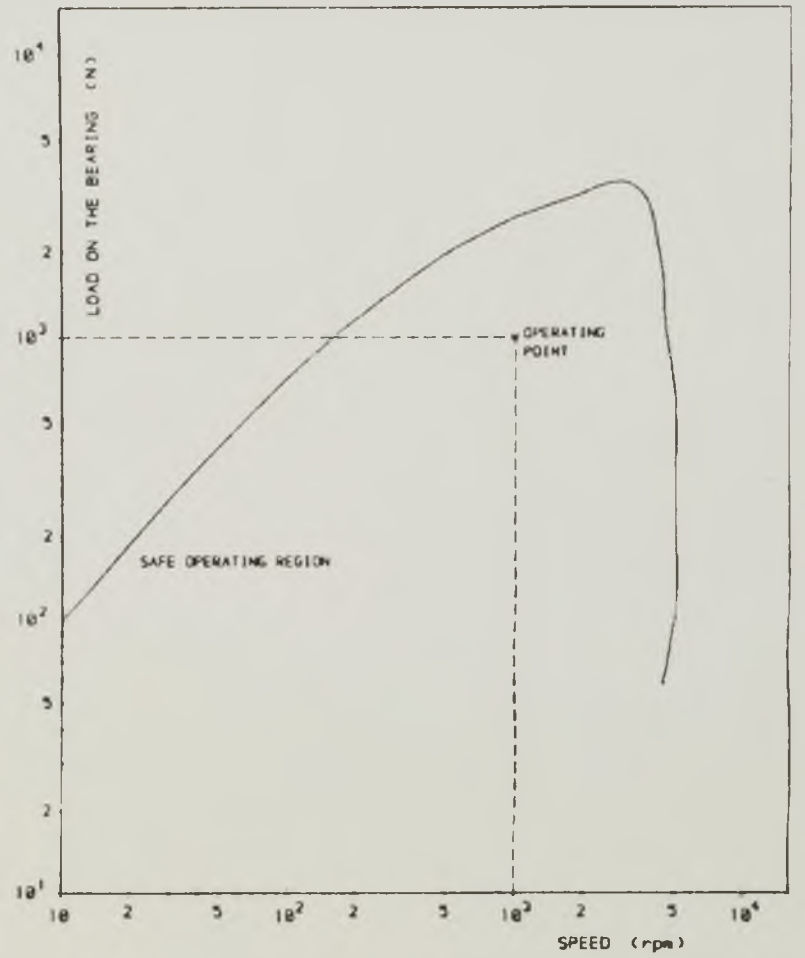

LOAD-SPEED DIAGRAM

OPTIMIZATION PROCESS

IF REQUIRED IT UILL BE POSSIBLE TO SEE THE EFFECT OF A CHANGE IN D, B, CD OR OIL TYPE UPON THE BEARING PERFORMANCE, FOR THE SPECIFIED LOAD AND SHAFT SPEED, AND SELECTED GROOVE SIZE AND OIL SUPPLY PRESSURE
IT UILL ALSO BE POSSIBLE TO CONSIDER COMBINED CHANGES OF THOSE PARAMETERS

UOULD YOU LIKE TO SEE THE EFFECT OF A CHANGE IN D (YES OR NO)
Y

ENTER FRACTIONAL CHANGE IN D TO EITHER SIDE
OF THE SELECTED VALUE. (EG. 0.1, 0.25, ETC.)
0.2

THE DIAGRAMS SHOW THE EFFECT ON THE BRG PERFORMANCE OF A CHANGE IN D ALONE

TO CONTINUE, PRESS <RETURN>

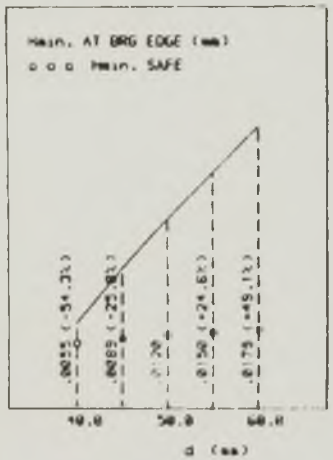

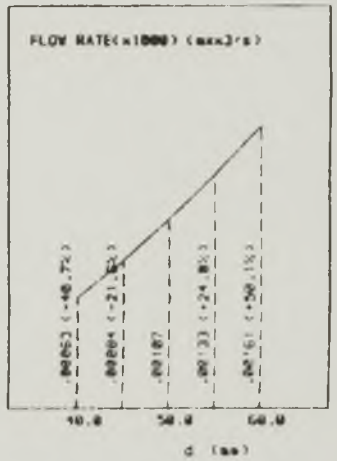

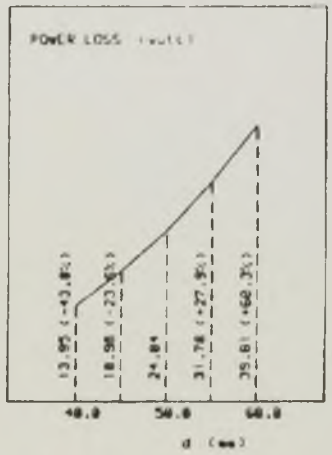

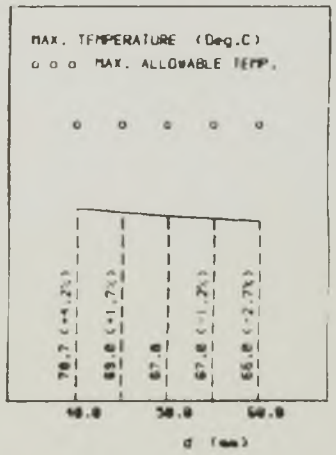

WOULD YOU LIKE TO SEE THE EFFECT OF A CHANGE IN B ON THE BRG PERFORMANCE (YES OR NO)
YES

ENTER FRACTIONAL CHANGE IN B/D TO EITHER SIDE OF THE SELECTED VALUE. (EG. 0.1, 0.25, ETC.)
0.2

THE DIAGRAMS SHOW THE EFFECT ON THE BRG PERFORMANCE OF A CHANGE IN B ALONE

TO CONTINUE, PRESS <RETURN>

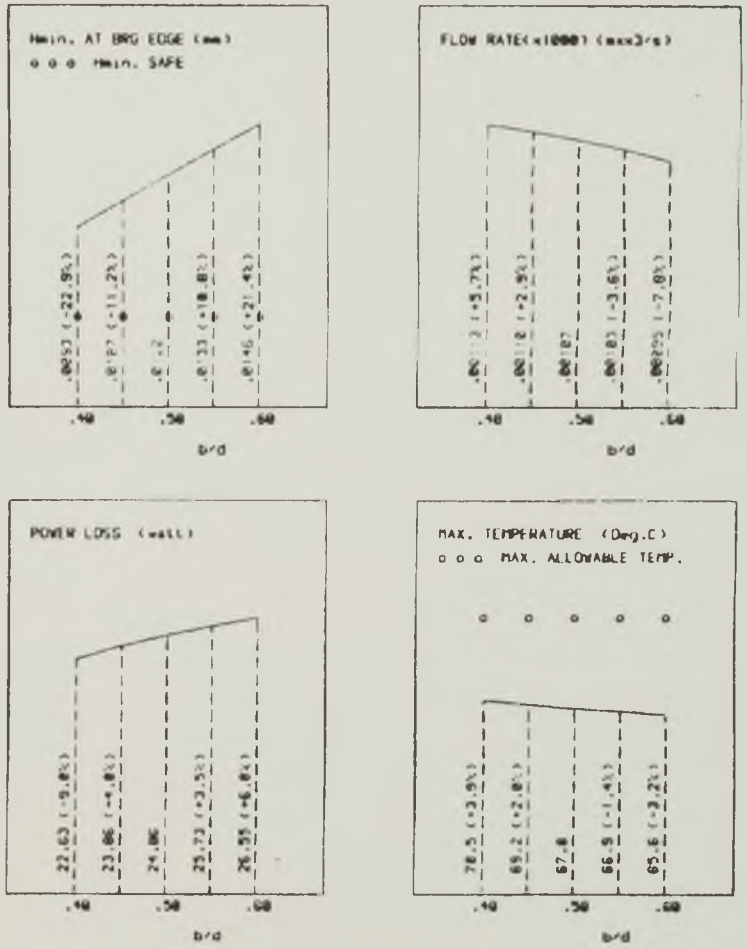

WOULD YOU LIKE TO SEE THE EFFECT OF A CHANGE
IN CD ON THE BRG PERFORMANCE (YES OR NO)
Y

ENTER FRACTIONAL CHANGE IN CD/D TO EITHER SIDE
OF THE SELECTED VALUE. (EG. 0.1, 0.25, ETC.)
0.3

THE DIAGRAMS SHOW THE EFFECT ON THE BRG PERFORMANCE OF A
CHANGE IN CD ALONE

TO CONTINUE, PRESS <RETURN>

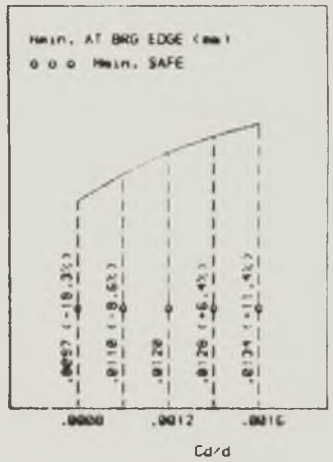

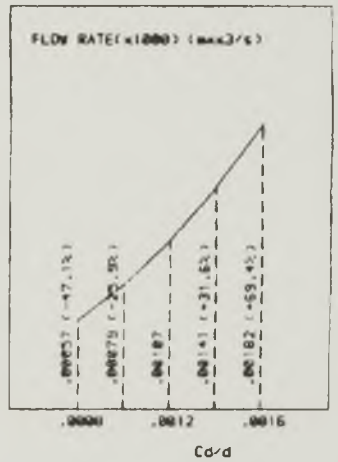

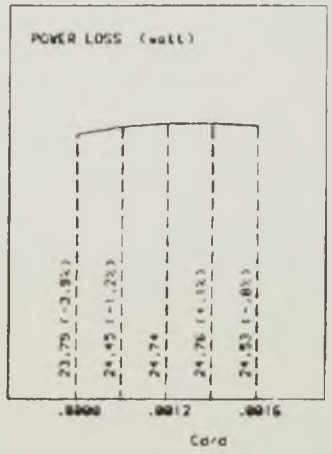

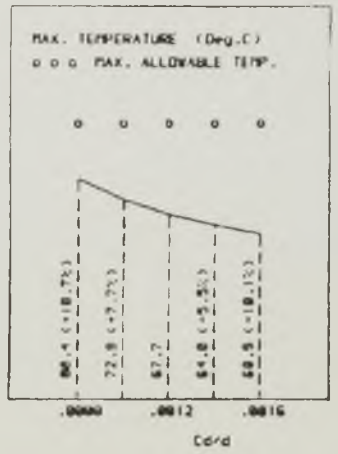

```
WOULD YOU LIKE TO CHANGE THE OIL AND SEE THE
EFFECT ON THE BRG PERFORMANCE  (YES OR NO)
Y

THE SELECTED OIL WAS OIL  2

ENTER INTEGER (1,2 OR 3) CORRESPONDING TO A THINNER OIL
THAN THE ONE SELECTED
IF THE SELECTED OIL WAS OIL 1, TYPE ALSO 1
1

ENTER INTEGER (2,3 OR 4) CORRESPONDING TO A THICKER OIL
THAN THE ONE SELECTED
IF THE SELECTED OIL WAS OIL 4, TYPE ALSO 4
3
```

THE DIAGRAMS SHOW THE EFFECT ON THE BRG PERFORMANCE OF A CHANGE IN OIL ALONE

TO CONTINUE, PRESS <RETURN>

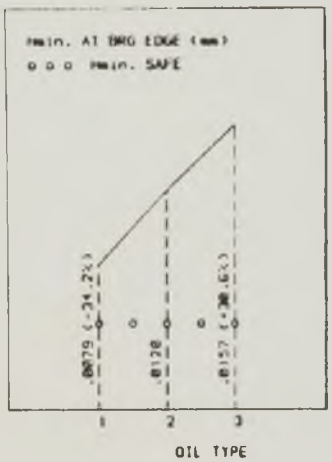

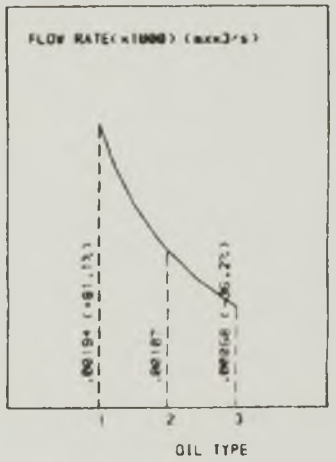

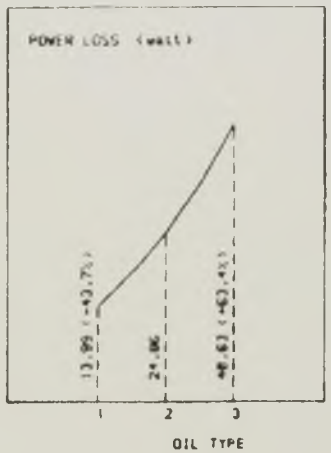

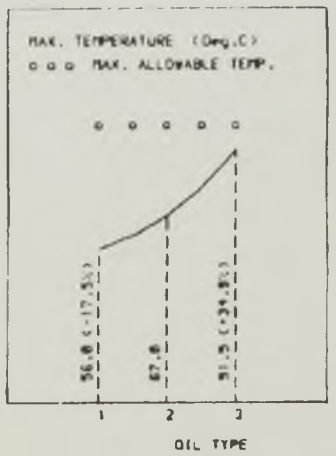

```
WOULD YOU LIKE TO SEE THE EFFECT OF COMBINED CHANGES
IN THE VALUES OF THE PARAMETERS, ON THE PERFORMANCE OF
THE BEARING  (YES OR NO)
Y
ENTER DIAMETER (MM)    (SELECTED D =   50.0)
50
ENTER B/D   (SELECTED B/D= 0.50)
0.5
ENTER CD/D   (SELECTED CD/D= 0.0012)
0.0012
ENTER INTEGER CORRESPONDING TO THE OIL
FOR A NON-STANDARD OIL, TYPE 5
(OIL  2  WAS THE ONE SELECTED)
2
-----------------------------------------------------------------
 D(MM)   B/D   CD/D   HMIN(MM)  Q(M**3/S)  H(WATT)  MAX.T(DEG.C)
   50.  0.50  0.0012   0.0120   0.0000011     24.8      67.8
OIL  2
THE BRG WILL BE  27.6% STARVED
MAX.ALLOWABLE TEMP.(DEG.C) = 100.0     HMIN.SAFE (MM) = 0.0047
-----------------------------------------------------------------

WOULD YOU LIKE TO TRY ANY OTHER COMBINATION OF
PARAMETERS  (YES OR NO)
WES
ENTER DIAMETER (MM)    (SELECTED D =   50.0)
50
ENTER B/D   (SELECTED B/D= 0.50)
0.5
ENTER CD/D   (SELECTED CD/D= 0.0012)
0.0015
ENTER INTEGER CORRESPONDING TO THE OIL
FOR A NON-STANDARD OIL, TYPE 5
(OIL  2  WAS THE ONE SELECTED)
2
-----------------------------------------------------------------
 D(MM)   B/D   CD/D   HMIN(MM)  Q(M**3/S)  H(WATT)  MAX.T(DEG.C)
   50.  0.50  0.0015   0.0132   0.0000017     24.6      61.8
OIL  2
THE BRG WILL BE  12.4% STARVED
MAX.ALLOWABLE TEMP.(DEG.C) = 100.0     HMIN.SAFE (MM) = 0.0047
-----------------------------------------------------------------

WOULD YOU LIKE TO TRY ANY OTHER COMBINATION OF
PARAMETERS  (YES OR NO)
Y
ENTER DIAMETER (MM)    (SELECTED D =   50.0)
50
ENTER B/D   (SELECTED B/D= 0.50)
0.5
ENTER CD/D   (SELECTED CD/D= 0.0012)
0.0015
ENTER INTEGER CORRESPONDING TO THE OIL
FOR A NON-STANDARD OIL, TYPE 5
(OIL  2  WAS THE ONE SELECTED)
5
-----------------------------------------------------------------
 D(MM)   B/D   CD/D   HMIN(MM)  Q(M**3/S)  H(WATT)  MAX.T(DEG.C)
   50.  0.50  0.0015   0.0166   0.0000012     35.6      72.7
NON-STANDARD OIL
THE BRG WILL BE  35.5% STARVED
MAX.ALLOWABLE TEMP.(DEG.C) = 100.0     HMIN.SAFE (MM) = 0.0047
-----------------------------------------------------------------

WOULD YOU LIKE TO TRY ANY OTHER COMBINATION OF
PARAMETERS  (YES OR NO)
YES
ENTER DIAMETER (MM)    (SELECTED D =   50.0)
50
ENTER B/D   (SELECTED B/D= 0.50)
0.5
ENTER CD/D   (SELECTED CD/D= 0.0012)
0.0012
ENTER INTEGER CORRESPONDING TO THE OIL
FOR A NON-STANDARD OIL, TYPE 5
(OIL  2  WAS THE ONE SELECTED)
1
-----------------------------------------------------------------
 D(MM)   B/D   CD/D   HMIN(MM)  Q(M**3/S)  H(WATT)  MAX.T(DEG.C)
   50.  0.50  0.0012   0.0079   0.0000019     14.0      56.0
OIL  1
MAX.ALLOWABLE TEMP.(DEG.C) = 100.0     HMIN.SAFE (MM) = 0.0047
-----------------------------------------------------------------

WOULD YOU LIKE TO TRY ANY OTHER COMBINATION OF
PARAMETERS  (YES OR NO)
NO

DO YOU WANT TO MAKE ANY CHANGES IN THE SELECTED
VALUES OF THE BRG PARAMETERS  (YES OR NO)

(YES-PERFORMANCE CHARACTERISTICS WILL BE RECALCULATED FOR
     THE NEW VALUES OF THE PARAMETERS

  NO-IT IS ASSUMED THAT THE PERFORMANCE CHARACTERISTICS ARE
     ACCEPTABLE. THE VALUES WILL BE LISTED TO THE TERMINAL)
YES

TAKE A NOTE OF D, B/D, CD/D, AND OIL TYPE
TO BE ADOPTED

TO CONTINUE, PRESS <RETURN>
```

```
DESIGN OF THE OPTIMIZED BEARING

ENTER DIAMETER (MM)   (IN THE RANGE 25-1000 MM)
50

ENTER B/D
0.5

ENTER CD/D
0.0012

ENTER INTEGER REPRESENTING THE OIL SELECTED
IF IT IS A NON-STANDARD OIL, TYPE 5
:
```

```
CHECKING IF THE DESIGN SELECTED WILL OPERATE WITHIN
THE RECOMMENDED REGION

TAKE ONE OF THE FOLLOWING ALTERNATIVES

  1 - THE USE OF A LOAD CAPACITY CHART ENABLING A
      CHECK OF THE OPERATING POINT WITH RESPECT TO A
      RECOMMENDED AREA OF OPERATION
  2 - NO DIAGRAM AVAILABLE, THE CHECK BEING MADE BY
      INTERNAL CALCULATIONS. GUIDANCE WILL BE GIVEN
      FOR CRITICAL OPERATING CONDITIONS

TYPE 1 OR 2 ACCORDING TO YOUR CHOICE
(YOU MUST TYPE 2 IF USING A NON-GRAPHICS TERMINAL)
2


B/D = 0.50

ECCENTRICITY RATIO = 0.69

THE DESIGN IS INSIDE THE RECOMMENDED AREA

DO YOU CONSIDER IT ACCEPTABLE AT THIS STAGE (YES OR NO)
Y


CHECK FOR LAMINAR FLOW

REYNOLDS NUMBER =      7.345

THE FLOW IN THE BEARING IS LAMINAR

TO CONTINUE, PRESS <RETURN>
```

DESIGN PARAMETERS OF THE BEARING
****

BEARING DIAMETER (MM) = 50.0

BEARING WIDTH (MM) = 25.0

DIAMETRAL CLEARNCE (MM) = 0.060

LUBRICANT SUPPLY PRESSURE (KN/M**2) = 100.00

LUBRICANT CHARACTERISTICS :

KINEMATIC VISCOSITY (CENTISTOKE) AT 40 DEG.C = 18.12
KINEMATIC VISCOSITY (CENTISTOKE) AT 100 DEG.C = 3.53

SINGLE SQUARE ENDED AXIAL GROOVE AT HMAX.

LENGTH OF THE GROOVE (MM) = 20.0

WIDTH OF THE GROOVE (MM) = 7.5

PERFORMANCE CHARACTERISTICS
****

ECCENTRICITY RATIO = 0.69

MINIMUM FILM THICKNESS AT THE EDGE (MM) = 0.0079

TOTAL POWER LOSS (WATTS) = 13.98

TOTAL FLOW RATE OF LUBRICANT (M**3/S) = 0.00000194

LUBRICANT OUTLET TEMPERATURE (DEG.C) = 43.4

MAXIMUM TEMPERATURE (DEG.C) = 56.0

ATTITUDE ANGLE (DEG) = 41.4

** SAFE MINIMUM FILM THICKNESS (MM) = 0.0047
(THE SAFETY FACTOR USED WAS 2)
IF ONLY LIMITED ATTENTION HAS BEEN PAID TO MISALIGNMENT
CONSIDERATIONS A LARGER SAFETY FACTOR MAY BE APPROPRIATE
(WITH A SAFETY FACTOR OF 3, HMIN.SAFE BASED ON THE
SURFACE ROUGHNESS CRITERION, IS 0.0070 MM)
** MAXIMUM ALLOWABLE TEMPERATURE (DEG.C) = 100.0
** ASSUMED OIL INLET TEMPERATURE (DEG.C) = 40.0

FORTRAN STOP
$

DO YOU WISH TO LOOK AT THE LOAD-SPEED CHARACTERISTICS
OF THE BEARING DESIGNED (YES OR NO) YES

TYPE 1 OR 2 ACCORDING TO YOUR CHOICE

1 - SHOWN IN THE FORM OF A DIAGRAM
2 - IN A TABULAR FORM
(YOU MUST TYPE 2 IF USING A NON-GRAPHICS TERMINAL) 1

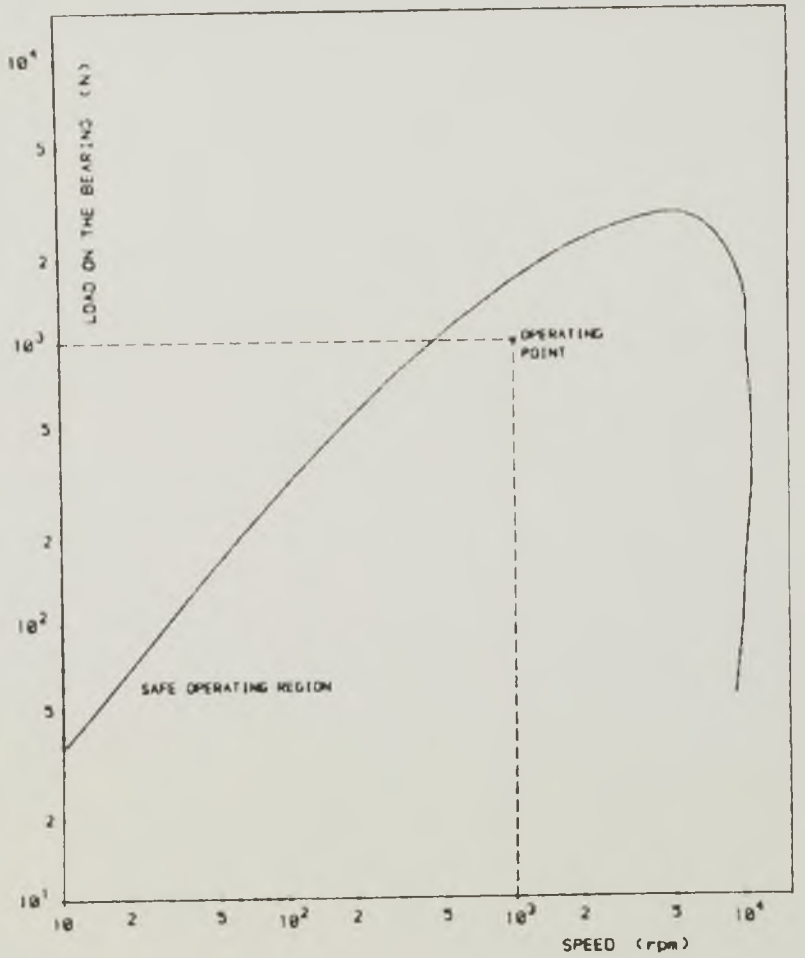

LOAD-SPEED DIAGRAM

2.4 Conclusions

An interactive computer program for the design of steadily loaded, liquid film, hydrodynamic journal bearings has been developed. The program procedure followed very closely that of ESDU Item No. 66023 (1966).

Two versions of the program were developed:

(1) The first version included two options

   a) A graphics option which employed some charts of ESDU Item No. 66023 (1966) and was able to generate diagrams for the study of the bearing performance at variable operating conditions,

   b) A non-graphics option in which graphical interaction was substituted by internal calculations from data in tabular form.

(2) The other version did not use any computer graphics. The procedure followed in this version of the program was similar to that of the graphics version running under the non-graphics option using, however, less computer memory space.

In the design of axially grooved bearings a major change in philosophy, with respect to that of ESDU Item No. 66023 (1966), concerning the design of the groove and the calculation of the lubricant supply pressure, was adopted. The computer program provided two alternatives:

(a) Selection of the size of the groove and calculation of the lubricant supply pressure for full flow

(b) Selection of both the groove size and the lubricant supply pressure without reference to fully flooded conditions.

CHAPTER 3

THE ANALYSIS OF FLUID FILM, FINITE, JOURNAL BEARINGS CONSIDERING FILM REFORMATION

3.1 Introduction

The Reynolds' equation, governing the distribution of pressure within the film of lubricant in a bearing, has no exact analytical solution for finite width journal bearings. Approximate solutions may, however, be obtained by the application of numerical methods to the solution of the Reynolds' equation resulting from the use of either finite difference or finite element techniques over the discretized film region.

The importance of the correct determination of the extent of the film in the bearing to which the Reynolds' equation is applicable, has been pointed out in Chapter 1. The film extent is accounted for in the equations by specifying the boundary conditions at the beginning and at the end of the fluid film, usually called the reformation and the rupture boundary conditions.

Various physical models have been proposed for rupture and reformation of the lubricant film in journal bearings. A summary of the work carried out in this field has been presented by Dowson and Taylor (1979).

A widely accepted film rupture condition is the Reynolds', or Swift-Steiber, boundary condition which assumes that pressure and

pressure gradients both take zero values when rupture occurs, a condition derived from flow continuity considerations across the rupture interface. The film is usually assumed to start at the position of maximum clearance where the build up of pressure begins, a condition that does not necessarily satisfy flow continuity and does not take into account the lubricant inlet conditions in real bearings. Cameron and Wood (1949) have used these boundary conditions in the analysis of finite width journal bearings with no oil grooves. A finite difference representation and relaxation techniques were used to solve the approximate Reynolds' equation.

In realistic journal bearings the lubricant is usually fed to the bearing through one or two axial grooves (or holes) at a supply pressure greater than the ambient. Cole and Hughes (1956), having noted that the measured friction torque was lower than that calculated on the assumption of a complete film, carried out visual studies of film extent and oil flow in journal bearings using transparent bushes of various sizes, clearance ratios and oil inlet arrangements. Photographs of the inlet region clearly showed that the geometry of the groove and the supply pressure significantly affected the film extent. The flow rate was also affected; the theoretical predictions of Cameron and Wood (1949) were at least three times greater than the experimental values for the operating conditions investigated by Cole and Hughes (1956).

Clearly, the condition of zero pressure at the maximum clearance where the build up of pressures was assumed to start, could not accommodate realistic lubricant supply arrangements. A boundary condition accounting for the groove geometry and the lubricant supply pressure would appear necessary. Jakobsson and Floberg (1957) derived both the rupture and the reformation boundary conditions from flow continuity considerations.

A balance of the lubricant flow rates entering and leaving a control volume on the boundaries, led to zero pressure gradients at the rupture boundary and to the establishment of a reformation boundary condition relating the local film thickness and pressure gradients to the film thickness at rupture. Their method of solution of the approximate finite difference form of Reynolds' equation using a relaxation technique, and for the rupture and reformation boundary conditions derived, was outlined.

The Jakobsson and Floberg (1957) reformation boundary condition, although generally accepted as being adequate to model the film inlet conditions was, however, difficult to incorporate into an analysis and only with the development of high speed, large storage, digital computers in more recent times, has it become possible.

The first successful attempt to locate automatically the reformation boundary in journal bearings with realistic supply conditions seems to have been the work of McCallion et al (1971). Finite difference approximations and a Gauss-Seidel iterative solution technique were used to solve the Reynolds' equation. The presence of the groove and the lubricant supply pressure were accounted for by keeping the pressure at every node over the groove at a constant value, corresponding to the dimensionless supply pressure. The method of solution was as follows:

(a) The Reynolds' equation was first solved for $\bar{p} = \frac{\partial \bar{p}}{\partial \bar{x}} = 0$ at the rupture and the reformation boundaries, and a first estimate of the extent of the cavitation region was obtained.

(b) Each circumferential mesh line was examined to detect the mesh point where a condition derived from the Jakobsson and Floberg

(1957) reformation boundary condition was satisfied. A new location of the reformation boundary was then found.

(c) All pressures in the new cavitation region were set to zero and the Reynolds' equation was solved for the new region. The procedure was repeated from (b) until the newly determined boundaries did not differ from the previous ones.

An adequate mesh size was found by comparing the location of the reformation boundary obtained using a given mesh size with that obtained when the number of mesh lines in the circumferential direction was doubled. Good correlation was reported between the solutions for flow for a single axial groove and an oil hole at the load line, and the experimental results of Clayton (1946).

Etsion and Pinkus (1974) showed in their analysis of 'short' journal bearings that an incomplete film of lubricant at the inlet has a drastic effect on the lubricant flow rate. In Etsion and Pinkus (1975), their theory was extended to the analysis of finite journal bearings with incomplete films. Solutions were presented for different groove geometries but they appeared to be applicable only to zero supply pressure conditions. The Reynolds rupture boundary condition was adopted and the lubricant inlet conditions were expressed in terms of the width of the incomplete film at an angular location (α) downstream from the groove. A flow balance in the incomplete film region allowed the local film width (ℓ) to be expressed as a function of the pressure gradients, the axial dimension of the groove and the film thickness (equation (4) of the paper). This equation for the width of the incomplete film as a function of the angular location was solved simultaneously with the Reynolds' equation using finite difference approximations and an iterative solution

procedure. A first approximation for the width of the film was assumed, giving an initial shape for the reformation boundary. The Reynolds' equation was then solved with the condition of zero pressure along the reformation line. The new values for film thickness and pressure gradients obtained from the current solution were introduced into the equation derived from flow continuity considerations (equation (4) of the paper), resulting in a new approximation for the width of the incomplete film. The process was terminated when convergence in film width and pressure distribution was achieved.

The equation expressing flow continuity in the incomplete film region (Etsion and Pinkus (1975), equation (2)) appears to be imprecise in its consideration of the recirculating flow over the groove, which is included in two of the terms. Such flow was already included in the first term of the right hand side of the equation and therefore should not have been included in the second term. The Etsion and Pinkus (1975) flow continuity condition is shown on Figure 3.1. This implied, for example, that the width of the continuous film at the location of the groove for a 'short' bearing, was bigger than the groove length ($\ell > L_o$). If as a limiting case the groove extended for the full width of the bearing (L), then the fact that $\ell > L$ as predicted by the model used, could probably be interpreted as meaning that some side flow had occurred in a region where the axial pressure gradient should be zero. The influence of the model adopted by Etsion and Pinkus (1974, 1975) on the prediction of flow rates is discussed further in Section 3.5.8.

McCallion et al (1971) and Etsion and Pinkus (1974, 1975) incorporated in their solution scheme a zero pressure condition at the reformation boundary, and the calculated pressure gradients at the boundary were checked for flow continuity conditions before a new iteration was started. Hargreaves (1981), in his studies of film formation and lubricant

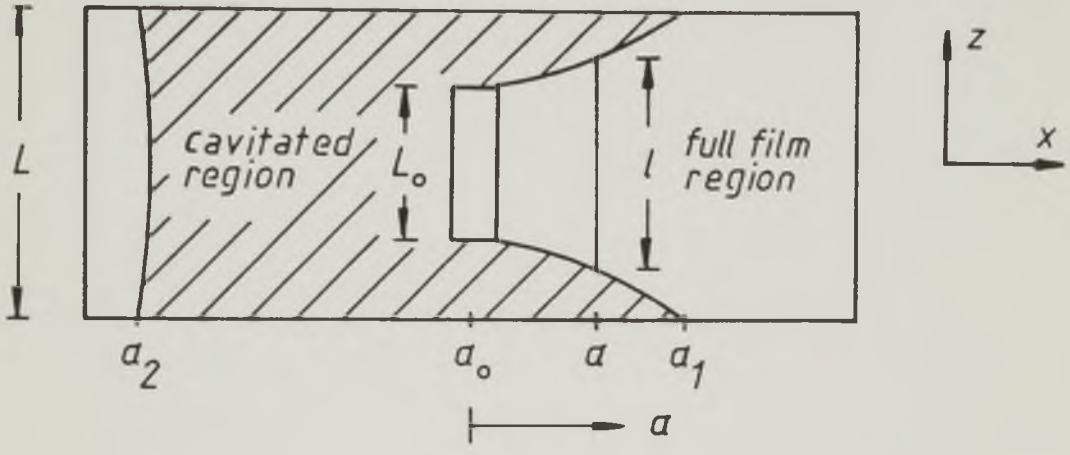

$$\int_0^{\ell/2} q_x \, dz = \int_0^{L_o/2} (q_x)_o \, dz + \int_0^{\ell/2} (q_x)_2 \, dz$$

where (q_x) is the flow per unit width.

Figure 3.1 The Etsion and Pinkus (1975) flow continuity condition in the incomplete film region ($\alpha_o \leq \alpha \leq \alpha_1$)

flow rate in thrust bearings, adopted a different approach; the pressure gradient boundary condition was incorporated into the equation to be solved at the current reformation boundary location and a check for constant cavitation pressure along the boundary was carried out after the solution for the pressure had been obtained. The relocation of the boundary was made at every mesh line by simple interpolation or extrapolation between the point on the boundary and the node just inside the boundary.

Ruddy (1979) carried out a numerical analysis of circumferentially grooved bearings as part of a more extensive programme of work concerning both static and a dynamic analyses of various fluid film journal bearing types. Using the Reynolds boundary conditions at film rupture and the condition of zero pressure at the film reformation, a cavitation region was obtained by setting all negative nodal pressures in each iteration cycle to zero. The calculated flow rates into and out of the bearing were found to be different and this lack of flow continuity in the axial direction was attributed to an incorrect reformation boundary condition. The Jakobsson and Floberg (1957) reformation boundary condition was then incorporated. The computer solution technique was as follows. An initial estimate of the cavitation zone was obtained putting all negative pressures equal to zero in each cycle. The pressure gradient at a number of nodes on the current reformation boundary was calculated and compared with the pressure gradient required to satisfy continuity. This provided a criterion for moving the reformation boundary to start the next iteration. After each iteration the axial flow rates into and out of the bearing were calculated and compared. The solution was taken to have converged when the two axial flow rates had converged to within a given tolerance.

The programming complexities arising from film reformation considerations, requiring the location of the reformation boundary and the determination of pressure gradients at the interface, were completely eliminated in a new approach to the problem of locating cavities initially proposed by Elrod and Adams (1974) and later refined by Elrod (1981), which was seen as an important step forward in the analysis of liquid lubricated bearings. Elrod (1981) presented a computational algorithm which allowed the automatic delimitation of the cavitation region without explicit reference to boundary conditions, and was valid for both steady and transient operating conditions. A 'universal' differential equation was employed throughout the whole lubricating region. This equation incorporated a 'cavitation index' (g) which, by taking the value zero (in the cavitation region) or unity (in the full film region), allowed the equation to change its form. In the full film region the equation was elliptic and was basically the Reynolds' equation. In the cavitation zone the equation became parabolic in form. Mass flow continuity was achieved in the cavitation region as well as in the rupture and the reformation boundaries, and the Reynolds' rupture boundary condition and the Jakobsson and Floberg reformation boundary condition were automatically imposed.

To test the algorithm, the analysis of various bearing types was carried out by Elrod (1981). Good agreement was reported between the predictions of these analyses and exact solutions or experimental data provided by other workers.

Lebeck (1981) employed the Elrod cavitation algorithm in the analysis of mechanical face seals and reported good correlation with previous results and a significant decrease in computation time in

comparison with traditional techniques.

Finite difference approximations to the governing Reynolds' equation have been widely used in the study of the performance of hydrodynamic bearings. In recent years, however, finite element methods have also enjoyed the interest of lubrication researchers. Finite elementry may have an advantage over finite difference methods in the facility with which curved boundaries and complicated boundary conditions can be accommodated.

Milne (1974) presented a technique for calculating oil flow in bearings based upon computation of a stream function using the finite element method. The technique was applied to the case of a plane slider bearing to which the effect of the shape of the elements on the computation time and on the accuracy of the solutions was studied.

Hayashi and Taylor (1980) used a finite element approximation technique and the Newton-Raphson iterative solution method in the analysis of liquid film journal bearings. The predictions of the analysis for the location of the rupture boundary and the bearing performance were in good agreement with results obtained from a finite difference analysis and exact analytical solutions. Two advantages of using the finite element approach were mentioned:

(i) the ability to locate precisely curved boundaries
(ii) the ability to apply with ease flow boundary conditions

Film reformation was not considered but it was pointed out that the same approach would be equally successful for the more complex reformation boundary conditions.

The apparent simplicty and ability to incorporate realistic lubricant supply conditions exhibited by the Elrod cavitation algorithm

and the convincing results reported by Elrod (1981) and Lebeck (1981), seemed to make the algorithm attractive to the purposes of the present work.

The remainder of this chapter will be devoted to a discussion of the technique developed for the analysis of finite width journal bearings considering the lubricant supply conditions, which was based on Elrod's algorithm. A careful study of the effect of influential parameters on the computation time required for convergence of the solution and on the accuracy of the predictions, will be described.

3.2 Elrod's Cavitation Algorithm

In oil film bearing analysis, the oil is usually assumed to be incompressible. However, although mineral oils have low compressibility, their density does increase with increasing pressure. The compressibility is dependent on temperature and pressure, in general increasing with increasing temperature and decreasing with increasing pressure.

3.2.1 The Bulk Modulus of the Lubricant

The inverse of the compressibility is called the 'bulk modulus'. Peeler and Green (1959) defined the mean bulk modulus of a fluid (β) as,

$$\beta = V_o \left[\frac{p-p_o}{V_o-V}\right] \qquad (3.1)$$

where, (V) is the volume at the pressure (p)

(V_o) is the volume at the reference pressure (p_o), usually atmospheric

Galvin et al (1964) measured the percentage change in the volume of various mineral oils that occurred with a known pressure variation and at constant temperature (of 20^o and 100^oC). From their results the bulk modulus of lubricating oils was found to be in the range 10^7 - 10^8 N/m^2.

3.2.2 Elrod's Variable (θ)

Exploring the dependence of the lubricant density on pressure, Elrod (1981) expressed the pressure in the full film region of the bearing as

$$p = p_c + \beta (\theta - 1) \tag{3.2}$$

where (p_c) is the cavitation pressure and

$\theta = \frac{\rho}{\rho_c}$, is the ratio of the lubricant densities at the pressures (p) and (p_c) respectively. In the full film region, where $p \geq p_c$, $\theta \geq 1$.

In the cavitation region the pressure (p_c) was assumed to be constant and it was taken as zero in the present analysis. There was thus no flow of lubricant in the axial direction in this region and the Poiseuille component of the circumferential flow was zero. Due to changes in film thickness, the lubricant film breaks down and does not completely fill the clearance space. The Elrod variable (θ), when referring to the cavitation region, had a different meaning; it was defined as the fraction of the bearing width occupied by the lubricant.

3.2.3 The Cavitation Index (g)

A cavitation index (g) was defined from a knowledge of (θ) as follows:

$$g = 0 \quad \text{where } \theta < 1 \quad \text{(cavitation zone)} \tag{3.3}$$

$$g = 1 \quad \text{where } \theta \geq 1 \quad \text{(non cavitation zone)}$$

It will be seen in the next section that the introduction of (g) in the equations had the purpose of changing their form and thus making

them appropriate to the relevant film region.

3.2.4 The Cavitation Algorithm

Figure 3.2 represents the finite difference star and the computational cell (of dimensions (Δx), (Δy) and (h)) used by Elrod. The shaft surface speed (U_1) and the bush surface speed (U_2) were assumed to be greater than or equal to zero.

The following algorithm was proposed by Elrod (1981) for the convective (Couette) and pressure (Poiseuille) flow contributions to the mass flow entering the cell in the x-direction (the subscripts refer to points in the finite difference star).

(1) Convective mass flow per unit width of the bearing

$$(\dot{m}_x)_c = \frac{\rho_c (U_1+U_2)}{2} \left[\theta_{-1} h_{-1}(1-g_{-1})+g_{-1} h_{-1} + \frac{g_{-1} g_o}{2} (h_o - h_{-1})\right] \qquad (3.4)$$

When both nodes (-1,0) were in the full film region the film thickness at the cell wall was averaged. Otherwise it was taken as the film thickness at the upstream point (point -1)

(2) Pressure mass flow per unit width

$$(\dot{m}_x)_p = \left[\frac{h^3}{12\eta}\right]_{av} \beta\rho_c \left[\frac{g_{-1}(\theta_{-1}-1)-g_o (\theta_o-1)}{\Delta x}\right] \qquad (3.5)$$

which takes the usual form in the complete film region, is zero in the cavitation region and is interpolated at the rupture and reformation interfaces.

3.3 The Final Finite Difference Equation

The total mass flow per unit width entering the cell in the x-direction was given by the sum of expressions (3.4) and (3.5). Similar expressions could be obtained for the mass flow per unit width leaving the cell in the x-direction and for the mass flow in y-direction.

The finite difference equation having (θ) as the dependent variable was obtained from mass conservation considerations within the cell. For steady state operating conditions the mass of lubricant in the cell should not change. Thus,

$$(\Delta y)\ \dot{\Delta m}_x + (\Delta x)\ \dot{\Delta m}_y = 0 \qquad (3.6)$$

where ($\dot{\Delta m}_x$) and ($\dot{\Delta m}_y$) are the net mass flows per unit width entering the cell in the (x) and (y) directions.

The lubricant film was discretized by dividing the bearing area into a number of small areas defined by perpendicular mesh lines in the circumferential (x) and the axial (y) directions. Points in the grid were identified by the subscripts (i,j) corresponding to the intersection of the circumferential mesh line (i) with the axial mesh line (j). Figure 3.3 shows the computational cell, containing the grid point (i,j), surrounded by unequally spaced mesh lines.

Equations (3.4) and (3.5) were applied to the four walls of the cell and introduced into equation (3.6), thus allowing the derivation of an equation for ($\theta_{i,j}$). The bearing was assumed to be well aligned (film thickness not dependent on axial location).

The following dimensionless parameters were introduced at this stage

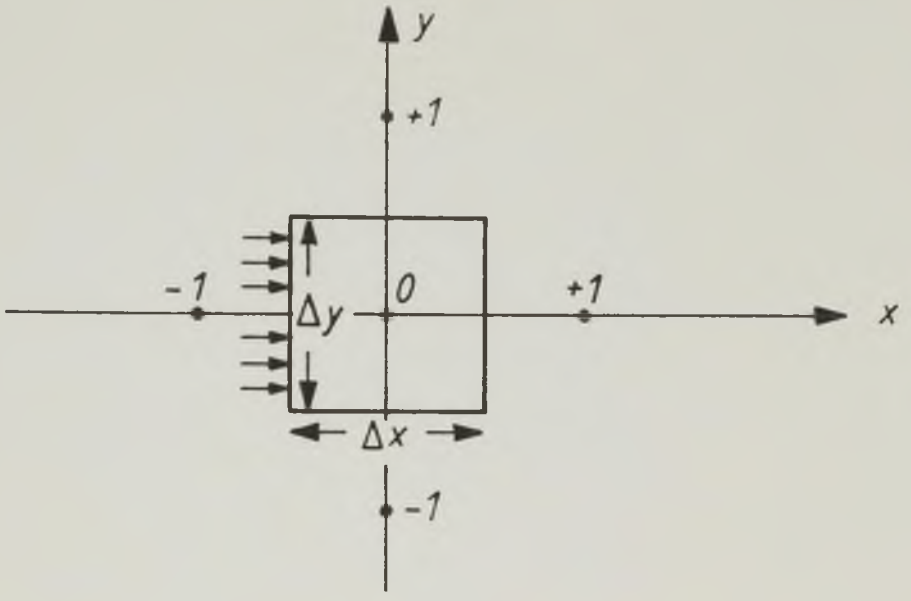

Figure 3.2 The finite difference star and the computational cell containing the central point.

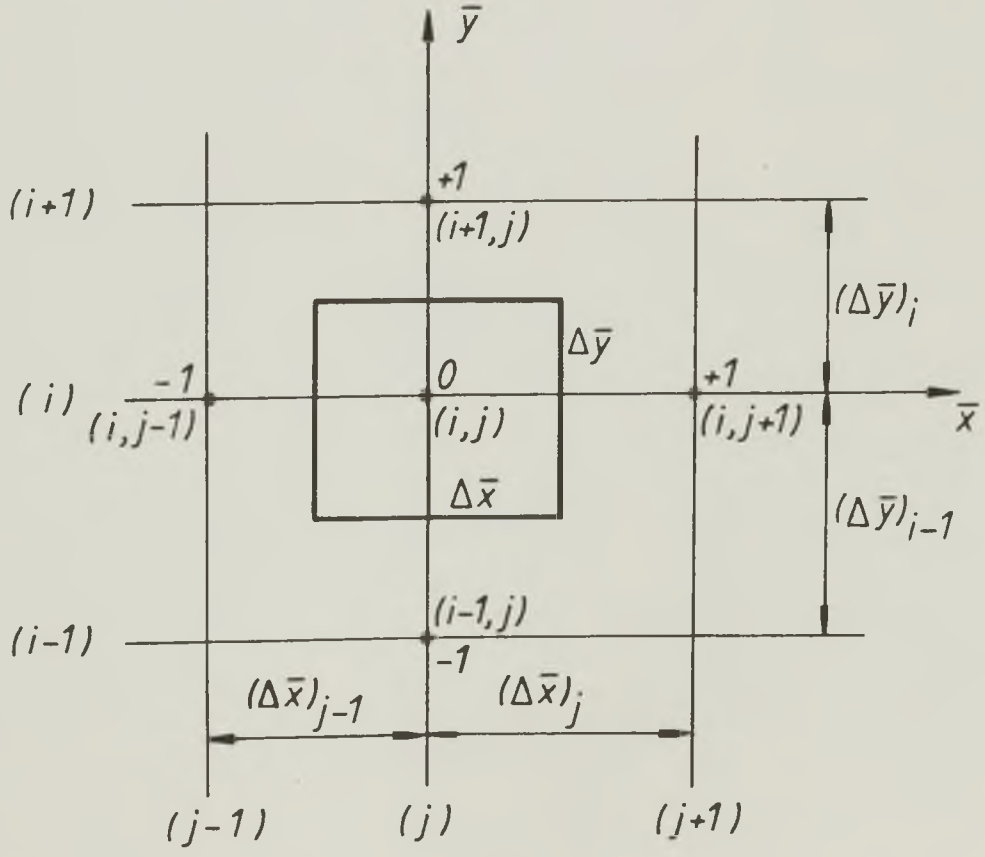

Figure 3.3 The computational cell surrounded by unequally spaced mesh lines

$$\bar{x} = \frac{x}{2\pi r} \qquad \bar{y} = \frac{y}{b}$$

$$\bar{h} = \frac{h}{c} \qquad \bar{\beta} = \frac{\beta}{\eta(\Omega_1+\Omega_2)} \left(\frac{c}{r}\right)^2$$

(Ω_1 and Ω_2 are the angular velocities of the shaft and the bush in rad/s)

The following equation for $(\theta_{i,j})$ was derived

$$\theta_{i,j} = \frac{(\pi/24)(\Delta\bar{x})\bar{\beta}(d/b)^2 E_{12} + (\Delta\bar{y}/2)E_{10} + (\Delta\bar{y}/96x2\pi)\bar{\beta}E_{11}}{(\pi/24)(\Delta\bar{x})\bar{\beta}(d/b)^2 E_9 + (\Delta\bar{y}/2)E_8 + (\Delta\bar{y}/96x2\pi)\bar{\beta}E_7} \qquad (3.7)$$

where,

$$E_7 = \frac{g_{i,j}(\bar{h}_j-\bar{h}_{j-1})^3}{(\Delta\bar{x})_{j-1}} + \frac{g_{i,j}(\bar{h}_j+\bar{h}_{j+1})^3}{(\Delta\bar{x})_j}$$

$$E_8 = \bar{h}_j(1-g_{i,j})$$

$$E_9 = \frac{\bar{h}_j^3 g_{i,j}}{(\Delta\bar{y})_{i-1}} + \frac{\bar{h}_j^3 g_{i,j}}{(\Delta\bar{y})_i}$$

$$E_{10} = E_3 - E_1$$

$$E_{11} = E_2 + E_4 + E_7$$

$$E_{12} = E_5 + E_6 + E_9$$

$$E_1 = g_{i,j}\bar{h}_{i,j} + \frac{g_{i,j}\, g_{i,j+1}}{2}(\bar{h}_{j+1} - \bar{h}_j)$$

$$E_2 = \frac{(\bar{h}_{j+1} + \bar{h}_j)^3 \, g_{i,j+1}\,(\theta_{i,j+1}{}^{-1})}{(\Delta\bar{x})_j}$$

$$E_3 = \theta_{i,j-1}\,\bar{h}_{j-1}\,(1-g_{i,j-1}) + g_{i,j-1}\,\bar{h}_{j-1} +$$

$$+ \frac{g_{i,j-1}\,g_{i,j}}{2}\,(\bar{h}_j - \bar{h}_{j-1})$$

$$E_4 = \frac{(\bar{h}_j+\bar{h}_{j-1})^3\, g_{i,j-1}\,(\theta_{i,j-1}{}^{-1})}{(\Delta\bar{x})_{j-1}}$$

$$E_5 = \frac{\bar{h}_j^3\, g_{i-1,j}\,(\theta_{i-1,j}{}^{-1})}{(\Delta\bar{y})_{i-1}}$$

$$E_6 = \frac{\bar{h}_j^3\, g_{i+1,j}\,(\theta_{i+1,j}{}^{-1})}{(\Delta\bar{y})_{i}}$$

$$\Delta\bar{x} = \frac{(\Delta\bar{x})_j + (\Delta\bar{x})_{j-1}}{2}$$

$$\Delta\bar{y} = \frac{(\Delta\bar{y})_i + (\Delta\bar{y})_{i-1}}{2}$$

3.4 The Analysis of Finite Width Journal Bearings With No Film Reformation

The prime purpose of the present work was to undertake an analysis of finite width journal bearings considering the lubricant supply conditions in some detail. It was intended to treat the case of lubricant supply via a single groove at the location of maximum film thickness and, possibly, via one or two grooves at any location. However, to gain confidence in the approach used and the predictions of the analysis, the computer program was initially designed for non-reformation conditions only. The lubricant was assumed to be supplied at ambient pressure via a full width line 'groove' at the maximum film thickness. Most of the journal bearing performance predictions available were obtained using this assumption and thus provided a good basis for comparison of results.

3.4.1 The Finite Difference Mesh

A system of equations written in a finite difference form, representing the application of equation (3.7) at each node, needed to be solved. A finite difference mesh covering the bearing area was set up by specifying the number of mesh lines parallel to the bearing axis (M) and the number of circumferential mesh lines (N). The values taken by the subscripts (i) and (j) in equation (3.7) were therefore in the range

i: 1 to N

j: 1 to M

The axial mesh line (1) was coincident with the axial mesh line (M) at the position of maximum film thickness. The circumferential lines (1) and (N) were coincident with the bearing edges. The mesh lines in both directions were equally spaced, the mesh size being dependent on the specified values of (M) and (N).

3.4.2 Boundary Conditions

The boundary conditions required were the values of (θ) at the bearing edges and at the lubricant supply line. The pressure was taken to be ambient at both locations. The lubricant was assumed to cavitate at ambient pressure, Thus,

$$p_c = p_{amb} = 0$$

In the full film region equation (3.2) applied. The boundary conditions adopted were;

(a) At the lubricant supply line,

$$p = p_c = 0 \quad \text{and} \quad \theta = 1$$

(b) At the nodes on the bearing edges where a full width film existed,

$p = p_c = 0$ and $\theta = 1$

(c) Within the cavitation region equation (3.2) was not applicable. The values of (θ) in this region were not related to the cavitation pressure, they were obtained from the solution of the system of equations (3.7). Due to the technique used which required a knowledge of (θ) at the nodes on the circumferential mesh line (1) to calculate (θ) at the nodes on the circumferential mesh line (2), the following conditions were imposed.

$$\theta_{1,j} = \theta_{2,j}$$

and $$\theta_{N,j} = \theta_{N-1,j}$$

for all nodes (2,j) and (N-1,j) in the cavitation region.

3.4.3 Method of Solution of the Finite Difference Equation

Approximations of the type represented by equation (3.7) resulted in as many equations as grid points and the solution of a system of simultaneous linear equations was required. The parameters involved were (b/d), (ε) (which determined ($\bar{h}$)) and ($\bar{\beta}$). A Gauss-Seidel iterative method was used. The following steps were involved in the procedure;

(1) Initially, the values of (θ) and (g) at every node were set to unity

(2) For any iteration cycle (m>1) the value of (θ) at every node (excluding those where boundary conditions had been specified) was obtained from

$$\theta_{(m)} = \theta_{(m-1)} + R_f \left(\theta_{(cal)} - \theta_{(m-1)}\right) \qquad (3.8)$$

where $\theta_{(m-1)}$ is the value calculated in the previous iteration

$\theta_{(cal)}$ is the value determined in the current iteration, from equation (3.7)

R_f is the relaxation factor

(3) After each iteration new values were given to (g) at every node, according to the new values of (θ) and equations (3.3)

(4) The iterative process was terminated once the solution had converged. The convergence criterion was

$$g_{(m)} = g_{(m-1)} \quad \text{and} \qquad (3.9)$$

$$\left|\frac{\theta_{(m)} - \theta_{(m-1)}}{\theta_{(m-1)}}\right| \leq \text{tolerance}$$

at all nodes. The procedure returned to step (2) until convergence was achieved.

3.4.4 Pressure Distribution in the Lubricant Film

Equation (3.2) which was applicable to the full film region only, was written in dimensionless form as

$$\bar{p} = \bar{\beta}\ (\theta-1) \qquad (3.10)$$

where the dimensionless pressure ($\bar{p}$) was given by

$$\bar{p} = \frac{p}{\eta(\Omega_1+\Omega_2)} \left(\frac{c}{r}\right)^2 \qquad (3.11)$$

The pressure distribution was determined from the distribution of (θ) according to

$$\bar{p}_{i,j} = \bar{\beta}\ (\theta_{i,j} - 1) \quad \text{if} \quad \theta_{i,j} \geq 1$$

and $$\bar{p}_{i,j} = 0 \quad \text{if } \theta_{i,j} < 1$$

3.4.5 Load Capacity and Attitude Angle

The load capacity was determined by integration of the pressure distribution around the bearing. For the coordinate system represented in Figure 3.4, the components of the resultant film pressure force along and perpendicular to the line of centres ((z) and (x) directions respectively) were

$$P_x = \int_0^{2\pi} \int_{-b/2}^{b/2} pr \sin\alpha \, dy \, d\alpha$$

$$P_z = -\int_0^{2\pi} \int_{-b/2}^{b/2} pr \cos\alpha \, dy \, d\alpha \qquad (3.12)$$

where (α) is the circumferential variable measured from the position of maximum film thickness in the direction of the shaft rotation.

Using equation (3.11) for the dimensionless pressure and taking

$$dy = b \, d\bar{y}$$

and $$d\alpha = 2\pi \, d\bar{x}$$

a dimensionless form of equation (3.12) was obtained

$$\bar{P}_x = 2\pi \int_0^1 \int_0^1 (\bar{p} \sin\alpha) \, d\bar{y} \, d\bar{x}$$

$$\bar{P}_z = -2\pi \int_0^1 \int_0^1 (\bar{p} \cos\alpha) \, d\bar{y} \, d\bar{x} \qquad (3.13)$$

where the normal force components (P_x,P_z) were made dimensionless according to

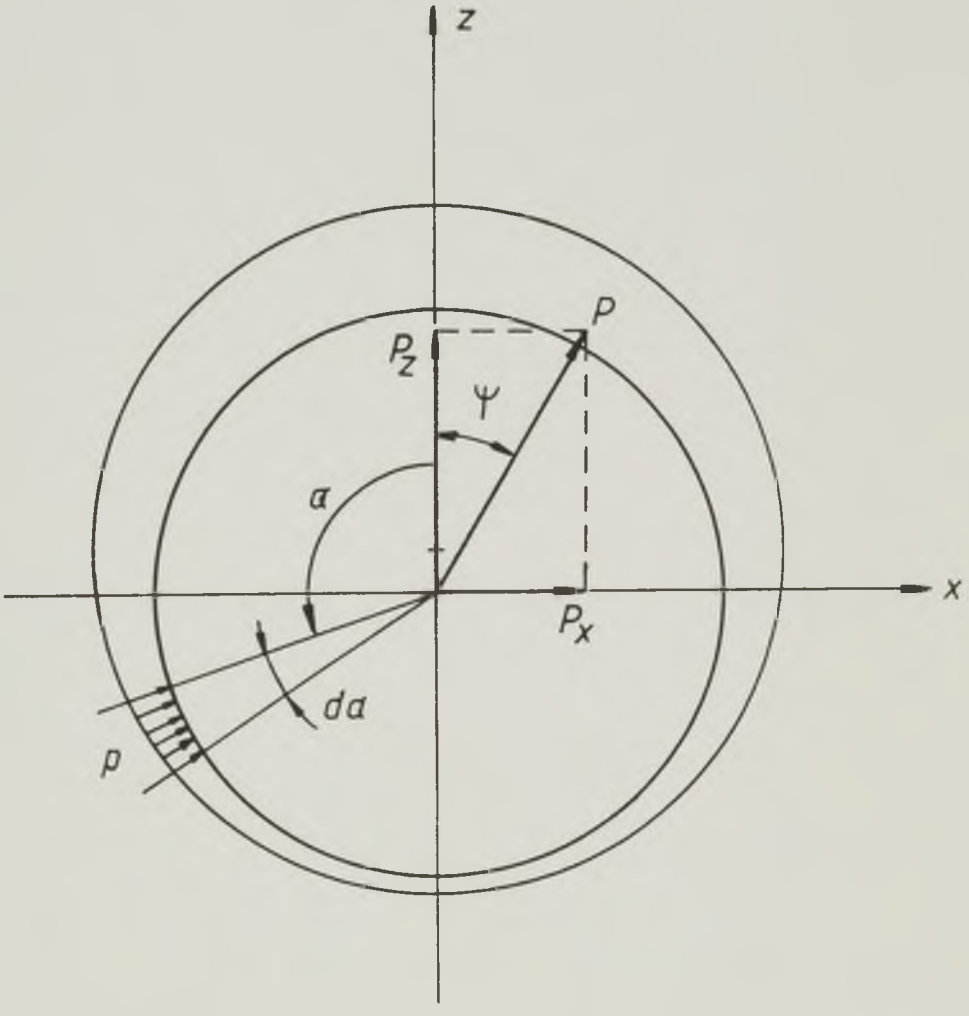

Figure 3.4 Coordinate system and normal force components of the resultant pressure.

$$\bar{P} = \frac{P}{br\eta(\Omega_1+\Omega_2)} \left(\frac{c}{r}\right)^2 \qquad (3.14)$$

Simpson's rule was used to integrate each of the equations (3.13).

The dimensionless load capacity of the bearing and the attitude angle were then determined from

$$\bar{W} = \sqrt{\bar{P}_x^{\,2} + \bar{P}_z^{\,2}} \qquad (3.15)$$

and $$\psi = \tan^{-1}\left(\frac{\bar{P}_x}{\bar{P}_z}\right)$$

3.4.6 Lubricant Flow Rates

The computer program calculated the dimensionless flow rate from the sides of the bearing ($\bar{Q}_s$), the flow rate into the cavitation region ($\bar{Q}_c$) and the net flow issuing from the groove ($\bar{Q}_{gr}$) when, at a later stage of the analysis, the lubricant inlet conditions were considered. The approach adopted for the evaluation of the net flow issuing from the groove is discussed in Section 3.5.3.

In the full film region, the flow in the circumferential direction included both Couette and Poiseuille components. The flow in the axial direction was pressure flow only.

The circumferential flow rate across a bearing section of width (y_1) was given by

$$Q_x = \int_0^{y_1} \left[-\frac{h^3}{12\eta}\frac{\partial p}{\partial x} + \frac{(U_1+U_2)h}{2}\right] dy \qquad (3.16)$$

The axial flow rate across a section of circumferential length (x_1) was determined from

$$Q_y = \int_0^{x_1} \left(-\frac{h^3}{12\eta} \frac{\partial p}{\partial y} \right) dx \qquad (3.17)$$

In dimensionless form, equations (3.16) and (3.17) were written as

$$\bar{Q}_x = \int_0^{\bar{y}_1} \left(-\frac{\bar{h}^3}{24\pi} \frac{\partial \bar{p}}{\partial \bar{x}} + \frac{\bar{h}}{2} \right) d\bar{y} \qquad (3.18)$$

$$\bar{Q}_y = \pi \left(\frac{d}{b}\right)^2 \int_0^{\bar{x}_1} \left(-\frac{\bar{h}^3}{24} \frac{\partial \bar{p}}{\partial \bar{y}} \right) d\bar{x} \qquad (3.19)$$

where the flow rates were made dimensionless acording to

$$\bar{Q} = \frac{Q}{cb(U_1+U_2)} \qquad (3.20)$$

A knowledge of the pressure gradients at every relevant nodal point was required before the numerical integration of equations (3.18) and (3.19) could be carried out.

The Evaluation of Pressure Gradients

Figure 3.5 illustrates the method used to approximate the pressure gradient (say in $\bar{x}$-direction) at a node 'O'. It was assumed that in a small interval [O, 3δ], where (δ) is the mesh size, the pressure variation could be represented by a polynomial of degree three

$$\bar{p}\ (\bar{x}) = A + B\bar{x} + C\bar{x}^2 + D\bar{x}^3$$

the coefficients of which were calculated from a knowledge of the pressure at the four nodes involved and denoted O, 1, 2, 3 (see Figure 3.5).

The coefficient (B) was found to be given by

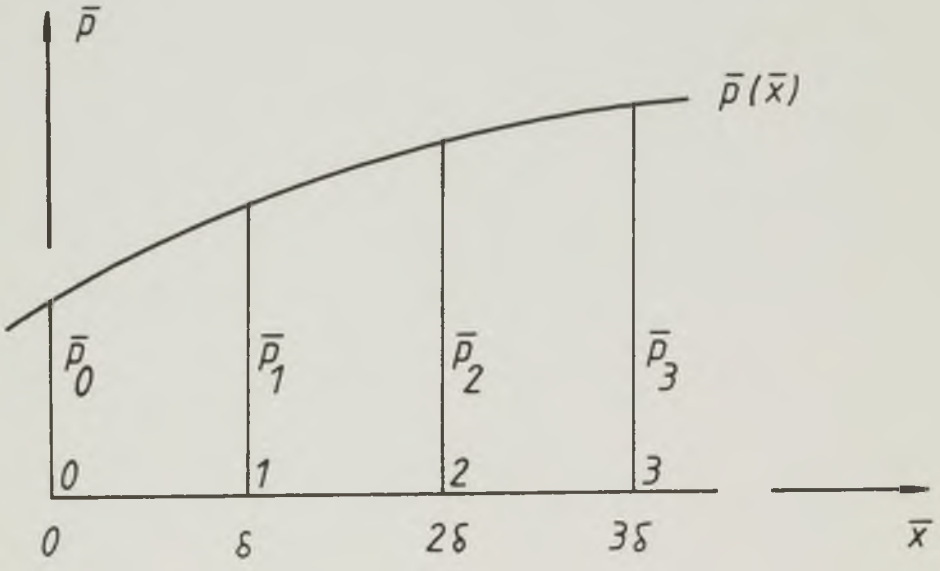

$$\bar{p}(\bar{x}) = A + B\bar{x} + C\bar{x}^2 + D\bar{x}^3$$

Solve for (B) given that

$\bar{p} = \bar{p}_0$ at $\bar{x} = 0$

$\bar{p} = \bar{p}_1$ $\bar{x} = \delta$

$\bar{p} = \bar{p}_2$ $\bar{x} = 2\delta$

$\bar{p} = \bar{p}_3$ $\bar{x} = 3\delta$

Figure 3.5 Approximation used to calculate the pressure gradient at the node '0'.

$$B = \frac{-11\,\bar{p}_o + 18\,\bar{p}_1 - 9\,\bar{p}_2 + 2\bar{p}_3}{6\delta}$$

and the required pressure gradient at node '0' was

$$\left(\frac{\partial \bar{p}}{\partial \bar{x}}\right)_{\bar{x}=0} = B \qquad (3.21)$$

The flow rates were determined using Simpson's rule to integrate numerically equations (3.18) and (3.19).

3.4.7 The Computer Program Flow Chart

The program procedure was similar to that employed when film reformation was considered. It will be discussed in Section 3.5.4.

3.4.8 A Study of the Convergence of the Solution

The parameters affecting the convergence of the iterative process for given operating conditions (b/d, ε), were the mesh size, the tolerance adopted in the convergence criterion, the relaxation factor (R_f) and the bulk modulus parameter of the lubricant ($\bar{\beta}$).

The smaller the mesh size or the tolerance adopted, the larger the number of iterative cycles required to achieve convergence and also more accurate the solution obtained.

Elrod and Adams (1974) and Elrod (1981) have mentioned the possibility of numerical instabilities for particular values of ($\bar{\beta}$) and in the former paper the use of $\beta = 6.9 \times 10^7$ N/m^2 was reported for reasons of stability of the solution.

Elrod (1981) showed that, providing convergence had been achieved, the value of ($\bar{\beta}$) used had no significant effect on the bearing performance predictions. A preliminary investigation on the influence of (R_f) and ($\bar{\beta}$) seemed to suggest that whatever the value of ($\bar{\beta}$), convergence within a minimum number of cycles was achieved for a value of (R_f) of about

unity. A more detailed study was carried out to investigate these effects fully.

Influence of the Bulk Modulus Parameter

Solutions were obtained for a number of operating conditions taking $R_f = 1$, tolerance = 10^{-5}, M x N = 51 x 11 and for variable $(\bar{\beta})$. It was found that the optimum value of $(\bar{\beta})$ for a minimum number of cycles for convergence was dependent on (b/d) and (ε), and for a given (b/d) the optimum value of $(\bar{\beta})$ increased with increasing (ε), as shown in Figure 3.6. The following was also observed;

(a) The value of $(\bar{\beta})$ used did not affect the performance predictions except for very high values of $(\bar{\beta})$. For values of $(\bar{\beta})$ corresponding to $\beta > 10^{10}$ it has been observed in a number of cases that convergence was achieved, but to the wrong pressure distribution. This was cured by using a smaller tolerance.

(b) Although the final pressure distribution was not affected by the value of $(\bar{\beta})$ used, the values of (θ) in the full film region were obviously affected. For values of $(\bar{\beta})$ corresponding to $\beta < 10^{6}$, (θ) was much greater than unity in the full film region due to the assumed relatively high compressibility of the lubricant.

(c) In the cavitation zone (θ) was almost unaffected by changes in $(\bar{\beta})$.

As an example, for typical operating conditions,
$C_d/d = 0.002$, $\Omega_1 = 125$ rad/s, $\Omega_2 = 0$, $\eta = 0.02$ Pa.s and
$\beta = 5 \times 10^{7}$ N/m^2, the value of $(\bar{\beta})$ would be 80.

The influence of the bulk modulus parameter on the convergence of the solution will be discussed further in Section 3.5.6.

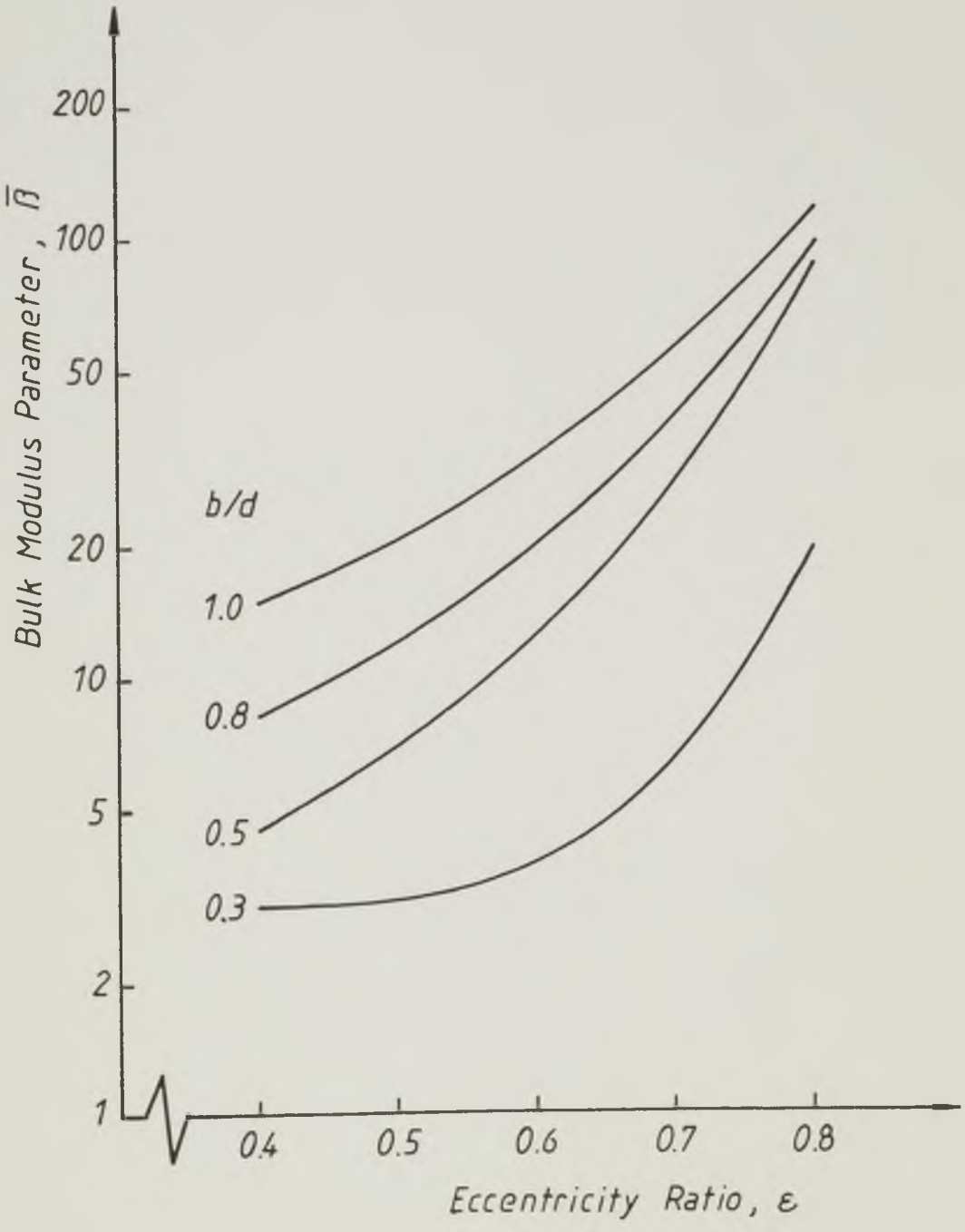

Figure 3.6 Values of ($\bar{\beta}$) for convergence within a minimum number of cycles.
M x N = 51 x 11, R_f = 1

Optimum Relaxation Factor

The influence of the relaxation factor on the number of cycles for convergence is shown in Figure 3.7 where three different operating conditions are considered. The values of ($\bar{\beta}$) used were obtained from the previous study to ensure rapid convergence.

A decrease in the number of cycles was initially observed as (R_f) increased from a value less than unity. Convergence within a minimum number of cycles was in general achieved for (R_f) in the range (1-1.05). A further increase in the value of (R_f) resulted in either the number of cycles for convergence to increase very sharply or, more commonly, the program to be interrupted due to 'overflow'.

Case 2 (Figure 3.7) was chosen for a closer look into the iterative process for values of (R_f) in the neigh bourhood of its optimum value. It was observed that when (R_f) varied from 1 to 1.04 the number of cycles decreased further to 72 and for R_f = 1.047 to 1.04718 the number of cycles was 71. Then, suddenly at R_f = 1.04719 'overflow' occurred. When the values of (θ) at various nodes and for successive iterative cycles were printed out, it was found that with a given number of cycles performed some of the nodes had already converged. With the continuation of the iterative process the values $\theta_{(m-1)}$ and $\theta_{(m)}$ at those nodes, stayed for a while within the tolerance varying in an oscillatory fashion. However, after a number of cycles, variable from node to node, the value $\theta_{(m)}$ started moving away from $\theta_{(m-1)}$. For a given value of $\theta_{(m-1)}$ the resulting $\theta_{(m)}$ became bigger and bigger as the iteration progressed and 'overflow' eventually occurred.

The value R_f = 1 was therefore adopted. This consideration of optimum relaxation factor and instability will be discussed further in Section 3.5.7.

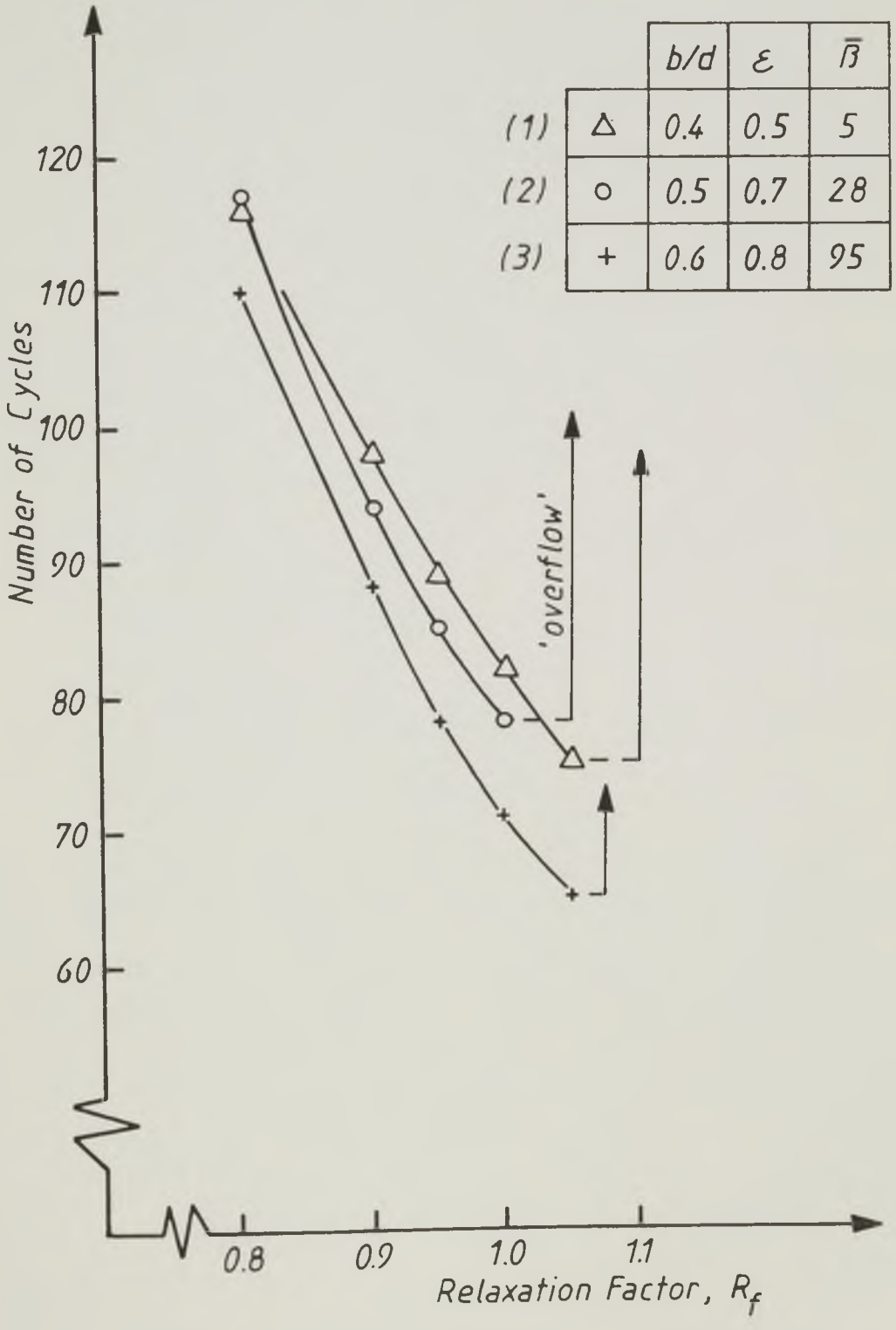

Figure 3.7 Influence of the relaxation factor on the number of cycles for convergence
M x N = 51 x 11, tolerance = 10^{-5}

Optimum Tolerance

The influence of the tolerance on the number of cycles for convergence and on the accuracy of the solution, is shown in Figure 3.8. The ratio of the values of load capacity ($\bar{W}$), attitude angle (ψ) and side flow ($\bar{Q}_s$), to the values of the same quantities for the tolerance 10^{-8} (e.g. $\bar{W}_r = \bar{W}/\bar{W}_{tol=10^{-8}}$) are quoted.

The tolerance 10^{-5} was considered to represent a satisfactory compromise between accuracy and number of cycles required for convergence. It was therefore adopted.

3.4.9 Comparison of the Predictions of the Current Analysis with Published Results

The results of the current analysis were checked against the predictions of ESDU Item No. 66023 (1966), Ashton (1973) and King (1975) for load capacity and flow rates. Figures 3.9 and 3.10 show very good correlation for b/d = 0.5. Equally good was the correlation observed for b/d = 0.75 and b/d = 1. The dimensionless flow rates of ESDU Item No. 66023 (1966) corresponding to the inlet flow ($\bar{Q}_i$) and to the side flow ($\bar{Q}_s$) were (Q'_E) and (Q'_v) respectively (apart from a constant).

3.5 The Analysis of Finite Width Journal Bearings Considering Film Reformation

The analysis discussed in Section 3.4 was extended to include a detailed study of the lubricant supply/reformation conditions. Only the case of a single axial groove (or single 'square' hole) at the position of maximum film thickness was studied.

Three more parameters were introduced to enable consideration of the new situation of lubricant being supplied to the bearing via a groov

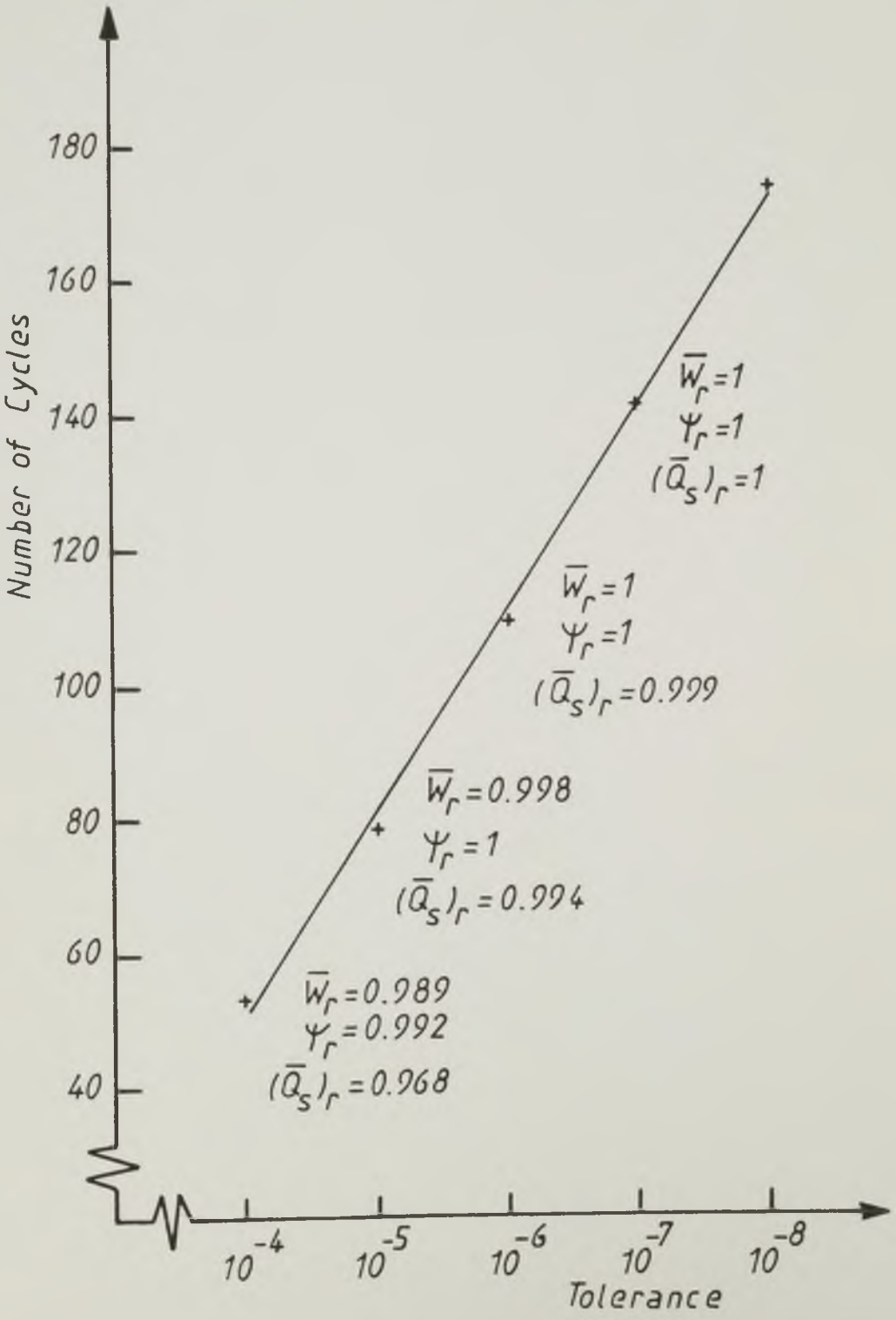

Figure 3.8 Influence of the tolerance on the number of cycles for convergence and on the accuracy of the solution.
b/d = 0.5, ε = 0.7, $\bar{\beta}$ = 28
M x N = 51 x 11, R_f = 1

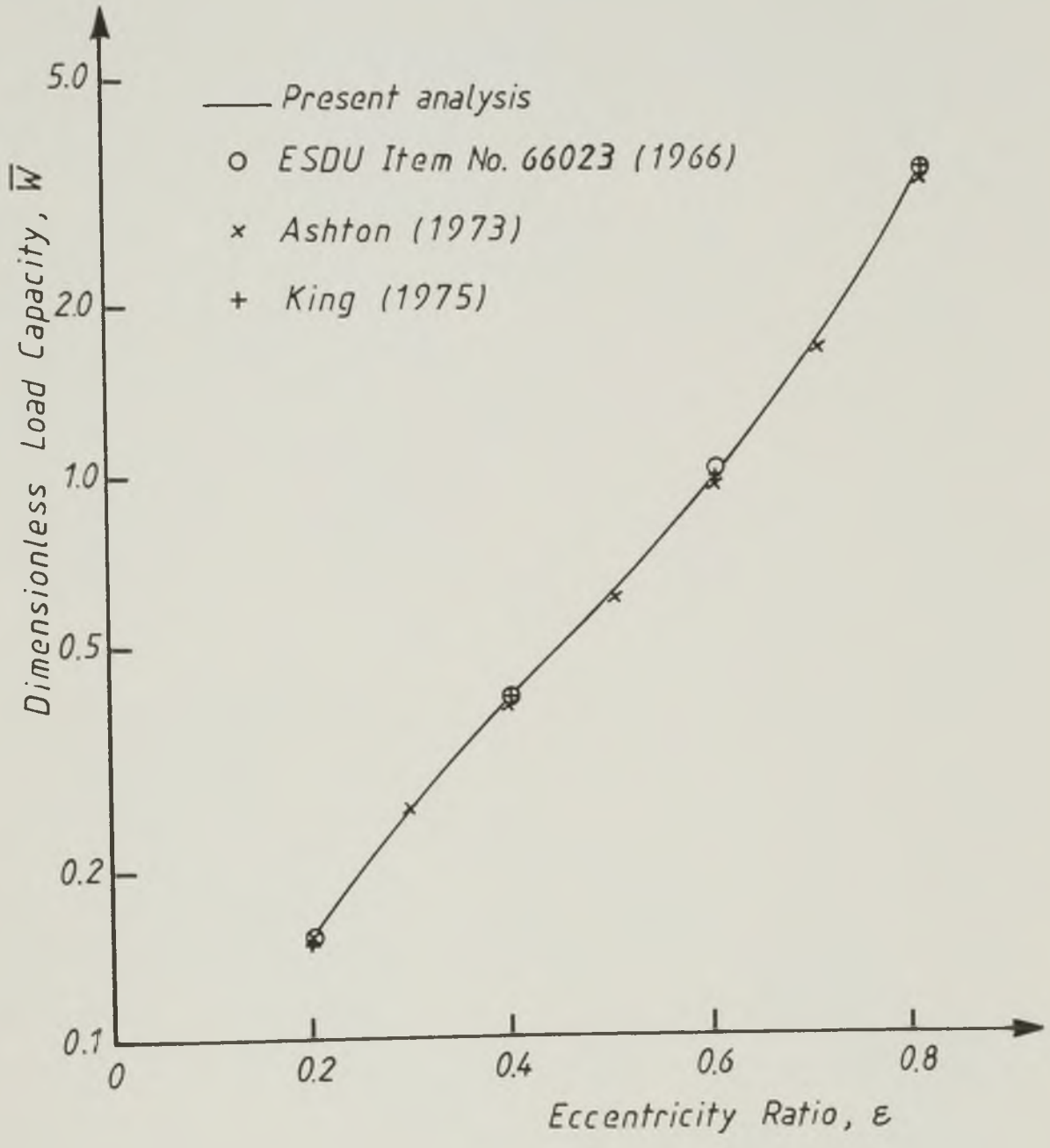

Figure 3.9 Comparison of theoretical results for dimensionless load capacity without considering reformation. b/d = 0.5

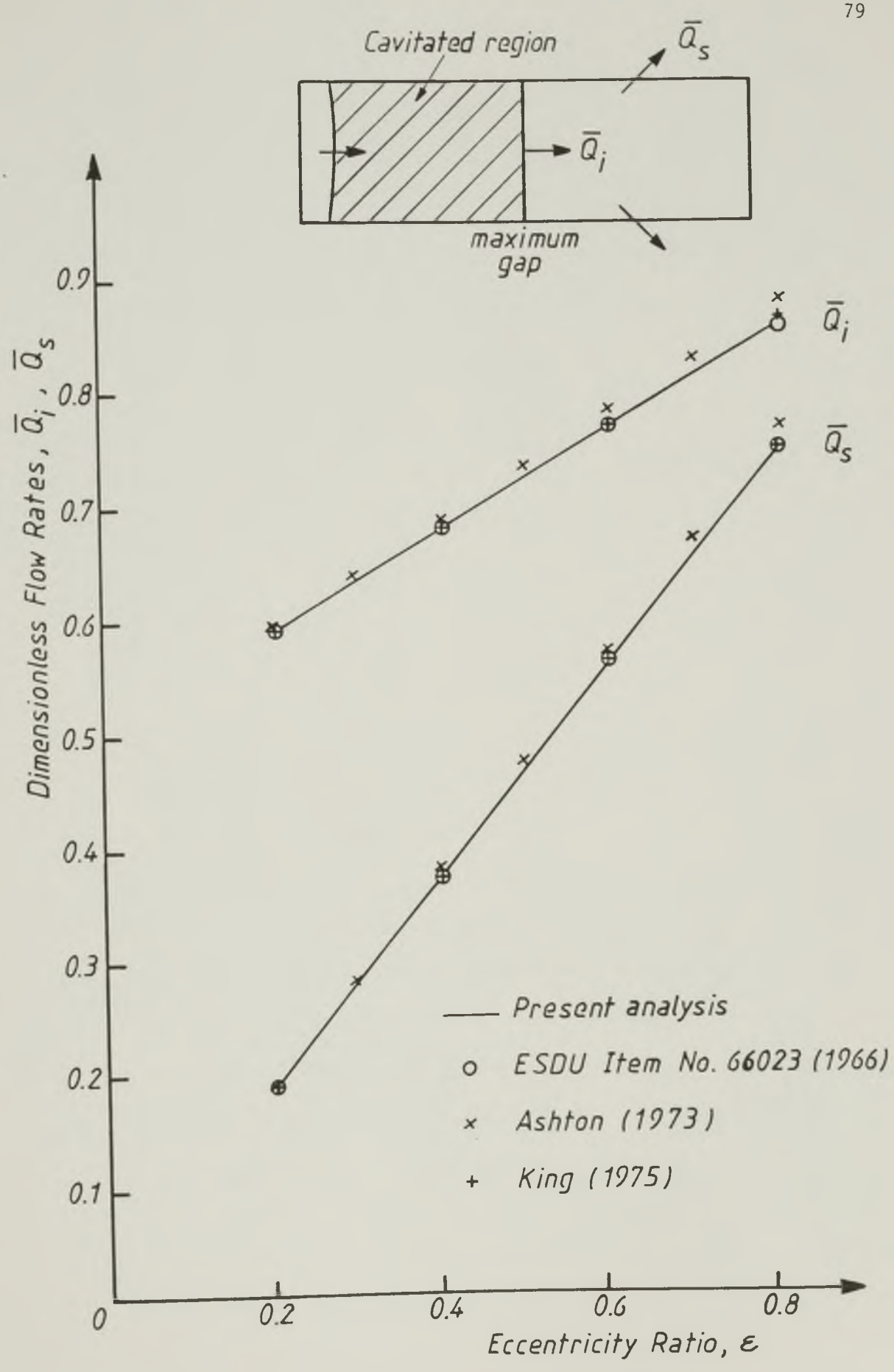

Figure 3.10 Comparison of theoretical results for dimensionless flow rate without considering reformation. b/d = 0.5

at a supply pressure greater than ambient. The groove geometry was accounted for by the introduction of the parameters (a/b) and (w/d) related to the axial and the circumferential dimensions of the groove. The lubricant supply pressure was introduced by means of the dimensionless supply pressure ($\bar{p}_f$).

3.5.1 The Variable Finite Difference Mesh

The axis of the journal was assumed to be parallel to the bearing axis. The distribution of pressures was symmetric about the bearing centre line and it was therefore sufficient to solve equations (3.7) for half the bearing area only.

The accuracy of the location of the reformation boundary was found to affect the calculated flow rates, a matter which will be discussed in Section 3.5.5.

A mesh of variable size was used to cope with the presence of the groove and the degree of accuracy required in the location of the reformation boundary. Only (M) and (N), the number of mesh lines in the (x) and the (y) directions respectively, needed to be specified. A variable mesh covering half the bearing area was set up automatically by the computer program with the following features;

(a) One mesh line was always coincident with each groove edge

(b) The number of grid intervals over the groove was dependent on the groove size

(c) There was always at least three equally spaced intervals around the groove edges and near the bearing edge, such that equation (3.21) could be used to calculate pressure gradients

(d) The number of grid intervals over the film reformation region in the circumferential direction was dependent on ($\bar{p}_f$) and (a/b).

Figure 3.11 shows two automatically generated grids for two different lubricant inlet conditions. Details on the automatic generation of the variable mesh are given in Appendix A.

3.5.2. Boundary Conditions at the Groove

The boundary conditions at the bearing edge were the same as those discussed in Section 3.4.2. At the groove the pressure was assumed to be constant and equal to the lubricant supply pressure. The values of (θ) at all nodes over the groove were kept constant throughout the solution procedure at a value given by equation (3.10).

A simple calculation of the pressure drop associated with the acceleration of the oil from the groove into the bearing showed that it was of about 0.01 bar (1 kN/m^2) for a tangential speed of the shaft of 3 m/s, and of about 0.25 bar (25 kN/m^2) for a tangential shaft speed of 15 m/s.

3.5.3 Evaluation of the Flow of Lubricant Issuing From the Groove

The flow rate of lubricant supplied to the bearing through the groove should be equal to the flow rate from the bearing sides. These flow rates were obtained from different calculations and the correlation between them was used to assess the accuracy of the solution.

The evaluation of flow rates has been discussed in general terms in Section 3.4.6. The approach adopted for the evaluation of the dimensionless flow rate issuing from the groove ($\bar{Q}_{gr}$) is sketched in Figure 3.12. Three situations were considered covering the full range of supply pressures.

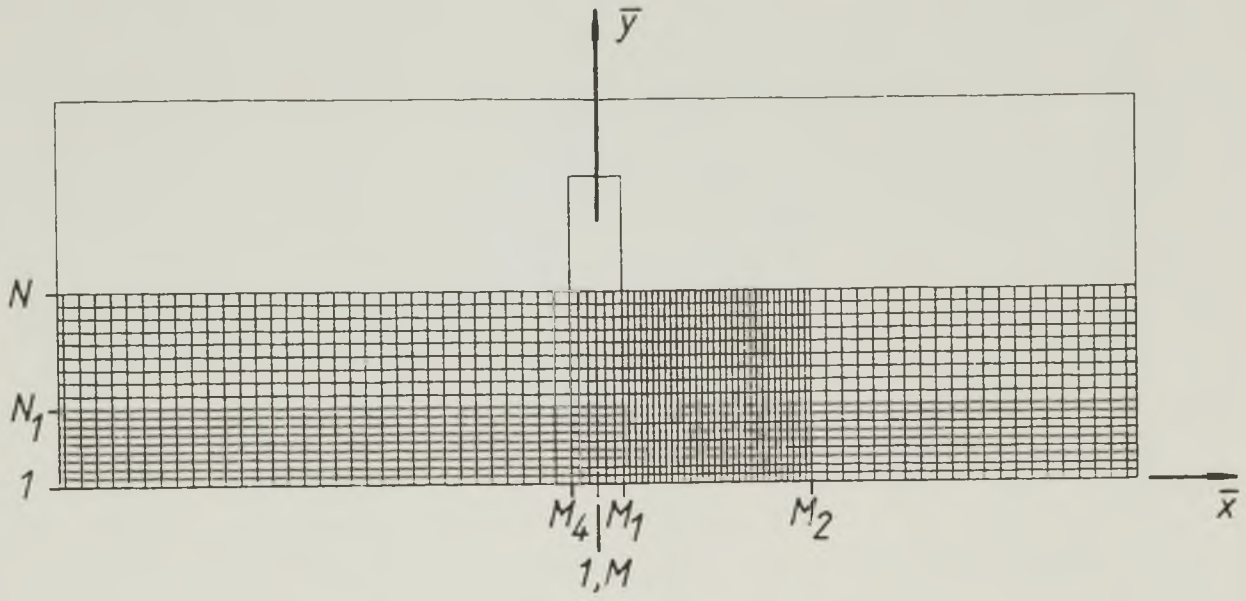

(a) $\bar{p}_f = 0$, $a/b = 0.6$, $w/d = 0.15$

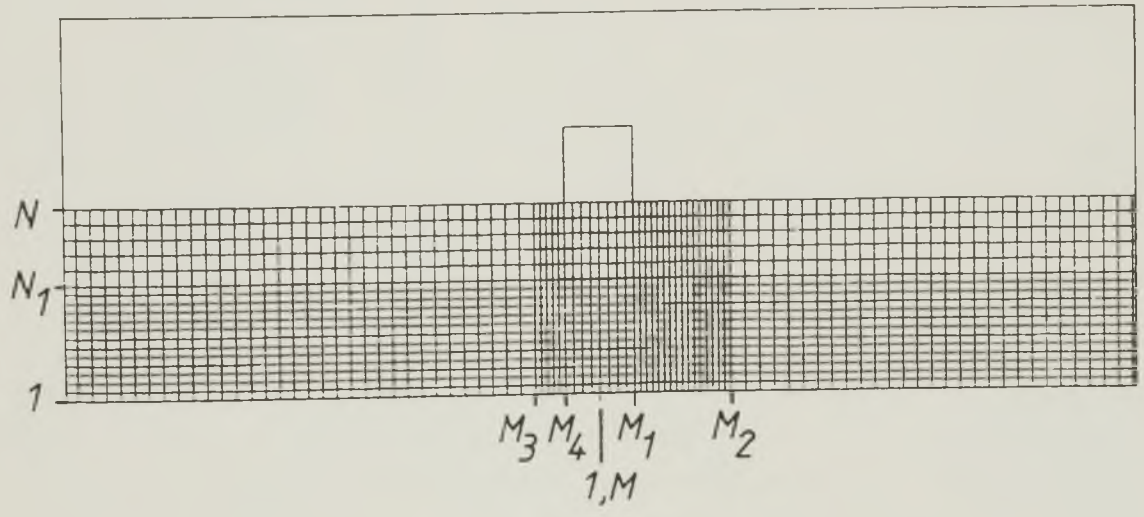

(b) $\bar{p}_f = 0.25$, $a/b = 0.4$, $w/d = 0.2$

Figure 3.11 Two automatically generated grids showing the dependence of mesh size on groove geometry and supply pressure
(M x N = 91 x 19)

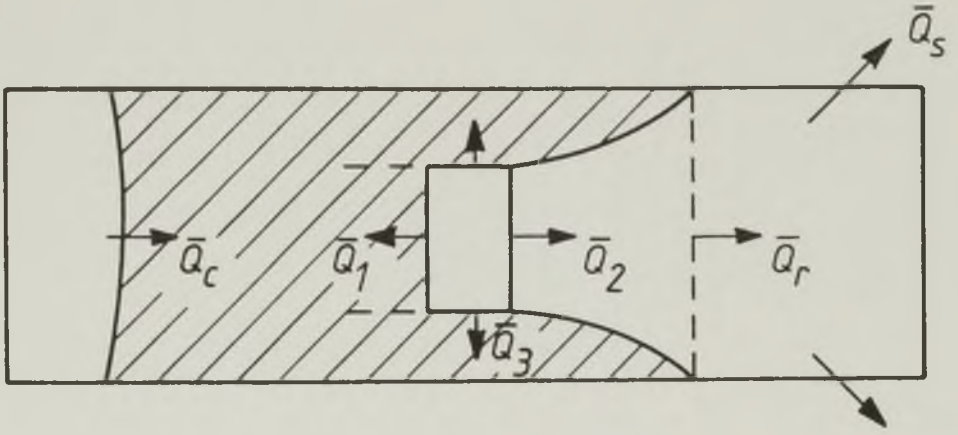

(a) $\bar{p}_f = 0$ $(\bar{Q}_3 = 0,\ \bar{Q}_1 = -\bar{Q}_c\,(a/b))$

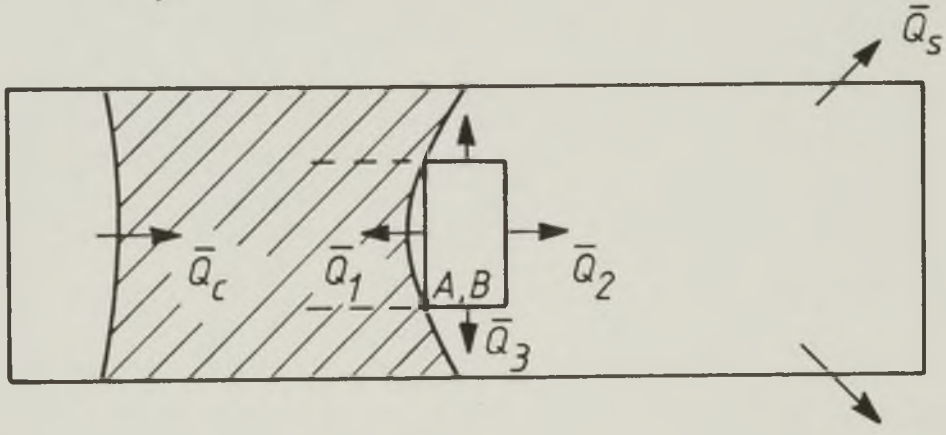

(b) $\bar{p}_f > 0$ (small) $(\bar{Q}_1 = -\bar{Q}_c\,(a/b))$

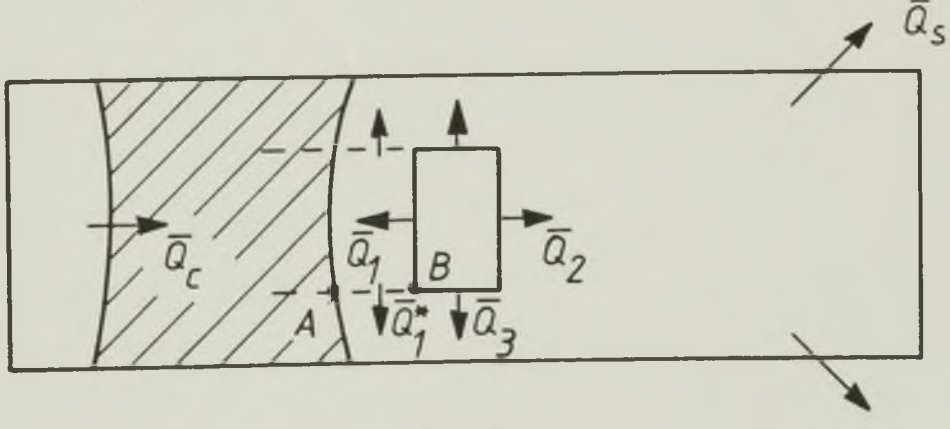

(c) $\bar{p}_f >> 0$ $(\bar{Q}_1 = \bar{Q}_1^* - (\bar{Q}_c \cdot a/b))$

Figure 3.12 A sketch of the partial flows considered in the calculation of the flow of lubricant issuing from the groove
($\bar{Q}_{gr} = \bar{Q}_1 + \bar{Q}_2 + \bar{Q}_3$)

(a) $\bar{p}_f = 0$

The flow over the downstream edge of the groove ($\bar{Q}_2$) contained both Couette and Poiseuille components. The lubricant pressure at the groove was ambient and there was therefore no axial flow from the sides of the groove ($\bar{Q}_3$=0), The flow past the upstream edge of the groove ($\bar{Q}_1$) was actually into the groove resulting from the recirculating flow and given by,

$$\bar{Q}_1 = -\bar{Q}_c \frac{a}{b}$$

(b) $\bar{p}_f$>0, but small (points A and B coincided).

Low lubricant supply pressures and/or high shaft speeds could result in the situation sketched in Figure 3.12(b), where the dimensionless supply pressure was not sufficiently high to cause the reformation boundary to move away from the groove into the diverging film region of the bearing.

The flow from the sides of the groove ($\bar{Q}_3$) was Poiseuille flow only. ($\bar{Q}_1$) and ($\bar{Q}_2$) were similar to case (a)

(c) $\bar{p}_f$>>0

The reformation boundary is now considered to be well away from the groove edge, a situation detected by the program by comparing the location of the nodes (A) and (B). The approach initially used to calculate the flow ($\bar{Q}_1$) was based on a direct calcualtion of the Couette and the Poiseuille components across the upstream edge of the groove. For low/moderate dimensionless supply pressure, however, the determination of pressure gradients could be very inaccurate due to the fact that the pressure could have non-zero values at two or three nodes only, for each circumferential mesh line. A different approach was devised. The axial flow over the section (A - B) was calculated ($\bar{Q}_1^*$) and the flow ($\bar{Q}_1$) was determined from

$$\bar{Q}_1 = \bar{Q}_1^* - (\bar{Q}_c \frac{a}{b})$$

This expression ensured a consistent variation of $(\bar{Q}_1)$ with $(\bar{p}_f)$. If (A) and (B) were coincident $\bar{Q}_1^* = 0$ and $(\bar{Q}_1)$ was reduced to case (b). As the dimensionless supply pressure increased, $(\bar{Q}_1^*)$ increased and there was a value of $(\bar{p}_f)$ for which $(\bar{Q}_1^* = \bar{Q}_c \frac{a}{b})$. As a result the net flow past the upstream edge of the groove would be zero. A further increase in $(\bar{p}_f)$ resulted in a positive value of $(\bar{Q}_1)$, indicating that there was a net flow out of the groove from its upstream edge.

The total net dimensionless flow issuing from the groove was given by

$$\bar{Q}_{gr} = \bar{Q}_1 + \bar{Q}_2 + \bar{Q}_3 \qquad (3.22)$$

3.5.4 The Computer Program

A computer program incorporating the previously discussed details was written in Fortran IV, the flow chart for which is shown in Figure 3.13. Double precision was employed throughout the program to minimize the effect of truncation errors.

The solution of a number of cases of different operating conditions was allowed for during one run of the program. The number of cases was read in as (NCASE) and (IC) was the counter for the number of cases which had already converged. Two parameters were controlled during the execution of the program.

(a) The number of cycles performed during the solution of each case which was held in (NCYCLE). The program was stopped if convergence had not been achieved in a number of cycles smaller than a maximum preset value (NCYMAX)

(b) The total cpu time used. The program was stopped when the total

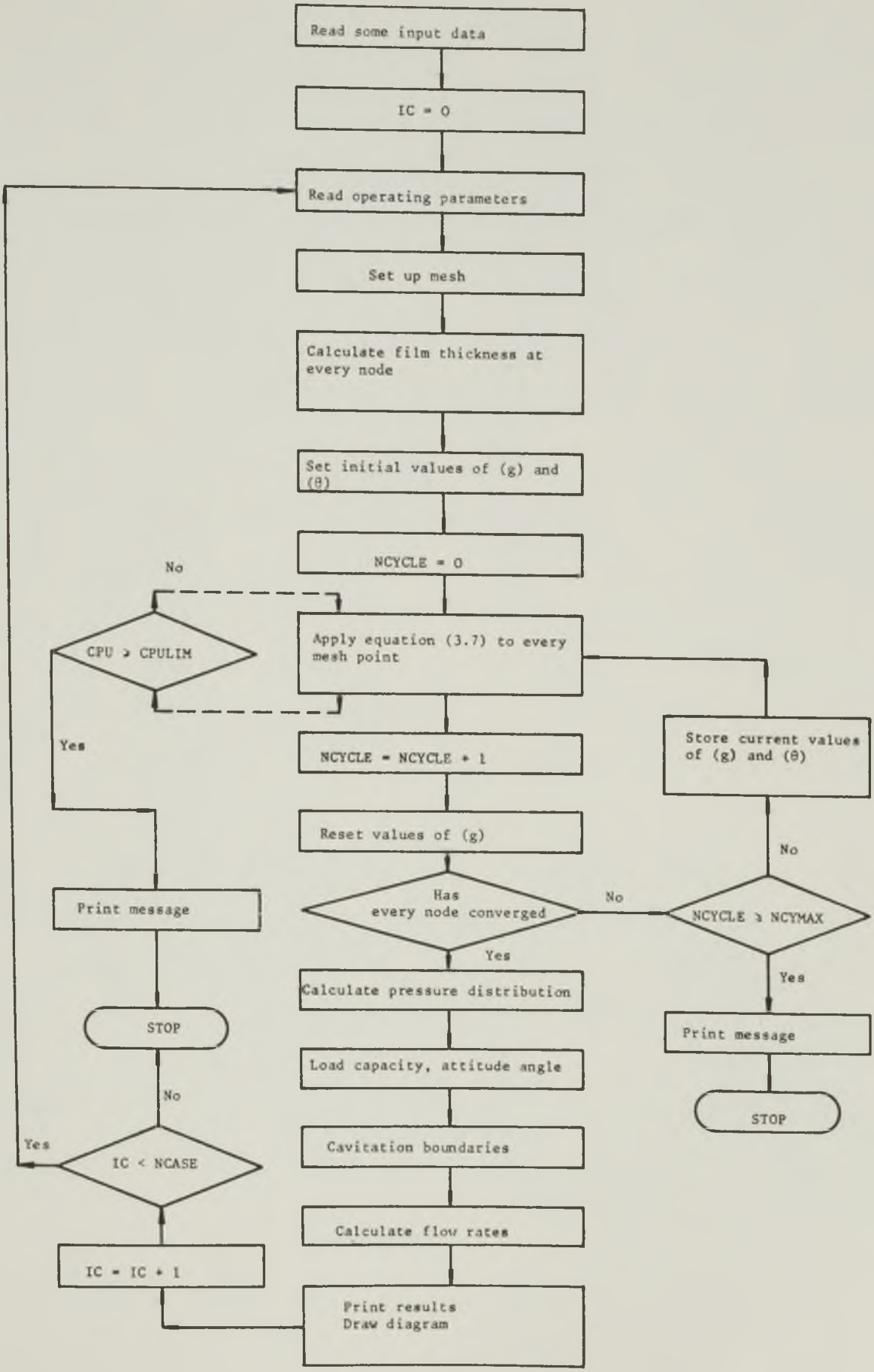

Figure 3.13 Computer program flow chart

cpu time (CPU) exceeded the preset maximum cpu time (CPULIM). The solutions already obtained were kept in an output file, including a record of the cpu time used in each solution.

The program was implemented on the Amdahl 470 Computer System at the University of Leeds.

The program coding and sample input and output data are listed in Appendix B.

3.5.5 Mesh Size and the Accuracy of the Solution

In the first instance, apart from the region over the groove, the mesh lines parallel to the (y) axis were equally spaced. When a grid of (51x11) nodal points over half the bearing area was used, significant discrepancies were observed between the calculated values of ($\bar{Q}_{gr}$) and ($\bar{Q}_s$). To invesitgate the cause of such discrepancies the simpler case of $\bar{p}_f = 0$ was considered.

For flow continuity to be satisfied with $\bar{p}_f = 0$ the circumferential flow rate of lubricant over the bearing section corresponding to the intersection of the calculated reformation boundary with the bearing edges ($\bar{Q}_r$, in Figure 3.12(a)), should be equal to the flow over the bearing section at the downstream edge of the groove. That is, for flow continuity in the reformation region the following equation should be satisfied

$$\bar{Q}_r = \bar{Q}_2 + \bar{Q}_c \left(1 - \frac{a}{b}\right) \qquad (3.23)$$

The discrepancy observed between the left and the right hand sides of equation (3.23) was, in general, in the range 5-8%. At low (a/b), however, this discrepancy was as high as 12%.

Considerable time and effort was invested in the investigation of this discrepancy. The calculated pressure gradients and the numerical integrations were checked against hand calculations for a pre-fixed pressure distribution. They were found to be correct. When a balance of flows at nodes on the reformation boundary were worked out, it was found that flow continuity was not satisfied. This could be due partly to the approximations involved in the cavitation algorithm or, more likely, to inaccurate location of the reformation boundary. If, for example, the reformation boundary intersected the bearing edge at 40^{o} from the groove location, the maximum error in the location of that point of intersection would be one circumferential mesh interval (about 7^{o} for M = 51). The error introduced in the dimensionless film thickness ($\bar{h}$) would be of about 4.5% at $\varepsilon = 0.8$, and because the pressure flow is a function of $\bar{h}^3$, the error introduced in the determination of flow rates could be as much as 13%.

The number of mesh lines was increased in both circumferential and axial directions. The general results could be summarized as follows:

(1) An increase in the number of node points resulted in a decrease in the discrepancy observed between both sides of equation (3.23), but also an increase in the computer cpu time required.

(2) The values that changed significantly were ($\bar{Q}_r$) and ($\bar{Q}_s$) only, ($\bar{Q}_c$), ($\bar{Q}_2$) and ($\bar{W}$) were not much affected by a change in mesh size. This reinforced the idea that the discrepancies observed were mainly due to inaccuracy in the location of the reformation boundary.

(3) For the same total number of nodes, the cpu time was higher for higher values of (N). For a grid of (M = 125, N = 25) or higher, it simply was not possible to get a solution in an acceptable cpu time.

(4) At M = 91, N = 19 the maximum discrepancy observed was 7.5% corresponding to the case to which a 12% discrepancy had been observed at M = 51, N = 11. The cpu times used were in general acceptable.

A mesh with a total number of grid points (91 x 19) was therefore adopted.

A much more acceptable discrepancy in the flow continuity condition (3.23) was observed when a variable mesh was used, as discussed in Section 3.5.1. The mesh intervals in the circumferential direction over the reformation region upstream and downstream of the groove corresponded to about 2^{o}.

A matrix of solutions obtained with a variable mesh of (91x19) nodes, for variable (b/d), (ε), (a/b) and($\bar{p}_f$), showed that the discrepancy between ($\bar{Q}_{gr}$) and ($\bar{Q}_s$) was now usually less than 5% (often between 3% and 5%). At $\bar{p}_f$=0 and a/b $\leq$ 0.5 this figure could rise to 6.5%. A significant increase in cpu time with respect to the case of an even mesh with the same number of nodes, was also observed.

Bearing in mind the purpose of the computer solutions obtained, a variable mesh of (91x19) nodes seemed to be an acceptable compromise between accuracy and computation time.

3.5.6 Computation Time for a Single Solution

The influence of relaxation factor, tolerance and bulk mudulus parameter on the convergence of the Gauss-Seidel iteration has been discussed in Section 3.4.8 for the case where film reformation was not considered.

In the present analysis where the lubricant supply conditions were considered and a variable mesh with an increased total number of nodes

was adopted, a relaxation factor of unity usually gave minimum cpu time at given values of $(\bar{\beta})$ and tolerance. Here again the values unity for relaxation factor and 10^{-5} for tolerance were adopted. When the values of $(\bar{\beta})$ recommended for non-reformation conditions were used in the present analysis many situations of 'overflow' were encountered. A detailed study of the influence of $(\bar{\beta})$ on the convergence of the solution showed that now convergence was, in general, only achieved with values of $(\bar{\beta})$ equal to or less than 0.1. Figure 3.14 shows the effect of the value of $(\bar{\beta})$ on the number of cycles for convergence for the operating conditions indicated in the figure.

A minimum number of cycles was normally obtained with values of $(\bar{\beta})$ in the range (0.01-0.03). The cpu time required for a single solution using values of $(\bar{\beta})$ within that range was usually of 250 to 350 cpu seconds and seemed to be affected more significantly by the values of (a/b) and $(\bar{p}_f)$. Those figures could, however, be doubled in some cases at low (a/b) and ambient supply pressure.

The value of $(\bar{\beta})$ adopted did not affect significantly the solution; performance predictions at given operating conditions obtained using different values of $(\bar{\beta})$ were normally equal to the third decimal place.

3.5.7 An Attempt to Reduce the Computation Time

An attempt was made to reduce the cpu time required for convergence by using over-relaxation in the full film region only. Elrod (1981) pointed out that equations of the type (3.7) were elliptic in the full film region and parabolic in the cavitation region, and Smith (1971) showed that the Gauss-Seidel over-relaxation iterative method was the most efficient for the solution of elliptic partial differential equations.

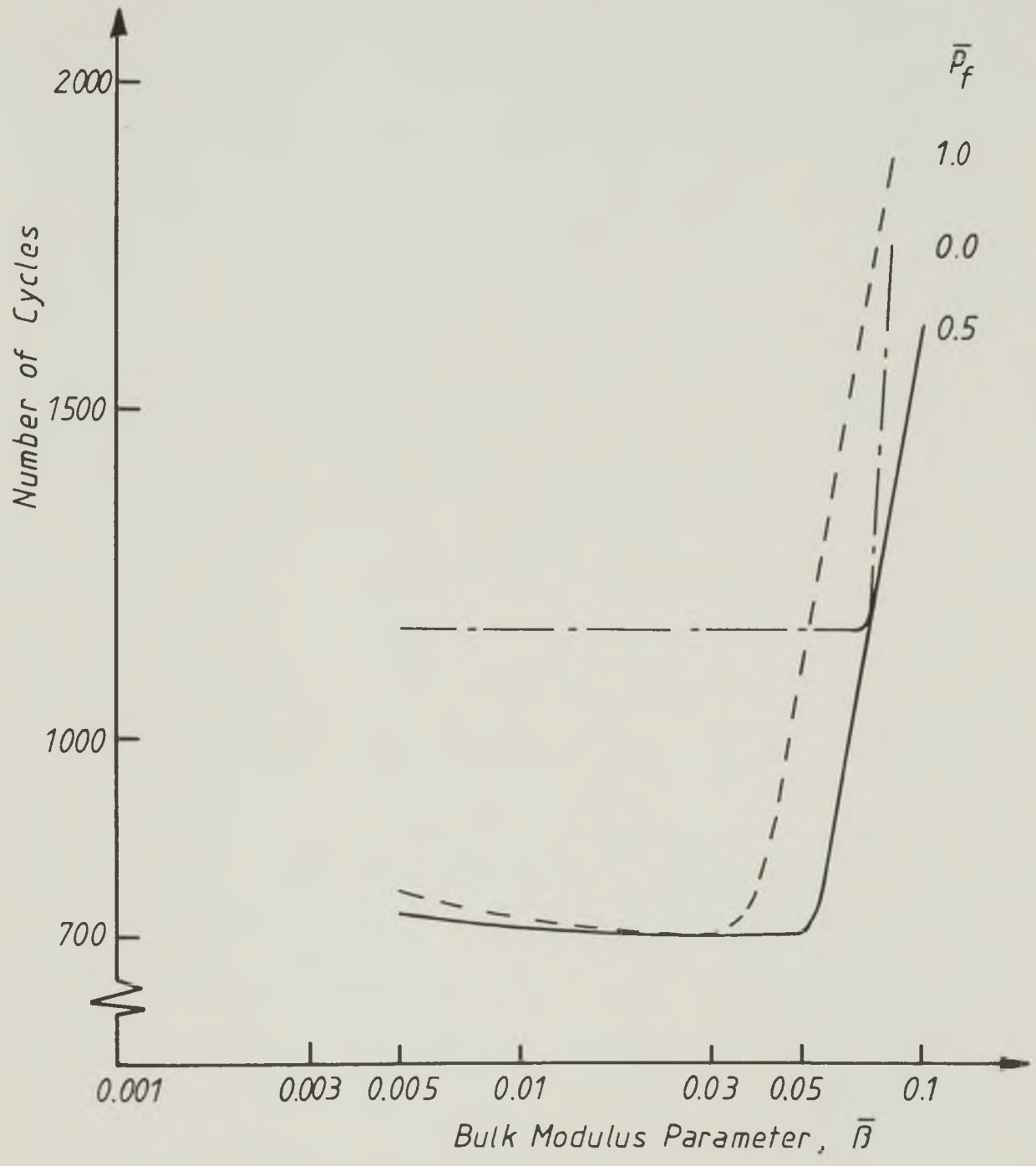

Figure 3.14 Influence of the value of ($\bar{\beta}$) on the number of cycles for convergence

MxN = 91 x 19, variable mesh size
b/d = 0.5, ε = 0.7
a/b = 0.8, w/d = 0.2
R_f = 1, tolerance = 10^{-5}

Over-relaxation was used with the equations corresponding to nodes in a full film region initially guessed using the same approach as used before to define the variable mesh (Section 3.5.1). For the end of the continuous film region a conservative location of the rupture boundary at $\alpha = 190^{\circ}$ was assumed. The over-relaxation factor used was either entered as data or, alternatively, an optimum over-relaxation factor was calculated by the program according to the method proposed by Randall (1968). For grid points outside the guessed full film region (R_f) was unity.

Very good results were obtained for a number of cases studied, with reductions in cpu time of the order of 50%. Unfortunately, cases of 'overflow' and consequent interruption of the solution were also encountered without it being possible to make any improvement on the situation. The use of two different values of (R_f) was therefore abandoned.

3.5.8 Comparison of the Predictions of the Analysis With Published Results

Published results of a direct analysis of finite width journal bearings considering the lubricant inlet conditions were scarce and usually only applicable to situations of lubricant supplied at ambient pressure.

McCallion et al (1971) considered both the groove geometry and the lubricant supply pressure but only the case of a groove located at the load line. The similarity in the shape of the rupture and reformation boundaries compared with the predictions of the present analysis is, however, worth noting.

Etsion and Pinkus (1975) presented results of the analysis of finite width journal bearings with incomplete films for a range of values

of (b/d), (ε) and (a/b), the lubricant supply pressure being ambient. Very poor agreement was observed when their results were compared with those of the present analysis. The most significant discrepancies were observed for side flow and for the location of the reformation boundary, at low values of (a/b). The comparative results are shown in Figures 3.15 and 3.16.

The discrepancies observed could be partly explained by the continuity condition used by Etsion and Pinkus in the film reformation region (equation (2) of their paper), and already discussed in Section 3.1. Such a condition would be equivalent to an increase in the flow rate past the downstream edge of the groove, by a fraction of the cavitation flow corresponding to the groove length. This increased inlet flow was responsible for the higher values of ($\bar{Q}_s$) and the lower values of (α_r) observed. Also the increase on the observed discrepancies for decreasing eccentricity ratio, was seen as the effect of the increasing significance of the recirculating flow.

Non-reformation conditions could be simulated in the present analysis by taking $\bar{p}_f = 0$, a/b = 0.999 and w/d = 0.001. When the results for load capacity and flow rates, for b/d = 0.5, were compared with those obtained from the non-reformation analysis discussed in Section 3.4, the correlation observed was within 0.5%.

3.6 Conclusions

(1) Prior to the presentation of a cavitation algorithm by Elrod (1981), a refinement of previous work by Elrod and Adams (1974), the delineation of the region of the bearing where the film cavitates was dependent on an explicit reference to some boundary conditions. Normally, film reformation has not been considered; the lubricant has been assumed to be supplied at ambient pressure via a line

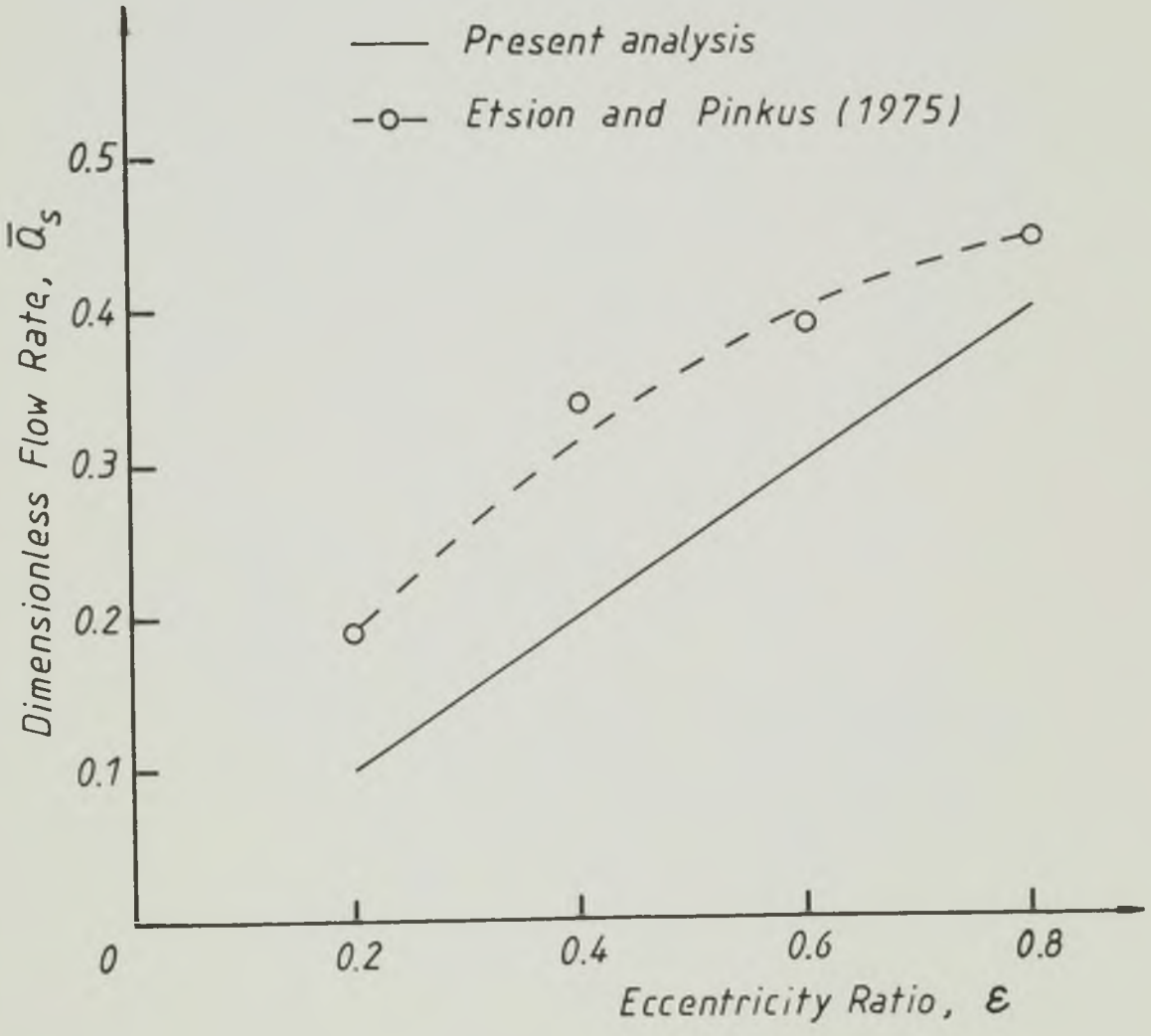

Figure 3.15 A comparison of the predictions of dimensionless side flow rate from the present analysis with those presented by Etsion and Pinkus (1975). b/d = 0.5, a/b = 0.5, $\bar{p}_f = 0$

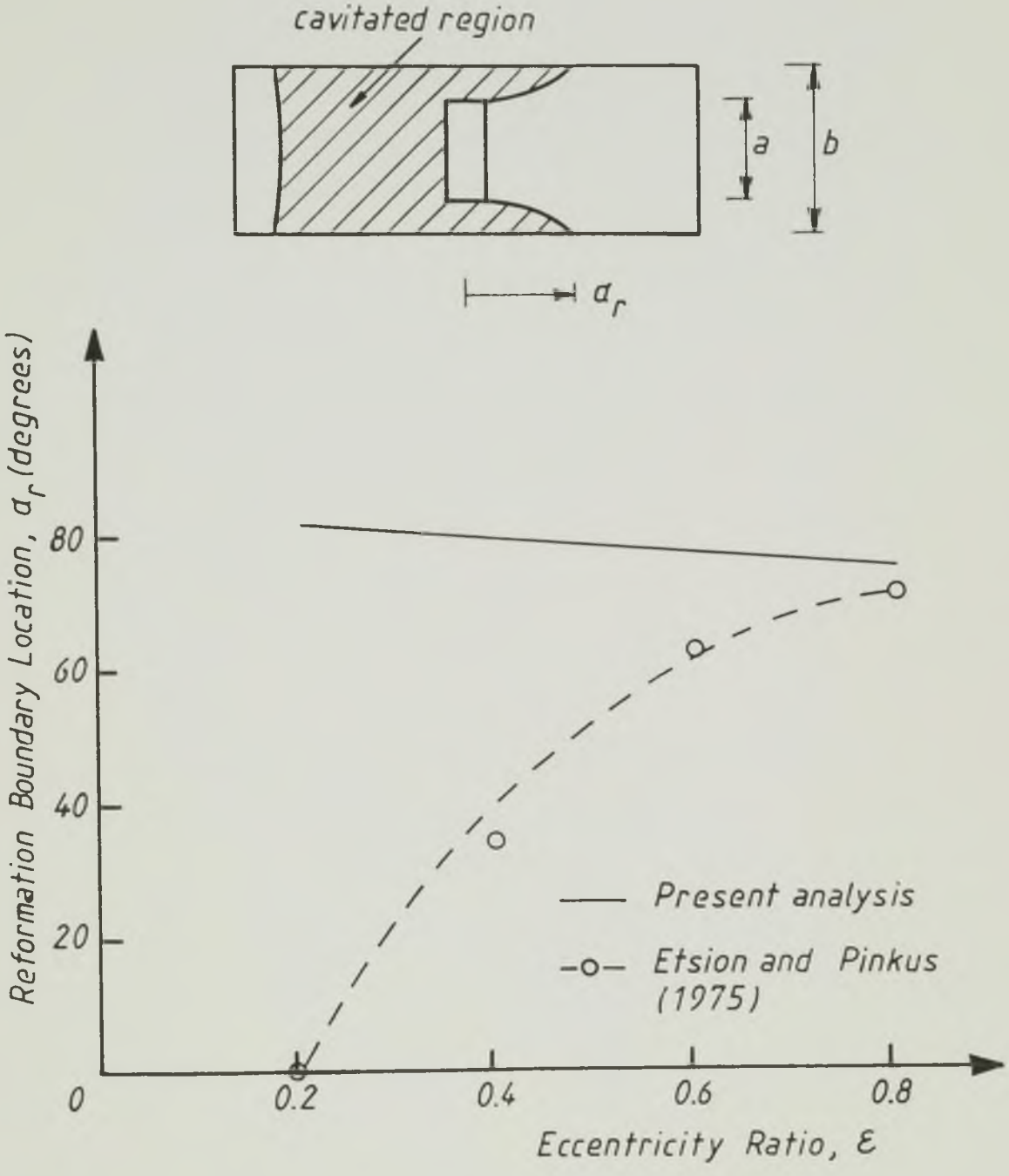

Figure 3.16 A comparison of the predictions of the present analysis for the reformation boundary location with those of Etsion and Pinkus (1975). $b/d = 0.5$, $a/b = 0.5$, $\bar{p}_f = 0$

groove located at the maximum film thickness. A condition based on flow continuity has normally been used to locate the rupture boundary. Such an analysis has been largely adopted for two main reasons:

(i) The difficulties arising from the inclusion of a reformation boundary condition in the numerical analysis

(ii) The fact that the load capacity would not be significantly influenced by the lubricant inlet conditions.

The development of high speed, large storage digital computers made possible the consideration of both the rupture and the reformation boundary conditions. McCallion et al (1971) and Etsion and Pinkus (1975), among others, obtained solutions for finite width journal bearings considering the film inlet conditions. Elrod (1981) proposed a cavitation algorithm which was able to deal with the cavitation region without the explicit formulation of its boundary conditions. Flow continuity was achieved within the cavitation region and across the boundaries. Very satisfactory results of analyses incorporating the Elrod cavitation algorithm were reported by Elrod (1981) and Lebeck (1981).

(2) A technique was developed for the analysis of finite width journal bearings based on Elrod's algorithm. A system of simultaneous equations in finite difference form derived from the application of the algorithm and involving the normalized bearing parameters, was solved over the bearing area using a Gauss-Seidel iterative method.

The case of non-reformation was first considered. A computer program for determining the bearing performance under non-reformation conditions was written. A study of the parameters

affecting the convergence of the Gauss-Seidel iteration was carried out, its conclusions being summarized as follows:

(a) There existed an optimum value for the bulk modulus parameter ($\bar{\beta}$) for quickest convergence which was dependent on (b/d) and (ε). Although affecting the number of cycles for convergence, the value of ($\bar{\beta}$) used did not affect significantly the bearing performance predictions.

(b) A number of tests carried out using the optimum values of ($\bar{\beta}$) suggested that the optimum value for the relaxation factor (R_f) would be about unity. 'Overflow' caused the program operation to be interrupted in most of the cases to which $R_f > 1$.

(c) The tolerance adopted as a compromise between accuracy of the solution and number of cycles required was 10^{-5}.

The predictions of this analysis showed very good correlation with published results.

(3) The analysis was extended to include the lubricant inlet conditions for a single groove at the maximum film thickness. For reasons of accuracy of the solution, a finer mesh (of about 2° intervals) was used over the film reformation region. The flow of lubricant issuing from the groove was calculated directly and the discrepancy between this and the calculated side flow, was used as a measure of the accuracy of the solution. For a grid of (91x19) nodes the discrepancies observed were, in general, within the range 3-5%. At $\bar{p}_f = 0$ and $a/b \leq 0.5$ this discrepancy could, however, go up to a maximum of 6.5%. This was mainly attributable to the inaccurate location of the reformation boundary.

A value of (R_f) of unity and values of ($\bar{\beta}$) within the range (0.01-0.03) resulted, in general, in a minimum number of cycles for convergence of the solution.

Published results of a direct analysis considering the groove geometry and the lubricant supply pressure were not available. Etsion and Pinkus (1975) presented solutions for the lubricant supplied at ambient pressure. Correlation between the predictions of the present analysis and those of Etsion and Pinkus (1975) was not good. This was attributed mainly to their formulation of the flow continuity condition in the film reformation region.

When conditions of non reformation were simulated by taking $\bar{p}_f = 0$, $a/b = 0.999$ and $w/d = 0.001$, the results given by the program were within 0.5% of the predictions of the analysis that considered no reformation.

(4) Only the case of a single groove at the maximum film thickness has been considered. It would not be difficult to extend the analysis to the case of one axial groove at any location or indeed to a consideration of two axial grooves. An iteration would then be required to determine the correct attitude angle, and the cpu time would be greatly increased. Thus, every effort to speed up the convergence of the Gauss-Seidel iteration would be worthwhile.

CHAPTER 4

A COMPARISON OF RESULTS FROM THE PRESENT ANALYSIS WITH THE PREDICTIONS OF ESDU ITEM No. 66023 (1966) AND THE DEVELOPMENT OF DATA CHARTS

4.1 Introduction

Most of the journal bearing design procedures available have been based on numerical solutions of the Reynolds' equation which have incorporated the assumption of lubricant supplied at ambient pressure via a line 'groove' at the location of maximum film thickness. With real lubricant inlet conditions film reformation would be unlikely to occur at the line of maximum film thickness and, therefore, such an assumption will lead to inaccurate predictions of the flow of lubricant in the bearing (Cole and Hughes (1956), McCallion et al (1971), Etsion and Pinkus (1974)). The influence of the lubricant flow rate upon bearing performance as a whole has already been stressed in Chapter 1.

A commonly used procedure for the design of steadily loaded, liquid film, hydrodynamic journal bearings, is the one described in ESDU Item No. 66023 (1966) which has been briefly discussed in Section 2.2. This procedure relied very heavily upon the use of design charts based on data obtained from numerical solutions of the Reynolds equation in which the lubricant inlet conditions were not fully considered .

One objective of the journal bearing analysis undertaken was to carry out an investigation of the correlation of the bearing performance predictions (flow rate in particular) of ESDU Item No. 66023 (1966), with the predictions of a more accurate analysis in which film reformation was considered. For this purpose, computer solutions were obtained for all combinations of the values of the parameters shown in Table 4.1. Additional solutions have been computed for the development of data charts.

Parameter	Values
b/d	0.5, 0.75, 1.0
ε	0.2, 0.4, 0.6, 0.8
a/b	0.5, 0.8, 1.0 (0.999)
w/d	0.2
$\bar{p}_f$	0.0, 0.1, 0.25, 0.5, 1.0

Table 4.1 Values of the Parameters Considered

The maximum value of dimensionless supply pressure considered ($\bar{p}_f$=1.0) corresponded to a bearing with a clearance ratio of 0.002 operating at a journal speed of 500 r.p.m. (8.33 Hz) with a lubricant supplied at 250 kN/m^2 and an effective viscosity of 0.019 N.s/m^2.

The performance predictions computed included:

(i) The dimensionless pressure distribution in the lubricant film

(ii) The dimensionless load carrying capacity ($\bar{W}$)

(iii) The attitude angle (ψ)

(iv) The dimensionless flow rate of lubricant issuing from the groove ($\bar{Q}_{gr}$).

(v) The dimensionless flow rate out from the bearing sides ($\bar{Q}_s$)

(vi) The dimensionless flow rate into the cavitation region ($\bar{Q}_c$)

(vii) The location of the reformation and the rupture boundaries.

The performance predictions (i) to (vi) were printed out (see Appendix B) and the locations of the rupture and the reformation boundaries were shown in a diagram of the 'developed' bearing area. Figure 4.1 shows two of these diagrams for two different operating conditions.

In this chapter, a study of the correlation between results from the analysis undertaken and the predictions of ESDU Item No. 66023 (1966) will be described and the development of data charts based on computer solutions will be discussed.

4.2 A Comparison of the Results for Load Capacity and Attitude Angle

Results for dimensionless load capacity and attitude angle from the present analysis were compared with the predictions of ESDU Item No. 66023 (1966) for all combinations of the values of the parameters shown in Table 4.1. The correlation observed could be summarized as follows:

(a) For non-reformation conditions ($\bar{p}_f$ =0 and a/b=1) the correlation observed for both ($\bar{W}$) and (ψ) was good at all values of (b/d) and (ε) considered.

(b) For realistic lubricant inlet conditions the degree of correlation was dependent on the values of the operating parameters. Figures 4.2 and 4.3 show the comparative results for dimensionless load capacity and attitude angle for fixed b/d=0.5, a/b=0.8 and w/d=0.2 The discrepancies observed were more significant at low values of

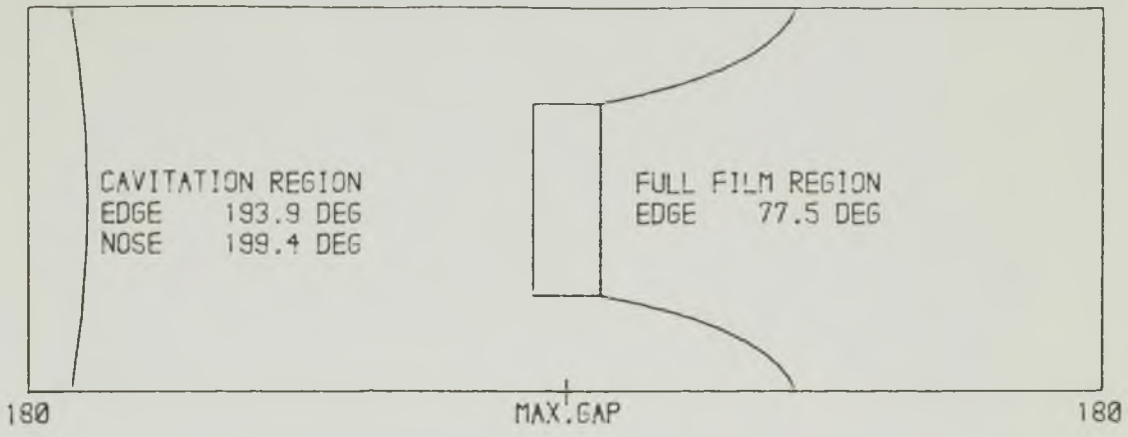

SHAFT ROTATION FROM LEFT TO RIGHT

NORMALIZED SUPPLY PRESSURE = .000

b/d = .500 ECC = .600

a/b = .500 w/d = .200

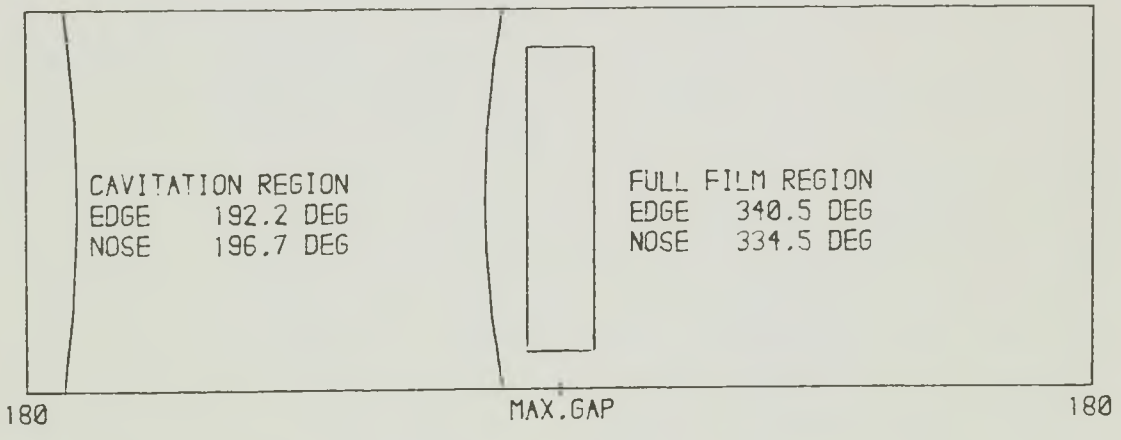

SHAFT ROTATION FROM LEFT TO RIGHT

NORMALIZED SUPPLY PRESSURE = .500

b/d = .500 ECC = .600

a/b = .800 w/d = .200

Figure 4.1 The location of the reformation and the rupture boundaries for two different sets of operating parameters.

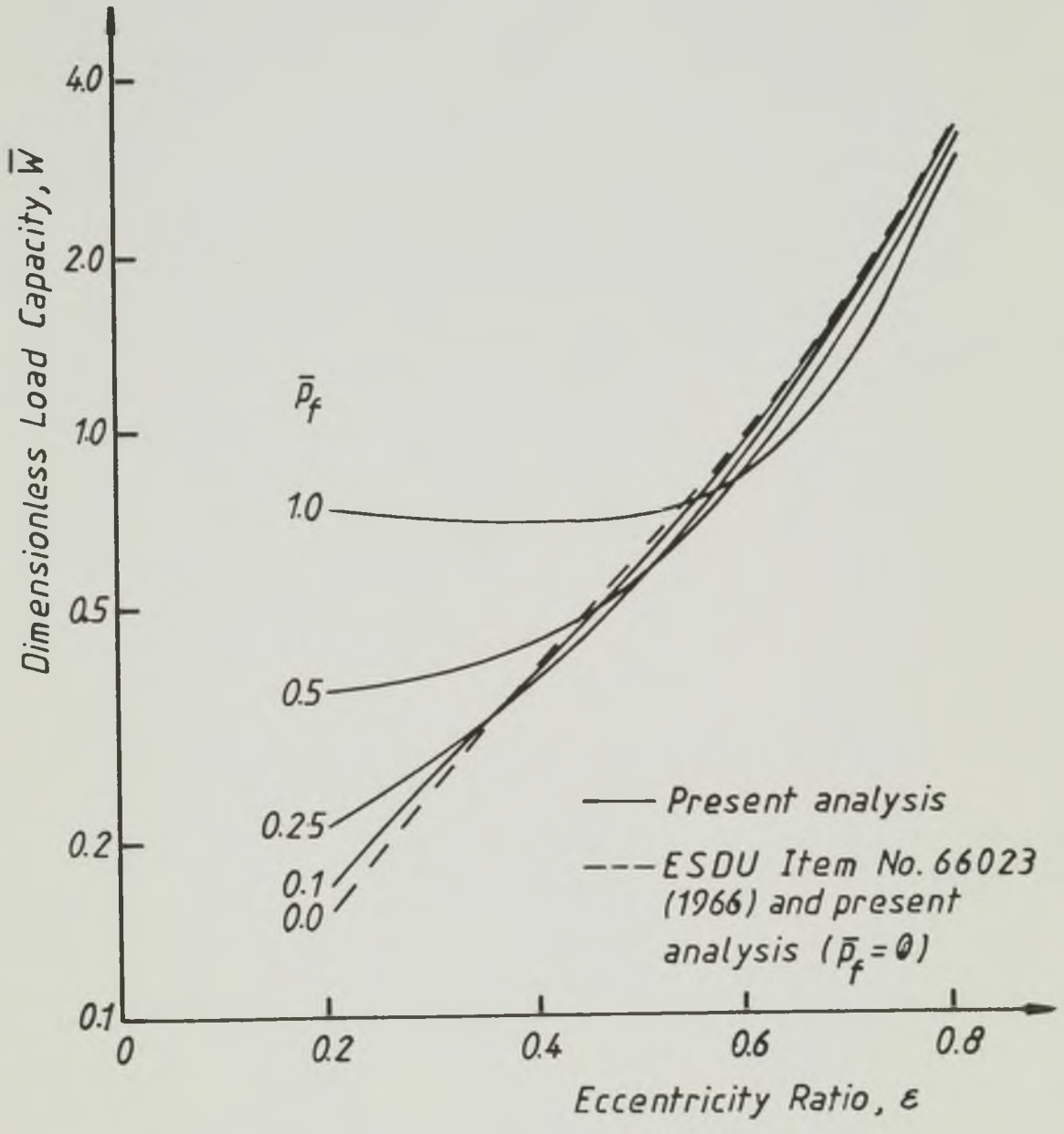

Figure 4.2 Comparison of results for load capacity from the present analysis with the predictions of ESDU Item No. 66023 (1966) b/d = 0.5, a/b = 0.8, w/d = 0.2

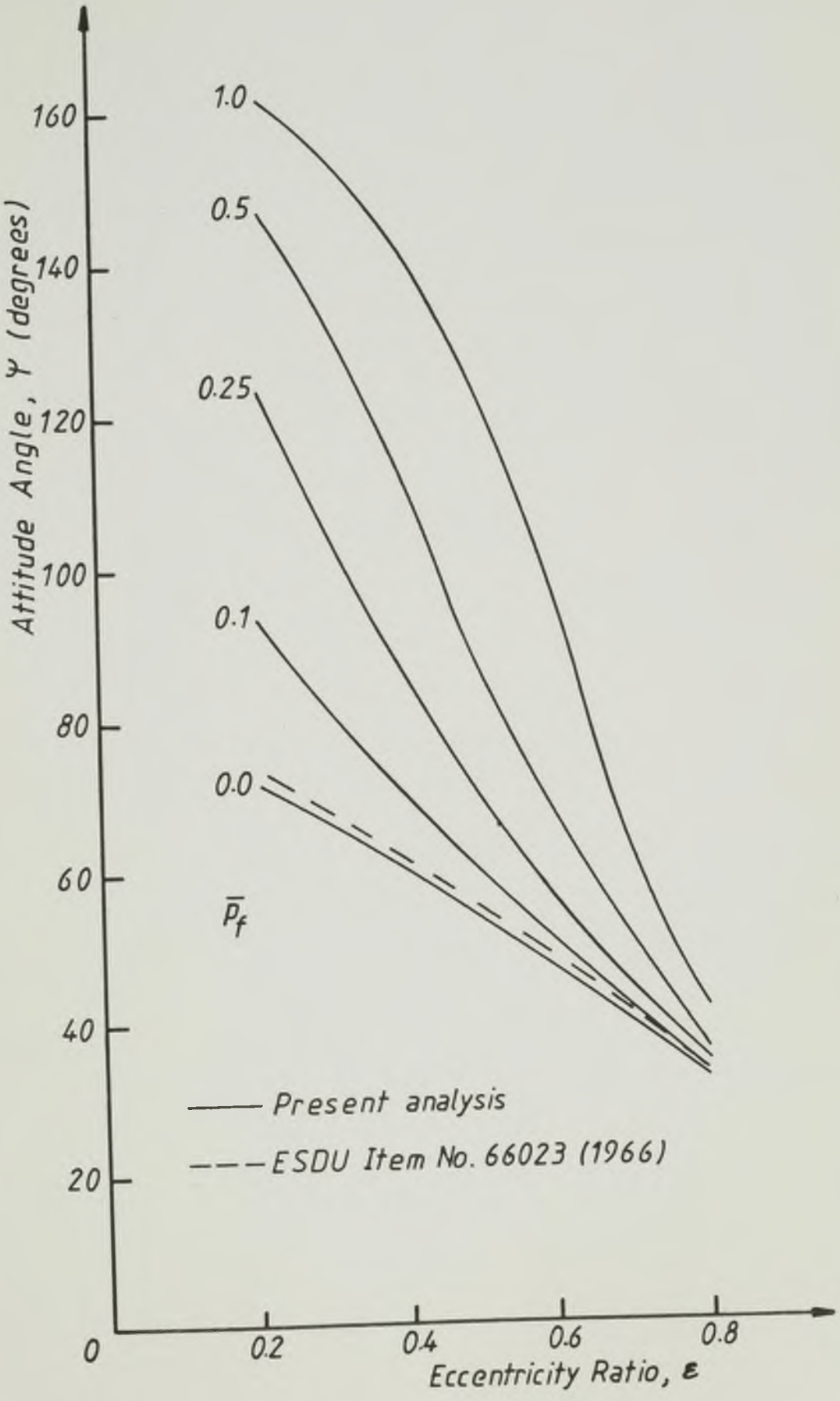

Figure 4.3 Comparison of results for attitude angle from the present analysis with the predictions of ESDU Item No. 66023 (1966)
b/d = 0.5, a/b = 0.8, w/d = 0.2

(ε), increasing for increasing values of ($\bar{p}_f$). This was a consequence of the hydrostatic pressures in the groove region, the significance of which, in comparison with the hydrodynamic pressures developed in the film, was dependent on the lubricant supply pressure and the size of the groove.

This pattern was unchanged at higher values of (b/d), the discrepancies being, however, slightly smaller as (b/d) increased.

(c) Figure 4.4 shows the effect of groove length on the dimensionless load capacity at ambient supply pressure. The discrepancies here were more significant at low values of (ε), increasing for decreasing values of (a/b). Severe 'starved' inlet conditions ($\bar{p}_f$=0, a/b < 0.5) can be seen to affect significantly the load carrying capacity of the bearing at low values of the eccentricity ratio (ε < 0.6).

At finite lubricant supply pressures and low values of (ε) the computer solutions for load capacity were greater than the predictions of ESDU Item No. 66023 (1966) (see Figure 4.2).

In conclusion it can be said that;

(i) The accuracy of the predictions of dimensionless load carrying capacity from ESDU Item No. 66023 (1966) at ambient supply pressure and with a/b $\geq$ 0.5, is good (with a maximum discrepancy of 9%) for all values of (ε) and (b/d) considered. At higher values of ($\bar{p}_f$) the accuracy of the predictions was dependent on ($\bar{p}_f$) and (ε). In general, for a given eccentricity ratio, the degree of accuracy decreased with increasing values of ($\bar{p}_f$), the discrepancies being more significant at low values of (ε). At ε > 0.3 and $\bar{p}_f \leq$ 0.25,

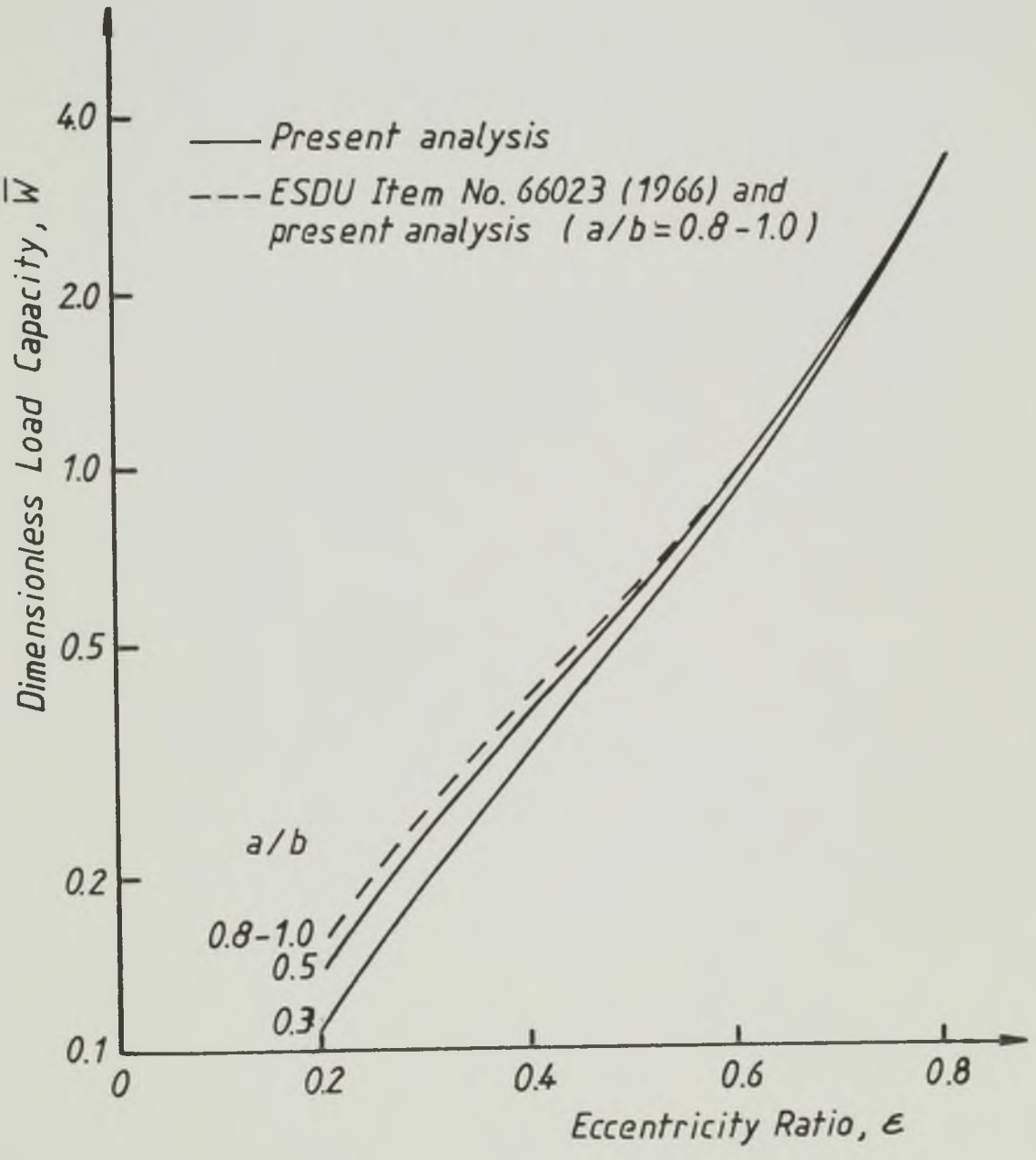

Figure 4.4 Comparison of results for load capacity from the present analysis with the predictions of ESDU Item No. 66023 (1966) b/d = 0.5, w/d = 0.2, $\bar{p}_f = 0$

a practical maximum value of dimensionless supply pressure, the maximum discrepancy observed was about 10%.

(ii) The predictions for atttitude angle of ESDU Item No. 66023 (1966) at $\bar{p}_f=0$ and $a/b \geq 0.8$, were in good agreement with the predictions of the present analysis (with a maximum discrepancy of 4^o), for all values of (b/d) and (ε) considered. At finite values of dimensionless supply pressure significant discrepancies can occur between the predictions of the two procedures. These discrepancies increased with increasing values of $(\bar{p}_f)$ and decreased with increasing values of (ε). However, for practical values of eccentricity ratio and dimensionless supply pressure ($\varepsilon \geq 0.6$ and $\bar{p}_f \leq 0.25$) the discrepancies observed were not significant (8^o at the maximum).

At a limiting value of eccentricity ratio equal to zero there will be no hydrodynamic pressure generated. Hence, the load carrying capacity of the bearing will be a consequence of the hydrostatic pressure in the groove region alone, resulting in an attitude angle of about 180^o.

4.3 Comparison of Results for Side Flow

In ESDU Item No. 66023 (1966) the lubricant flow rate in the bearing was determined as the sum of a 'zero supply pressure' flow (Q_v) with a 'zero speed' flow (Q_p), a method proposed by McKee (1952). (Q_v) was defined as the lubricant flow rate induced into the clearance space by the rotation of the journal. It was actually side leakage but incorporated a correction factor accounting for the length of the groove.

The flow (Q_p) was defined as the flow rate of lubricant forced through the groove, into the bearing, by the supply pressure and was

determined on the assumption of a stationary journal.

At zero supply pressure (Q_p) became zero and the side flow rate, according to ESDU Item No. 66023 (1966), was reduced to (Q_v). Figure 4.5 shows a comparison of results for dimensionless side flow from the present analysis with the predictions of ESDU Item No. 66023 (1966), at b/d=0.5 and $\bar{p}_f$=0. The correlation was good at a/b=1 and a/b=0.8. As (a/b) decreased the discrepancies increased, being about 12% at a/b=0.3 and ε=0.8. The same trend was observed for the other values of (b/d) considered, the discrepancies showing, however, a slight tendency to increase with increasing values of (b/d) for given values of (a/b) and (ε).

At finite lubricant supply pressures the side flow predictions from ESDU Item No. 66023 (1966) were given by (Q_p+Q_v). The presence of the viscosity of the lubricant in the formula giving the flow rate (Q_p), made a comparison of flows in dimensionless terms difficult, thus preventing a comparative study of results for a wide range of operating conditions. The option left was to compare the dimensional side flow rates at different operating conditions. A bearing with the following specifications was considered:

d = 50 mm

b/d = 0.5

C_d/d = 0.0015

Journal speed = 800 r.p.m. (13.33 Hz)

Single groove at the maximum film thickness

a/b = 0.4 and a/b = 0.8

w/d = 0.2

The oil supply pressures chosen were 150 kN/m^2 and 300 kN/m^2 and the oil characteristics were as follows

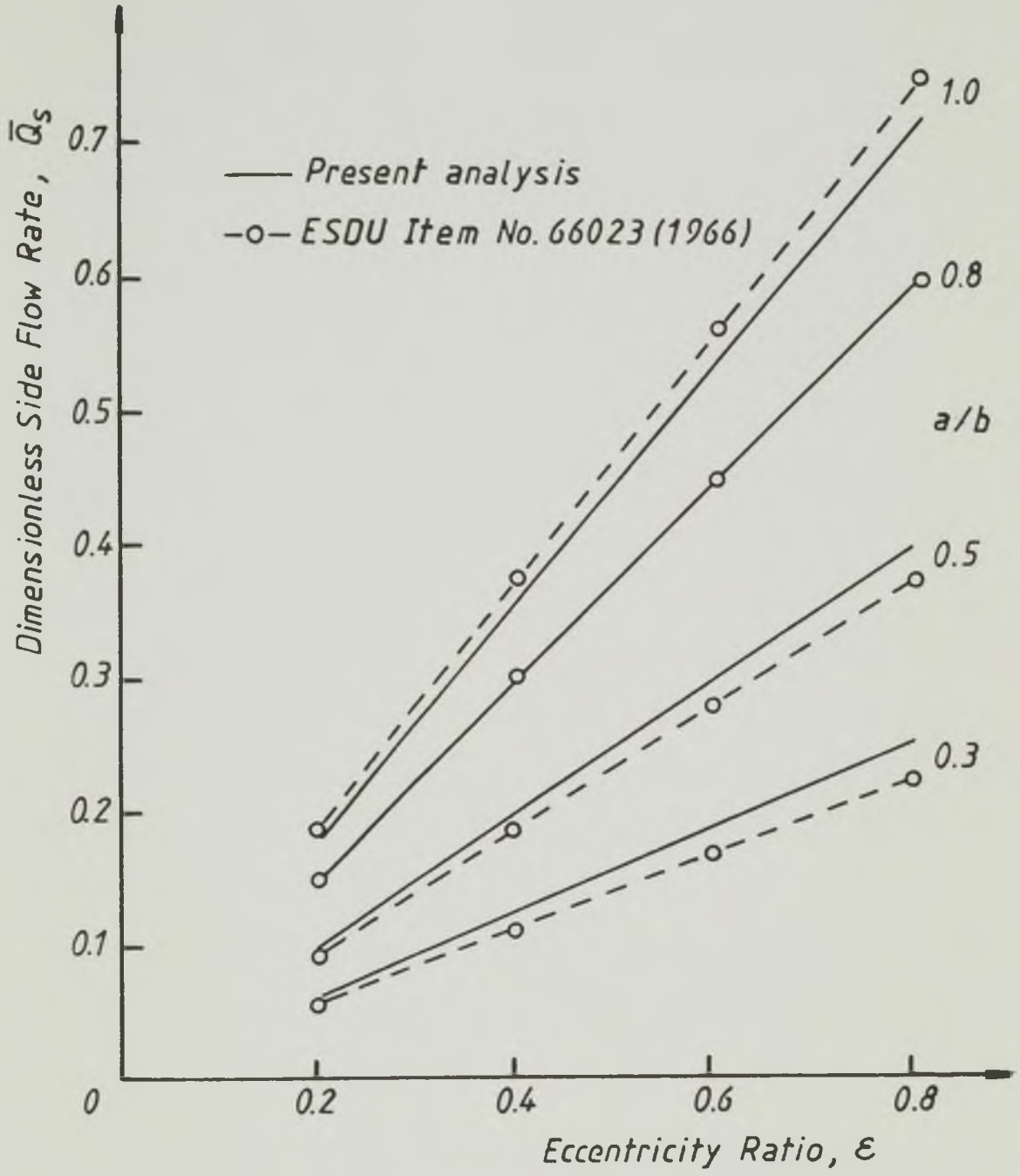

Figure 4.5 Comparison of results for dimensionless side flow from the present analysis with the predictions of ESDU Item No. 66023 (1966), at zero supply pressure.
b/d = 0.5, w/d = 0.2

Kinematic viscosity at $40^{o}C$ - 25.88 cSt ($25.88 \times 10^{-6} m^2/s$)

Kinematic viscosity at $100^{o}C$ - 4.64 cSt ($4.64 \times 10^{-6} m^2/s$)

Density at $20^{o}C$ - 867.5 Kg/m^3

For each combination (p_f, a/b) the side flow rate at various loading conditions was determined according to the ESDU Item No. 66023 (1966) procedure. The value of the effective viscosity of the oil determined in each case was then used to obtain the dimensionlesss supply pressure ($\bar{p}_f$). The values of ($\bar{p}_f$) and (ε) thus found, along with the parameters (b/d), (a/b) and (w/d), were used in the computer solutions from the present analysis.

A comparison of results for the supply pressure p_f=150 kN/m^2 is shown in Figure 4.6. Good correlation was observed at a/b=0.8. At a/b=0.4 the correlation was not so good, discrepancies of 10% to 16% were observed. At p_f=300 kN/m^2 good correlation was observed for both a/b=0.8 and a/b=0.4 (with a maximum discrepancy of about 5%).

The conclusions of a comparison of results for side flow rate from the present analysis with the predictions of ESDU Item No. 66023 (1966) may be summarized as follows:

(i) At zero lubricant supply pressure and a/b=0.8, a common value, the correlation was good for all values of (b/d) considered. Increasing discrepancies were observed at decreasing values of (a/b). At a/b=0.3, b/d=0.5 and ε=0.8, a discrepancy of about 12% was observed.

(ii) At finite supply pressures, a comparison of results for a wide range of operation conditions was not possible. For a given bearing specification results for dimensional side flow rate at

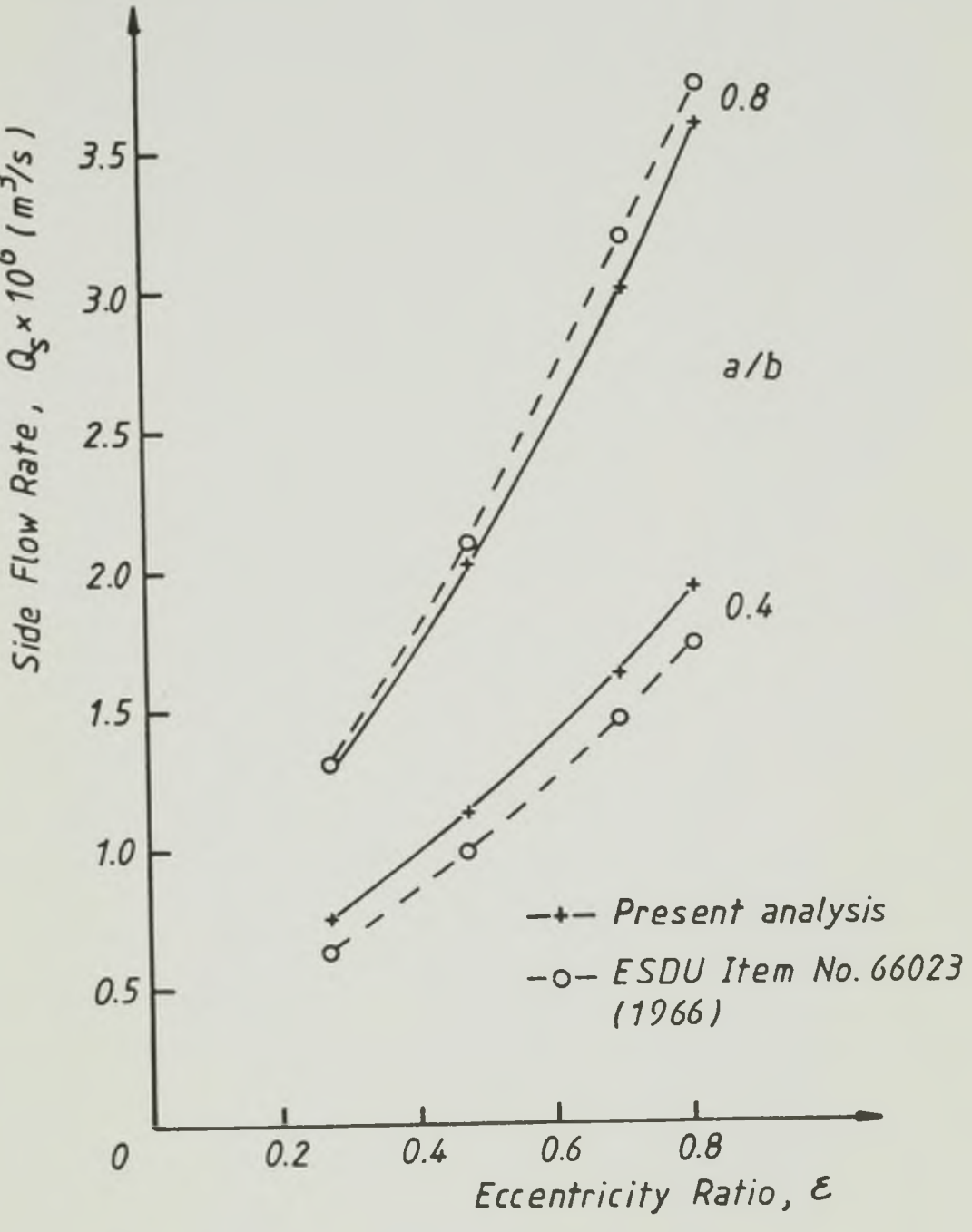

Figure 4.6 Comparison of results for side flow from the present analysis with the predictions of ESDU Item No. 66023 (1966), at a supply pressure p_f = 150 kN/m^2.

the supply pressures of 150 kN/m^2 and 300 kN/m^2, and a/b=0.4 and a/b=0.8, were compared showing acceptable agreement (within 5%) with the exception of the case where a/b=0.4 and p_f=150 kN/m^2 in which discrepancies of 10% to 16% were observed.

4.4 The Development of Charts for Predicting the Dimensionless Load Capacity

Data charts for predicting the dimensionless load capacity and the dimensionless side flow rate were developed from a matrix of computer solutions.

The independent parameters involved were five: (b/d), (ε), (a/b), (w/d) and ($\bar{p}_f$). The parameter (w/d), when in the range (0.1 - 0.3), was not expected to influence significantly the load capacity of the bearing. The charts were drawn from solutions in which (w/d) was fixed at the value 0.2 and were subsequently checked against solutions for random values of the parameters, including values of (w/d) varying in the range (0.1 - 0.3).

Attempts made to incorporate the four remaining parameters in only one chart were unsuccessful. Therefore it was necessary to construct a number of charts incorporating three of the four parameters, one chart for each value of the parameter omitted. The parameters finally chosen to be incorporated in each chart were (ε), (b/d) and (a/b). One chart was drawn for each value of ($\bar{p}_f$).

It was realised that, from a bearing design stand-point, it would have been more convenient to have a number of charts, each for a particular value of (b/d), incorporating the parameter ($\bar{p}_f$) instead. This type of chart has been shown to be inconvenient for practical use due to the relatively small effect of ($\bar{p}_f$) on load capacity at high

eccentricity ratios (see Figure 4.2).

The dimensionless load capacity charts developed are shown in Figures 4.7 to 4.9. They may be used for values of the parameters varying in the following ranges;

(ε)	0.2 to 0.8
(b/d)	0.5 to 1.0
(a/b)	0.3 to 0.8
(w/d)	0.1 to 0.3

and for values of $(\bar{p}_f)$ of 0.0, 0.25 and 0.5.

The charts were constructed as follows. For each value of $(\bar{p}_f)$ a basic chart was drawn from a matrix of computer results obtained for variable values of (ε) and (b/d) and fixed a/b=0.8 and w/d=0.2. The correction curves for values of (a/b) smaller than 0.8 were then drawn such that, at a fixed value of b/d=0.7, the value of $(\bar{W})$ corresponding to a given pair of values (ε, a/b) should be read on the b/d=0.7 line. The way the charts should be used is indicated in each Figure.

Each chart was tested for at least twenty five random combinations of the values of the parameters (ε), (b/d), (a/b) and (w/d). The accuracy varied from chart to chart. The maximum error in the prediction of load capacity detected when using the chart for $\bar{p}_f$=0.0 was ± 1.8% and for $\bar{p}_f$=0.25 was ± 3%. For $\bar{p}_f$=0.5 the error detected was usually not bigger than ±2.5%, maximum errors of 7% were, however, detected for low values of (a/b) at lower values of (ε) ($\varepsilon < 0.4$, $a/b < 0.5$).

At higher values of $(\bar{p}_f)$ and low eccentricity ratios, the influence of (a/b) on load capacity became more and more significant as (ε) decreased and the curves of constant (a/b) were dependent on the

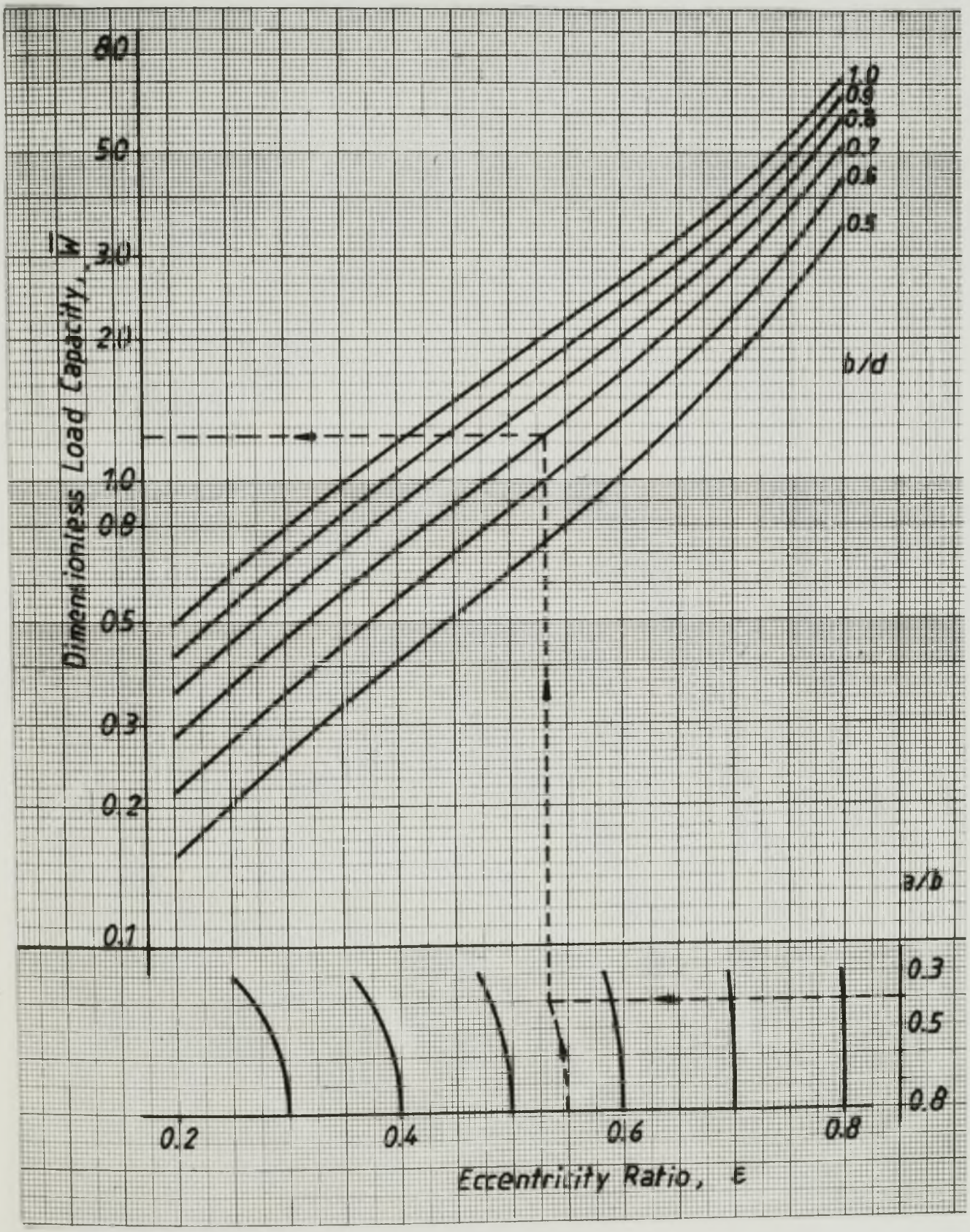

Figure 4.7 Dimensionless load capacity chart.
Valid for (w/d) in the range (0.1-0.3)
and $\bar{p}_f = 0.0$

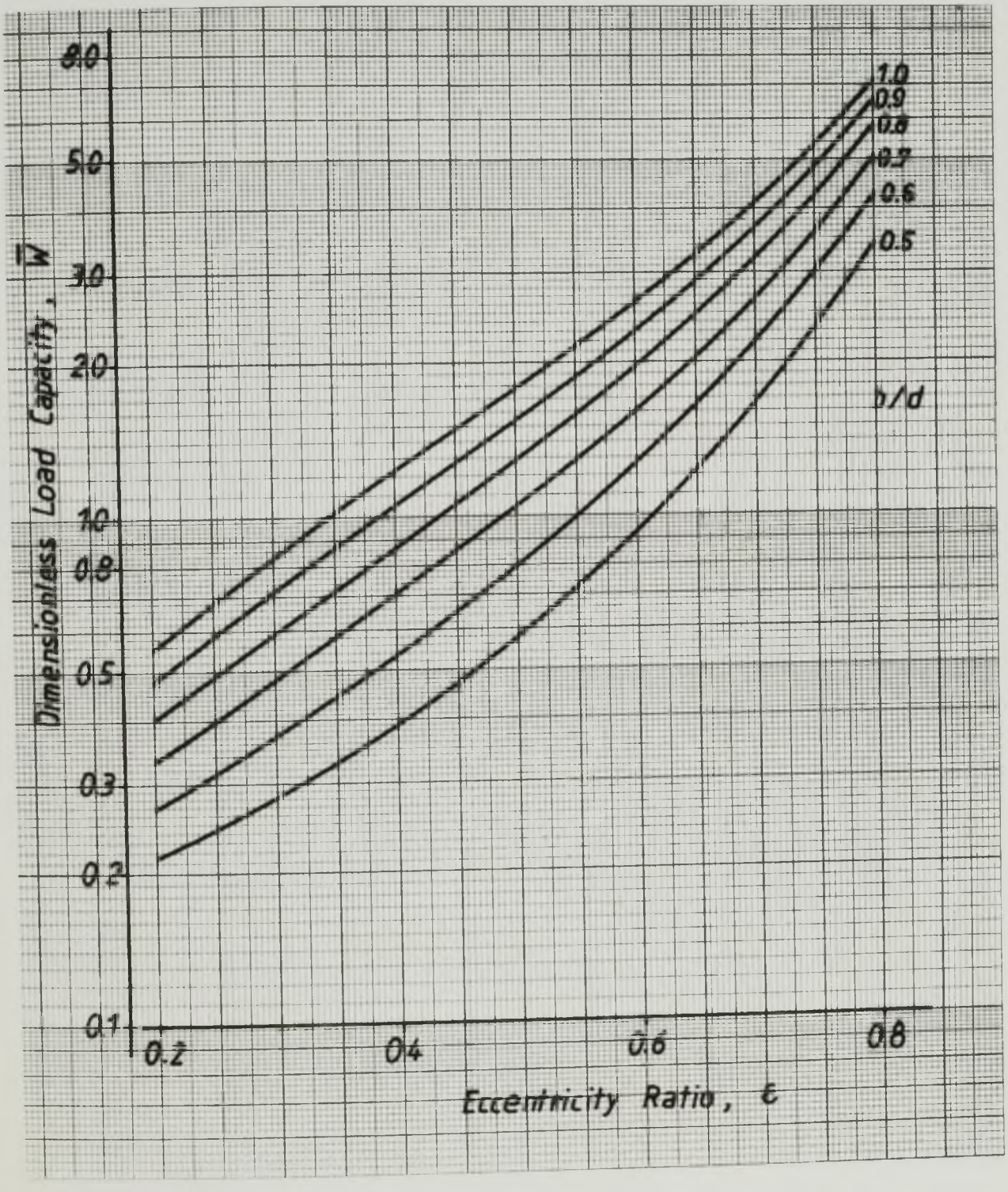

Figure 4.8 Dimensionless load capacity chart.
Valid for (w/d) in the range (0.1-0.3),
(a/b) in the range (0.3-0.8) and $\bar{p}_f = 0.25$

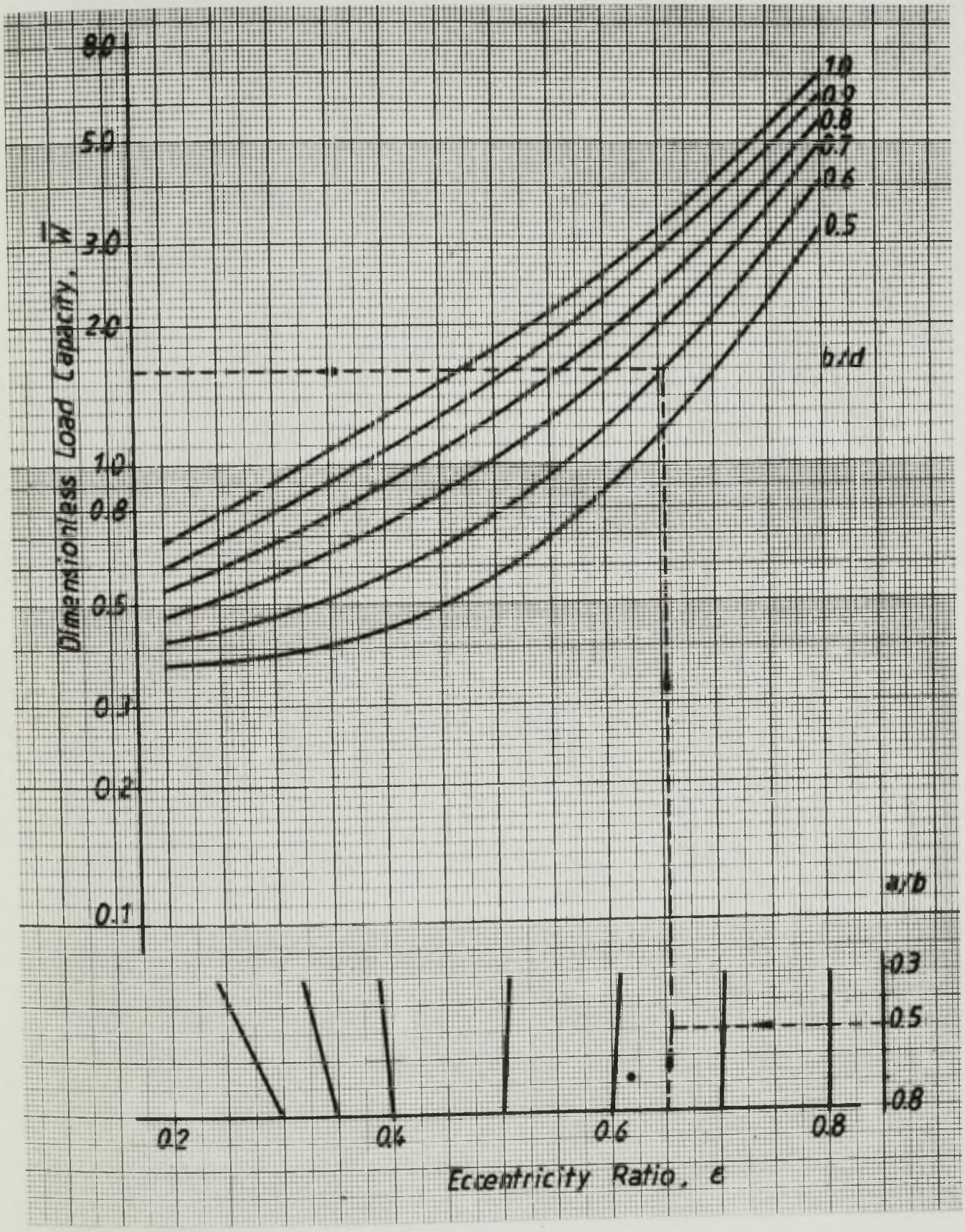

Figure 4.9 Dimensionless load capacity chart. Valid for (w/d) in the range (0.1-0.3) and $\bar{p}_f = 0.5$

value of (b/d). This made the construction of a load capacity chart for $\bar{p}_f$=1.0, giving acceptably accurate predictions at low values of (a/b) and (ε), impossible. It would still be acceptably accurate at high values of (ε), but for such situations the effect of (a/b) on load capacity was not very significant (see Figures 4.7 to 4.9). It was therefore decided not to include a chart for load capacity predictions at $\bar{p}_f$=1.0.

Computer solutions for dimensionless load capacity at a/b=0.8 and w/d=0.2 are included in a table of bearing performance predictions given in Appendix C.

4.5 The Development of Charts for Predicting the Dimensionless Side Flow Rate

Here again it was not possible to find a satisfactory way of incorporating more than three independent parameters in one chart. The chart developed for dimensionless side flow predictions incorporated the parameters (b/d), (ε) and ($\bar{p}_f$), and was drawn for fixed values of a/b=0.8 and w/d=0.2. The chart, shown in Figure 4.10, was obtained as follows. The lines of constant flow rate were based on a matrix of results for dimensionless side flow at b/d=0.75, a/b=0.8, w/d=0.2 and variable (ε) and ($\bar{p}_f$). Points on those lines were defined by the function $\bar{Q}_s$ ($\bar{p}_f$) at a given (ε). The parameter (b/d) was then introduced in the chart. The curves for constant dimensionless supply pressure, on the left hand side of Figure 4.10, represented the effect of (b/d) on side flow rate for a given eccentricity ratio. Each pressure curve was drawn in such a way that, for given values of (b/d) and (ε), the intersection of the horizontal dashed line - corresponding to the pair of values (b/d, $\bar{p}_f$) - with the vertical dashed line corresponding to the value of (ε), indicated the known value of ($\bar{Q}_s$).

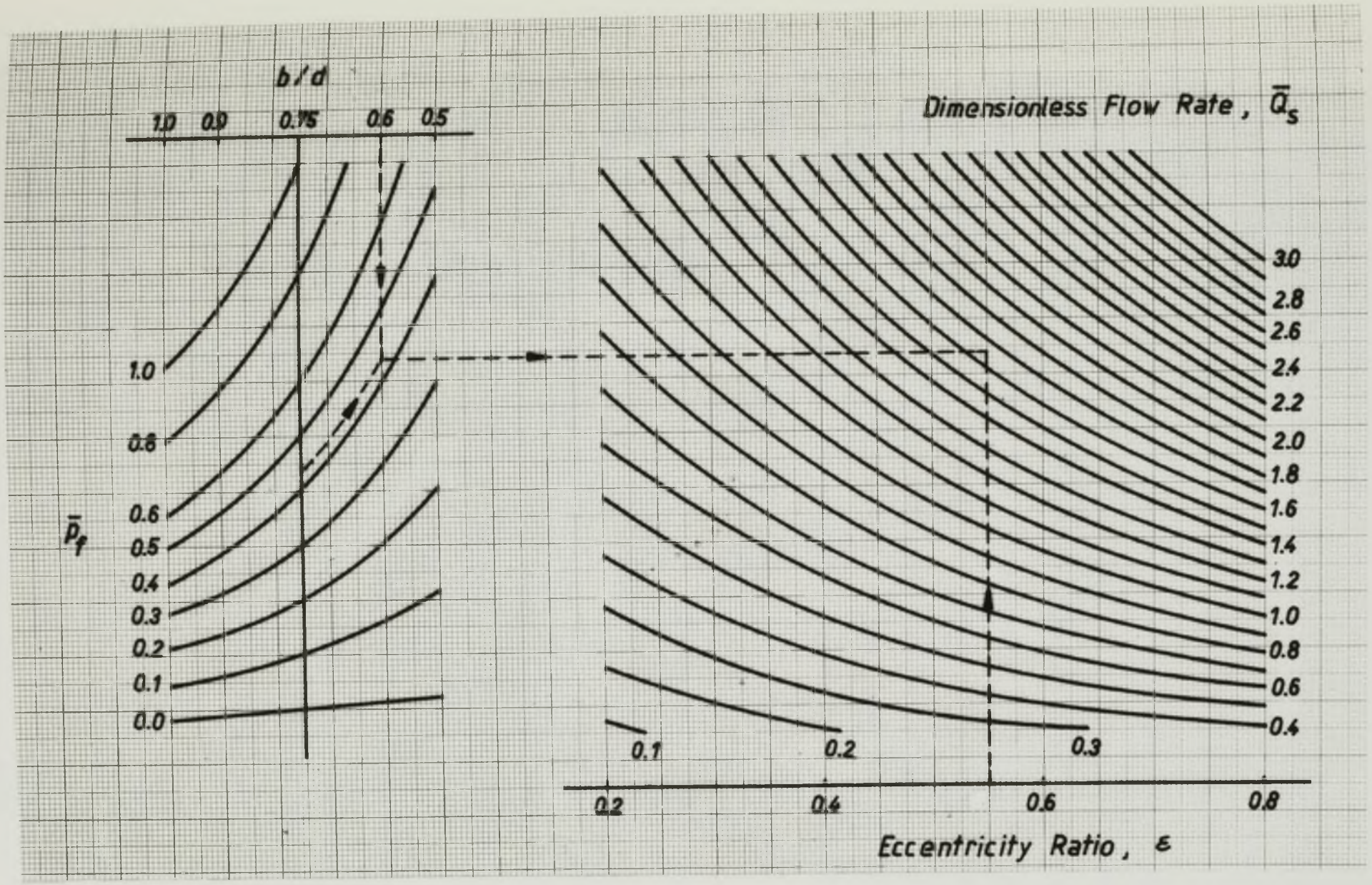

Figure 4.10 Dimensionless side flow chart. Valid for a/b = 0.8 and w/d = 0.2

Checks carried out for various values of (ε) and fixed values of (b/d) and ($\bar{p}_f$), showed that the constant pressure curves were independent of (ε), a feature required for the success of this type of chart.

Figure 4.10 may therefore be used to obtain dimensionless side flow predictions for journal bearings with a single oil groove at the maximum film thickness and fixed values of $a/b=0.8$ and $w/d=0.2$. However, both (a/b) and (w/d) affected the side flow rate. The possibility of predicting the dimensionless side flow by affecting the value read out from Figure 4.10 by some factor accounting for values of (a/b) and (w/d) not equal to 0.8 and 0.2 respectively was investigated. It was found that at fixed values of $b/d=0.75$ and $a/b=0.8$, and for (w/d) varying in the range (0.1-0.3), the ratio $q_w = \bar{Q}_s/\bar{Q}_{chart}$ (where $\bar{Q}_s$ is the dimensionless side flow rate for the specified operating parameters and $\bar{Q}_{chart}$ is the value given by Figure 4.10), was dependent on (w/d) and ($\bar{p}_f$) but was almost unaffected by the values of (ε) or (b/d).

The ratio (q_w) was plotted against values of (w/d) for various values of ($\bar{p}_f$). This diagram, which allowed the determination of the 'groove width flow factor' (q_w) for values of (w/d) in the range (0.1-0.3) and for fixed $a/b=0.8$, is shown in Figure 4.11.

A similar reasoning for a fixed value of $w/d=0.2$ and variable values of (a/b) in the range (0.3-0.8) led to the construction of a diagram for the determination of the 'groove length flow factor' (q_a), also defined by the ratio ($\bar{Q}_s/\bar{Q}_{chart}$). This diagram is shown in Figure 4.12.

Because of the process used to construct the dimensionless flow chart (Figure 4.10) and the diagrams of Figures 4.11 and 4.12, predictions of dimensionless side flow rate were only possible for values of $a/b=0.8$ and (w/d) within the range (0.1-0.3) or for $w/d=0.2$ and (a/b) within the

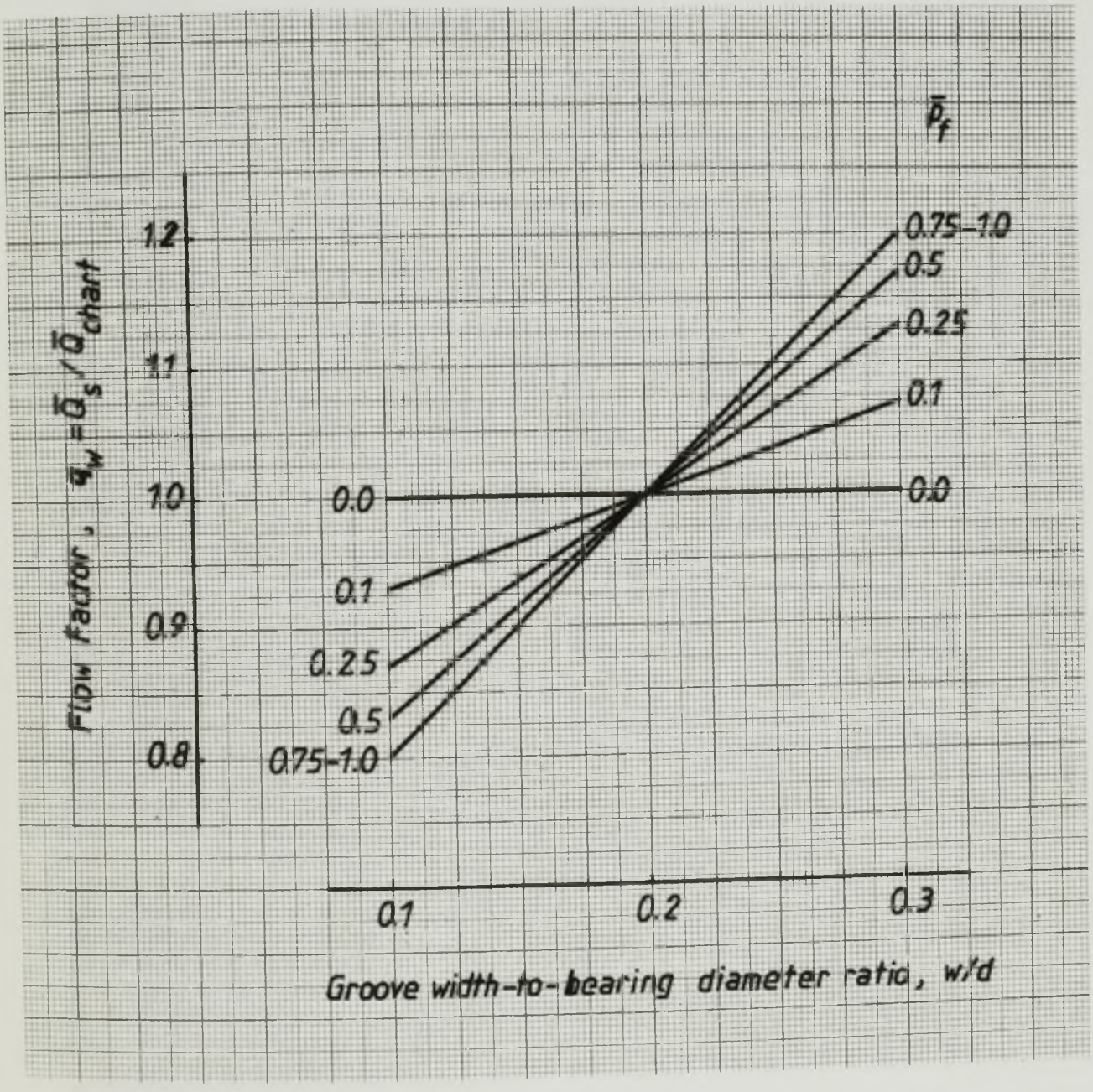

Figure 4.11 Groove width flow factor (q_w).
Valid for a/b = 0.8 only

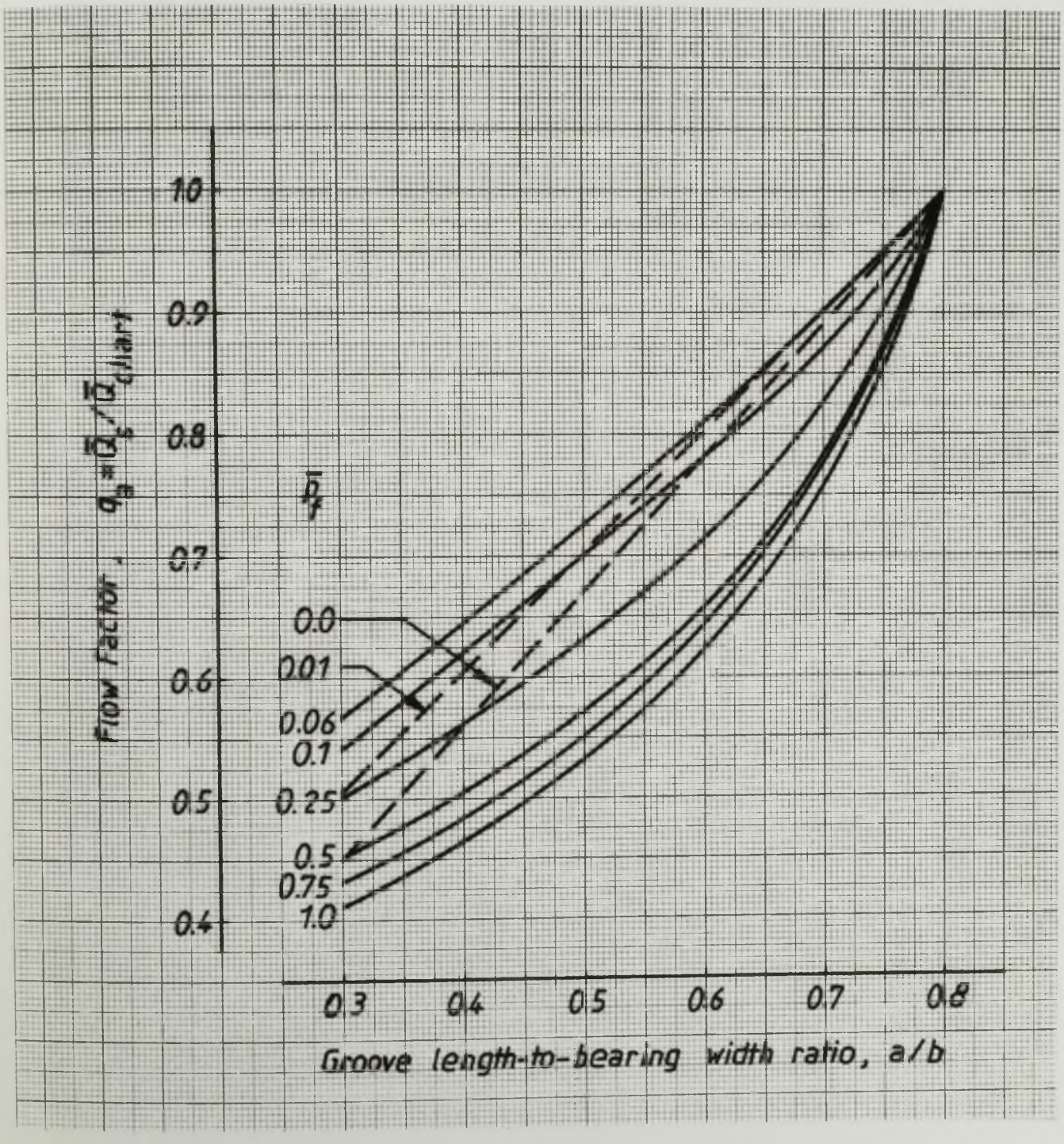

Figure 4.12 Groove length flow factor (q_a).
Valid for w/d = 0.2 only

range (0.3-0.8).

For values of (a/b) and (w/d) satisfying this condition and for any combinations of the parameters (b/d), (ε) and ($\bar{p}_f$) within the limits of the chart, the dimensionless side flow rate was obtained from

$$\bar{Q}_s = \bar{Q}_{chart} \times \text{Flow Factor } (q_w \text{ or } q_a)$$

The accuracy of the predictions for side flow rate from Figures 4.10 to 4.12 was checked against computer solutions for more than sixty random combinations of values of the parameters. The error incorporated in these predictions was generally found to be in the range ±2% to ±4% and the maximum error detected was ±5%.

Computer solutions for dimensionless side flow rate at a/b=0.8 and w/d=0.2 are given in Appendix C.

4.6 Predictions of the Attitude Angle and the Location of the Cavitation Boundaries

Predictions of the attitude angle and the location of the reformation and the rupture boundaries from the present analysis are given in Appendix C, for fixed values of a/b=0.8 and w/d=0.2.

4.7 Conclusions

(1) One objective of the present journal bearing analysis was to carry out an investigation on the correlation between the performance predictions from ESDU Item No. 66023 (1966), in which film reformation was not considered, and those which incorporated the lubricant inlet conditions. The conclusions of such a study for the predictions of dimensionless load capacity, attitude angle and side flow rate can be summarized as follows:

(a) Dimensionless Load Capacity.

At ambient supply pressure the correlation between the predictions of dimensionless load capacity of the two procedures was good at values of groove length-to-bearing width ratio (a/b) greater than or equal to 0.5, for all values of eccentricity ratio.

Severe 'starved' inlet conditions ($\bar{p}_f$=0, a/b < 0.5) were shown to affect the dimensionless load capacity significantly at low values of eccentricity ratio (ε <0.6).

At finite values of dimensionless supply pressure the degree of correlation varied with ($\bar{p}_f$) and (ε). In general, for a given eccentricity ratio the degree of correlation decreased with increasing values of ($\bar{p}_f$), the discrepancies being more significant at low values of (ε). Figure 4.13 shows the degree of correlation between the predictions of the two procedures within regions of variation of the parameters. The predictions of the present analysis were taken as the reference values. The two diagrams were based on results shown in Figures 4.2 and 4.4 for fixed b/d=0.5. In general, at increasing values of (b/d) the maximum discrepancy in each region decreased.

(b) Attitude Angle.

At ambient supply pressure and (a/b) greater than or equal to 0.8, there was good correlation between the predictions of attitude angle from the two procedures. At finite values of ($\bar{p}_f$) large discrepancies can occur at low values of eccentricity ratio and high values of dimensionless supply pressure. For practical operating conditions ($\varepsilon \geq 0.6$, $\bar{p}_f \leq 0.25$) the maximum discrepancy was about 8°.

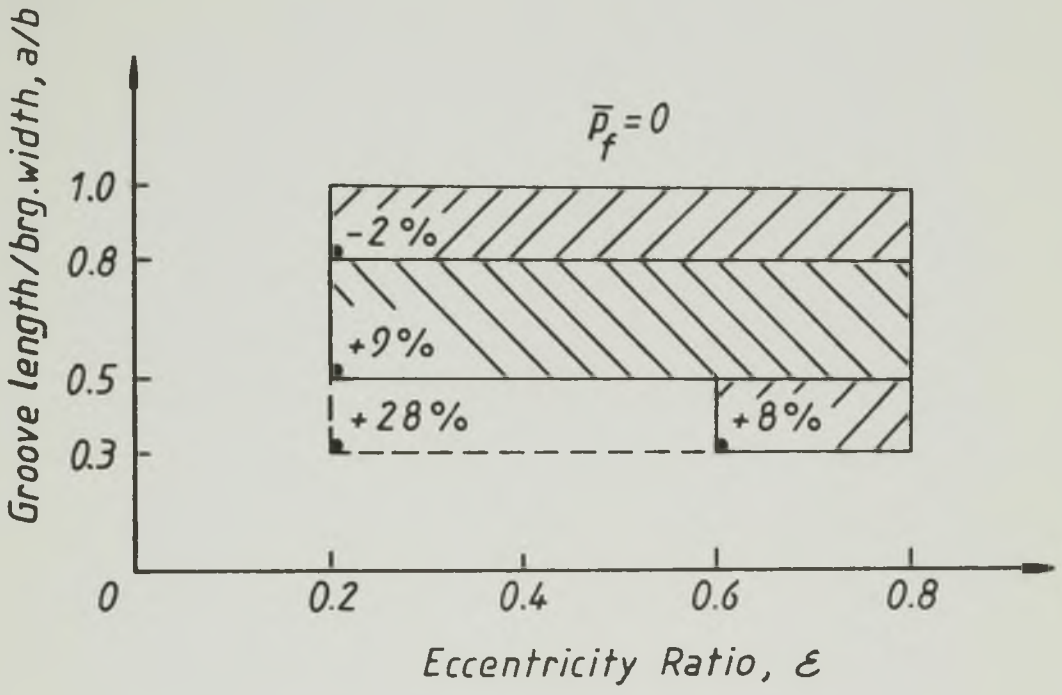

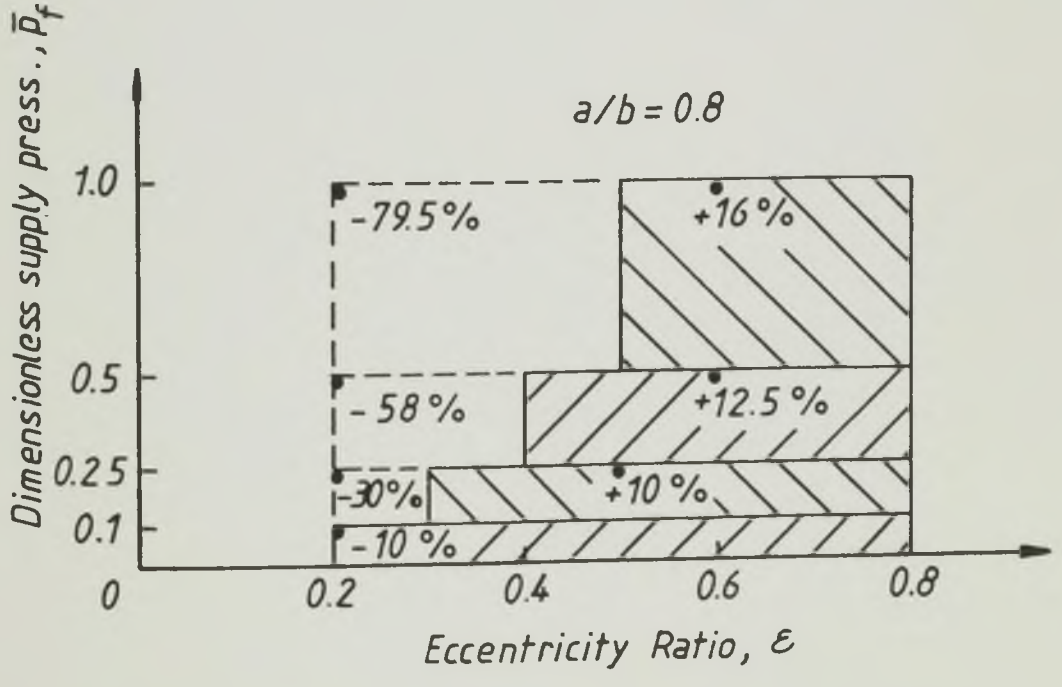

Figure 4.13 The degree of correlation between the predictions of dimensionless load capacity from ESDU Item No. 66023 (1966) and those of the present analysis (taken as the reference values). The points indicate the conditions at which the maximum discrepancy in each region occurred.

(c) Side Flow Rate.

The side flow rate at ambient supply pressure obtained from ESDU Item No. 66023 (1966), (Q_v), was based on solutions for a full width film at the inlet which were multiplied by the factor (a/b). A comparison of the predictions of dimensionless side flow rate at ambient supply pressure of ESDU Item No. 66023 (1966) with those of the present analysis for a range of values of (a/b) and (ε), showed good agreement. The observed discrepancies increased as (a/b) decreased being only slightly affected by the value of (ε). For b/d=0.5 and a/b=0.8 no significant discrepancy occurred and a maximum difference of about 12% was observed at a/b=0.3.

The use of the correction factor (a/b) by ESDU Item No. 66023 (1966) for the determination of the side flow rate (Q_v), appeared to give a remarkably good approximation to the predictions of the present analysis which incorporated flow reformation considerations. Neglecting flow inlet conditions can cause significant errors on side flow rate as pointed out by Cole and Hughes (1956), McCallion et al (1971), Etsion and Pinkus (1975) and others. Figure 4.5 shows that such errors can be as large as 25% at a/b=0.8 and 66% at a/b=0.3.

At finite supply pressures, a comparison of a few results for the dimensional side flow rate obtained for combinations of moderate and high values of supply pressure and (a/b), showed good correlation (within 5%) in all cases but one, in whcih discrepancies of 10% to 16% were observed.

(2) Charts for dimensionless load capacity and dimensionless side flow predictions were developed from a matrix of computer solutions for combinations of the five independent parameters (b/d), (ε), (a/b), (w/d) and ($\bar{p}_f$). A table of performance predictions for variable values of ($\bar{p}_f$), (b/d) and (ε) and fixed values of a/b=0.8 and w/d=0.2, is given in Appendix C.

CHAPTER 5

DESCRIPTION AND COMMISSIONING OF THE EXPERIMENTAL APPARATUS

5.1 Introduction

The bearing analysis presented in this thesis, which incorporates a consideration of the lubricant supply conditions, has provided theoretical predictions for the performance of hydrodynamic journal bearings with a single axial groove (or oil hole) located at the position of maximum film thickness.

An experimental apparatus was conceived and designed with the purpose of obtaining experimental measurements of side flow rate and of the location of the rupture and of the reformation boundaries thus enabling a study of the correlation between present theory and experiments to be carried out. The test facility was required to allow a visualization of the flow in the bearing and to enable variation of eccentricity ratio, shaft rotational speed and oil supply pressure. A number of existing glass bushes of width-to-diameter ratio equal to unity were to be used as the test bearings.

The alternative of setting the bearing for a given value of eccentricity ratio was preferred to that of applying a known load and determining the resulting eccentricity ratio. This avoided predictable difficulties in the measurement of the minimum film thickness. It was

recognised in the early stages of the design that the success of the apparatus would depend on its ability to allow bush settings at various values of eccentricity ratio with good accuracy. It was found during the commissioning of the apparatus that the solution adopted did not result entirely as intended at the design stage but proved, nevertheless, to be satisfactory for the purposes of the experimental programme.

A description of the experimental apparatus and associated equipment, the measurement techniques used and the results of the commissioning tests will be presented in this chapter.

5.2 General Assembly of the Apparatus

A photograph of the experimental apparatus is shown in Plate 5.1. Basically it consisted of two brackets; a fixed bracket (1) which supported the main shaft assembly, and a floating bracket (2) supporting the glass bush mounting assembly. The position of the floating bracket with respect to the fixed bracket was dependent on the thicknesses of an interchangeable packing plate (3) and of a pair of interchangeable packing blocks (4). According to the design, a pre-selected eccentricity of the test bush could be obtained by using packing blocks and a packing plate of adequate thicknesses.

A steel shaft (5) was mounted on two SKF 30311 taper roller bearings which were pre-loaded to remove any radial clearance and to increase their stiffness. The pre-loading system (6) consisted of six helical springs, each having a spring constant of 93 kN/m, the force of which was transmitted to the bearing through the end cap (7). The shaft was driven through a speed increasing pulley system by a 1.1 kW motor (8) of infinitely variable speed controlled by a Fenner control unit.

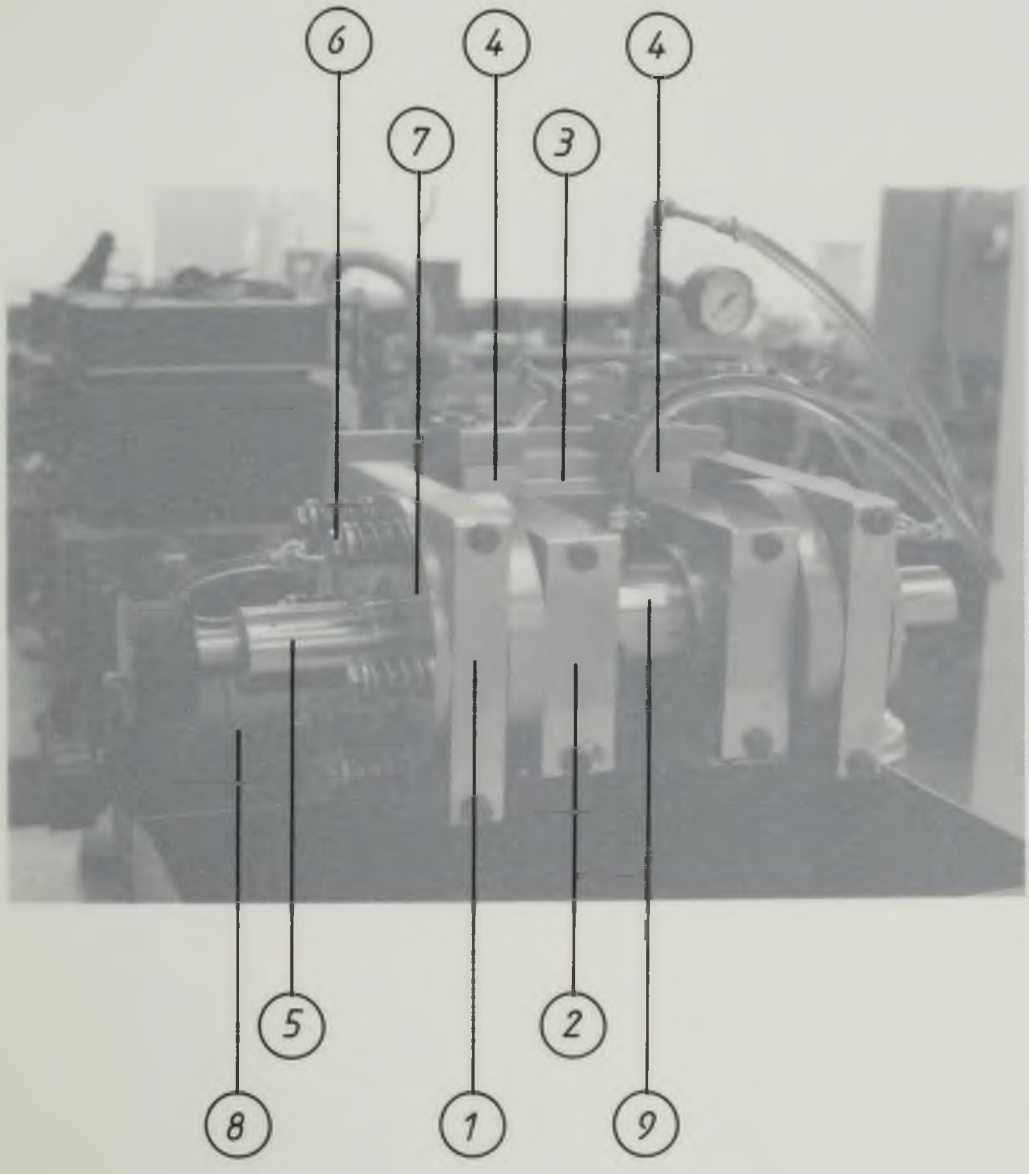

Plate 5.1 A photograph of the experimental apparatus

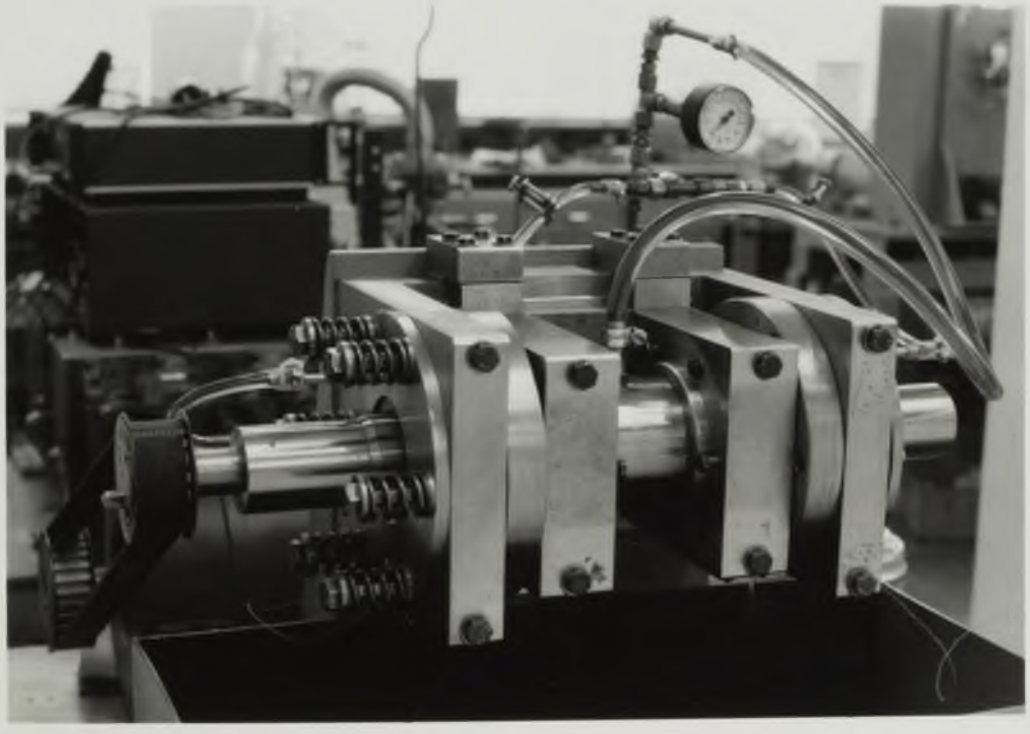

Plate 5.1 A photograph of the experimental apparatus

The test bush (9) was mounted on brass clamp sleeves (10) as shown in Figure 5.1. The clamp sleeves were pulled against the tapered ends of the glass bushes by means of six clamping screws (11), three on each side, 120° apart. In addition, six adjustment screws (12) existed to assist in the setting of the test bushes.

5.2.1 The Test Bushes

The bushes used in the experiments were in glass and had been supplied by Chance Brothers Ltd., Pickersleigh Avenue, Malvern, Worcs., UK. Tests for bore roundness carried out using a Rank Taylor Hobson Talyrond machine showed a maximum departure from circularity of 18.7 μm, a value that appeared to be acceptable when compared with the radial clearance of the bearings, c = 138 μm. Three bushes were used in the experiments the dimensions of which, apart from the geometry of the oil supply recess, were not significantly different. Table 5.1 shows the dimensions of each of the bushes used. Their wall thickness was approximately 6.5mm.

Considering a test bush as a simply supported beam, the maximum deflection of the bush for a bearing load corresponding to an operating eccentricity ratio of 0.8, shaft speed of 1000 r.p.m. (16.66 Hz) and oil effective temperature of 25°C, would be 0.3 μm. Taking the bush as an open ended pressure vessel subjected to an axisymmetric internal pressure equal to the bearing specific loading, the increase in the diameter of the bush would be about 3.6 μm. It was determined that the changes in film shape due to deformation of the glass bushes when subjected to the film pressures developed during the experiments were not significant.

The technique used to machine the oil supply recess on a glass bush was as follows. The hole required for the lubricant supply pipe was drilled on the bush centre line using a diamond impregnated core drill of

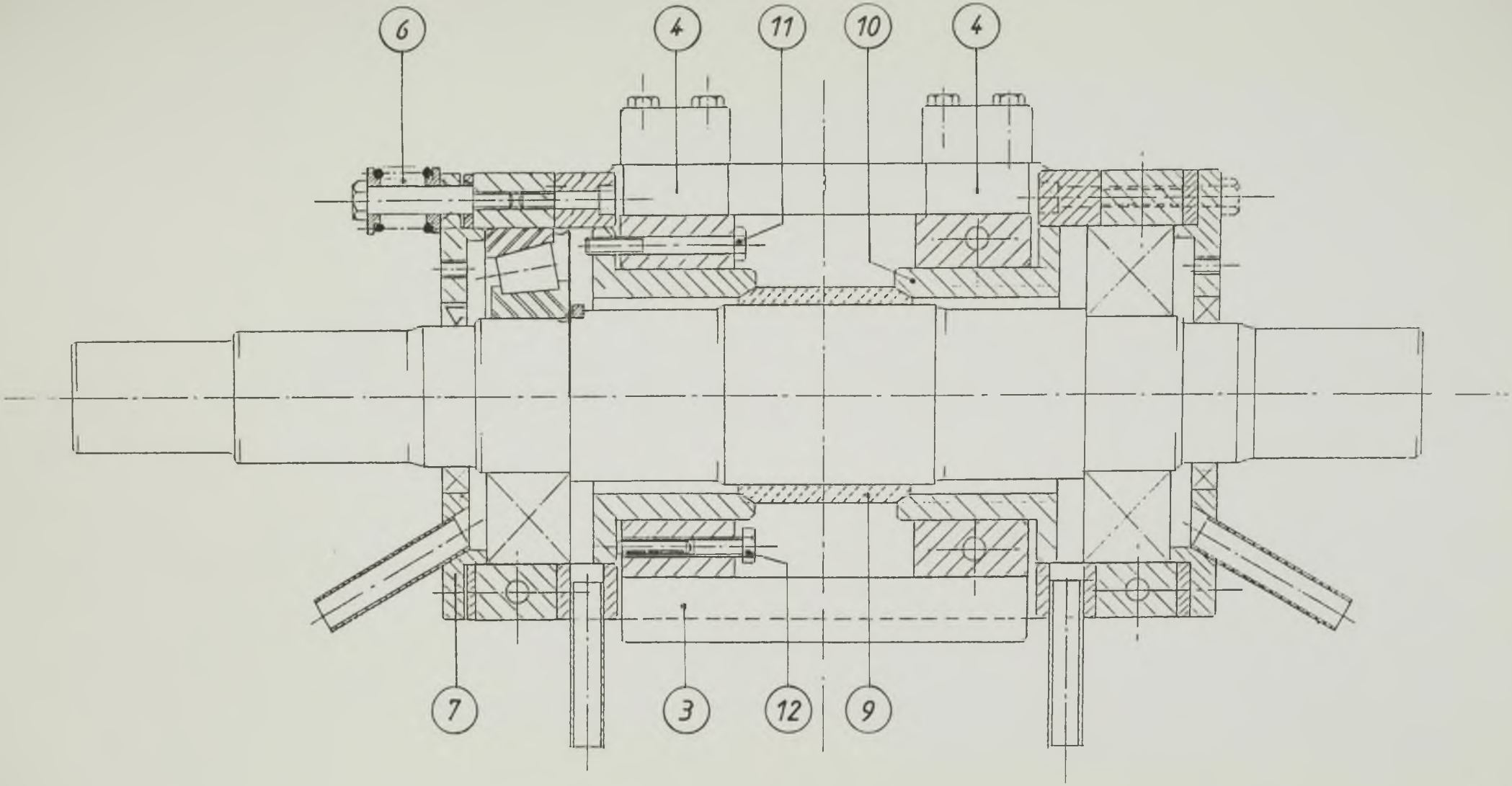

Figure 5.1 Detailed drawing of the main shaft and the bush assemblies

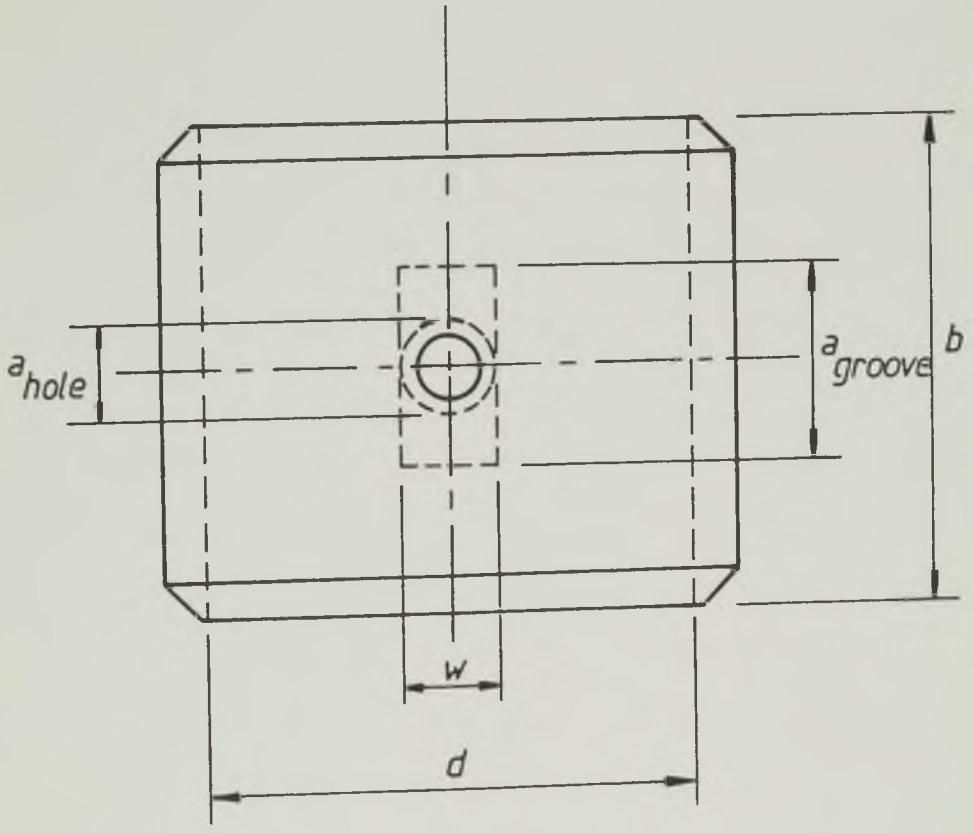

	Supply Geometry	d	b	a	w	Resulting C_d
Bush 1	oil hole	63.501	63.5	12	12	0.276
Bush 2	axial groove	63.502	63.5	26	12	0.277
Bush 3	axial groove	63.501	63.5	45	12	0.276

Table 5.1 Dimensions of the glass bushes used in the experimental programme (mm).
Shaft diameter, 63.225 mm

8mm in diameter. A brass tool of cylindrical shape attached to the head of a vertical milling machine was then used to machine the axial groove. This operation is sketched in Figure 5.2 The length of the tool was the same as the required groove length (a); the diameter of the tool was calculated to give specified values of groove width and depth at the groove centre. The tools used had a diameter of 18 mm which produced a groove 12 mm wide with a maximum depth of 2.3 mm. The bush was clamped to the universal table of the milling machine which was then moved to position. The contact surface of the brass tool was fed with Carborundum, a grinding compound (silicon carbide and grease mixed), while rotating in contact with the bush surface. The table of the machine was moved slowly in the horizontal direction (as indicated in Figure 5.2) keeping the surface of the glass bush slightly pressed against the surface of the brass tool. The current depth of the groove was equal to the total displacement of the table.

The technique used with Bushes 2 and 3 to drill the hole for the lubricant supply pipe, was also employed to drill the oil hole in Bush 1. A core drill of 12 mm diameter was used. The recess was formed by the brass pipe when it was glued to the bush. The diameter of the oil inlet pipe was 6 mm, a value common to all the bushes.

5.2.2 The Lubricant Supply System

A line diagram of the lubricant supply system is shown in Figure 5.3. The lubricant used was a Shell oil designated as H.V.I. 60, a straight mineral oil to which red dye (Waxoline red) was added to facilitate visual observations of the oil film in the bearing. A screw pump pumped oil from the supply tank (containing about 12 litres of oil) to the bearing. The pump had been supplied by Mono Pumps Ltd. with a

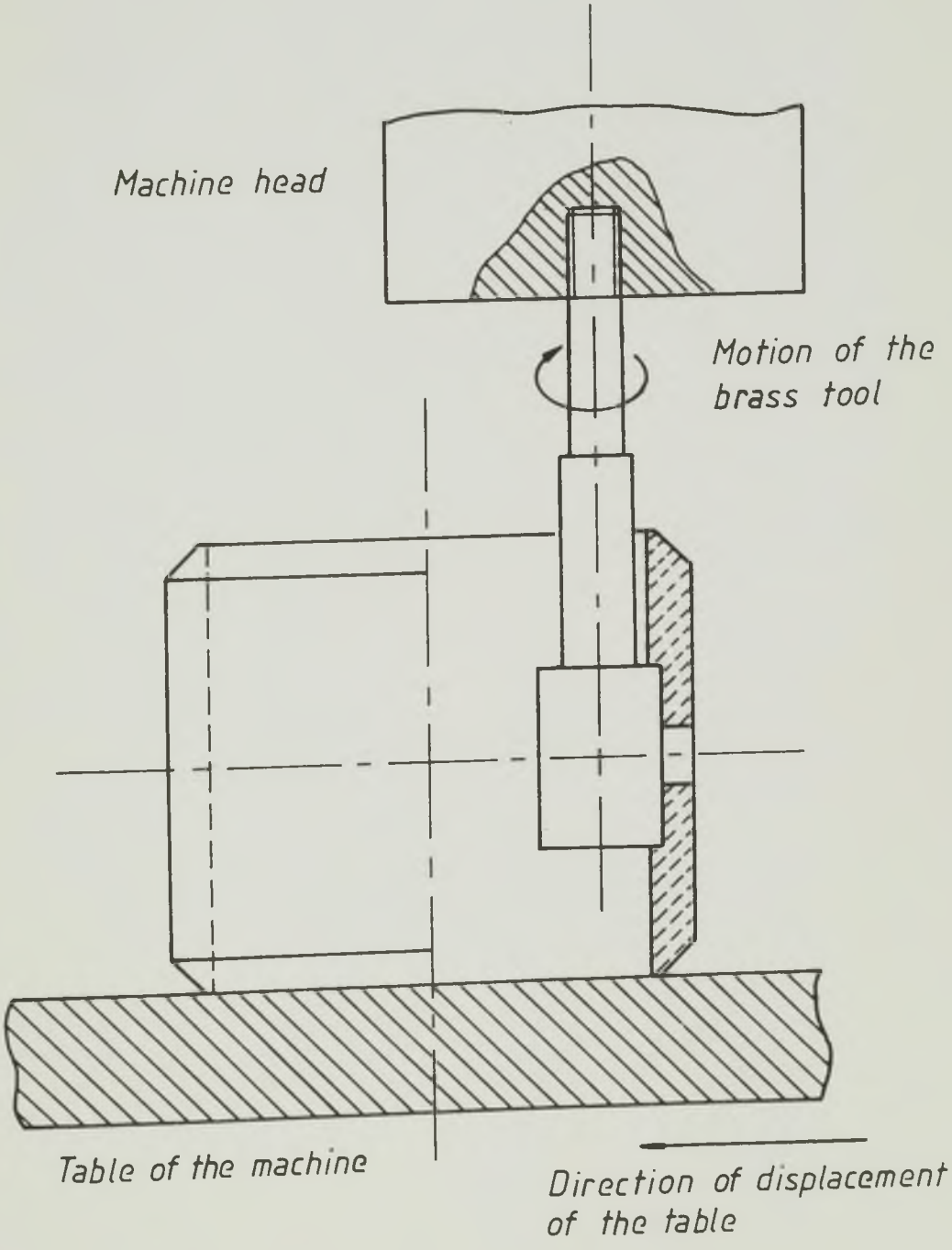

Figure 5.2 The technique used for machining the axial groove in a glass bush

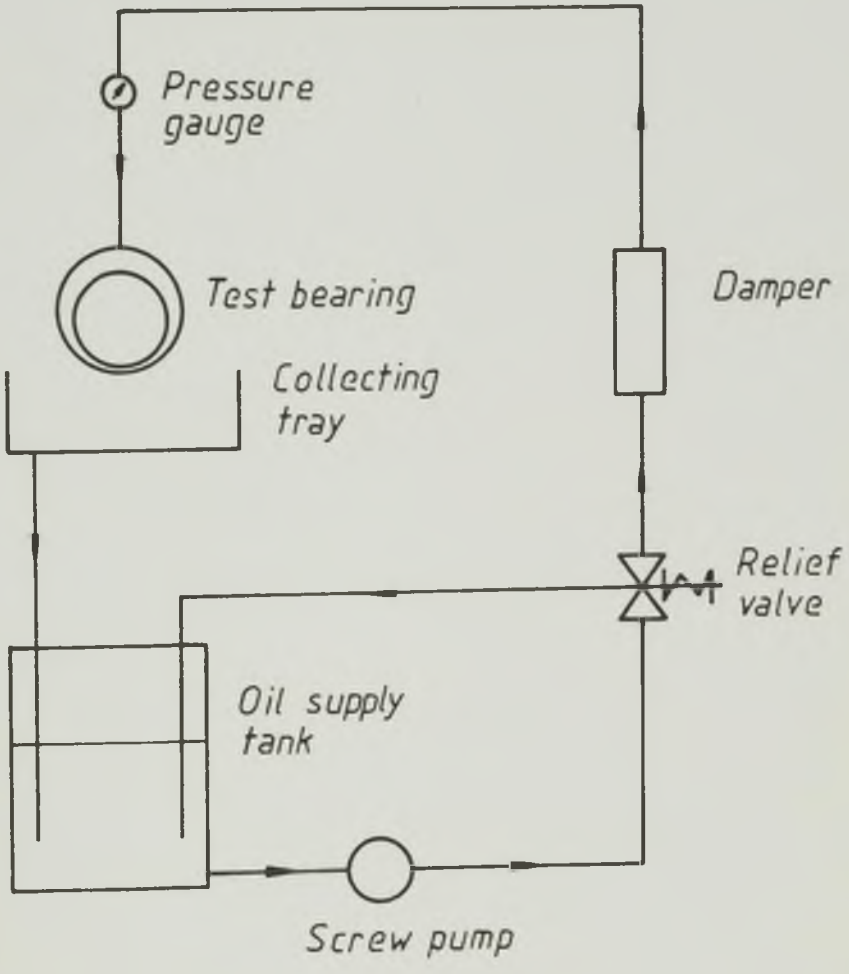

Figure 5.3 A line diagram of the lubricant supply system

constant speed electric motor. In the present experimental programme tests for variable oil supply pressure at fixed values of eccentricity ratio were performed and the resulting oil flow rate in the bearing measured. A variable oil supply pressure was achieved by altering the flow rate delivered by the pump, that is, by varying the rotational speed of the oil pump. The constant speed motor supplied with the pump was, therefore, removed and replaced by a 0.37kW, variable speed motor, controlled by a Fenner control unit.

It was observed that at supply pressures greater than 1.5-2 bar (150-200 kN/m^2) the flow delivered by the pump was a pulsating one resulting in oscillations in the value of the supply pressure. To smooth down the output from the pump a pulsation damper was mounted on the oil supply circuit. Inside the damper the oil passed through a rubber sleeve housed in a chamber where there was air under pressure. For the damping to be effective in the conditions of the experiments the air pressure in the chamber, which was controlled by a pressure gauge mounted on a pressure tapping provided, had to be at least 2.5 bar (250 kN/m^2).

From the damper the oil was conducted directly to the test bearing. The oil issuing from the sides of the bearing was discharged via two holes, one on each side (see Figure 5.1), into a collecting tray placed beneath the apparatus from where it was returned by gravity to the supply tank. A relief valve was installed downstream of the pump.

5.3 Measurement Techniques

A number of parameters were measured, some were used in a direct comparison with the predictions of the theory, others were combined in dimensionless groups for a comparative study of results for a wide range

of operating conditions. The measurement techniques used will be discussed in the following sections.

5.3.1 Lubricant Characteristics

The kinematic viscosity of the lubricant was determined by using a suspended level U-tube capillary viscometer. From a knowledge of the kinematic viscosity at two different values of temperature an equation for the viscosity - temperature relationship can be obtained as discussed in Miranda (1983). For the Shell H.V.I. 60 oil used the following viscosity - temperature relationship was derived,

$$\log \log (\nu + 0.8) = 9.567 - 3.772 \log (t + 273) \qquad (5.1)$$

where (ν) is the kinematic viscosity of the oil in centistoke and (t) is the oil temperature in degrees Celsius.

The oil density, required for determining the oil flow rate and to convert kinematic viscosity to dynamic viscosity, was determined by using a specific gravity bottle. At a temperature of $19^{o}C$ the density was found to be 867.5 kg/m^3. Variations of oil density with temperature were not significant for the temperature variations observed in the experiments.

5.3.2 Eccentricity Ratio

By design, the value of the eccentricity ratio and the location of the position of maximum film thickness would be determined by the thicknesses of the packing blocks and of the packing plate used. Different sets of packing blocks and packing plates of convenient thicknesses would allow bush settings at any pre-selected value of eccentricity ratio. However, during the commissioning of the apparatus it was found that after a pair of packing blocks had been mounted and

the resulting eccentricity ratio checked, if this pair of packing blocks was then removed and mounted again the same value of eccentricity ratio was usually not obtained. This was attributed to the method of holding the floating bracket which relied on screws tightened up against the packing blocks and the packing plate and also to the test bush clamping technique (see Plate 5.1 and Figure 5.1). The design technique of setting the bush for a pre-selected value of eccentricity ratio, was therefore, not reliable.

All the tests were performed with the oil inlet port located at the position of maximum film thickness. This permitted the use of sets of packing blocks of different thicknesses in conjunction with an unchanged packing plate, in order to obtain variable values of eccentricity ratio. Four sets of packing blocks which would allow settings with eccentricity ratios in the range (0.2 - 0.8) were manufactured (the pair of packing blocks and the packing plate which produced a concentric bush-shaft position were supplied with the apparatus). The pair of packing blocks with the most suitable thicknesses to produce an eccentricity ratio approximate to the value required was used and the resulting eccentricity ratio was determined as follows. The plunger of a clock dial test indicator (hereafter referred to as dial gauge) was introduced into the inlet brass pipe of the glass bush to make contact with the surface of the shaft. The dial gauge was fixed to the bush inlet brass pipe by means of a sleeve and contact screws as shown in Plate 5.2. The plunger could be freely moved. A displacement of the plunger was converted into a rotational movement of the needle of the dial gauge in a circular scale with 100 divisions, each division corresponding to a displacement of the plunger by 0.01 mm. When the glass bush was rotated around the stationary shaft, the position of maximum clearance could be detected by the change

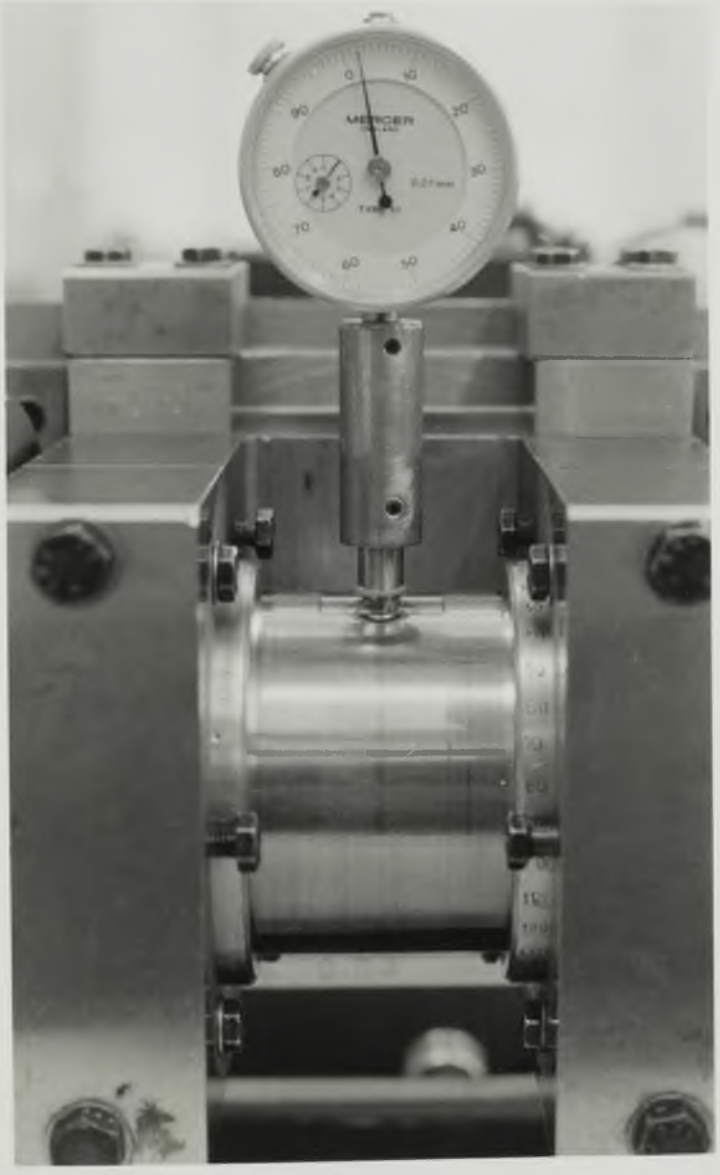

Plate 5.2 A photograph illustrating the arrangement used to determine the eccentricity ratio

in the direction of movement of the needle of the dial gauge. If (ΔC) was the change in the dial gauge reading when the glass bush was rotated from the positions of maximum to minimum film thickness, the eccentricity ratio is given by

$$\varepsilon = \frac{\Delta C}{C_d} \qquad (5.2)$$

5.3.3 Rotating Shaft Speed

The rotational speed of the shaft was measured using a hand mechanical tachometer.

5.3.4 Lubricant Supply Pressure

The pressure at which oil was supplied to the bearing was measured using a Bourdon-tube pressure gauge. A flexible plastic pipe (9 mm in diameter, 0.8 m long) connected the point where the pressure gauge was positioned (see Figure 5.3) with the bush inlet pipe. The pressure drop in the plastic pipe due to viscous effects was calculated as being of about 0.06 bar ($6kN/m^2$) for average operating conditions, a value which is not significant in comparison with the values of finite supply pressure used in the experiments.

5.3.5 Lubricant Temperatures

The oil temperature was measured by nickel-chromium/nickel-aluminium thermocouples in conjunction with a 'Comark' electronic thermometer. The zero temperature reading was checked by a thermocouple immersed in a bath of iced water.

The temperature of the side leakage oil was measured by thermocouples positioned in the holes which conducted the oil to the collecting tray. For the measurement of the inlet temperature of the oil

a thermocouple was positioned just upstream of the bush inlet brass pipe. Measurements of the oil inlet temperature were only performed in the commissioning tests. Oil film temperatures were not measured.

5.3.6 Lubricant Flow Rate

A comparison of experimental results of side flow rate with theoretical predictions was one of the main aims of the experimental programme. The method used to measure the side flow rate was simple and reliable; the oil discharged from the sides of the bearing during an interval of time (Δt) was collected in a portable tray the weight of which, when empty, had been previously measured. The time of oil collection was measured using a stop watch and was normally of 60 seconds and 30 seconds at low and high values of oil supply pressure respectively. The tray containing the oil collected was then weighed and the weight of the oil collected determined. The side flow rate was evaluated from a knowledge of the weight of the oil collected, the time interval (Δt) and the oil density.

5.3.7 Location of the Rupture and the Reformation Boundaries

The datum for the angular location of the rupture and the reformation boundaries was the position of the groove (or of the oil hole) which was located at the maximum film thickness. A scale graduated in degrees was engraved on one of the brass clamp sleeves holding the glass bush. The zero of the scale was in the top vertical position and the scale was graduated from 0^{o} to 180^{o} in the direction of greater visibility, and from 0^{o} to 90^{o} in the opposite direction. The smallest division of the scale corresponded to an angular change of 5^{o}.

5.4 The Commissioning of the Apparatus

5.4.1 Observations

To find out whether the apparatus was functioning as designed, introductory testing was performed without recording any results. Variable values of eccentricity ratio could be obtained using different sets of packing blocks. Repeatability in the value of the eccentricity ratio for the same pair of packing blocks was, however, not normally achieved as discussed in Section 5.3.2. The location of the position of maximum film thickness, as well as the eccentricity ratio, could be determined using a dial gauge. The maximum error in the location of the position of maximum film thickness was estimated as being of $\pm 5^{o}$ and $\pm 10^{o}$ at high and low values of eccentricity ratio respectively.

A variable flow rate was obtained by varying the rotational speed of the oil pump. No visible fluctuation in the oil flow rate issuing from the open end of the supply pipe was observed. With the supply pipe connected to the bearing, oscillations of the needle of the pressure gauge were noticeable at supply pressures greater than 1.5-2 bar (150-200 kN/m^2) increasing in amplitude as the supply pressure increased. This fluctuation in the value of supply pressure, due to a pulsating delivery from the oil pump, was completely eliminated when a pulsation damper was installed as discussed in Section 5.2.2.

Film rupture and film reformation could be observed as well as the effect of oil supply pressure on the location of the film reformation boundary. For some bush settings it was observed that the reformation boundary was clearly assymetrical with respect to the bearing centre line; this was caused by misalignment between the bush and the shaft axes.

Thermal equilibrium was generally achieved after a 4 - 5 hours

run at constant operating conditions. At a shaft speed of 600 r.p.m. (10 Hz) and oil supply pressure of 1 bar (100kN/m^2), the observed increase in the temperature of the oil after thermal equilibrium had been reached was about 10°C when the shaft ran concentric with the bush, and of about 12°C at an eccentricity ratio of 0.76. The rise in the temperature of the oil as it passed through the test bearing was about 1°C at concentric shaft/bush and about 2°C at ε=0.76. It is worth noting here that the effective temperature of the oil in the bearing was assumed to be equal to the measured outlet temperature for the purpose of calculating the dimensionless supply pressure.

Despite the difficulties encountered in setting the test bearing for pre-selected values of eccentricity ratio and to achieve a satisfactory alignment between the shaft and the bush axes, the apparatus was operating satisfactorily.

5.4.2 Commissioning Tests

Two tests were carried out, both with Bush 3 with the groove located at the position of maximum film thickness, for a comparison of experimental flow rates with theoretical predictions from other sources. A first test was run with the shaft stationary. The oil flow rate at four values of supply pressure in the range 0.68-1.69 bar (68 - 169 kN/m^2) was measured for each value of eccentricity ratio tested. Figure 5.4 shows a comparison of the experimental results of dimensionless flow rate with the theoretical predictions of ESDU Item No. 66023 (1966) and Martin and Lee (1982). The flow rate was made dimensionless according to the expression shown in the same figure. The experimental results at a fixed value of (ε) varied slightly with the value of supply pressure (p_f). Very good correlation was achieved, the biggest percentage difference observed being 34.3% at

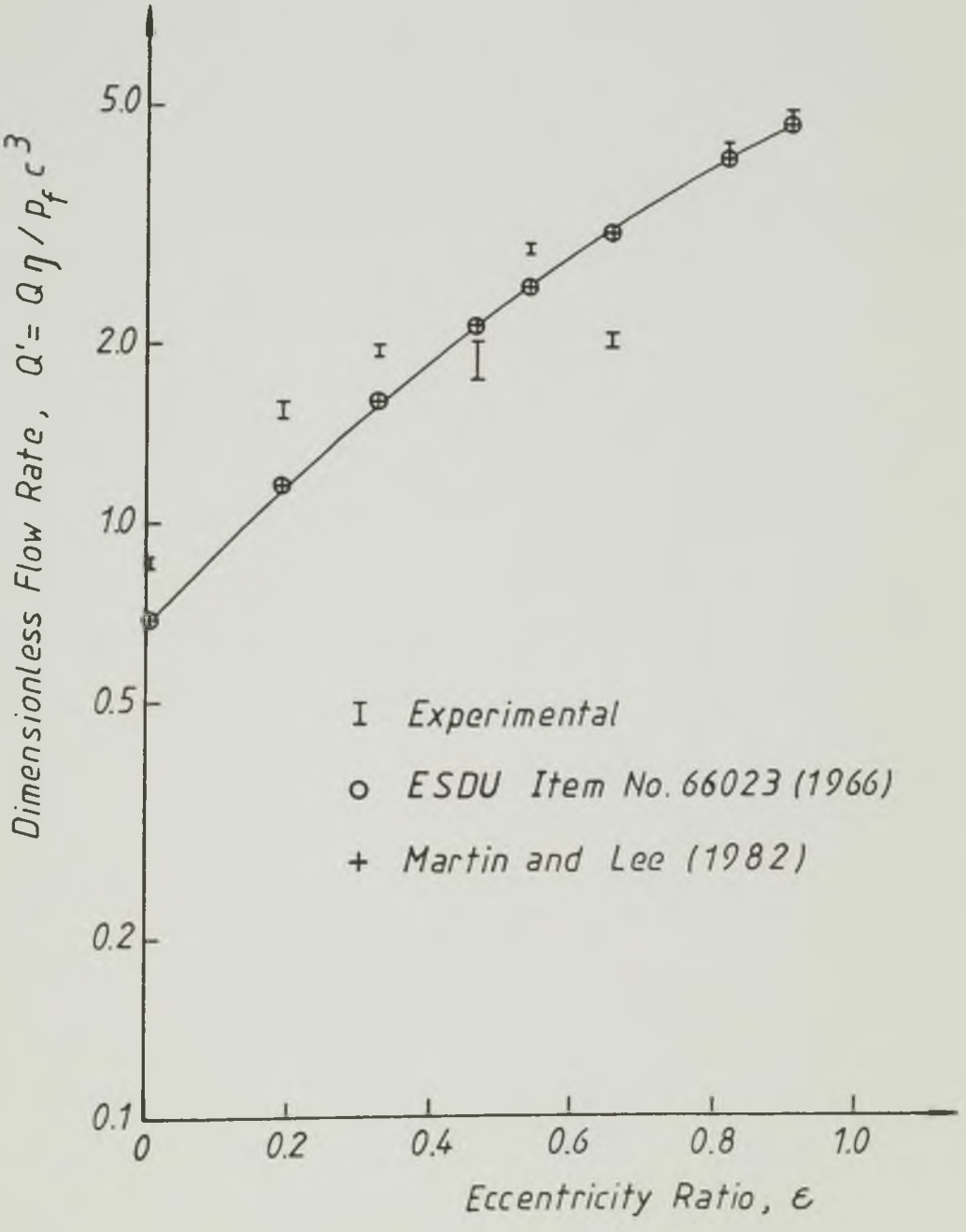

Figure 5.4 A comparison of the experimentally determined dimensionless flow rate when using Bush 3 with a stationary shaft, with the theoretical predictions of ESDU Item No. 66023 (1966) and Martin and Lee (1982)

ε=0.65. Errors in the location of the position of maximum film thickness and bearing misalignment were probably the cause for the discrepancies observed.

A second test was run at fixed values of eccentricity ratio and oil supply pressure and at variable shaft speed. Figure 5.5 shows the correlation observed between the experimentally determined side flow rate and the theoretical predictions of ESDU Item No. 66023 (1966). Again, very good agreement was observed the maximum difference being 14.9%.

The very good correlation between experimental results and theoretical predictions of other sources achieved in those two tests indicated that the apparatus could be used with confidence to obtain experimental results for a wide range of operating conditions. An experimental programme was carried out in order to study the correlation between experiment and the predictions of the theoretical analysis presented in this thesis. A discussion of results of the experimental programme will be dealt with in the next chapter.

5.5 Conclusions

(1) An apparatus for the study of oil flow in journal bearings has been designed. The use of glass bushes permitted a visual study of the film extent in the bearing.

(2) The commissioning of the apparatus has been performed. Operation at a wide range of conditions was possible and the effect of operating parameters on flow rate and on the location of the film reformation boundary was observed to be as expected.

It was found that it was difficult to establish a bush setting for a pre-selected value of eccentricity ratio and a careful setting was

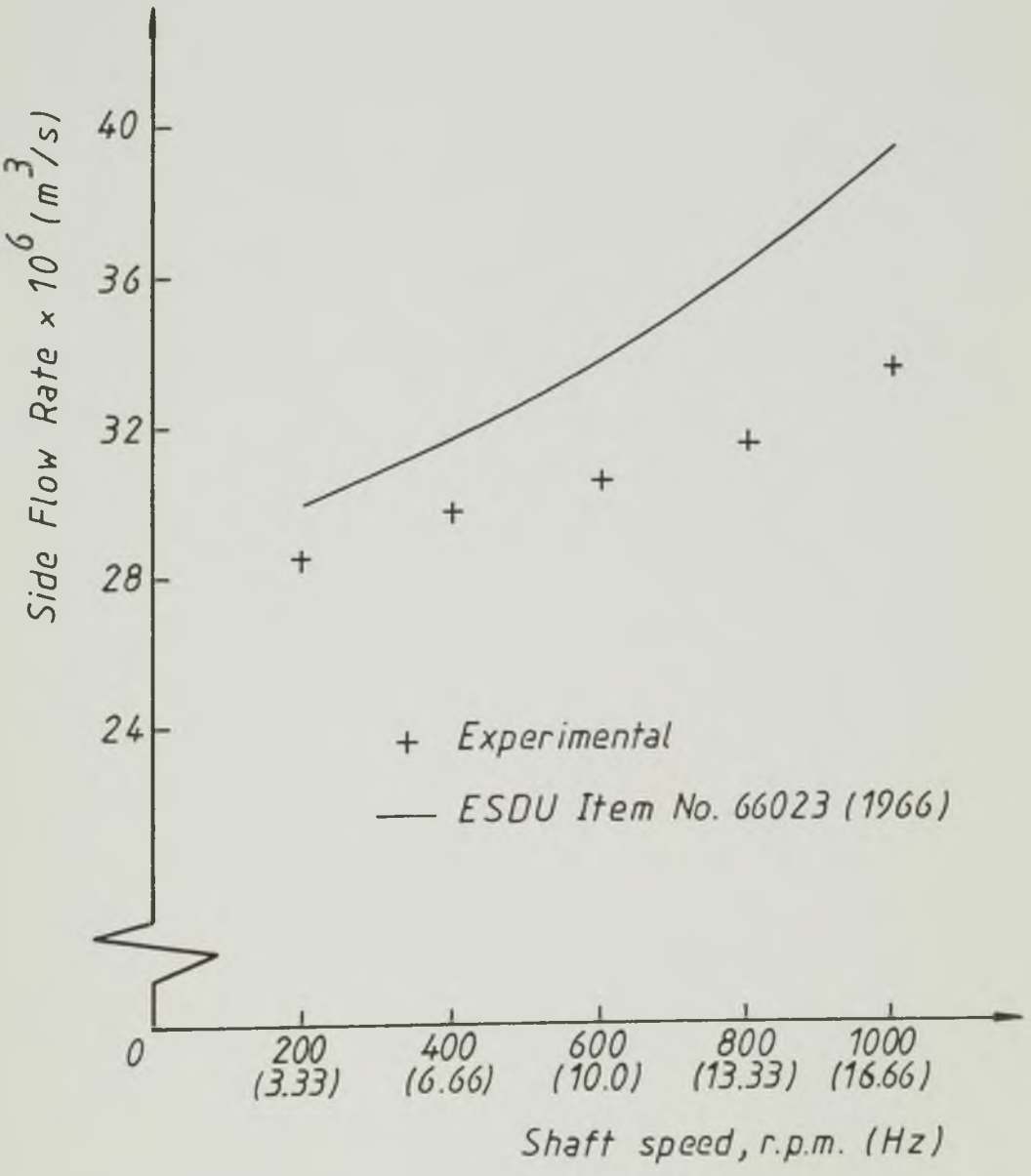

Figure 5.5 A comparison between the experimentally determined side flow rate and the predictions of ESDU Item No. 66023 (1966), with Bush 3 at fixed eccentricity ratio and oil supply pressure (ε = 0.67, p_f = 1.69 bar (169 kN/m^2)

required to minimize bearing misalignment. However, this would not affect the aims of the experimental programme.

Preliminary tests have been performed which gave very good correlation between the experimentally determined side flow rate and the theoretical predictions of ESDU Item No. 66023 (1966) and Martin and Lee (1982).

The commissioning of the experimental apparatus has confirmed that it could be used with confidence to carry out a programme of tests.

CHAPTER 6

THE EXPERIMENTAL PROGRAMME AND DISCUSSION OF RESULTS

6.1 Introduction

The experimental apparatus has been described in Chapter 5. The commissioning tests carried out identified some limitations of the apparatus, for example a difficulty in obtaining a bearing setting corresponding to a pre-selected value of eccentricity ratio, and also showed that a very careful bush setting was required to minimize axial misalignment and to prevent errors in the determination of the operating eccentricity ratio and in the location of the position of the maximum clearance. Misalignment affects the flow rate of lubricant in the bearing (Hargreaves (1981), Siew and Reason (1982)) and in addition it would affect the measurements of the angular extent of the full film region in the present experiments.

The results of the commissioning tests showed good correlation with theoretical predictions from other sources, indicating that the apparatus could, nevertheless, be used with confidence to provide a wide range of experimental results for comparison with the predictions of the present theoretical analysis. For this purpose a detailed programme of tests was prepared.

This chapter will deal with the experimental programme and a discussion on the correlation between the experimental results and the theoretical predictions.

6.2 The Experimental Programme

The computer program used in the present journal bearing analysis was able to generate solutions for a range of values of bearing width-to-diameter ratio (b/d), eccentricity ratio (ε), groove length-to-bearing width ratio (a/b), groove width-to-bearing diameter ratio (w/d) and dimensionless supply pressure ($\bar{p}_f$). The bushes used in the experiments had fixed values for (b), (d), (w) and (C_d) as indicated in Table 5.1. The parameters (b/d), (w/d) and (C_d/d) were therefore the same for all bushes. The length of the groove (a) varied from bush to bush. The operating eccentricity ratio and the dimensionless supply pressure could of course be varied. Table 6.1 gives the values of the bearing parameters corresponding to each bush tested (based on the bearing dimensions shown in Table 5.1).

	Supply geometry	b/d	C_d/d	a/b	w/d
Bush 1	oil hole	1	4.365×10^{-3}	0.189	0.189
Bush 2	axial groove	1	4.365×10^{-3}	0.409	0.189
Bush 3	axial groove	1	4.365×10^{-3}	0.708	0.189

Table 6.1 Bearing parameters and groove size corresponding to each bush used in the experiments

6.2.1 The Tests

To allow a comparison of results over a wide range of operating conditions to be carried out, the experiments were programmed in a way that permitted the results to be expressed in dimensionless form whenever possible.

The parameters that could be varied in the tests were the eccentricity ratio and the dimensionless supply pressure. The latter was dependent on the oil supply pressure, on the shaft speed and on the effective temperature of the oil. The oil supply pressure and the shaft speed were set, the oil temperature was measured. Tests involving the three bushes provided results at variable (a/b).

Two sets of experiments were carried out. The tests included in the 'set of experiments 1' involved all three bushes and were performed at fixed journal speed. Each bush was usually set to six different values of eccentricity ratio in the range (0.2-0.8). For each bush setting tests for four values of oil supply pressure were carried out. The 'set of experiments 2' involved only one bush and was designed to show the effect of shaft speed on the bearing performance. The tests were carried out at fixed eccentricity ratio for five values of shaft speed, in the range 200-1000 r.p.m. (3.33-16.66 Hz), and at two different values of oil supply pressure. Table 6.2 gives the details of the programme of tests.

6.2.2 The Test Procedure

The apparatus was assembled as described in Chapter 5. The test procedure was as follows.

	Bush Involved	Eccentricity Ratio	Oil Supply Pressure, bar	(kN/m^2)	Journal Speed, r.p.m. (Hz)
SET OF EXPERIMENTS 1	Bush 1	0.27			
		0.44	0		
		0.57	0.678	(67.8)	600
		0.67	1.695	(169.5)	(10)
		0.74	2.712	(271.2)	
	Bush 2	0.26			
		0.41	0		
		0.47	0.678	(67.8)	600
		0.58	1.695	(169.5)	(10)
		0.67	2.712	(271.2)	
		0.76			
	Bush 3	0.29			
		0.38	0		
		0.47	0.678	(67.8)	600
		0.58	1.695	(169.5)	(10)
		0.67	2.712	(271.2)	
		0.74			
SET OF EXPERIMENTS 2	Bush 2	0.67	0		200 (3.33)
					400 (6.66)
			1.695	(169.5)	600 (10)
					800 (13.33)
					1000 (16.66)

Table 6.2 The programme of tests

(1) The 'adjustment screws' were unscrewed to make sure that they were not operating. The 'clamping screws' were tightened up gently pulling the bush holders against the bush. At the end of this operation the bush should not be loose but should be able to be rotated over its tapered ends.

(2) The pair of packing blocks which was supposed to provide a setting with the closest value of eccentricity ratio to the one desired, were screwed tight in place.

(3) A dial gauge was used to detect the position of maximum film thickness and to measure the change in clearance from this position to the position of minimum film thickness. The value of the eccentricity ratio was calculated from a knowledge of this change in clearance, as discussed in Chapter 5 (Section 5.3.2).

(4) 'Adjustment' and 'clamping' screws were altered until a suitable value of eccentricity ratio was achieved.

(5) The oil groove was centered in the position of maximum film thickness and a little action on one of the 'adjustment' or of the 'clamping' screws usually sufficed for holding the bush tight in that position.

(6) The dial gauge was then taken off the bush inlet brass pipe and the oil supply pipe was connected to the bearing. A clamp was used to prevent separation of the plastic pipe from the inlet brass pipe at high oil supply pressures.

(7) The oil pump drive motor and the shaft drive motor were switched on and operated at a low speed to check the bearing misalignment. The procedure returned to step (4) until acceptable bearing alignment was achieved. Sometimes this proved to be a tedious and

time-consuming operation

(8) The shaft speed was set to the required value and the rotational speed of the oil pump was then altered until the desired value for the oil supply pressure was indicated by the pressure gauge. The shaft speed was checked regularly during the tests.

(9) The measurements required were recorded.

(10) Once the tests with the current bush setting had been completed the eccentricity ratio was checked with the dial gauge. The value for eccentricity ratio measured after the tests was, in general, not significantly different from the one corresponding to the initial setting. The eccentricity ratio adopted for that set of tests was the mean of the two values measured.

6.2.3 The Measurements Recorded

During the setting up of the bush two measurements were recorded:

(i) The angular location of the position of maximum film thickness

(ii) The change in clearance from the position of maximum to the position of minimum film thickness which allowed the determination of the eccentricity ratio.

For a given bush setting the following measurements were recorded during every test:

(iii) The rotational speed of the shaft

(iv) The oil supply pressure

(v) The weight of the collected side leakage oil and the time in which it was collected. This allowed the determination of the side flow rate as discussed in Chapter 5 (Section 5.3.6). In order to compare the experimental results for side flow with the theoretical predictions the flow rate measured was usually normalized according

to the expression adopted in this thesis.

(vi) The location of the rupture and of the reformation boundaries. The location of a boundary was defined by an angle measured from the groove centre line to the boundary in the direction of the shaft rotation. The groove was assumed to be located at the position of maximum film thickness. The angular location of the rupture boundary was recorded as an angle (α_c) measured at the bearing centre line. At low oil supply pressures the upstream end of the full film region usually coincided with the upstream edge of the groove. In such a situation only the angular location of the beginning of the full width film (α_r, at the bearing edge) was recorded. When, at moderate/high values of supply pressure, the reformation boundary was located upstream of the groove (see Plate 6.1) both (α_r) and the angular location of the nose of the boundary (at the bearing centre line) were recorded.

(vii) The outlet temperature of the oil. It has been pointed out in Chapter 5 that oil temperatures could take four hours to stabilize under constant operating conditions. The operating conditions changed from test to test due to changes in oil supply pressure or shaft speed (see Table 6.2) and it would have been impractical to wait until a stabilized temperature had been reached in every test. On the other hand, the rate of increase in the oil temperature at given operating conditions was usually small and, therefore, in the period of time required to collect the oil and to read out the angular location of the boundaries of the cavitation region, the observed increase in temperature was not significant ($0.5^{o}C$ was the maximum increase observed). Two readings of the outlet temperature

of the oil were recorded; the first was taken immediately before and the second was taken immediately after the collection of the oil and the reading of the angular location of the boundaries of the cavitation region. The oil outlet temperature was taken as the mean of those two readings and was assumed to be equal to the effective temperature of the oil for the purpose of determining the dimensionless supply pressure.

6.3 Experimental Results and Discussion

The main purpose of this experimental programme was to provide results for comparison with the predictions of the theoretical analysis discussed in this thesis. The use of glass bearings enabled the visualization of the film of oil in the bearing. The effect of the operating conditions on the extent of the full width film was investigated and other qualitative observations recorded.

The remainder of this chapter will be concerned with some experimental observations and with a comparison of experimental results for side flow rate and for the location of the rupture and the reformation boundaries, with the predictions of the theoretical analysis.

6.3.1 Qualitative Observations

In the tests carried out with Bush 1 (oil hole) at low values of eccentricity ratio ($\varepsilon < 0.3$) and at constant shaft speed (600 r.p.m. (10 Hz)) a complete film of oil was observed all around the bearing at any of the supply pressures tested. When the speed was increased a value was reached at which air bubbles appeared in the divergent film region of the bearing completely surrounded by a complete film of oil. This minimum value of shaft speed was dependent on the supply pressure and decreased as the latter increased. Some of the air forming these air bubbles, which were not fixed in position, had been driven along

by the oil supply stream and moved upstream after leaving the oil groove. In the experiments involving Bush 2 (axial groove, a/b = 0.409) at ε = 0.26, air bubbles appeared in the region upstream of the groove when the supply pressure was greater than the ambient. At zero supply pressure a complete film of oil around the bearing occurred. With Bush 3 (axial groove, a/b = 0.708) at ε = 0.29, air bubbles were observed in the divergent region of the bearing at all supply pressures tested.

As the eccentricity ratio was increased a well defined cavitation region was observed in all tests where the rupture and the reformation boundaries could be identified clearly. If some axial misalignment between bush and shaft existed it would be detected by the lack of symmetry of the film pattern in the cavitation zone with respect to the bearing centre line and, in particular, by the shape of the reformation boundary.

In the cavitation region all the oil appeared to be carried over by the oil streamers and none between the air cavities and the moving shaft.

Whilst the rupture boundary was more or less straight, the reformation boundary at either low or high supply pressure conditions had a curved shape very similar to that predicted by the theory. Plate 6.1 shows the experimentally observed reformation boundaries and the corresponding theoretical predictions at two different sets of operating conditions.

The influence of the oil supply pressure on the extent of the complete width film was clearly seen in the tests involving Bush 1 (oil hole) and Bush 2 (axial groove, a/b = 0.409). At given shaft speed and eccentricity ratio, the supply pressure being the ambient, the cavitation

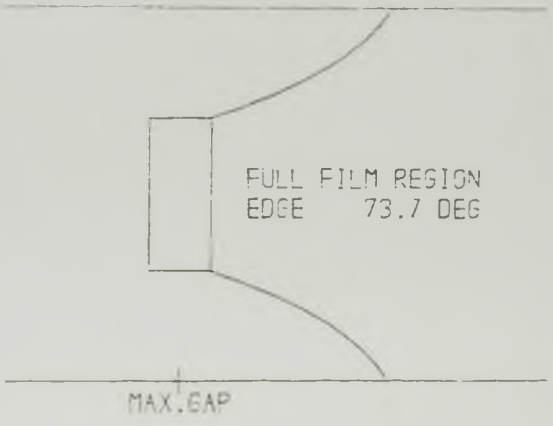

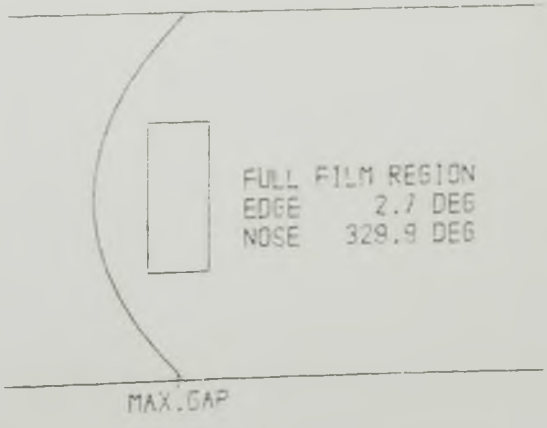

Plate 6.1 The experimentally observed (left) and the theoretically predicted (right) shapes of the film reformation boundary for Bush 2 at $\varepsilon = 0.67$, $\bar{p}_f = 0$ (upper) and $\varepsilon = 0.67$, $\bar{p}_f = 0.64$ (lower). Shaft rotation was from left to right.

region extended well downstream of the groove. As the supply pressure increased the reformation boundary moved upstream due to the increased inlet flow of oil (see Figure 6.7). The location of the rupture boundary was not significantly affected by changes in oil supply pressure, an observation that is in agreement with the theoretical predictions (see Appendix C).

When running tests at variable speed a stable film reformation boundary was observed for all speeds tested at low values of supply pressure. At the higher values of supply pressure, however, an instability was observed at the air-oil interface in the film reformation zone characterized by the local break down of the air-oil interfaces due to what seemed to be the collapse of air bubbles carried by the oil inlet stream and moving upstream from the groove to the film reformation boundary. At given values of eccentricity ratio and oil supply pressure there existed a value of shaft speed above which this instability occurred. This phenomenon has also been observed by Cole and Hughes (1956) and Hargreaves (1981).

6.3.2 Interpolation of the Experimental Results

Experimental results were obtained for the range of operating conditions shown in Table 6.2. The tests included in the 'set of experiments 1' were designed to give results for dimensionless side flow rate and for the location of the rupture and of the reformation boundaries at constant shaft speed and variable eccentricity ratio and oil supply pressure. For a given test bush (fixed(a/b)) and at fixed eccentricity ratio, results were obtained at four values of oil supply pressure. A convenient way of presenting a comparison of experimental results with theoretical predictions seemed to be the graphical form with the dimensionless supply pressure as the parameter, incorporating

the rotational speed, the oil supply pressure and the effective temperature of the oil. Although the speed was the same for all tests and the same values of supply pressure were used at each eccentricity ratio, the values for dimensionless supply pressure (corresponding to a given value of oil supply pressure) calculated at two different values of eccentricity ratio, usually differed due to differences in the effective temperature of the oil. To convert experimental results at variable values of eccentricity ratio and variable determined dimensionless supply pressure into results at variable eccentricity ratio and pre-fixed values of dimensionless supply pressure, graphical interpolation was used for every value of the eccentricity ratio. The procedure was as follows.

(i) Experimental results for dimensionless side flow and for the location of the rupture and of the reformation boundaries were plotted against the experimental values of dimensionless supply pressure. These plots were usually straight lines for the dimensionless flow rate and smooth curves for the location of the rupture and of the reformation boundaries.

(ii) The required interpolated values corresponding to pre-fixed values of dimensionless supply pressure (0, 0.5, 1.0 and 1.5) were then simply read out on the diagram.

An alternative to interpolation of experimental results was the adjustment of the values of shaft speed and/or oil supply pressure such that when combined with the measured effective temperature they resulted in a pre-fixed value of dimensionless supply pressure. This method was not adopted because it would have required more or less complicated calculations 'on the spot' with the additional difficulty of a non stabilized effective temperature of the oil.

For the presentation of the experimental results obtained at fixed eccentricity ratio interpolation was not required.

6.3.3 Lubricant Flow Rates

Results of lubricant side flow rate for all bushes at variable values of eccentricity ratio and oil supply pressure were obtained from the 'set of experiments 1'. Based on these, results of dimensionless side flow rate at pre-selected values of dimensionless supply pressure (0.0, 0.5, 1.0 and 1.5) and for the same values of eccentricity ratio as used in the experiments were determined by interpolation as discussed in Section 6.3.2. The interpolated experimental results were then compared with the predictions of the theoretical analysis presented in this thesis.

Figures 6.1 to 6.3 are plots of dimensionless side flow rate against eccentricity ratio for four values of dimensionless supply pressure. Very good correlation has been achieved for all bushes. The theoretical results for Bush 1 were obtained with the assumption of a 'square hole' of dimensions equal to the diameter of the oil hole of the bush, a condition which was expected to cause slightly greater theoretical predictions of dimensionless flow rate at supply pressures greater than the ambient. At $\bar{p}_f = 0.5$ the maximum percentage difference observed between the interpolated experimental results and the theoretical predictions was 17.2%. At higher values of dimensionless supply pressure the correlation was better with a maximum discrepancy of 12.7% at $\bar{p}_f = 1.5$.

With Bushes 2 and 3 very good correlation was achieved at low dimensionless supply pressure (0.0 and 0.5) for all values of eccentricity ratio. At higher values of ($\bar{p}_f$) with Bush 2 the experimental results showed some scatter, the biggest deviation from the

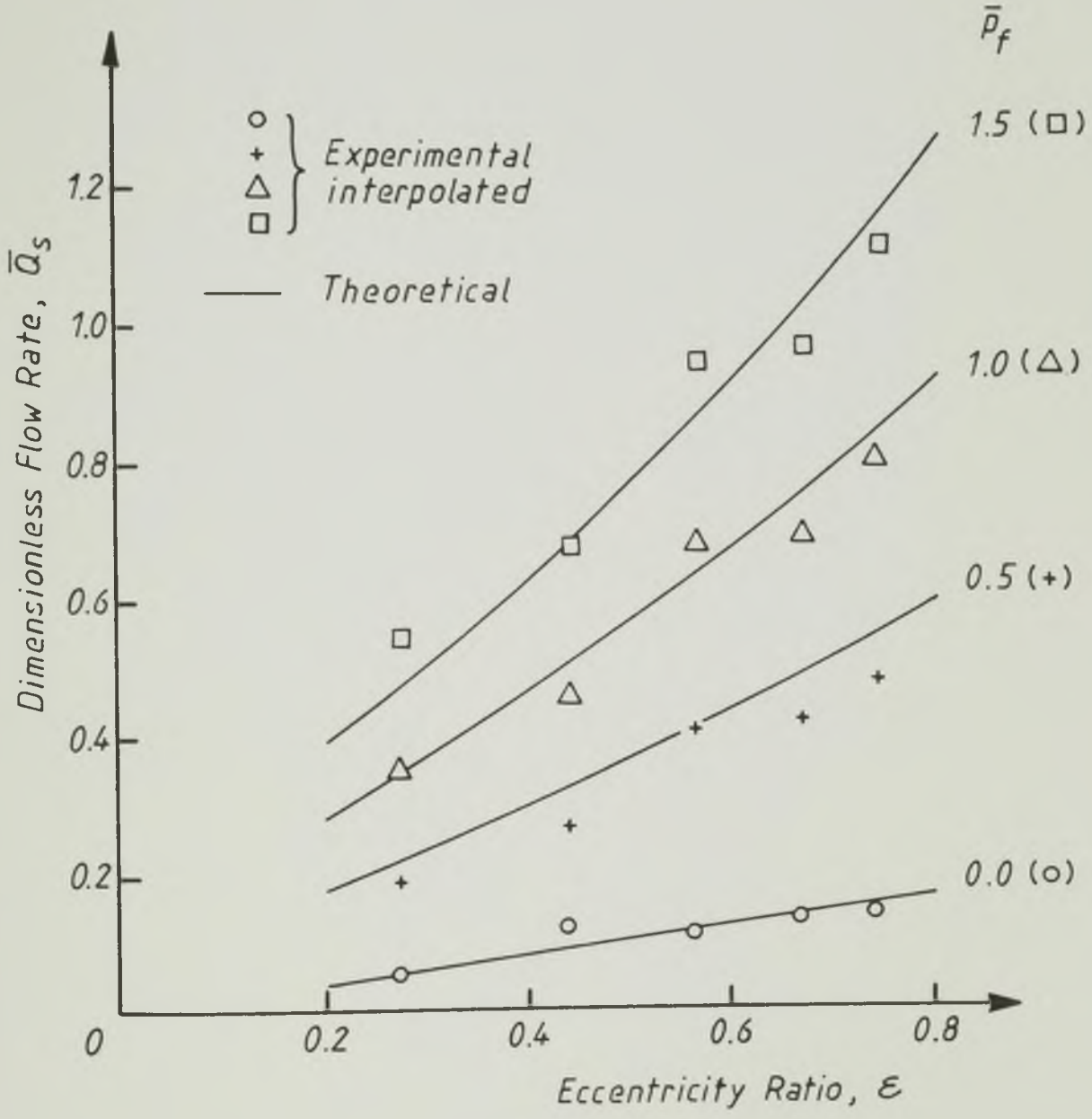

Figure 6.1 A comparison of the interpolated experimental results of dimensionless side flow rate with the theoretical predictions for Bush 1 (oil hole). Rotational speed of the shaft, 600 r.p.m., (10 Hz)

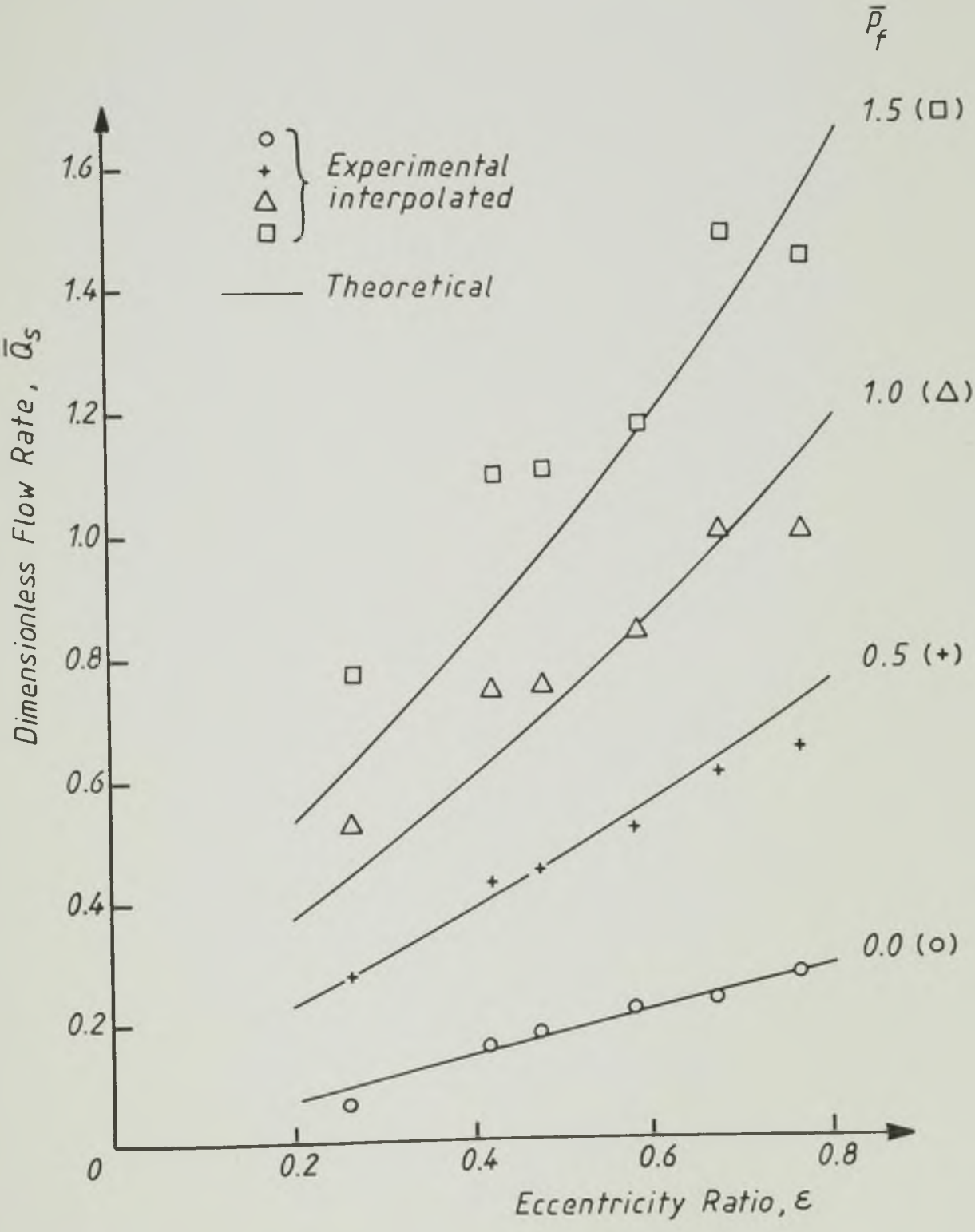

Figure 6.2 A comparison of the interpolated experimental results of dimensionless side flow rate with the theoretical predictions for Bush 2 (axial groove, a/b = 0.409). Rotational speed of the shaft, 600 r.p.m. (10 Hz).

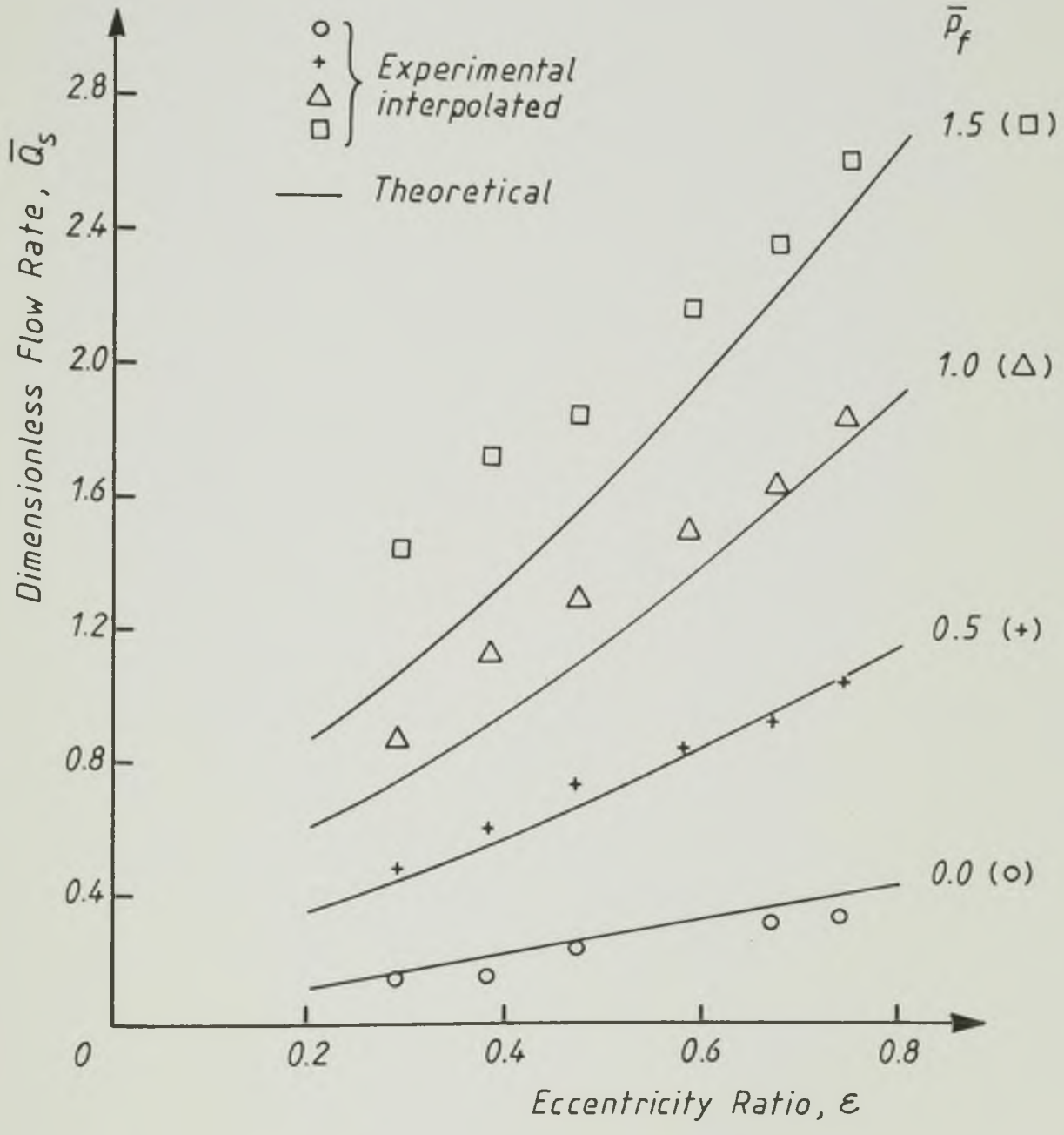

Figure 6.3 A comparison of the interpolated experimental results of dimensionless side flow rate with the theoretical predictions for Bush 3 (axial groove, a/b = 0.708). Rotational speed of the shaft, 600 r.p.m. (10 Hz)

theoretical predictions being of 22.8% at $\bar{p}_f = 1.5$. With Bush 3 the experimental results at high values of $(\bar{p}_f)$ were consistently greater than the theoretical predictions, the differences being more significant at low values of (ε). The results exhibited the same trend as the theoretical predictions with a maximum percentage difference of 27.1% at $\bar{p}_f = 1.5$ and $\varepsilon = 0.29$.

Possible errors in the location of the position of maximum film thickness and in the determination of the eccentricity ratio could have been partly responsible for the deviations from the theoretical predictions observed. Misalignment was, however, thought to have caused most of the discrepancies. Hargreaves (1981) showed that misalignment would result in an increase in oil flow rate. When misalignment existed its effect on the measured flow rate would become increasingly significant at increasing values of dimensionless supply pressure.

Figures 6.1 to 6.3 also show the dependence of dimensionless side flow rate on eccentricity ratio, groove size and dimensionless supply pressure. The effect of the rotational speed of the shaft on side flow rate is shown in Figure 6.4 for two values of oil supply pressure, namely, ambient and 1.695 bar (169.5 kN/m^2). The experimental results were obtained with Bush 2 at fixed $\varepsilon = 0.67$. The increase in the outlet temperature of the oil observed during the tests was, 1.3°C and 2.5°C at the ambient supply pressure and at $p_f = 1.695$ bar respectively. The effect of these relatively small changes in oil temperature on the side flow rate was negligible in comparison with the effect of shaft speed. Very good correlation with the theoretical predictions was achieved. At the supply pressure of 1.695 bar (169.5 kN/m^2) the

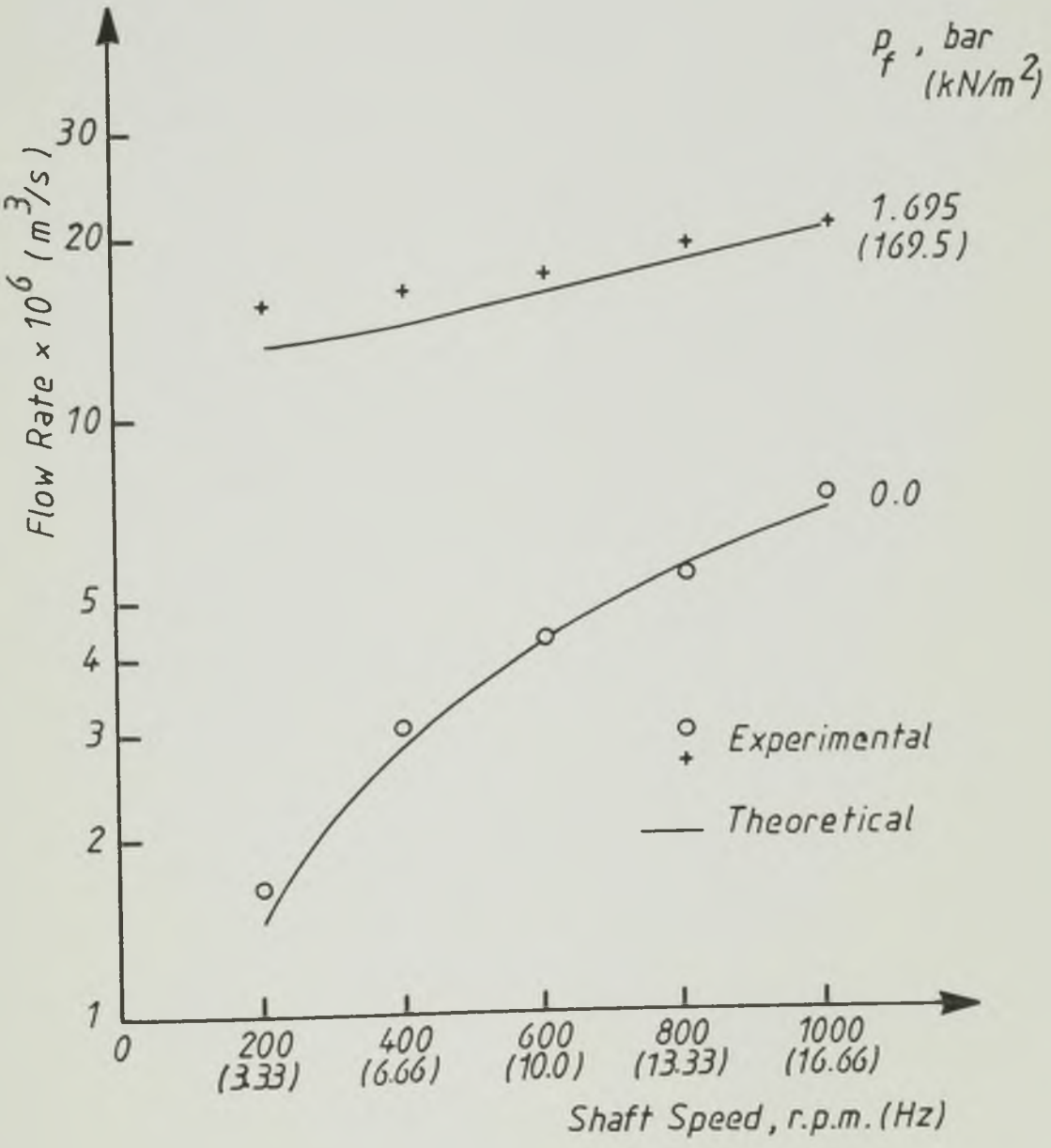

Figure 6.4 The influence of shaft speed on side flow rate for Bush 2 (axial groove, a/b = 0.409) at fixed ε = 0.67

experimentally determined oil flow rates were all greater than the theoretical predictions, the maximum percentage difference being of 14.2% at the lowest value of the shaft speed. This small discrepancy could again be due to some degree of bearing misalignment.

When the differences between the results for side flow rate at the supply pressure of 1.695 bar (169.5 kN/m^2) and at the ambient supply pressure were calculated for all values of shaft speed tested, it was found that those differences were all within the range (13.49×10^{-6} - 14.17×10^{-6} m^3/s). This supports the approach adopted by some journal bearing design procedures in which the side flow rate is calculated as the sum of two flow components: a 'zero supply pressure flow' which is not dependent on the oil supply pressure and a 'zero velocity flow' which depends on the oil supply pressure and is calculated assuming a stationary journal.

6.3.4 The Location of the Film Rupture and the Film Reformation Boundaries

The measurements recorded concerning the location of the film rupture and the film reformation boundaries have been discussed in Section 6.2.3. A comparison of the experimental results for the angular location of the beginning of the full width film (α_r) and for the angular location of the film rupture boundary (α_c), with the theoretical predictions was carried out for all the experimental results obtained. The correlation observed in the comparison of results for the various bushes was qualitatively similar, hence results obtained with one bush only will be presented in each case.

Figure 6.5 shows a comparison of the interpolated experimental results for the location of the film reformation boundary with the theoretical predictions at fixed shaft speed. Very good correlation was achieved at high values of dimensionless supply pressure for all values of eccentricity ratio. The experimentally determined values of (α_r) were consistently lower than the theoretical predictions at low and moderate values of (ε) and were higher than the theoretical predictions at high values of (ε). This trend was also observed with Bush 1 and with Bush 3. The maximum discrepancies observed at high values of ($\bar{p}_f$) were 7^o and 5^o at $\bar{p}_f = 1.0$ and $\bar{p}_f = 1.5$ respectively. At $\bar{p}_f = 0$ and $\bar{p}_f = 0.5$ correlation was good at high values of (ε). Maximum differences of about 20^o were observed at low values of (ε). At $\varepsilon > 0.5$ the maximum discrepancy observed was 9^o and 6^o at $\bar{p}_f = 0$ and $\bar{p}_f = 0.5$ respectively.

Possible sources of error in the measurement of the angular location of the rupture and of the reformation boundaries were:

(i) Bearing misalignment

(ii) Imprecise location of the position of maximum film thickness. An estimate of the maximum error introduced by this means was $\pm 10^o$ at low values of (ε) and $\pm 5^o$ at high values of (ε).

(iii) The fact that the bearing edge could not actually be seen due to the bush clamping technique used. The location of the point on the bearing edge where a full width film occurred was estimated by visual extrapolation.

(iv) The instability observed at the downstream end of the air cavities under particular operating conditions discussed in Section 6.3.1. This could affect the identification of the real reformation boundary.

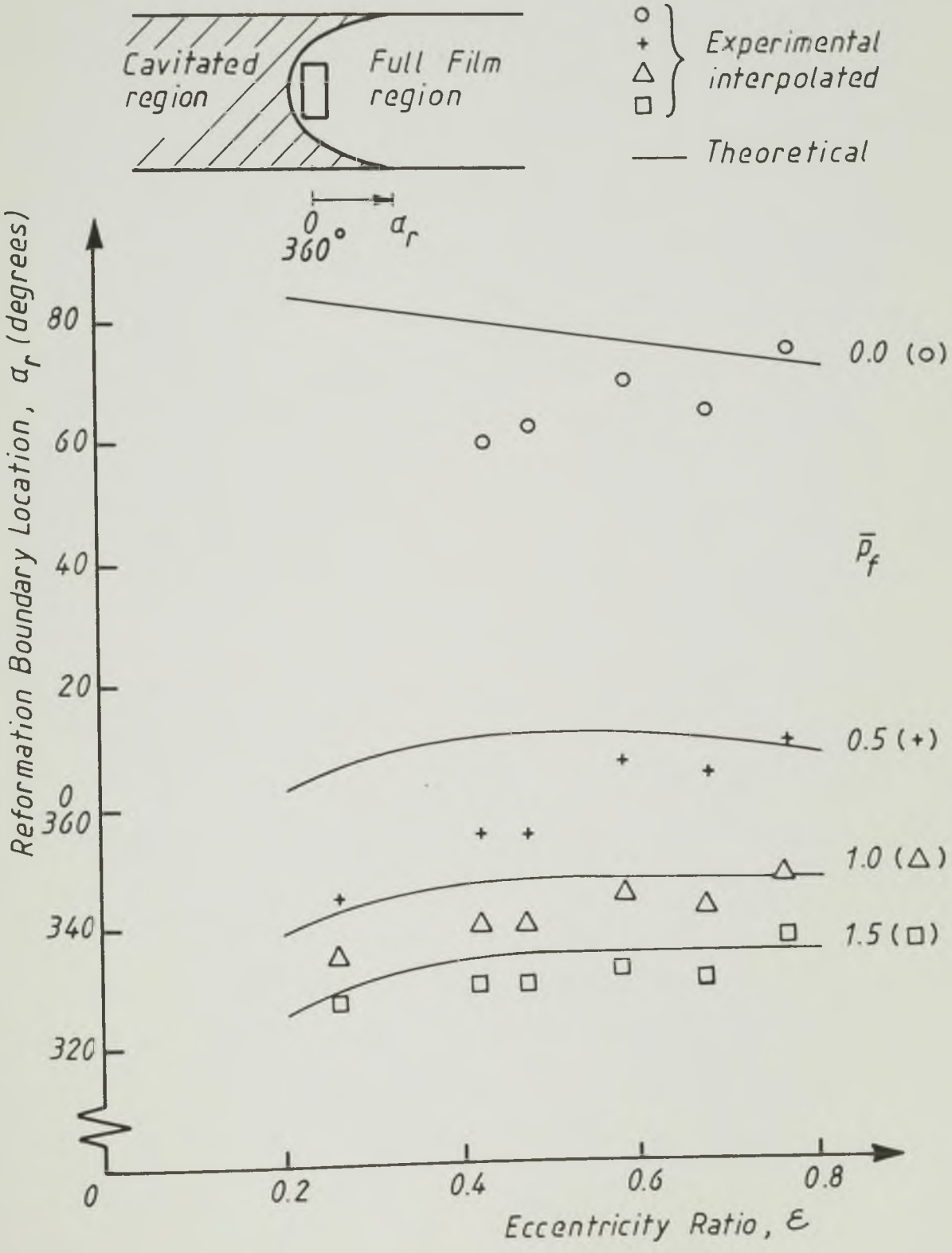

Figure 6.5 A comparison of the interpolated experimental results for the location of the film reformation boundary with the theoretical predictions for Bush 2 (axial groove, a/b = 0.409). Shaft speed 600 r.p.m. (10 Hz)

(v) Approximations associated with the interpolation of experimental results.

It was felt that causes (i) and (ii) were the major sources of errors in the experimental results under discussion.

The discrepancies observed in Figure 6.5 at $\varepsilon < 0.5$ for $\bar{p}_f = 0$ and $\bar{p}_f = 0.5$ occurred with the tests on all bushes and in all cases the experimental results were lower than the theoretical predictions. It did not seem reasonable to attribute those differencies to the possible causes of error enumerated above. It is worth noting that very good agreement in dimensionless side flow rate was achieved at all values of (ε) for $\bar{p}_f = 0$ and $\bar{p}_f = 0.5$ (see Figure 6.2). A plausible explanation for these discrepancies could not be found.

Figure 6.6 shows a comparison of the experimental results for the angular location of the film rupture boundary (α_c) with the theoretical predictions, observed with Bush 3. The experimentally determined values of (α_c) were not significantly affected by the oil supply pressure. The theoretical predictions showed a very slight variation of (α_c) with ($\bar{p}_f$) for a given (ε). The solid curve represented in Figure 6.6 gives the theoretical predictions for all values of ($\bar{p}_f$) with a maximum error of 3.5^o. Large experimental discrepancies (within the range 30^o-42^o) with the theoretical predictions were observed at all values of eccentricity ratio. They could be partly due to experimental errors but it was belived that they were mainly a result of the physical model for film rupture adopted and incorporated in the theoretical analysis. Elrod's cavitation algorithm, which formed the basis of the present theoretical analysis, incorporated the Reynolds boundary conditions which assume that pressure and pressure gradients take the value zero at the

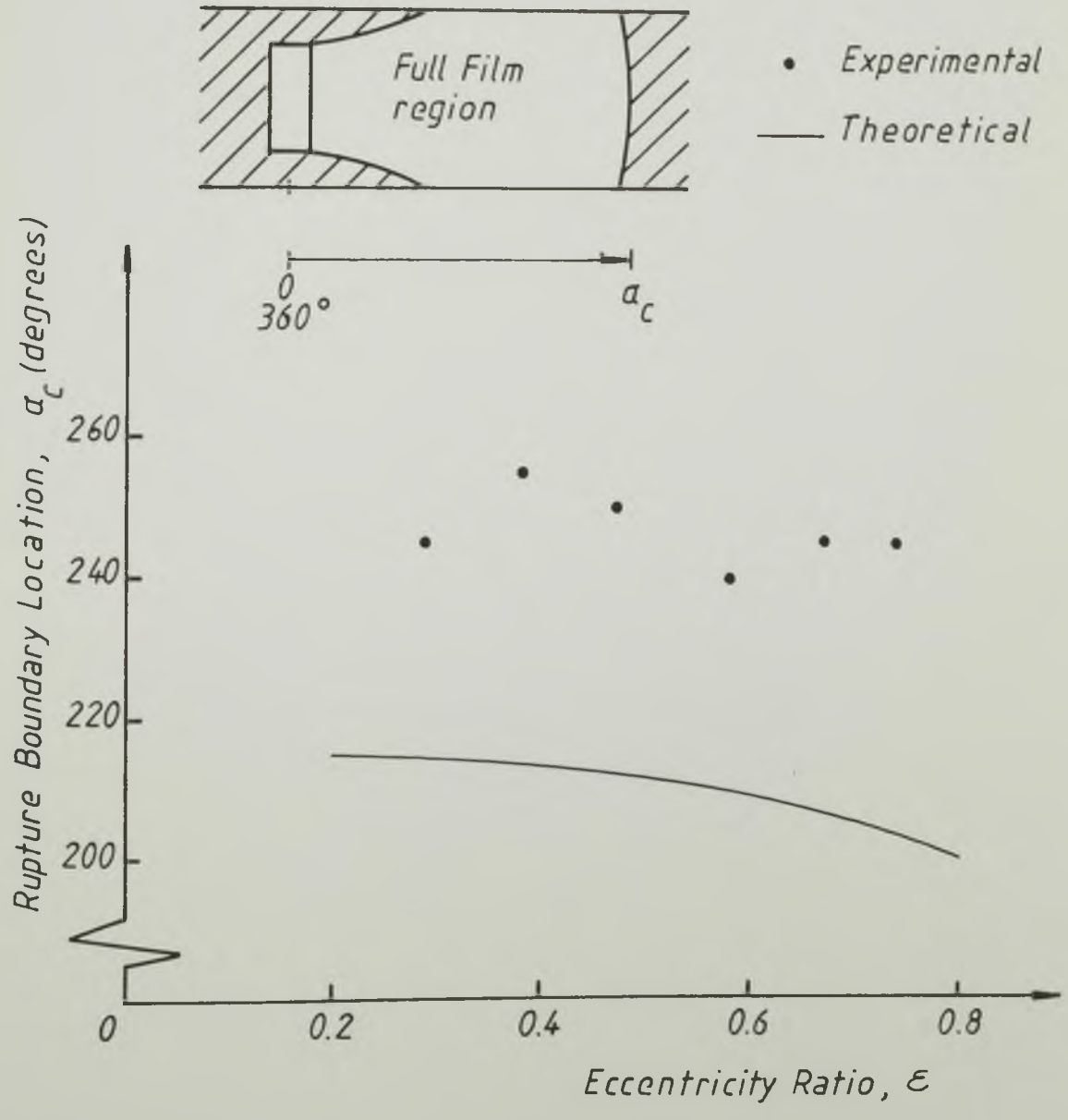

Figure 6.6 A comparison of the experimental results for the location of the film rupture boundary with the theoretical predictions for Bush 3 (axial groove, a/b = 0.708) at all values of supply pressure. Shaft speed, 600 r.p.m. (10 Hz).

film break down. Although commonly used, the Reynolds boundary conditions for film rupture cannot predict the negative pressure loop which has been observed by a number of researchers immediately upstream of film break down (McKee and McKee (1932), Dowson (1957), Floberg (1965), Etsion and Ludwig (1982)).

The occurrence of a sub-ambient pressure loop results in an extended full film region in comparison with theoretically predicted by solutions incorporating Reynolds' conditions. Theoretical models for film rupture have been presented also by Floberg (1965, 1968) and Coyne and Elrod (1970, 1971) both predicting a sub-cavity pressure loop upstream of the cavitating region. Taylor (1973) investigated the effect of the theoretical model used on the prediction of the angular location of the film rupture boundary for infinite width journal bearings. The boundary conditions considered were the Reynolds boundary conditions and a condition derived from a flow separation theory presented by Birkhoff and Hays (1963) which assumes a full width film and no liquid-gas interface (this theory was later extended by Coyne and Elrod (1970, 1971) to consider the presence of a liquid-gas interface). The comparative results showed that by using the separation condition the angular location of the rupture boundary was extended by as much as 60^{o} at $\varepsilon = 0.4$ and 25^{o} at $\varepsilon = 0.7$, in comparison with the results obtained using Reynolds' conditions. These results seemed to indicate that the large differences observed in Figure 6.6 were mainly attributable to the rupture boundary conditions incorporated in the theoretical analysis.

Using Coyne and Elrod (1970, 1971) flow separation conditions at film rupture, Taylor (1975) carried out a theoretical analysis of infinite width journal bearings and found that there exists a minimum value of eccentricity ratio below which separation does not occur. It has been pointed out in Section 6.3.1 that cavitation was not observed in some experiments with Bush 1 and Bush 2 contrary to the

predictions of the present theoretical analysis. The findings of Taylor (1975) show that such a situation can be predicted theoretically by using more appropriate rupture boundary conditions. If a rupture cavitation boundary does not occur below a certain value of (ε) a reformation boundary will not occur below the same value of (ε). It would be interesting to know what would be the predictions of (α_r) from a theoretical analysis incorporating both the Coyne and Elrod (1970, 1971) rupture boundary conditions and the Jakobsson and Floberg (1957) reformation boundary conditions, as (ε) gradually increases, and if this could provide some explanation for the large discrepancies observed in Figure 6.5 at low values of (ε) and ($\bar{p}_f$).

The Influence of Dimensionless Supply Pressure on the Location of the Film Reformation Boundary

Figure 6.7 shows the effect of dimensionless supply pressure on the location of the film reformation boundary for Bush 1 at ε = 0.74 and a shaft speed of 600 r.p.m. (10 Hz). The correlation between the experimental results and the theoretical predictions was good. A maximum discrepancy of 11° was observed at $\bar{p}_f$ = 0.384 and could probably be due to some of the possible causes of errors already discussed.

The results shown in Figure 6.7 are consistent with the results for dimensionless flow rate shown in Figure 6.1 corresponding to the maximum value of (ε) tested (ε = 0.74); the experimentally determined dimensionless side flow rate was always smaller than the theoretical predictions and it is interesting to note that the biggest discrepancy occurred at a value of ($\bar{p}_f$) approximately equal to the one that produced the biggest discrepancy in Figure 6.7.

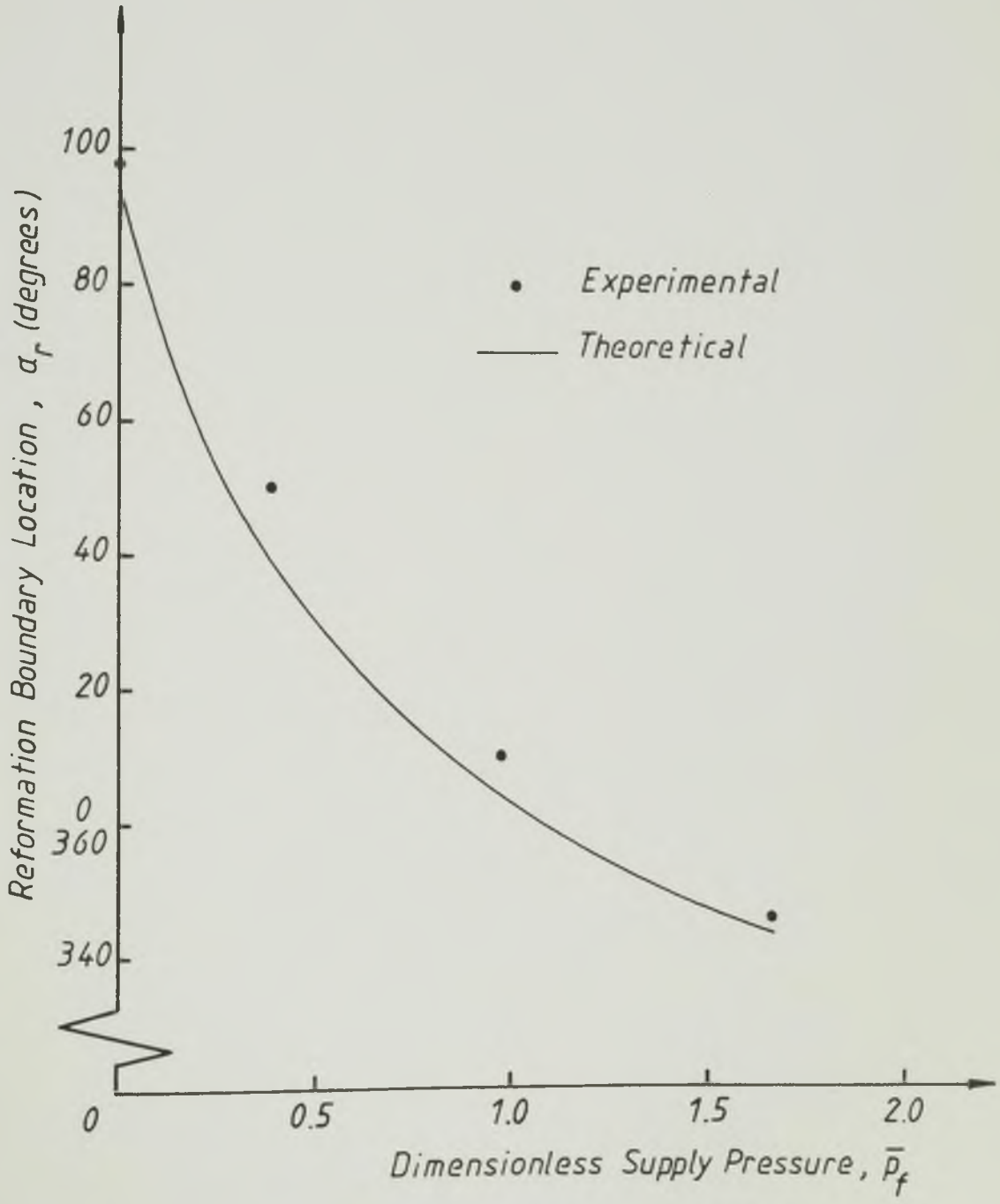

Figure 6.7 The influence of dimensionless supply pressure on the location of the film reformation boundary. Bush 1(oil hole). Shaft speed, 600 r.p.m. (10 Hz). Eccentricity ratio, ε = 0.74

The Influence of Shaft Speed on the Location of the Film Reformation Boundary

The effect of shaft speed on the angular location of the film reformation boundary is shown in Figure 6.8 for Bush 2, at two values of oil supply pressure and fixed $\varepsilon = 0.67$.

According to the predictions of the theoretical analysis, at constant ambient supply pressure the value of (α_r) should be independent of the rotational speed of the shaft. The experimental results showed approximately the same trend with discrepancies similar in magnitude to those observed in Figure 6.5 at $\bar{p}_f = 0$ and $\varepsilon > 0.5$. At a constant supply pressure of 1.695 bar (169.5 kN/m^2) increasing values of speed resulted in decreasing values of dimensionless supply pressure which varied from 2.697 to 0.738 during the test. A maximum discrepancy of 16^o between the experimentally determined and the theoretically predicted values of (α_r) was observed at a shaft speed of 800 r.p.m. (13.33 Hz). At speeds greater than 600 rp.m. (10 Hz) the instability of the film immediately upstream of the reformation boundary already discussed was observed and might have affected the identification of the reformation boundary.

The experimental results for (α_r) were lower than the theoretical predictions for all values of shaft speed. Again this is consistent with the correlation observed in Figure 6.4 for side flow rate at the same operating conditions.

6.4 Conclusions

The experimental programme has been outlined in this chapter and a comparison of experimental results and theoretical predictions discussed. The following conclusions can be made.

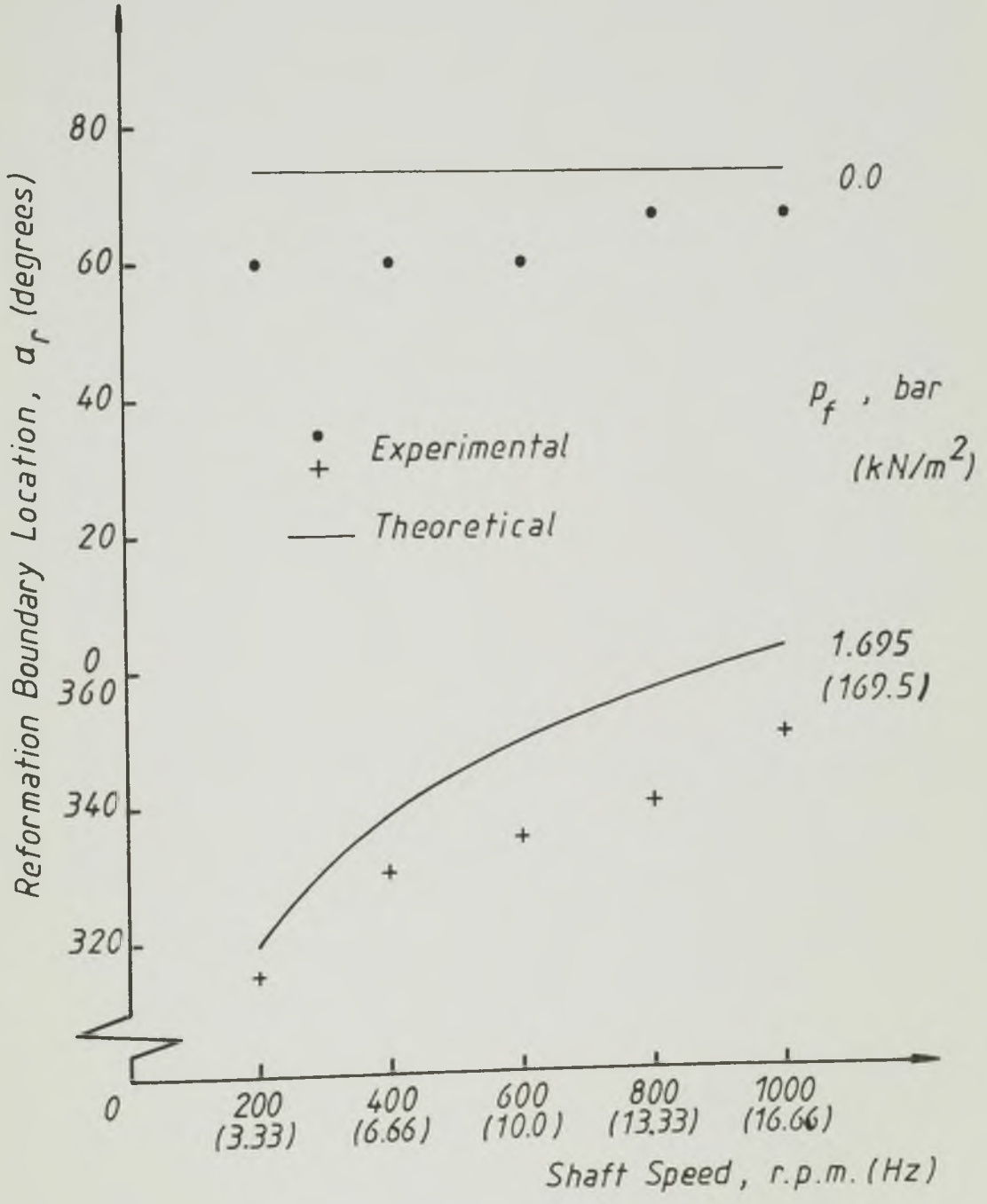

Figure 6.8 The influence of shaft speed on the location of the film reformation boundary.
Bush 2 (axial groove, a/b = 0.409)
Eccentricity ratio, ε = 0.67

(1) Despite the limitations of the experimental apparatus it was possible to carry out the experimental programme as planned. Tests were performed with three bushes of different groove sizes. The parameters that could be varied were the eccentricity ratio (ε), the dimensionless supply pressure ($\bar{p}_f$) and the groove length-to-bearing width ratio (a/b) by using different bushes. The fixed parameters were b/d = 1 and w/d = 0.189. The groove was located at the position of maximum film thickness.

(2) Correlation between the experimentally determined dimensionless flow rate and the theoretical predictions was shown to be very good. With Bush 1, the maximum percentage difference observed was 17.2% at $\bar{p}_f = 0.5$ and $\varepsilon = 0.67$. Results obtained with Bush 2 and Bush 3 showed very good correlation with the theoretical predictions especially at low/moderate values of dimensionless supply pressure. At high values of ($\bar{p}_f$) and low eccentrcity ratio the correlation was not so good, the maximum percentage differences were 22.8% at $\bar{p}_f = 1.5$ and $\varepsilon = 0.41$ with Bush 2, and 27.1% at $\bar{p}_f = 1.5$ and $\varepsilon = 0.28$ with Bush 3.

The possible sources of error in the experimental results have been discussed, the most influential was believed to be bearing misalignment.

The good correlation achieved in the present study between theory and experiment for dimensionless flow rate is certainly a result of a consideration of the lubricant inlet conditions in the theoretical analysis. Most predictions of side flow rate presented in the past have been based on solutions which did not incorporate the lubricant inlet conditions, and this has been recognized by a

number of authors as the primary cause of the large discrepancies observed between experimental results and theoretical predictions.

(3) The correlation observed when the experimental results for the location of the film reformation boundary were compared with the theoretical predictions was, in general, good. At values of dimensionless supply pressure $\bar{p}_f = 1.0$ and $\bar{p}_f = 1.5$ the maximum differences observed were 7^o and 5^o respectively. At lower values of dimensionless supply pressure ($\bar{p}_f = 0$ and $\bar{p}_f = 0.5$) correlation was good only at values of eccentricity ratio greater than 0.5. At lower values of (ε) large discrepancies were observed which could not be entirely due to experimental errors; however, the correlation observed for dimensionless side flow rate at the same operating conditions was very good. A plausible explanation for this 'poor' correlation at low values of (ε) and ($\bar{p}_f$) has not been found.

The consistency between the experimental results for the angular location of the film reformation boundary and those of side flow rate has been highlighted in various points in the discussion. This consistency shows the interrelation between the extent of the full width film and the side flow rate.

(4) Large discrepancies (ranging from 30^o to 42^o) were observed in a comparison of experimental results with theoretical predictions for the location of the film rupture boundary. This was mainly attributable to the rupture boundary conditions incorporated in the theoretical analysis (Reynolds boundary conditions) which could not accommodate the sub-ambient pressure loop that usually occurs immediately upstream of the rupture boundary.

CHAPTER 7

OVERALL CONCLUSIONS AND SUGGESTIONS FOR FUTURE WORK

The present research work has been carried out according to the programme initially established and its main objectives have been achieved.

Conclusions specifically related to individual sections of the work have been dealt with at the end of the respective chapters. In this chapter a summary of the major conclusions and suggestions for future work will be presented.

7.1 Conclusions

(1) An interactive computer program for the design of steadily loaded, fluid film hydrodynamic journal bearings based on the design procedure of ESDU Item No. 66023 (1966), has been developed. Two versions of the program have evolved;

(i) A graphics version, which used some of the design charts of ESDU Item No. 66023 (1966) and also data in tabular form. Interpolation from the tabular data was possible as an alternative to graphical interaction.

(ii) A non-graphics version, in which all design charts have been substituted by tabulated data. This version used less computer memory than the graphics version.

A study of the effect of changes in some bearing parameters (either individual changes or combined changes) on the bearing performance could be carried out enabling the design of an optimized bearing to be undertaken.

(2) A numerical analysis technique for the study of the performance of journal bearings considering the groove geometry and the lubricant supply pressure has been developed. Finite difference approximations associated with a cavitation algorithm developed by Elrod (1981) have been used to determine the pressure distribution and the extent of the full width film in the bearing, without explicit reference to rupture or reformation boundary conditions. A Gauss-Seidel iterative technique was used to solve the resulting system of simultaneous equations.

An investigation of the effect of influential parameters on the convergence of the Gauss-Seidel iteration has been carried out.

(3) The predictions of dimensionless load capacity and dimensionless flow rate for non-reformation conditions have been shown to be in excellent agreement with those of ESDU Item No. 66023 (1966), Ashton (1973) and King (1975).

The performance predictions of the analysis which considered the lubricant inlet conditions for journal bearings with a single axial groove (or oil hole) located at the position of maximum film thickness, have been compared with those of Etsion and Pinkus (1975) for ambient supply pressures only. The significant discrepancies observed, in particular in the dimensionless flow rate, have been attributed mainly to the Etsion and Pinkus (1975) flow continuity condition which appeared to be incorrect.

(4) The performance predictions of ESDU Item No. 66023 (1966), based on solutions of Reynolds' equation which did not incorporate detailed lubricant inlet conditions, have been compared with those of the analysis presented in this thesis which incorporated the lubricant inlet conditions. Remarkably good agreement was observed for the predictions of dimensionless side flow rate at ambient supply pressure, for a wide range of operating conditions. A correction factor (a/b), accounting for the length of the groove, has been included in the calculation of the 'velocity induced flow rate' in ESDU Item No. 66023 (1966). The introduction of this factor is responsible for the agreement noted and is an outstanding example of engineering judgement in design. At finite values of supply pressure, a comparison of predictions of flow rates was possible only in dimensional terms. Good correlation has been observed, with a maximum discrepancy of 16%, for the few cases considered.

A comparison of the predictions of dimensionless load capacity and attitude angle from both procedures has shown a reasonly good correlation at practical operating conditions (high eccentricity ratio and low/moderate dimensionless supply pressure). If, however, the hydrostatic pressure in the groove region becomes comparable to the hydrodynamic pressure then the predictions of dimensionless load capacity and attitude angle from ESDU Item No. 66023 (1966) have been shown to be inadequate.

(5) The study referred to in (4) above has also shown that the dimensionless side flow rate and the extent of the full width film of lubricant in journal bearings may be greatly affected by the lubricant inlet conditions. These may also influence significantly

the predictions of dimensionless load capacity and attitude angle when the hydrostatic pressures in the bearing are comparable to the hydrodynamic pressures.

(6) Charts for predicting dimensionless load capacity and dimensionless side flow rate have been developed.

(7) An experimental programme has been carried out in conjunction with the theoretical work. An apparatus has been designed and commissioned specifically for this study. The performance of three glass bushes, all of width-to-diameter ratio of unity, clearance ratio of 4.365×10^{-3} and of variable groove length was studied experimentally. Measurements of side flow rate and of the location of the rupture and the reformation boundaries were performed at values of eccentricity ratio and oil supply pressure within the ranges (0.2-0.8) and (0-271 kN/m^2) respectively. Excellent correlation has been achieved between the theoretical predictions of dimensionless side flow rate and the experimental measurements for all bushes. The agreement between theoretical predictions and experimental measurements of the location of the film reformation boundary was good except at low values of eccentricity ratio and dimensionless supply pressure.

Discrepancies ranging from 30° to 42° have been observed between the theoretical predictions of the location of the rupture boundary and the experimental measurements. This has been attributed mainly to the rupture boundary conditions incorporated into the thoeretical analysis (the Reynolds' rupture boundary conditions).

7.2 Suggestions for Future Work

(1) It has been shown that the lubricant inlet conditions affect significantly the flow rate and the extent of the full width film in journal bearings. Theoretical predictions of power loss in the bearing, which may be influenced by the extent of the full width film, have not been determined. In view of its importance, together with the lubricant flow rate, on the calculation of the effective temperature of the lubricant, it would be of interest to know how the inclusion of film reformation considerations into the analysis might affect the power loss.

(2) The numerical analysis developed could be extended to cope with more practical grooving arrangements. The extension of this analysis to journal bearings with axial grooves at specific locations in relation to the load line would not be difficult, but it would require another iterative loop in order to determine the attitude angle. The computation time would, therefore, be substantially increased.

The same technique could also be applied to the study of the effect of film reformation considerations on the performance of circumferentially grooved journal bearings.

(3) The computation time required for a single solution was normally about 250-350 cpu seconds on the Amdahl V/470 computer. An investigation of alternative schemes of solution leading to the reduction of the computational time would be worthwhile, particularly if the analysis presented in this thesis was to be applied to journal bearings with alternative, practical grooving arrangements or to dynamically loaded bearings.

(4) The journal bearing analysis has been carried out for an isoviscous lubricant, a common assumption in bearing analysis. In reality, however, the viscosity of the lubricant in the bearing varies, mainly due to temperature variations, and this affects the bearing performance. With confidence in flow rate predictions established, a detailed consideration of thermal effects would seem to be justified.

REFERENCES

Ashton, J.N. (1973), 'Optimum Computerized Design of Hydrodynamic Journal Bearings', Ph.D. Thesis, University of Leeds.

Birkhoff, G. and Hays, D.F. (1963), 'Free Boundaries in Partial Lubrication', J. Math. Phys., Vol. 42.

Cameron, A. and Wood, W.L. (1949), 'The Full Journal Bearing', Proc. Inst. Mech. Eng., Vol. 161.

Clayton, D. (1946), 'An Exploratory Study of Oil Grooves in Plain Bearings', Proc. Inst. Mech. Eng., Appl. Mech., Vol. 155.

Cole, J.A. and Hughes, C.J. (1956), 'Oil Flow and Film Extent in Complete Journal Bearings', Proc. Inst. Mech. Eng., Vol. 170.

Connors, H.J. (1962), 'An Analysis of the Effect of Lubricant Supply Rate on the Performance of the 360° Journal Bearing', Trans. A.S.L.E., Vol. 5.

Coyne, J.C. and Elrod, H.G. (1970), 'Conditions for the Rupture of a Lubricating Film. Part I: Theoretical Model', Trans. A.S.M.E., J. Lub. Techn., Vol. 92, No. 3.

Coyne, J.C. and Elrod, H.G. (1971), 'Conditions for the Rupture of a Lubricating Film - Part II: New Boundary Conditions for Reynolds Equation', Trans. A.S.M.E., J. Lub. Techn., Vol. 93, No. 1.

Dowson, D. (1957), 'Cavitation in Lubricating Films Supporting Small Loads', Proc. Inst. Mech. Eng., Conf. on Lubrication and Wear.

Dowson, D. and Ashton, J.N. (1976), 'Optimum Computerized Design of Hydrodynamic Journal Bearings', Int. J. Mech. Sci., Vol. 18.

Dowson, D. and Taylor, C.M. (1979), 'Cavitation in Bearings', Ann. Rev. Fluid Mech., Vol. 11.

Dubois, G.B. and Ocvirk, F.W. (1953), 'Analytical Derivation and Experimental Evaluation of Short Bearing Approximation for Full Journal Bearings', N.A.C.A. Techn. Note 1157.

Elrod, H.G. and Adams, M.L. (1974), 'A Computer Program for Cavitation and Starvation Problems', Proc. 1st Leeds-Lyon Symposium on Tribology.

Elrod, H.G. (1981), 'A Cavitation Algorithm', Trans. A.S.M.E., J. Lub. Techn., Vol. 103, No. 3.

ESDU Item No. 66023 (1966), 'Calculation Methods for Steadily Loaded Pressure Fed, Hydrodynamic Journal Bearings', Inst. Mech. Eng. London.

Etsion, I. and Pinkus, O. (1974), 'Analysis of Short Journal Bearings With New Upstream Boundary Conditions', Trans. A.S.M.E., J. Lub. Techn., Vol. 96, No. 3.

Etsion, I. and Pinkus, O. (1975), 'Solutions of Finite Journal Bearings With Incomplete Films', Trans. A.S.M.E., J. Lub. Techn., Vol. 97, No. 1.

Etsion, I. and Ludwig, L.P. (1982), 'Observation of Pressure Variation in the Cavitation Region of Submerged Journal Bearings', Trans. A.S.M.E., J. Lub. Tech., Vol. 104, No. 2.

Floberg, L. (1965), 'On Hydrodynamic Lubrication With Special Reference to Sub-cavity Pressures and Number of Streamers in Cavitation Regions', Acta Polytech. Scand. Mech. Eng. Ser., ME 19.

Floberg, L. (1968), 'Sub-cavity Pressures and Number of Oil Streamers in Cavitation Regions With Special Reference to the Infinite Journal Bearing', Acta Polytech. Scand. Mech. Eng. Ser., ME 37.

Galvin, G.D., Naylor, H. and Wilson, A.R. (1964), 'The Effect of Pressure and Temperature on Some Properties of Fluids of Importance in Elastohydrodynamic Lubrication', Proc. Inst. Mech. Eng., Lub. and Wear Second Convention, Vol. 178, Pt. 3N.

Hargreaves, D.J. (1981), 'An Experimental and Theoretical Study of Film Formation and Lubricant Flow Rate in Grooved Rectangular Thrust Bearings', Ph.D. Thesis, University of Leeds.

Hayashi, H. and Taylor, C.M. (1980), 'A Determination of Cavitation Interfaces in Fluid Film Bearings Using Finite Element Analysis', J. Mech. Eng. Sci., Inst. Mech. Eng., Vol. 22, No. 6.

Jakobsson, B. and Floberg, L. (1957), 'The Finite Journal Bearing Considering Vaporization', Transactions of Chalmers University of Technology, No. 190.

King, K.F. (1975), 'Two Computer Programs For Turbulent Thin Film Flow', Internal Report, Dept. Mech. Eng., University of Leeds.

Lebeck, A.O. (1981), 'Design of an Optimum Moving Wave and Tilt Mechanical Face Seal for Liquid Applications', BHRA Fluid Eng., 9th International Conference on Fluid Sealing, Paper E2.

Martin, F.A. (1981), Private Communication.

Martin, F.A. and Lee, C.S. (1982), 'Feed Pressure Flow in Plain Journal Bearings', Paper presented at the A.S.L.E. Annual Meeting, Cincinnati, Ohio, U.S.A.

McCallion, H., Lloyd, T. and Yousif, F.B. (1971), 'The Influence of Oil Supply Conditions on the Film Extent and Oil Flow in Journal Bearings', Proc. Inst. Mech. Eng. Tribology Convention.

McKee, S.A. and McKee, T.R. (1932), 'Pressure Distribution in Oil Films of Journal Bearings', Trans. A.S.M.E., Vol. 54.

McKee, S.A. (1952), 'Oil Flow in Plain Journal Bearings', Trans. A.S.M.E., Vol. 74.

Milne, A.A. (1974), 'A Finite Element Method for Calculating Oil Flow in Bearings', N.E.L. Report No. 569.

Miranda, A.A.S. (1983), 'Interactive Computer Aided, Design of Steadily Loaded, Liquid Film, Hydrodynamic Plain Journal Bearings', Research Report, Dept. Mech. Eng., University of Leeds.

Peeler, R.L. and Green, J. (1959), 'Measurement of Bulk Modulus of Hydraulic Fluids', A.S.T.M. Bulletin.

Randall, T.J. (1968), 'A Note on the Estimation of the Optimum Successive Over-relaxation Parameter for Laplace's Equation', Computer Journal, Vol. 10.

Reynolds, O. (1886), 'On the Theory of Lubrication and its Application to Mr. Beauchamp Tower's Experiments, Including an Experimental Determination of the Viscosity of Olive Oil', Phil. Trans. Roy. Soc. London, Ser. A, Vol. 177.

Ruddy, A.V. (1979), 'The Dynamics of Rotor-Bearing Systems With Particular Reference to the Influence of Fluid-Film Journal Bearings and the Modelling of Flexible Rotors', Ph.D. Thesis, University of Leeds.

Seireg, A. and Ezzat, H. (1969), 'Optimum Design of Hydrodynamic Journal Bearings', Trans. A.S.M.E., J. Lub. Techn., Vol. 91, No. 3.

Siew, A.H. and Reason, B.R. (1982), 'A New Approach to Journal Bearing Design', 59th Symposium of the AGARD Propulsion and Energetics Panel, Ottawa, Canada.

Smith, G.D. (1971), 'Numerical Solution of Partial Differential Equations', Oxford University Press, London.

Sommerfeld, A. (1904), 'Zur Hydrodynamiscien Theorie der Schmiermittehreibung', Z. Maths. Phys., 50.

Taylor, C.M. (1971), 'A Survey of Computerized Bearing Design Programmes', Tribology, Vol. 4, No. 2.

Taylor, C.M. (1973), 'Separation Cavitation; Solutions for the Infinite Width Cylinder-Plane and Journal Bearing Configurations', J. Mech. Eng. Sci., Vol. 15, No. 3.

Taylor, C.M. (1975), 'Gaseous Cavitation in Lightly Loaded Liquid Film Journal Bearings', Int. J. Mech. Sci., Vol. 17.

Tribology Handbook (1973), Edited by M.J. Neale, Butterworths.

APPENDIX A AUTOMATIC GENERATION OF THE VARIABLE MESH

In the discussion that follows refer to Figure 3.11, Chapter 3.

(1) Number of Mesh Intervals in the Axial Direction

The total number of mesh intervals in the axial direction was (N-1). There were two different mesh sizes in this direction: one for the region over the groove and the other for the region between the bearing edge and the groove edge.

(i) The number of mesh intervals over the groove $(N-N_1)$ was dependent on (a/b). It was given by the approximation to the nearest integer of the value of

$$(N-1) \times (a/b) - 2 \qquad (A.1)$$

(ii) The number of mesh intervals over the region between the groove edge and the bearing edge was then determined from

$$(N_1-1) = (N-1) - (N-N_1)$$

Two extra mesh intervals, with respect to the proportion ((1-a/b) x (N-1)),were normally given to this region (see expression (A.1)) to allow for a more accurate location of the film reformation boundary. The minimum number of mesh intervals in this region was three $((N_1-1)_{min} = 3)$ such that four significant pressure values were always used in the calculation of pressure gradients.

(2) Number of Mesh Intervals in the Circumferential Direction

The total number of mesh intervals in the circumferential direction was (M-1).

There were three different mesh sizes in this direction: one in the region over the groove, another in the film reformation region and a third one in the remaining bearing area.

(i) The number of mesh intervals over the groove $((M_1-1) + (M-M_4))$ was dependent on the value of (w/d) as shown in Table A.1.

Value of (w/d)	No. of mesh intervals
$w/d \leq 0.1$	4
$0.1 < w/d \leq 0.15$	6
$0.15 < w/d \leq 0.25$	8
$w/d > 0.25$	10

Table A.1 Number of mesh intervals over the groove in the circumferential direction.

(ii) Over the film reformation region, for reasons of accuracy in the determination of the reformation boundary location, a finer mesh size was used which corresponded to an arc of approximately 2°.

An estimate of the angular extent of the film reformation region was obtained using expressions derived from results previously obtained for a grid of (51x11) nodes and even mesh size in the circumferential direction (apart from the

region over the groove).

The angle (α_{1-2}) corresponding to the number of mesh intervals (M_2-M_1) was determined from

$$\alpha_{1-2} \text{ (degrees)} = (1.22 - a/b)/0.01 \quad \text{if } \bar{p}_f < 0.025$$
$$\alpha_{1-2} \text{ (degrees)} = ((1.22- a/b)/0.01) - (10 + 160\ \bar{p}_f) \quad \text{if } \bar{p}_f \geq 0.025 \qquad (A.2)$$

To allow for better accuracy in the determination of pressure gradients at the downstream edge of the groove the angle (α_{1-2}) was never less than 8^o.

At a supply pressure greater than zero the finer mesh extended to the region upstream of the groove. The angle (α_{3-4}) corresponding to the number of mesh intervals (M_4-M_3) was determined from

$$\alpha_{3-4} \text{ (degrees)} = 40\ \bar{p}_f \qquad (A.3)$$

Minimum and maximum values of (α_{3-4}) were taken as 8^o and 30^o respectively.

The number of mesh intervals of finer size over the film reformation region in the circumferential direction was given by the integer part of the following reals,

$$\frac{\alpha_{1-2}}{2} \quad \text{for } (M_2-M_1)$$

and

$$\frac{\alpha_{3-4}}{2} \quad \text{for } (M_4-M_3)$$

(iii) The number of mesh intervals over the remaining part of the bearing area was found by difference to the total number of mesh intervals in the circumferential direction (M-1).

APPENDIX B SAMPLE INPUT AND OUTPUT DATA AND LISTING OF THE COMPUTER PROGRAM

A flow chart of the computer program developed for the analysis of fluid film, finite width, hydrodynamic journal bearings has been discussed in Chapter 3. A sample of input and output data and the listing of the program and its subroutines are presented in this appendix.

```
PRINT OUT PRESSURES (1=YES, 0=NO)
0
NUMBER OF NODES (CIRCUMF.- AXIAL)
91    19
MESH REPRESENTATION REQUIRED (1=YES, 0=NO)
0
BULK MODULUS PARAMETER
0.03
RELAXATION FACTOR, TOLERANCE
1.0    1.0D-05
MAXIMUM CYCLES ALLOWED PER CASE
5000
LIMIT IN CPU TIME (BATCH-290/BIGBATCH-1790/
                   MAXBATCH-7190)
1790
NUMBER OF CASES
1
B/D     ECCRAT.    A/B     W/D    SUPPLY PRESS
0.5       0.7      0.8     0.2       0.2
```

(I)

SAMPLE INPUT DATA, (I)

SAMPLE OUTPUT DATA, (O)

```
APPLICATION OF ELRODS ALGORITHM TO JOURNAL BEARINGS


WIDTH-DIAMETER RATIO   B/D =  0.500
ECCENTRICITY RATIO = 0.700
AXIAL GROOVE AT THE MAX. FILM THICKNESS
GROOVE SIZE     A/B =  0.800
                W/D =  0.200
NORMALIZED SUPPLY PRESSURE =   0.200
BULK MODULUS PARAMETER OF THE OIL =     0.030


RELAXATION FACTOR = 1.000
TOLERANCE =  0.10D-04
NUMBER OF CYCLES PERFORMED :   711
CPU TIME USED =  226.7 SECONDS


PRESSURE DISTRIBUTION SYMMETRICAL ABOUT THE BRG CENTRE LINE
ANGLE MEASURED FROM THE POSITION OF MAXIMUM FILM THICKNESS


DIMENSIONLESS LOAD CAPACITY  =   1.6526
ATTITUDE ANGLE =  44.0  DEGREES
DIMENSIONLESS FLOW RATES :
FLOW ISSUING FROM THE GROOVE =  1.4811
FLOW FROM THE BEARING SIDES =  1.5447
FLOW INTO THE CAVITATION REGION =  0.1588
```

(O)

```
C
C  ---------------------------------------------------------
C  A PROGRAM FOR THE ANALYSIS OF FINITE WIDTH JOURNAL BEARINGS
C  CONSIDERING FILM REFORMATION.
C  IT INCORPORATES THE ELROD CAVITATION ALGORITHM AND USES A
C  GAUSS-SEIDEL ITERATIVE METHOD TO SOLVE THE RESULTING
C  SYSTEM OF FINITE DIFFERENCE EQUATIONS.
C  A DIAGRAM SHOWING THE LOCATION OF THE RUPTURE AND OF THE
C  REFORMATION BOUNDARIES MAY BE DRAWN.
C  ONLY THE CASE OF A SINGLE AXIAL GROOVE (OR HOLE) LOCATED AT
C  THE POSITION OF MAXIMUM FILM THICKNESS IS CONSIDERED
C  ---------------------------------------------------------
C
C       M - NUMBER OF NODES IN THE CIRCUMFERENTIAL DIRECTION.
C           201  IS THE MAXIMUM ALLOWABLE
C       N - NUMBER OF NODES IN THE AXIAL DIRECTION.
C           31  IS THE MAXIMUM ALLOWABLE
C      BD - BEARING WIDTH-TO-BEARING DIAMETER RATIO
C     ECC - ECCENTRICITY RATIO
C      AB - GROOVE LENGTH-TO-BEARING WIDTH RATIO
C      WD - GROOVE WIDTH-TO-BE ARING DIAMETER RATIO
C   PFBAR - NORMALIZED SUPPLY PRESSURE
C    BBAR - NORMALIZED BULK MODULUS OF THE OIL
C      RF - RELAXATION FACTOR
C     TOL - TOLERANCE
C  NCYMAX - MAXIMUM NUMBER OF CYCLES ALLOWABLE IN GAUSS-
C           SEIDEL ITERATION
C    SECS - CPU TIME (SECONDS) USED IN EACH RUN
C     CPU - TOTAL CPU TIME USED
C  CPULIM - MAXIMUM CPU TIME ALLOWABLE TO RUN THE PROGRAM
C     IPR - INDICATOR. IPR=0 MEANS THAT PRINT OUT OF PRESSURE
C           DISTRIBUTION IS NOT REQUIRED
C   IGRID - INDICATOR. NGRID=0 MEANS THAT A DRAWING
C           REPRESENTING THE MESH IS NOT REQUIRED
C   NCASE - NUMBER OF CASES TO BE CONSIDERED IN EACH RUN
C      IC - COUNTER FOR THE NUMBER OF CASES PERFORMED
C
      IMPLICIT REAL*8(A-H,O-Y)
      COMMON/BLOCK1/PI
      COMMON/BLOCK2/H(202),ANGLE(202),DXBAR(201),DYBAR(31)
      COMMON/BLOCK3/IG(32,202),NG(32,202),TPREV(32,202)
      COMMON/BLOCKT/THETA(32,202)
      COMMON/BLOCK4/P(31,201)
      COMMON/BLOCK5/PFUN(201),AFUN(201)
      COMMON/BLOCK7/XBCAV(61),YBCAV(61),XBREF(61),YBREF(61),
     +              XBREF1(31),YBREF1(31),XBREF2(61),YBREF2(61)
      COMMON/BLOCK8/QSIDE,QGR,QGR1,QGR2,QGR3,QCAV
      COMMON/BLOCKZ/ZXCUR(3),ZYCUR(3)
C
C  COUNTING THE CPU TIME - TIMER INITIALIZATION
C
      SECS=0.0
      SAUX=0.0
      CALL SETTIM
C
C  NOMINATION OF THE PLOTTER TO DRAW THE GRAPHS
C
      CALL C1012
      CALL DEVPAP(430.0,250.0,1)
C
C  ---------------------
C  READING THE DATA FILE
C  ---------------------
C
      PI=3.1415926536
      IC=0
      READ(5,100)TITLE
100   FORMAT(10A5)
      READ(5,*)IPR
      READ(5,100)TITLE
      READ(5,*)M,N
      READ(5,100)TITLE
      READ(5,*)IGRID
      READ(5,100)TITLE
      READ(5,*)BBAR
      READ(5,100)TITLE
      READ(5,*)RF,TOL
      READ(5,100)TITLE
      READ(5,*)NCYMAX
      READ(5,100)TITLE
      READ(5,100)TITLE
      READ(5,*)CPULIM
      READ(5,100)TITLE
      READ(5,*)NCASE
      READ(5,100)TITLE
70    READ(5,*)BD,ECC,AB,WD,PFBAR
C
C  ---------------------------------------------------------
C  CALCULATION OF THE DIMENSIONLESS FILM THICKNESS AT EVERY
C  NODAL POINT. DETERMINATION OF THE GRID SPACINGS
C  ---------------------------------------------------------
C
      CALL FILM(M,N,ECC,AB,WD,NIGRX,NIEDY,PFBAR)
C
C  ---------------------------------------------------------
C  USING A GAUSS-SEIDEL ITERATIVE METHOD TO SOLVE THE FINITE
C  DIFFERENCE EQUATIONS
C  ---------------------------------------------------------
C
      CALL GAUSS(M,N,NCYCLE,NCYMAX,PFBAR,TOL,RF,NIGRX,NIEDY,
```

```
     +            BBAR,BD,CFULIM,CPU)
      IF(CPU.GE.CPULIM)GOTO 10
      IF(NCYCLE.GE.NCYMAX)GOTO 10
C
C  ------------------------------------------------------
C  CALCULATION OF THE PRESSURE DISTRIBUTION AND LOAD CAPACITY
C  ------------------------------------------------------
C
      CALL PRESS(M,N,BBAR)
      CALL LOAD(M,N,WBAR,ATTA)
C
C  ------------------------------------------------------
C  LOCATION OF THE CAVITATION AND THE REFORMATION BOUNDARIES
C  ------------------------------------------------------
C
      CALL CVRF(M,N,NIGRX,NIEDY,PFBAR,JJ,JCAV,JR,JR1,JREF)
C
C  -------------------------
C  DETERMINATION OF FLOW RATES
C  -------------------------
C
      CALL FLOW(M,N,BD,AB,NIGRX,NIEDY,JJ,JR1)
C
C  COUNTING THE CPU TIME
C
      SAUX=SAUX+SECS
      SECS=CPUTIM(X)-SAUX
C
C  -------------------------------
C  WRITING OUT THE CALCULATED VALUES
C  -------------------------------
C
10    WRITE(10,150)BD
150   FORMAT(1H1,//,' APPLICATION OF ELRODS ALGORITHM TO JOURNAL',
     +1X,'BEARINGS',/////,' WIDTH-DIAMETER RATIO   B/D =',F7.3,/)
      WRITE(10,200)ECC
200   FORMAT(' ECCENTRICITY RATIO =',F6.3,/)
      WRITE(10,250)AB,WD
250   FORMAT(' AXIAL GROOVE AT THE MAX. FILM THICKNESS',//,
     +' GROOVE SIZE    A/B =',F7.3,//,
     +'                W/D =',F7.3,/)
      WRITE(10,300)PFBAR
300   FORMAT(' NORMALIZED SUPPLY PRESSURE =',F8.3,/)
      WRITE(10,350)BBAR
350   FORMAT(' BULK MODULUS PARAMETER OF THE OIL =',F10.3,///)
      WRITE(10,400)RF
400   FORMAT(' RELAXATION FACTOR =',F6.3,/)
      WRITE(10,450)TOL
450   FORMAT(' TOLERANCE =',D10.2,/)
      IF(CPU.GE.CPULIM)GOTO 80
      IF(NCYCLE.GE.NCYMAX)GOTO 20
      WRITE(10,500)NCYCLE
500   FORMAT(' NUMBER OF CYCLES PERFORMED :',I6,/)
      WRITE(10,550)SECS
550   FORMAT(' CPU TIME USED =',F7.1,' SECONDS')
      WRITE(10,600)
600   FORMAT(1H ,///,' PRESSURE DISTRIBUTION SYMMETRICAL ABOUT THE ',
     +'BRG CENTRE LINE',//,
     +' ANGLE MEASURED FROM THE POSITION OF MAXIMUM FILM THICKNESS')
      WRITE(10,650)WBAR,ATTA
650   FORMAT(1H ,///,' DIMENSIONLESS LOAD CAPACITY  =',F9.4,//,
     +' ATTITUDE ANGLE =',F6.1,' DEGREES')
      WRITE(10,700)
700   FORMAT(1H ,/,' DIMENSIONLESS FLOW RATES :')
      WRITE(10,750)QGR,QSIDE,QCAV
750   FORMAT(1H ,/,' FLOW ISSUING FROM THE GROOVE =',F8.4,//,
     +' FLOW FROM THE BEARING SIDES =',F8.4,//,
     +' FLOW INTO THE CAVITATION REGION =',F8.4)
      IF(IPR.EQ.0)GOTO 30
      WRITE(10,800)
800   FORMAT(1H1,//,50X,' NORMALIZED PRESSURE DISTRIBUTION',//,
     +' ANGLE',48X,'. . . AXIAL NODES . . .',/,
     +' -----   ------------------------------------------------',
     +'-------------------------------------------------',
     +'--')
      DO 50 J=1,M
      WRITE(10,850)ANGLE(J),(P(I,J),I=1,N)
50    CONTINUE
850   FORMAT(1X,F6.1,3X,19F6.3)
C
C  ------------------------------------------------------
C  DRAWING THE CAVITATION AND THE REFORMATION BOUNDARIES
C  ------------------------------------------------------
C
30    CALL DIAG(M,N,NIGRX,NIEDY,JJ,JCAV,JR,JR1,JREF,BD,
     +         ECC,AB,WD,PFBAR,IGRID)
      GOTO 60
20    WRITE(10,900)NCYMAX
900   FORMAT(1H ,///,' CONVERGENCE NOT ACHIEVED WITHIN',I6,
     +' CYCLES')
60    IC=IC+1
      IF(IC.LT.NCASE)GOTO 70
      GOTO 90
80    WRITE(10,950)
950   FORMAT(1H ,///,' MAXIMUM CPU TIME EXCEEDED - ',
     +'JOB NOT COMPLETE')
90    CALL DEVEND
      STOP
      END
```

```
      SUBROUTINE FILM(M,N,ECC,AB,WD,NIGRX,NIEDY,PFBAR)
C
C     ------------------------------------------------
C     SETS UP THE NORMALIZED MESH AND CALCULATES THE FILM
C     THICKNESS AT EVERY NODAL POINT
C     ------------------------------------------------
C
C     M - NUMBER OF NODES IN THE CIRCUMFERENTIAL DIRECTION.
C         MUST BE ODD. MAXIMUM M=201
C     N - NUMBER OF NODES IN THE AXIAL DIRECTION OVER HALF THE
C         BEARING WIDTH. IT MUST BE ODD. MAXIMUM N=31
C     NIGRX - NUMBER OF INTERVALS IN THE CIRCUMFERENTIAL DIRECTION
C             OVER THE GROOVE. IT MUST BE EVEN.
C     NIGRY - NUMBER OF INTERVALS OVER HALF THE GROOVE IN THE AXIAL
C             DIRECTION. IT VARIES WITH A/B
C     NIEDY = (N-1)-NIGRY
C     NIDWX - NUMBER OF INTERVALS OVER THE FILM REFORMATION
C             REGION DOWNSTREAM OF THE GROOVE IN THE CIRCUMFERENTIAL
C             DIRECTION (INTERVALS OF APPROXIMATELY 2 DEGREES)
C     NIUPX - NUMBER OF INTERVALS OVER THE FILM REFORMATION
C             REGION UPSTREAM OF THE GROOVE IN THE CIRCUMFERENTIAL
C             DIRECTION (INTERVALS OF APPROXIMATELY 2 DEGREES)
C
      IMPLICIT REAL*8(A-H,O-Y)
      COMMON/BLOCK1/PI
      COMMON/BLOCK2/H(202),ANGLE(202),DXBAR(201),DYBAR(31)
C
C     DETERMINATION OF THE MESH SPACINGS
C
      NIUPX=0
      FFUP=0.0
C     MESH INTERVALS OVER THE GROOVE IN THE CIRCUMFERENTIAL DIRECTION
      IF(WD.LE.0.1)NIGRX=4
      IF((WD.GT.0.1).AND.(WD.LE.0.15))NIGRX=6
      IF((WD.GT.0.15).AND.(WD.LE.0.25))NIGRX=8
      IF(WD.GT.0.25)NIGRX=10
      IF((PFBAR.EQ.0.0).AND.(WD.GT.0.1))NIGRX=NIGRX-2
      DXGR=WD/(FLOAT(NIGRX)*PI)
C     MESH INTERVALS OVER THE FILM REFORMATION REGION IN THE
C     CIRCUMFERENTIAL DIRECTION
      FFDW=(1.22-AB)/0.01
      IF(PFBAR.GE.0.025)FFDW=FFDW-(10.0*160.0*PFBAR)
      IF(FFDW.LT.8.0)FFDW=8.0
      ZFDW=SNGL(FFDW/2.0)
      NIDWX=IFIX(ZFDW)
      DXDW=(FFDW/360.0)/FLOAT(NIDWX)
      IF(PFBAR.EQ.0.0)GOTO 5
      FFUP=PFBAR*40.0
      IF(FFUP.LT.8.0)FFUP=8.0
      IF(FFUP.GT.30.0)FFUP=30.0
      ZFUP=SNGL(FFUP/2.0)
      NIUPX=IFIX(ZFUP)
      DXUP=(FFUP/360.0)/FLOAT(NIUPX)
5     DX=(1.0-WD/PI-(FFDW+FFUP)/360.0)/(M-1-NIDWX-NIGRX-NIUPX)
C     MESH INTERVALS IN THE AXIAL DIRECTION
      AUX=FLOAT(N-1)*(1.-AB)+0.5
      Z=SNGL(AUX)
      NIEDY=IFIX(Z)
C     FOR GOOD ACCURACY ON THE DETERMINATION OF THE
C     REFORMATION BOUNDARY LOCATION
      IF((N-1-NIEDY).GE.4)NIEDY=NIEDY+2
      IF(NIEDY.LT.3)NIEDY=3
      DYED=(1.-AB)/(2.*FLOAT(NIEDY))
      DYGR=AB/(2.*FLOAT(N-1-NIEDY))
C     STORING THE NORMALIZED INTERVALS IN ARRAYS
      JFF=1+NIDWX+NIGRX/2
      JRN=M-NIUPX-NIGRX/2
      DO 10 J=1,M
      IF((J.LE.(NIGRX/2)).OR.(J.GE.(M-NIGRX/2)))DXBAR(J)=DXGR
      IF((J.GT.(NIGRX/2)).AND.(J.LT.JFF))DXBAR(J)=DXDW
      IF((J.GE.JFF).AND.(J.LT.JRN))DXBAR(J)=DX
      IF(PFBAR.EQ.0.0)GOTO 10
      IF((J.GE.JRN).AND.(J.LT.(M-NIGRX/2)))DXBAR(J)=DXUP
10    CONTINUE
      DO 20 I=1,N
      IF(I.GT.NIEDY)GOTO 25
      DYBAR(I)=DYED
      GOTO 20
25    DYBAR(I)=DYGR
20    CONTINUE
C     CALCULATING THE NORMALIZED FILM THICKNESS
      M1=M+1
      DXT=0.0
      DO 30 J=1,M1
      ALPHA=2.*PI*DXT
      ANGLE(J)=360.*DXT
      H(J)=1.+ECC*DCOS(ALPHA)
      IF(J.EQ.M1)GOTO 30
      DXT=DXT+DXBAR(J)
30    CONTINUE
      RETURN
      END
C
C
      SUBROUTINE GAUSS(M,N,NCYCLE,NCYMAX,PFBAR,TOL,RF,NIGRX,
     +                 NIEDY,BBAR,BO,CPULIM,CPU)
C
C     ------------------------------------------------
C     SOLVES THE FINITE DIFFERENCE EQUATIONS AT EVERY NODE
C     USING A GAUSS-SEIDEL ITERATIVE TECHNIQUE
```

```
C  ------------------------------------------------
C
      IMPLICIT REAL*8(A-H,O-Z)
      COMMON/BLOCK1/PI
      COMMON/BLOCK2/H(202),ANGLE(202),DXBAR(201),DYBAR(31)
      COMMON/BLOCK3/IG(32,202),NG(32,202),TPREV(32,202)
      COMMON/BLOCKT/THETA(32,202)
C
      TGR=1.+PFBAR/BBAR
      DB2=(1./BD)**2
C
C  GIVING INITIAL VALUES TO G AND THETA
C
      NCYCLE=0
      CALL SETPAR(M,N,NCYCLE)
C
C  CALCULATING THETA AT EVERY NODE POINT
C
10    IF(NCYCLE.GE.NCYMAX)GOTO 20
      DO 3 I=1,N
      DO 3 J=1,M
3     TPREV(I,J)=THETA(I,J)
      DO 15 I=2,N
      DO 15 J=2,M
C  CHECKING THE CPU TIME USED
      CPU=CPUTIM(X)
      IF(CPU.GE.CPULIM)GOTO 20
C
      IF(I.NE.N)GOTO 4
      THETA(N+1,J)=THETA(N-1,J)
C  BOUNDARY CONDITIONS AT THE GROOVE - PRESSURES ALL
C  ROUND THE GROOVE SET EQUAL TO THE SUPPLY PRESSURE
4     IF(I.LE.NIEDY)GOTO 5
      IF((J.GT.(1+NIGRX/2)).AND.(J.LT.(M-NIGRX/2)))GOTO 5
      THETA(I,J)=TGR
      THETA(I,1)=TGR
C
      GOTO 15
5     IF(J.NE.M)GOTO 6
      THETA(I,M+1)=THETA(I,2)
6     RG1=FLOAT(NG(I,J))
      RG2=FLOAT(NG(I,J+1))
      RG3=FLOAT(NG(I,J-1))
      RG4=FLOAT(NG(I+1,J))
      RG5=FLOAT(NG(I-1,J))
      E1=(RG1*H(J)+RG1*RG2*(H(J+1)-H(J))/2.)
      E2=((H(J+1)+H(J))**3)*RG2*(THETA(I,J+1)-1.)/DXBAR(J)
      E31=THETA(I,J-1)*H(J-1)*(1.-RG3)+RG3*H(J-1)
      E32=RG3*RG1*(H(J)-H(J-1))/2.
      E3=E31+E32
      E4=((H(J)+H(J-1))**3)*RG3*(THETA(I,J-1)-1.)/DXBAR(J-1)
      E5=(H(J)**3)*RG5*(THETA(I-1,J)-1.)/DYBAR(I-1)
      E6=(H(J)**3)*RG4*(THETA(I+1,J)-1.)/DYBAR(I)
      E71=((H(J)+H(J-1))**3)*RG1/DXBAR(J-1)
      E72=((H(J)+H(J+1))**3)*RG1/DXBAR(J)
      E7=E71+E72
      E8=H(J)*(1.-RG1)
      E91=(H(J)**3)*RG1/DYBAR(I-1)
      E92=(H(J)**3)*RG1/DYBAR(I)
      E9=E91+E92
      E10=E3-E1
      E11=E2+E4+E7
      E12=E5+E6+E9
      DXB=(DXBAR(J)+DXBAR(J-1))/2.
      DYB=(DYBAR(I)+DYBAR(I-1))/2.
      T11=(PI*DXB*BBAR*DB2*E12/24.)+DYB*E10/2.
      T12=DYB*BBAR*E11/(192.*PI)
      T21=(PI*DXB*BBAR*DB2*E9/24.)+DYB*E8/2.
      T22=DYB*BBAR*E7/(192.*PI)
      TNEW=(T11+T12)/(T21+T22)
      THETA(I,J)=THETA(I,J)+RF*(TNEW-THETA(I,J))
      IF(J.NE.M)GOTO 15
      THETA(I,1)=THETA(I,M)
15    CONTINUE
C  BOUNDARY CONDITIONS AT THE BEARING EDGE
      DO 8 J=1,M
      IF(THETA(2,J).GE.1.)THETA(1,J)=1.
      IF(THETA(2,J).LT.1.)THETA(1,J)=THETA(2,J)
8     CONTINUE
C
C  RESETING THE VALUES OF G
C
      NCYCLE=NCYCLE+1
      CALL SETPAR(M,N,NCYCLE)
      DO 1 I=1,N
      DO 1 J=1,M
      IF(NG(I,J).NE.IG(I,J))GOTO 10
1     CONTINUE
      DO 2 I=1,N
      DO 2 J=1,M
      DIF=DABS(THETA(I,J)-TPREV(I,J))/TPREV(I,J)
      IF(DIF.GE.TOL)GOTO 10
2     CONTINUE
20    RETURN
      END
C
C
      SUBROUTINE SETPAR(M,N,NCYCLE)
C
C  ------------------------------------------------
```

```
C  SETS THE INITIAL VALUES OF G AND THETA
C  RESETS VALUES OF G AFTER A CYCLE, DEPENDING ON THETA.
C  PREVIOUS G'S ARE RETAINED
C  ------------------------------------------------------
C
      IMPLICIT REAL*8(A-H,O-Z)
      COMMON/BLOCK3/IG(32,202),NG(32,202),TPREV(32,202)
      COMMON/BLOCKT/THETA(32,202)
C
      N1=N+1
      M1=M+1
      IF(NCYCLE.GT.0)GOTO 10
      DO 1 I=1,N1
      DO 1 J=1,M1
      NG(I,J)=1
1     THETA(I,J)=1.
      GOTO 20
10    DO 2 I=1,N1
      DO 2 J=1,M1
      IG(I,J)=NG(I,J)
      IF(THETA(I,J).GE.1.)NG(I,J)=1
      IF(THETA(I,J).LT.1.)NG(I,J)=0
2     CONTINUE
20    RETURN
      END
C
C
      SUBROUTINE PRESS(M,N,BBAR)
C
C  ------------------------------------------------------
C  CALCULATES THE NORMALIZED GAUGE PRESSURES AT EVERY NODE
C  ------------------------------------------------------
C
      IMPLICIT REAL*8(A-H,O-Z)
      COMMON/BLOCK3/IG(32,202),NG(32,202),TPREV(32,202)
      COMMON/BLOCKT/THETA(32,202)
      COMMON/BLOCK4/P(31,201)
C
      DO 1 I=1,N
      DO 1 J=1,M
      IF(NG(I,J).EQ.0)GOTO 2
      P(I,J)=BBAR*(THETA(I,J)-1.)
      GOTO 1
2     P(I,J)=0.
1     CONTINUE
      RETURN
      END
C
C
      SUBROUTINE LOAD(M,N,WBAR,ATTA)
C
C  ------------------------------------------------------
C  CALCULATES THE DIMENSIONLESS LOAD CAPACITY BY NUMERICAL
C  INTEGRATION OF THE PRESSURE DISTRIBUTION
C  ------------------------------------------------------
C
      IMPLICIT REAL*8(A-H,O-Z)
      COMMON/BLOCK1/PI
      COMMON/BLOCK2/H(202),ANGLE(202),DXBAR(201),DYBAR(31)
      COMMON/BLOCK4/P(31,201)
      COMMON/BLOCK5/PFUN(201),AFUN(201)
C
      DO 10 I=1,N
      DO 15 J=1,M
      ALPHA=2.*PI*ANGLE(J)/360.
      PFUN(J)=-P(I,J)*DCOS(ALPHA)
15    CONTINUE
      AFUN(I)=SIMP(PFUN,1,M,DXBAR)
10    CONTINUE
      PYBAR=2.*PI*SIMP(AFUN,1,N,DYBAR)
      DO 25 I=1,N
      DO 30 J=1,M
      ALPHA=2.*PI*ANGLE(J)/360.
      PFUN(J)=P(I,J)*DSIN(ALPHA)
30    CONTINUE
      AFUN(I)=SIMP(PFUN,1,M,DXBAR)
25    CONTINUE
      PXBAR=2.*PI*SIMP(AFUN,1,N,DYBAR)
      ATTA=180.*DATAN(PXBAR/PYBAR)/PI
      IF(ATTA.GE.0.0)GOTO 20
      ATTA=180.0+ATTA
20    WBAR=2.*DSQRT(PXBAR**2+PYBAR**2)
      RETURN
      END
C
C
      FUNCTION SIMP(FUN,KI,K,DBAR)
C
C  ------------------------------------------------------
C  CALCULATES THE INTEGRAL OF A FUNCTION 'FUN' USING
C  SIMPSON'S RULE AND NON-EVEN MESH INTERVALS
C  ------------------------------------------------------
C
C    FUN - ARRAY HOLDING THE VALUES OF THE FUNCTION TO BE
C          INTEGRATED
C   KI,K - NODAL POINTS DEFINING THE DOMAIN OF INTEGRATION
C   DBAR - ARRAY HOLDING THE MESH INTERVALS
C
      IMPLICIT REAL*8(A-H,O-Z)
      DIMENSION FUN(K),DBAR(K)
```

```
C
      IF(KI.EQ.K)GOTO 20
      KK=K-1
      SIMP=0.0
      DO 10 I=KI,KK,2
      A1=2.*(DBAR(I)**2)
      A2=3.*DBAR(I)*DBAR(I+1)
      A3=(DBAR(I+1)**3)/DBAR(I)
      A4=6.*(DBAR(I)+DBAR(I+1))
      A=(A1+A2-A3)/A4
      B1=2.*(DBAR(I+1)**2)
      B2=(DBAR(I)**3)/DBAR(I+1)
      B=(2.*(A1+A2+B1)+A3+B2)/A4
      C=(A2-B2+B1)/A4
10    SIMP=SIMP+A*FUN(I)+B*FUN(I+1)+C*FUN(I+2)
      GOTO 30
20    SIMP=0.0
30    RETURN
      END
C
C
      SUBROUTINE CVRF(M,N,NIGRX,NIEDY,PFBAR,JJ,JCAV,JR,JR1,JREF)
C
C  ------------------------------------------------
C  DETERMINES THE LOCATION OF THE CAVITATION AND THE
C  REFORMATION BOUNDARIES
C  ------------------------------------------------
C
C   NIGRX - NUMBER OF MESH INTERVALS OVER THE GROOVE IN THE
C           CIRCUMFERENTIAL DIRECTION
C   NIEDY - NUMBER OF MESH INTERVALS IN BETWEEN THE GROOVE
C           AND THE EDGE OF THE BEARING
C    JCAV - CIRCUMFERENTIAL LOCATION OF THE POINT ON THE EDGE
C           OF THE BEARING WHERE FILM RUPTURE OCCURS
C    JREF - CIRCUMFERENTIAL LOCATION OF THE POINT ON THE BEARING
C           EDGE WHERE THE FULL WIDTH FILM BEGINS
C      JJ - CIRCUMFERENTIAL LOCATION OF THE NOSE OF THE
C           CAVITATION BOUNDARY
C      JR - CIRCUMFERENTIAL LOCATION OF THE NOSE OF THE
C           REFORMATION BOUNDARY
C     JR1 - CIRCUMFERENTIAL LOCATION OF THE NODE ON THE
C           REFORMATION BOUNDARY, THE AXIAL LOCATION OF WHICH
C           IS (NIEDY+1)
C   NPREF1,NPREF2 - NUMBER OF POINTS ON EACH PORTION OF THE
C           REFORMATION BOUNDARY WHEN SEPARATED INTO PARTS
C   XBCAV(K),YBCAV(K) - ARRAYS HOLDING NORMALIZED COORDINATES
C           OF POINTS ON THE CAVITATION BOUNDARY
C   XBREF(K),YBREF(K) - ARRAYS HOLDING NORMALIZED COORDINATES
C           OF POINTS ON THE REFORMATION BOUNDARY
C
      IMPLICIT REAL*8(A-H,O-Y)
      COMMON/BLOCK2/H(202),ANGLE(202),DXBAR(201),DYBAR(31)
      COMMON/BLOCKT/THETA(32,202)
      COMMON/BLOCK7/XBCAV(61),YBCAV(61),XBREF(61),YBREF(61),
     +          XBREF1(31),YBREF1(31),XBREF2(61),YBREF2(61)
C
      N1=N-1
      YBAR=0.0
      NIGRY=(N-1)-NIEDY
      NPREF1=NIEDY+1
      NPREF2=2*NIGRY+1
      DO 1 I=1,N
      IF(I.EQ.1)GOTO 10
      YBAR=YBAR+DYBAR(I-1)
C
C  LOCATION OF THE CAVITATION BOUNDARY AND COORDINATES OF POINTS
C
10    DO 2 J=2,M
      IF(I.GT.1)GOTO 15
      IF((THETA(I,J).LT.1.0).AND.(THETA(I,J-1).EQ.1.0))GOTO 20
      GOTO 2
15    IF((THETA(I,J).LE.1.0).AND.(THETA(I,J-1).GT.1.0))GOTO 20
2     CONTINUE
20    IF(I.EQ.N)JJ=J
      IF(I.EQ.1)JCAV=J
      XBCAV(I)=ANGLE(J)/360.0
      YBCAV(I)=YBAR
C
C  LOCATION OF THE REFORMATION BOUNDARY AND COORDINATES OF POINTS
C
      DO 3 K=2,M
      IF((THETA(I,K-1).LT.1.0).AND.(THETA(I,K).GE.1.0))GOTO 30
3     CONTINUE
30    XBREF(I)=ANGLE(K)/360.0
      YBREF(I)=YBAR
      IF(I.EQ.1)JREF=K
      IF(I.EQ.(NIEDY+1))JR1=K
      IF(I.EQ.N)JR=K
1     CONTINUE
C
C  CALCULATION OF POINTS ON THE OTHER HALF OF THE CURVES
C
      DO 4 I=1,N1
      XBCAV(N+I)=XBCAV(N-I)
4     YBCAV(N+I)=1.0-YBCAV(N-I)
      DO 5 I=1,N1
      XBREF(N+I)=XBREF(N-I)
5     YBREF(N+I)=1.0-YBREF(N-I)
50    DO 6 I=1,NPREF1
      XBREF1(I)=XBREF(I)
```

```
      IF((I.EQ.NPREF1).AND.(PFBAR.EQ.0.0))XBREF1(I)=DXBAR(1)*
     +       FLOAT(NIGRX)/2.0
6     YBREF1(I)=YBREF(I)
      NN2=(NPREF2+1)/2
      DO 7 I=1,NPREF2
      IF(I.GT.NN2)GOTO 60
      XBREF2(I)=XBREF(I+NIEDY)
      YBREF2(I)=YBREF(I+NIEDY)
      GOTO 7
60    II=I-NN2
      XBREF2(I)=XBREF2(NN2-II)
      YBREF2(I)=1.0-YBREF2(NN2-II)
7     CONTINUE
      RETURN
      END
C
C
      SUBROUTINE FLOW(M,N,BD,AB,NIGRX,NIEDY,JJ,JR1)
C
C     ------------------------------------------------
C     CALCULATES THE DIMENSIONLESS FLOW RATES. SIMPSON'S
C     RULE IS USED FOR NUMERICAL INTEGRATION.
C     ------------------------------------------------
C
C      NIGRX - NUMBER OF MESH INTERVALS OVER THE GROOVE IN
C              THE CIRCUMFERENTIAL DIRECTION
C      NIEDY - NUMBER OF MESH INTERVALS IN BETWEEN THE GROOVE
C              AND THE BEARING EDGE
C         JJ - CIRCUMFERENTIAL LOCATION OF THE NOSE OF THE
C              CAVITATION BOUNDARY
C        JR1 - CIRCUMFERENTIAL LOCATION OF THE NODE
C              (JR1,(NIEDY+1)) ON THE REFORMATION BOUNDARY
C      QSIDE - DIMENSIONLESS SIDE FLOW RATE
C       QCAV - DIMENSIONLESS FLOW RATE IN THE CAVITATION REGION
C        QGR - DIMENSIONLESS FLOW RATE ISSUING FROM THE GROOVE
C       QGR1 - FLOW FROM THE UPSTREAM EDGE OF THE GROOVE
C              QGR1<0 MEANS FLOW INTO THE GROOVE REGION
C       QGR2 - FLOW FROM THE DOWNSTREAM EDGE OF THE GROOVE
C       QGR3 - FLOW FROM THE SIDES OF THE GROOVE
C
      IMPLICIT REAL*8(A-H,O-Y)
      COMMON/BLOCK1/PI
      COMMON/BLOCK2/H(202),ANGLE(202),DXBAR(201),DYBAR(31)
      COMMON/BLOCKT/THETA(32,202)
      COMMON/BLOCK4/P(31,201)
      COMMON/BLOCK5/PFUN(201),AFUN(201)
      COMMON/BLOCK8/QSIDE,QGR,QGR1,QGR2,QGR3,QCAV
C
      DB2=(1.0/BD)**2
      I1=NIEDY+1
      J1=1+NIGRX/2
      N1=N-1
      J2=M-(NIGRX/2)
      NIGRY=(N-1)-NIEDY
      NGX=NIGRX+1
C
C  DIMENSIONLESS SIDE FLOW RATE
C
      DO 1 J=1,M
      PG=PGRAD(1,J,2,DYBAR(1),1)
      IF(PG.LT.0.0)PG=(P(2,J)-P(1,J))/DYBAR(1)
      IF(P(2,J).EQ.0.0)PG=0.0
1     AFUN(J)=-PG*(-H(J)**3)/24.0
      QSIDE=2.0*PI*DB2*SIMP(AFUN,1,M,DXBAR)
C
C  FLOW INTO THE CAVITATION REGION (CALCULATED AT
C  THE CIRCUMFERENTIAL POINT J=JJ)
C
      DO 2 I=1,N
2     AFUN(I)=THETA(I,JJ)
      QCAV=2.0*(H(JJ)/2.0)*SIMP(AFUN,1,N,DYBAR)
C
C  DIMENSIONLESS FLOW RATE ISSUING FROM THE GROOVE
C
C  FLOW OVER THE UPSTREAM EDGE OF THE GROOVE
      IF(P(I1,J2-1).GT.0.0)GOTO 10
      QGR1=-1.0*AB*QCAV
      GOTO 8
10    DO 3 J=JR1,J2
      PG=PGRAD(I1,J,2,DYBAR(1),-1)
3     AFUN(J)=PG*(-H(J)**3)/24.0
      IF(MOD((J2-JR1),2).NE.0)GOTO 20
      QLAT=2.0*PI*DB2*SIMP(AFUN,JR1,J2,DXBAR)
      GOTO 15
20    QLAT=2.0*PI*DB2*(SIMP(AFUN,JR1,(J2-1),DXBAR)+
     +     DXBAR(J2-1)*(AFUN(J2-1)+AFUN(J2))/2.0)
15    QGR1=QLAT-QCAV*AB
C  FLOW OVER THE DOWNSTREAM EDGE OF THE GROOVE
8     DO 4 I=I1,N
      PG=PGRAD(I,J1,1,DXBAR(J1),1)
      AFUN(I)=(PG*(-H(J1)**3)/(24.0*PI))+0.5*H(J1)
4     CONTINUE
      IF(MOD(NIGRY,2).NE.0)GOTO 30
      QGR2=2.0*SIMP(AFUN,I1,N,DYBAR)
      GOTO 40
30    QGR2=2.0*(SIMP(AFUN,I1,N1,DYBAR)+DYBAR(N1)*
     +    (AFUN(N1)+AFUN(N))/2.0)
C  FLOW OVER THE GROOVE SIDES
40    DO 5 K=1,NGX
      KJ=J2-1+K
```

```
      IF(KJ.GE.M)KJ=KJ-M+1
      PG=PGRAD(I1,KJ,2,DYBAR(1),-1)
5     AFUN(KJ)=PG*(-H(KJ)**3)/24.0
      AFUN(M)=AFUN(1)
      IF(MOD((M-J2),2).NE.0)GOTO 6
      S1=SIMP(AFUN,J2,M,DXBAR)
      S2=SIMP(AFUN,1,J1,DXBAR)
      GOTO 7
6     S1=SIMP(AFUN,J2,(M-1),DXBAR)+DXBAR(M-1)*(AFUN(M-1)+AFUN(M))/2.0
      S2=SIMP(AFUN,1,(J1-1),DXBAR)+
     +       DXBAR(J1-1)*(AFUN(J1-1)+AFUN(J1))/2.0
7     QGR3=2.0*PI*DB2*(S1+S2)
C  TOTAL NET FLOW ISSUING FROM THE GROOVE
      QGR=QGR1+QGR2+QGR3
      RETURN
      END
C
C
      FUNCTION PGRAD(IG,JG,KFLOW,SGRID,KG)
C
C  ------------------------------------------------
C  CALCULATES THE PRESSURE GRADIENT AT A NODAL POINT
C  ------------------------------------------------
C
C   IT IS ASSUMED THAT THE VARIATION OF PRESSURE IN THE
C   NEIGBOURHOOD OF A NODAL POINT CAN BE REPRESENTED BY
C   A POLYNOMIAL OF DEGREE 3.
C
C   IG,JG - GRID LOCATION OF THE NODE WHERE THE PRESSURE
C           GRADIENT IS REQUIRED
C   KFLOW - INDICATOR. KFLOW=1 IF IT IS REQUIRED THE FLOW
C           THROUGH A SECTION OF CONSTANT X
C           KFLOW=2 IF IT IS REQUIRED THE FLOW THROUGH A
C           SECTION OF CONSTANT Y
C   SGRID - SIZE OF MESH INTERVALS INVOLVED IN THE CALCULATIONS
C      KG - IS GIVEN THE VALUE 1 OR -1 DEPENDING  ON WHAT
C           DIRECTION IS BEING TAKEN TO CALCULATE THE PRESSURE
C           GRADIENT
C
      IMPLICIT REAL*8(A-H,O-Y)
      COMMON/BLOCK4/P(31,201)
C
      IF(KFLOW.EQ.2)GOTO 10
      PGRAD=(-11.0*P(IG,JG)+18.0*P(IG,JG+KG)-9.0*P(IG,2*KG+JG)+
     + 2.0*P(IG,3*KG+JG))/(6.0*SGRID)
      GOTO 20
10    PGRAD=(-11.0*P(IG,JG)+18.0*P(IG+KG,JG)-9.0*P(2*KG+IG,JG)+
     + 2.0*P(3*KG+IG,JG))/(6.0*SGRID)
20    RETURN
      END
C
C
      SUBROUTINE DIAG(M,N,NIGRX,NIEDY,JJ,JCAV,JR,JR1,JREF,BD,
     +                ECC,AB,WD,PFBAR,IGRID)
C
C  ------------------------------------------------------
C  DRAWS THE CAVITATION AND THE REFORMATION BOUNDARIES AND
C  THE MESH REPRESENTATION (IF REQUIRED)
C  ------------------------------------------------------
C
C  THE CALL TO DEVICE NOMINATION AND THE CALL TO 'DEVEND'
C  WERE MADE IN THE MAIN PROGRAM TO ALLOW FOR MORE THAN ONE
C  GRAPH TO BE STORED IN THE SAME PLOT FILE
C
      IMPLICIT REAL*8(A-H,O-Y)
      COMMON/BLOCK2/H(202),ANGLE(202),DXBAR(201),DYBAR(31)
      COMMON/BLOCK7/XBCAV(61),YBCAV(61),XBREF(61),YBREF(61),
     +          XBREF1(31),YBREF1(31),XBREF2(61),YBREF2(61)
      COMMON/BLOCKZ/ZXCUR(3),ZYCUR(3)
C
      NI=NIEDY+1
      JG=M-(NIGRX/2)
C
      CALL PICCLE
      CALL PENSEL(1,0.0,0)
C
C  DRAWING THE MESH OVER HALF THE BEARING AREA
C  XL,YW ARE THE SIDES OF A RECTANGLE REPRESENTING
C  THE BEARING AREA
C
      XL=140.0
      YW=50.0
      DXGR=FLOAT(NIGRX)*DXBAR(1)
      DYGR=FLOAT(2*(N-1-NIEDY))*DYBAR(N-1)
      XG=0.5-DXGR/2.0
      YG=FLOAT(NIEDY)*DYBAR(1)
C
      DO 100 I=1,2
      IF((I.EQ.1).AND.(IGRID.EQ.0))GOTO 100
      DX=120.0
      DY=195.0-FLOAT(I-1)*80.0
      CALL TRANSF(-1)
      CALL SHIFT2(DX,DY)
      CALL MOVTO2(0.0,0.0)
      CALL LINBY2(0.0,YW)
      CALL LINBY2(XL,0.0)
      CALL LINBY2(0.0,-YW)
      CALL LINBY2(-XL,0.0)
      CALL SCALE2(XL,YW)
C  DRAWING THE GROOVE
```

```
      CALL MOVTO2(0.5,0.0)
      CALL SYMBOL(3)
      CALL MOVTO2(XG,YG)
      CALL LINBY2(0.0,DYGR)
      CALL LINBY2(DXGR,0.0)
      CALL LINBY2(0.0,-DYGR)
      CALL LINBY2(-DXGR,0.0)
      IF(I.EQ.2)GOTO 100
C  DRAWING THE AXIAL MESH LINES
      DO 200 JGR=2,M
      XM=ANGLE(JGR)/360.0
      IF(XM.LT.0.5)GOTO 70
      XM=XM-0.5
      GOTO 80
70    XM=XM+0.5
80    CALL MOVTO2(XM,0.0)
200   CALL LINBY2(0.0,0.5)
C  DRAWING THE CIRCUMFERENTIAL MESH LINES
      YM=0.0
      DO 300 IGR=2,N
      YM=YM+DYBAR(IGR-1)
      CALL MOVTO2(0.0,YM)
300   CALL LINBY2(1.0,0.0)
100   CONTINUE
C
C  DRAWING THE CAVITATION BOUNDARY
C    - THREE POINTS ONLY -
C
      DO 1 I=1,3
      II=I+(I-1)*(N-2)
      ZXCUR(I)=SNGL(XBCAV(II))-0.5
      ZYCUR(I)=SNGL(YBCAV(II))
1     CONTINUE
      CALL CURTO2(ZXCUR,ZYCUR,3,0,0)
      CALL CHASIZ(2.0,2.5)
      CALL MOVTO2((ZXCUR(2)+2.0/XL),(ZYCUR(2)+1.0/YW))
      CALL CHAHOL(13HCAVITATION *.)
      CALL CHAHOL(8HREGION*.)
      CALL MOVTO2((ZXCUR(2)+2.0/XL),(ZYCUR(2)-3.0/YW))
      CALL CHAHOL(8HEDGE  *.)
      CALL CHAFIX(ANGLE(JCAV),7,1)
      CALL CHAHOL(6H DEG*.)
      CALL MOVTO2((ZXCUR(2)+2.0/XL),(ZYCUR(2)-7.0/YW))
      CALL CHAHOL(8HNOSE  *.)
      CALL CHAFIX(ANGLE(JJ),7,1)
      CALL CHAHOL(6H DEG*.)
C
C  DRAWING THE REFORMATION BOUNDARY
C
      IF(PFBAR.EQ.0.0)GOTO 10
      IF((JREF.LE.JG).AND.((XBREF(1)+0.5).GT.1.0))GOTO 60
      IF((JR1-JR).GE.2)GOTO 60
10    AUX=FLOAT(NI)/2.0
      Z=SNGL(AUX)
      NP=IFIX(Z)+1
      DO 3 I=1,3
      II=I+(I-1)*(NP-2)
      IF((I.EQ.3).AND.(MOD(NI,2).EQ.0))II=II-1
      ZXCUR(I)=SNGL(XBREF1(II))
      ZYCUR(I)=SNGL(YBREF1(II))
      IF(ZXCUR(I).GE.0.5)GOTO 30
      ZXCUR(I)=ZXCUR(I)+0.5
      GOTO 3
30    ZXCUR(I)=ZXCUR(I)-0.5
3     CONTINUE
      CALL CURTO2(ZXCUR,ZYCUR,3,0,0)
C
      DO 4 I=1,3
4     ZYCUR(I)=1.0-ZYCUR(I)
      CALL CURTO2(ZXCUR,ZYCUR,3,0,0)
      IF(PFBAR.EQ.0.0)GOTO 20
C
      NP=N-NIEDY
      DO 5 I=1,3
      II=I+(I-1)*(NP-2)
      ZXCUR(I)=SNGL(XBREF2(II))-0.5
      ZYCUR(I)=SNGL(YBREF2(II))
5     CONTINUE
      CALL CURTO2(ZXCUR,ZYCUR,3,0,0)
      GOTO 20
C
60    DO 2 I=1,3
      II=I+(I-1)*(N-2)
      ZXCUR(I)=SNGL(XBREF(II))
      ZYCUR(I)=SNGL(YBREF(II))
      IF(ZXCUR(I).GE.0.5)GOTO 50
      ZXCUR(I)=ZXCUR(I)+0.5
      GOTO 2
50    ZXCUR(I)=ZXCUR(I)-0.5
2     CONTINUE
      CALL CURTO2(ZXCUR,ZYCUR,3,0,0)
C
C  WRITING STRINGS OF CHARACTERS
C
20    CALL MOVTO2((DXGR/2.0+0.5+5.0/XL),(0.5+1.0/YW))
      CALL CHAHOL(18HFULL FLUM REGION*.)
      CALL MOVTO2((DXGR/2.0+0.5+5.0/XL),(0.5-3.0/YW))
      CALL CHAHOL(7HEDGE *.)
      CALL CHAFIX(ANGLE(JREF),7,1)
      CALL CHAHOL(6H DEG*.)
```

```
      IF(JR.EQ.JG)GOTO 40
      CALL MOVTO2((DXGR/2.0+0.5+5.0/XL),(0.5-7.0/YW))
      CALL CHAHOL(7HNOSE *.)
      CALL CHAFIX(ANGLE(JR),7,1)
      CALL CHAHOL(6H DEG*.)
40    CALL TRANSF(-1)
      CALL SHIFT2(DX,DY)
      CALL MOVTO2(-3.0,-4.0)
      CALL CHAHOL(5H180*.)
      CALL MOVTO2((XL/2.0-6.5),-4.0)
      CALL CHAHOL(9HMAX.GAP*.)
      CALL MOVTO2((XL-3.0),-4.0)
      CALL CHAHOL(5H180*.)
      CALL MOVTO2(30.0,-20.0)
      CALL CHAHOL(17HSHAFT ROTATION *.)
      CALL CHAHOL(20HFROM LEFT TO RIGHT*.)
      CALL MOVTO2(30.0,-30.0)
      CALL CHAHOL(30HNORMALIZED SUPPLY PRESSURE =*.)
      CALL CHAFIX(PFBAR,5,3)
      CALL MOVTO2(34.0,-40.0)
      CALL CHAHOL(9H*LB/D =*.)
      CALL CHAFIX(BD,5,3)
      CALL MOVBY2(18.0,0.0)
      CALL CHAHOL(7HECC =*.)
      CALL CHAFIX(ECC,5,3)
      CALL MOVTO2(34.0,-50.0)
      CALL CHAHOL(9H*LA/B =*.)
      CALL CHAFIX(AB,5,3)
      CALL MOVBY2(18.0,0.0)
      CALL CHAHOL(9H*LW/D =*.)
      CALL CHAFIX(WD,5,3)
      CALL TRANSF(-1)
C     NEXT TWO STATEMENTS ARE USED ONLY TO ENSURE THAT
C     THE NEXT GRAPH WILL BE DRAWN IN A NEW PAGE
      CALL MOVTO2(320.0,245.0)
      CALL LINBY2(0.0,2.0)
      RETURN
      END
```

APPENDIX C BEARING PERFORMANCE PREDICTIONS

The performance predictions shown in the table that follows apply to journal bearings with a single oil groove at the maximum film thickness and a/b = 0.8 and w/d = 0.2.

In a few cases, marked (*) in the table, convergence of the Gauss-Seidel iteration was not achieved. The results shown for these cases have been obtained for w/d = 0.19.

The following sketch of the developed bearing area serves to identify some of the parameters involved.

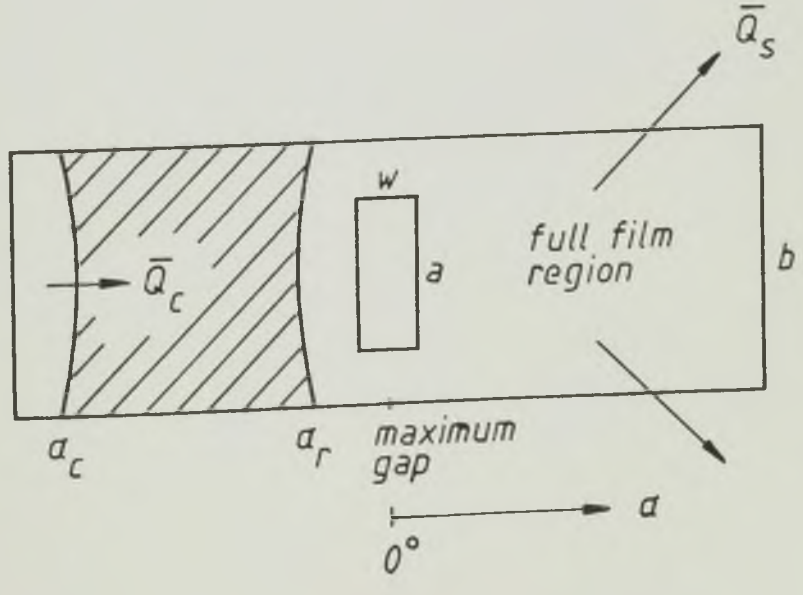

$\bar{p}_f$	b/d	ε	$\bar{W}$	$\bar{Q}_s$	$\bar{Q}_c$	ψ (deg)	α_r (deg)	α_c (deg)
0.0	0.5	0.2	0.154	0.151	0.404	72.1	49.5	193.7
		0.4	0.405	0.301	0.307	60.0	47.5	193.7
		0.6	1.001	0.449	0.209	47.1	47.5	193.7
		0.8	3.497	0.602	0.108	32.5	45.5	193.7
	0.6	0.2	0.214	0.146	0.405	70.1	49.5	194.0
		0.4	0.553	0.291	0.309	60.1	47.5	194.0
		0.6	1.332	0.435	0.211	47.5	47.5	194.0
		0.8	4.374	0.577	0.110	33.2	45.5	189.3
	0.7	0.2	0.278	0.141	0.407	71.4	49.5	198.7
		0.4	0.712	0.279	0.311	60.1	47.5	198.7
		0.6	1.665	0.417	0.213	48.0	45.5	194.0
		0.8	5.188	0.553	0.111	33.8	45.5	194.0
	0.8	0.2	0.346	0.135	0.408	70.9	49.5	198.7
		0.4	0.875	0.267	0.314	60.1	47.5	198.7
		0.6	1.997	0.397	0.216	48.3	45.5	194.0
		0.8	5.927	0.525	0.112	34.4	43.5	194.0
	0.9	0.2	0.416	0.129	0.410	70.5	49.5	198.7
		0.4	1.041	0.255	0.316	60.1	47.5	198.7
		0.6	2.320	0.376	0.218	48.6	45.5	194.0
		0.8	6.597	0.495	0.113	34.9	43.5	194.0
	1.0	0.2	0.487	0.124	0.412	70.1	49.5	203.4
		0.4	1.205	0.242	0.318	60.0	47.5	198.6
		0.6	2.624	0.356	0.220	49.0	45.5	193.7
		0.8	7.199	0.465	0.114	35.3	43.5	193.7

$\bar{P}_f$	b/d	ε	$\bar{W}$	$\bar{Q}_s$	$\bar{Q}_c$	ψ (deg)	α_r (deg)	α_c (deg)
0.25	0.5	0.2	0.213	0.609	0.404	123.7	344.5	194.3
		0.4	0.386	1.022	0.307	84.5	346.5	194.3
		0.6	0.926	1.518	0.209	56.3	346.5	194.3
		0.8	3.390	2.119	0.108	34.4	344.5	189.9
	0.6	0.2	0.267	0.484	0.405	113.9	344.5	194.3
		0.4	0.536	0.816	0.309	79.2	346.5	194.3
		0.6	1.261	1.211	0.211	55.0	346.5	194.3
		0.8	4.252	1.686	0.111	35.2	346.5	189.9
	0.7	0.2	0.330	0.405	0.407	106.5	344.5	198.7
		0.4	0.700	0.692	0.311	75.7	346.5	194.3
		0.6	1.603	1.025	0.213	54.5	346.5	194.3
		0.8	5.069	1.414	0.111	35.7	346.5	189.9
	0.8	0.2	0.400	0.348	0.408	100.9	346.5	198.7
		0.4	0.872	0.599	0.314	73.5	348.5	198.7
		0.6	1.946	0.885	0.216	54.2	348.5	194.3
		0.8	5.821	1.214	0.112	36.2	346.5	194.3
	0.9	0.2	0.474	0.304	0.410	96.6	346.5	198.7
		0.4	1.047	0.531	0.316	71.8	348.5	198.7
		0.6	2.281	0.783	0.218	54.0	348.5	194.3
		0.8	6.504	1.060	0.113	36.7	348.5	189.9
	1.0	0.2	0.551	0.274	0.412	93.3	346.5	203.0
		0.4	1.222	0.476	0.318	70.6	348.5	198.7
		0.6	2.599	0.697	0.219	54.0	351.4	194.3
		0.8	7.118	0.946	0.114	37.1	348.5	189.9

$\bar{p}_f$	b/d	ε	$\bar{W}$	$\bar{Q}_s$	$\bar{Q}_c$	ψ (deg)	α_r (deg)	α_c (deg)
0.5	0.5	0.2	0.363	1.099	0.404	147.3	338.5	196.7
		0.4	0.434	1.775	0.307	109.6	340.5	192.2
		0.6	0.863	2.642	0.209	67.4	340.5	192.2
		0.8	3.241	3.702	0.108	36.9	340.5	192.2
	0.6	0.2	0.410	0.845	0.405	138.4	338.5	196.7
		0.4	0.569	1.378	0.309	99.2	340.5	196.7
		0.6	1.196	2.043	0.211	63.8	340.5	192.2
		0.8	4.132	2.858	0.111	37.1	340.5	192.2
	0.7	0.2	0.466	0.683	0.407	130.3	338.5	196.7
		0.4	0.727	1.121	0.311	92.3	340.5	196.7
		0.6	1.544	1.659	0.213	61.7	340.5	196.7
		0.8	4.963	2.311	0.111	37.5	340.5	192.2
	0.8	0.2	0.529	0.574	0.408	123.4	338.5	201.3
		0.4	0.898	0.943	0.314	87.4	340.5	196.7
		0.6	1.893	1.390	0.216	60.6	342.5	196.7
		(*)0.8	5.728	1.898	0.112	37.9	341.1	192.2
	0.9	0.2	0.598	0.493	0.410	117.4	338.5	201.3
		0.4	1.076	0.811	0.310	83.9	342.5	196.7
		0.6	2.237	1.190	0.218	59.7	342.5	196.7
		0.8	6.382	1.650	0.113	38.6	342.5	192.2
	1.0	0.2	0.672	0.431	0.412	112.4	338.5	201.3
		0.4	1.256	0.708	0.319	81.2	342.5	196.7
		0.6	2.571	1.045	0.220	59.1	342.5	196.7
		0.8	7.005	1.429	0.114	39.0	342.5	192.2

$\bar{p}_f$	b/d	ε	$\bar{W}$	$\bar{Q}_s$	$\bar{Q}_c$	ψ (deg)	α_r (deg)	α_c (deg)
1.0	0.5	0.2	0.736	2.127	0.404	162.6	328.5	195.1
		0.4	0.696	3.369	0.307	140.6	332.5	195.1
		0.6	0.836	4.993	0.209	94.3	332.5	195.1
		0.8	2.972	7.047	0.108	41.9	332.5	190.4
	0.6	0.2	0.796	1.610	0.405	157.2	328.5	195.1
		0.4	0.799	2.555	0.309	129.9	332.5	195.1
		0.6	1.137	3.780	0.211	84.5	332.5	195.1
		0.8	3.851	5.314	0.110	41.6	332.5	190.4
	0.7	0.2	0.856	1.282	0.407	151.6	328.5	199.9
		0.4	0.928	2.033	0.312	120.5	332.5	195.1
		0.6	1.473	3.006	0.213	78.8	332.5	195.1
		(*) 0.8	4.685	4.126	0.111	41.6	333.1	190.4
	0.8	0.2	0.918	1.057	0.409	146.2	326.5	199.9
		0.4	1.079	1.677	0.314	112.8	332.5	195.1
		0.6	1.825	2.473	0.216	74.9	332.5	195.1
		0.8	5.434	3.455	0.112	42.1	332.5	190.4
	0.9	0.2	0.983	0.895	0.410	141.1	326.5	199.9
		0.4	1.245	1.419	0.317	106.6	332.5	199.9
		0.6	2.181	2.087	0.218	72.3	332.5	195.1
		(*)0.8	6.163	2.854	0.113	42.3	333.1	190.4
	1.0	0.2	1.050	0.772	0.412	136.3	326.5	199.9
		(*)0.4	1.417	1.197	0.319	101.4	332.8	199.9
		0.6	2.529	1.794	0.221	70.4	332.5	195.1
		0.8	6.803	2.491	0.114	42.7	332.5	195.1